TABLE OF CONTENTS

Page

LIST OF TABLES

LIST OF FIGURES

Page

LIST OF ABREVIATIONS

ETS	École de Technologie Supérieure
VTOL	Vertical Take-Off and Lnading
UAV	Unmanned Arial Vehicle
GPS	Global Positioning System
PID	Proportional Integral Derivative
LQR	Linear Quadratic Regulator
MPC	Model Predictive Control
NDO	Non-linear Disturbance Observer
SMC	Sliding Mode Control
DCM	Direction Cosine Matrix
PWM	Pulse Width Modulation
STO	Super-Twisting sliding model Observer
KDO	Kernal Disturbance Observer
GDOB	Generalized Disturbance Observer
ESO	Extended State Observer
MAVLink	Micro Air Vehicle Link
DOF	Degrees-Of-Freedom

LISTE OF SYMBOLS AND UNITS OF MEASUREMENTS

M_1	Motor number 1 of quadrotor
M_2	Motor number 2 of quadrotor
M_3	Motor number 3 of quadrotor
M_4	Motor number 4 of quadrotor
$(\mathcal{I})$	The earth fixed frame
(E_1, E_2, E_3)	The unit vector basis associated with the earth fixed frame
$(\mathcal{B})$	The body fixed frame
(E_1^b, E_2^b, E_3^b)	The unit vector basis associated with the body fixed frame
p	The position vector of the center of the quadrotor's mass
Θ	The attitude angles vector of the quadrotor
Ω	The angular velocity vector of attitude angles
$\ddot{\Theta}$	The angular acceleration vector of attitude angles
$\dot{p}$	The linear velocity vector of the translational system
$\ddot{p}$	The linear acceleration vector of the translational system
R	Rotation matrix
$M(\Theta)$	Euler matrix
x	The position of quadrotor in inertial frame along x-axis (m)
y	The position of quadrotor in inertial frame along y-axis (m)
z	The position of quadrotor in inertial frame along -axis (m)

ϕ	The orientation of quadrotor in inertial frame along Euler angle; roll (rad)
θ	The orientation of quadrotor in inertial frame along Euler angle; pitch (rad)
ψ	The orientation of quadrotor in inertial frame along Euler angle; yaw (rad)
I	The moment of inertia matrix of the quadrotor
I_x	Moment of inertia around the x-axis in the body frame ($\mathcal{B}$) (kg·m^2)
I_y	Moment of inertia around the y-axis in the body frame ($\mathcal{B}$) (kg·m^2)
I_z	Moment of inertia around the z-axis in the body frame ($\mathcal{B}$) (kg·m^2)
G	The gravitational force acting along the z-axis (m/s^2)
m	The mass of the quadrotor (Kg)
d_p	External disturbances along with the aerodynamical disturbances vector acting on the translational subsystem
d_Θ	External disturbances along with the aerodynamical disturbances vector acting on the orientation subsystem
d_x	External disturbance along with the aerodynamical disturbance acting on x-axis (N)
d_y	External disturbance along with the aerodynamical disturbance acting on y-axis (N)
d_z	External disturbance along with the aerodynamical disturbance acting on z-axis (N)
d_ϕ	External disturbance along with the aerodynamical disturbance acting on rotational roll angle (N.m)
d_θ	External disturbance along with the aerodynamical disturbance acting on rotational pitch angle (N.m)

d_ψ	External disturbance along with the aerodynamical disturbance acting on rotational yaw angle (N.m)
$S_{(\cdot)}$	sin(·)
$C_{(\cdot)}$	cos(·)
T_d	The resultant torques vector due to the gyroscopic effects (N.m)
J_r	The moment of inertia for each rotor of the quadrotor (Kg.m^2)
ω_i	The rotary speed of each rotor (rpm)
f_i	The force generated by the ith motor (N)
b	The thrust factor
F_{prop}	The three-dimensional translational force vector exerted by the propellers
T_{prop}	The three-dimensional reaction moment vector exerted by the propellers
T	The total thrust (N)
h	Distance from the center of mass to the rotor (m)
c	Drag factor coefficient
p_r	Desired position trajectory vector
ψ_r	Desired yaw
$\widehat{d_j}$	The estimation of the disturbance
z_j	The state vector of the observer
X	The state vector
L_j	the observer gain matrix

CHAPTER 1

INTRODUCTION

1.1 Background

The study of the Vertical Take-Off and Landing (VTOL) Unmanned Aerial Vehicle (UAV) has been growing intensively by researchers in the recent decades. The UAVs have gradually been adopted by the public to be used in several areas. In fact, several industries (automotive, medical, manufacturing, space,..etc.), require the use of UAVs. They are also starting to spread in the field of delivery especially with online shopping. Several structures and configurations of UAVs have been developed to allow 3D movements. For example, there are blimps, fixed-wing planes, single rotor helicopters, bird-like prototypes, quadrotors, Each of them has advantages and drawbacks.

Drones have evolved throughout this century to be used today in many areas. A drone is a flying machine that does not use a human pilot. These aircraft were used for the first time in the military field during the First World War. The evolution of technology, particularly in electronics, has significantly improved the performance of the drone. The drones are now employed in the medical field (Pulver *et al.*, 2016), audiovisual (Nägeli *et al.*, 2017) and engineering (McCabe *et al.*, 2017). Recently, among the developed rotary-wing UAVs is a particular fixed-pitch 4-rotor UAV, namely the quadrotor. The quadrotor is one of the existing drones that feature two sets of identical propellers that are powered by DC brushless motors to provide the required thrust force and perform maneuvers when they are in flight. Quadrotor has the advantages of light-weight configuration and inherent instability, which improves its flight maneuverability over fixed-wing UAV. More importantly, quadrotors have the capabilities to perform VTOL and hovering in mid-flight.

The Vertical Take-Off and Landing requirement of this project excludes some of the previous configurations. However, the platforms which show this characteristic have a unique ability for vertical, stationary and low-speed flight. The quadrotor architecture has been chosen for this research for its low dimension, good maneuverability, simple mechanics and payload ca-

pability. As the main drawback, the high energy consumption can be mentioned. However, the trade-off results are very positive. These properties are some of the reasons for the expansion of quadrotor research. In addition, this structure can be attractive in several applications, in particular for surveillance, imaging, dangerous environments, indoor navigation, and mapping. The goals of this thesis are the quadrotor identification, system modeling, the control algorithm design evaluation, the simulator design, and the real platform development.

The parameters of the quadrotor are identified to allow the implementation of several types of controllers. The study of the kinematics and dynamics is helpful to understand the physics of the quadrotor and its behavior. Together with the modelling, the determination of the control algorithm structure is very important to achieve a better stabilization. The whole system is validated and tested using Matlab-Simulink. Quadrotors are often used outdoors using a GPS (Global Positioning System). Most research, however, is done in laboratories where GPS cannot be used, and therefore another position detection system must be found. The most widespread solutions use motion sensors. These sensors can be however expensive, limiting the development of quadrotor research. The Microsoft Kinect, initially intended for entertainment, has been the subject of several types of research on the detection of human movements. This research was extended to the detection of objects. Some of the aspects that make researchers choose the Kinect are its price, which is affordable, and the interest to use the camera that has become important. In 2013, Microsoft released an improved version of the Kinect called Kinect One. This camera offers better accuracy and a high definition camera. Using the Kinect One, it becomes easy to detect the position of the quadrotor and makes it possible to test quadrotors in laboratories with an affordable equipment price. However, the limitation of the Kinect is its accuracy where the systematic error is around 3 cm, and it increases on the periphery of the range image and for increasing object-camera distance (Khoshelham & Elberink, 2012). In order to speed up the delivery order and supplementing manpower shortages, online retail giant Amazon (Amazon, 2015) exploited drones through the use of quadrotors to fly autonomously and make deliveries to its customers. Quadrotors can also be handily mounted with high-resolution cameras photographers and filmmakers to capture high altitude pictures with-

out having charter a flight during production. The popularity of the quadrotor extends to the field research laboratories as well. Quadrotors with their small size, VTOL and hovering capabilities can easily operate in an indoor environment of research laboratories. In recent years, commercial quadrotors such as crazyFly, AR Parrot,etc., have become increasingly popular and relatively cheap for UAV research.

However, commercial quadrotors are typically associated with their own hard-coded software and pre-programmed plant model. Therefore, to perform complex flight controls or modify their mathematical model, it is required to modify the quadrotor's autopilot embedded code. In academic research, the objective of the control system design would require implementing the Simulink system model and controller design as embedded software into autopilot hardware via a specific Micro-controller (MCU) platform and language implementation.
Amongst the commercial quadrotors, PX4 open hardware project elaborated in (Meier *et al.*, 2015) has designed the Pixhawk autopilot system that can be programmed using the PX4 flight stack software (L.Meier, 2015). Pixhawk uses PX4 flight stack software that runs on Nuttx RTOS and is able to support multiple applications that can be programmed individually. More importantly, PX4 is able to support system models and control algorithms developed using Simulink without for the need to be proficient in high-level programming. This capability allows for a research project to rapidly progress from the modeling and simulation to implementation phase on the actual hardware.
The quadrotor is listed under Rotary-wing UAVs category because it has several rotors. It is composed of five main elements: the four motors, the chassis, the IMU, the electronic card and the radio receiver. Quadrotor has attracted great interests in both control and robotics communities due to its simpler mechanism in comparison to the traditional helicopters.

1.2 Quadrotor Dynamics and control

This section provides a vast summary of some of the methods that have been engaged in the literature for the Modelling and robust control of quadrotor UAVs. The literature review provides

the motivation for the research areas on which this work focuses. Some of the issues discussed in this chapter are considered in detail in the relevant chapters of the dissertation.

1.2.1 UAV Modeling

A quadrotor UAV is considered as a rigid body in 3-dimensional space. It has 6 degrees of freedom, three translational and three rotational degrees of freedom. The first three translational degrees describe the UAV position which a trivial task and the other three degrees describe the UAV orientation which is a somewhat complicated task and has implications on the derived model. Some methods exist for defining the orientation of a generally rigid body in space. The most widely used methods in aeronautical applications are quaternions and Euler angles, (Jia, 2013a; Michael *et al.*, 2010). Euler angles shall be the focus of this discussion. They comprise three angles: yaw, pitch, and roll, which are used to describe the orientation of a rigid body. One of the advantages of the Euler angles approach is that it is intuitive and it is easy to visualize rotations described in this way. On the other hand, its disadvantage is the "gimbal lock" phenomenon which is an exhibition of singularities that restricts the trajectory tracking of the quadrotor. Due to this phenomenon, some of the control algorithms that are designed for UAV modeled using this approach are not capable of executing aggressive aerobatic maneuvers. Unlike Euler angles, the quaternion method does not suffer from the singularity issues and thus provides a globally valid way of representing UAV orientation. Additionally, in comparison to Euler angles, the quaternion is computationally efficient as it uses a 4 element vector to describe rotations compared to a 3x3 matrix in the case of Euler angles. Despite these advantages, quaternion is less used in modeling quadrotors because they are conceptually challenging to understand and are not very intuitive. In this work, Euler angles are used for representing the quadrotor UAV's orientation. Due to the limitations of Euler angles, the controller is designed in such a way that gimbal lock is avoided. A more detailed discussion of Euler angles is contained in Chapter 2 of this dissertation.

In order to derive the equations of motion of the quadrotor, it is common to assume that the vehicle is a rigid body. Euler angles method is used to describe the motion of a rigid body in

3-D space governed by the Newton-Euler equations. Given the full dynamics of the quadrotor, when it hovers at a certain height in the presence of small perturbations, the angular rotations of the quadrotor are independent on its linear translations, while the translational motions of the quadrotor depend on its orientations (Bouabdallah, 2007). Therefore, the dynamic system of the quadrotor can be divided into two subsystems: The position subsystem and the attitude subsystem. The control algorithm can be designed using two types of system structures: The outer-loop control structure to control the position (Lee *et al.*, 2009), (Alexis *et al.*, 2016) and the inner-loop control structure to control the attitude (Choi & Ahn, 2015), (Cao & Lynch, 2016).

In practice, the quadrotors motion cannot always be described by their exact dynamics due to the existing uncertainties mainly caused by model uncertainties, external disturbances, and inaccuracy of measurements. Each part of these uncertainties is described below.

- Model uncertainties

  Model uncertainties are mainly caused by the following reasons: 1) The linearized quadrotor dynamics are widely used to simplify the controller design. 2) Some system parameters are inaccurate including the inertia and the weight of the quadrotor. 3) The motor dynamics are assumed to be that of a first-/second-order system, which may not exactly describe the thrust generated by the propellers. The problem of the model inaccuracy can be solved by identifying the system dynamics through experiments (Bouffard *et al.*, 2012; Iskandarani *et al.*, 2013; Alexis *et al.*, 2011), or by considering it as an external disturbance (Lee *et al.*, 2009; Choi & Ahn, 2015; Bouffard *et al.*, 2012).

- External disturbances

  During the flight, the quadrotor is usually affected by external disturbances, including severe wind, actuator failure, and additional payload. In (Alexis *et al.*, 2012b), the quadrotor is operated under a strong wind. In (Dai *et al.*, 2014), an unknown payload is connected to the quadrotor by using a flexible cable. The loss of the motor effectiveness is considered and handled in (Sharifi *et al.*, 2010).

- Measurement inaccuracy

  The inaccurate measurement is usually produced for the following reasons: 1) There exist

sensor noises so that the measured data are inaccurate. 2) The sensor loses its effectiveness leading to the unavailable states. To solve this problem, observers are usually adopted; as described in (Berbra *et al.*, 2008).

1.2.2 Control methods

As stated above, the quadrotor is always subject to different uncertainties. In most ideal cases, quadrotor dynamics are considered accurate because perturbations are omitted. Thus, in such cases, the control methods need not be able to handle the uncertainties. For complex working environments, the robustness of control methods applied to the quadrotor is required due to external disturbances. In this subsection, the recent works on the control methods for the quadrotor will be presented.

1.2.2.1 Nominal system control methods

In this case, uncertainties are omitted, and the nonlinear model is assumed to describe the motions of the quadrotor accurately. The nonlinear model of the quadrotor has been widely studied in the literature and many nonlinear methods have been adopted to control the quadrotor. In (Mistler *et al.*, 2001), the quadrotor dynamics were linearized by using the exact linearization technique, and then a feedback controller was used to solve the trajectory tracking problem of the quadrotor. In (Bouabdallah & Siegwart, 2005), two nonlinear control methods were proposed; the backstepping method and the sliding mode method, in which the inner-outer loop structure is employed with the consideration of full quadrotor dynamics. The linear motion subsystems are controlled by using the backstepping technique. The sliding mode technique and the backstepping technique are applied to the attitude subsystems of the quadrotor, respectively.

As mentioned in Section 1.2.1, the nonlinearities of the quadrotor dynamics make the controller design and implementation sophisticated. To describe the quadrotor motions, the linearized quadrotor dynamics will be sufficiently accurate when the quadrotor is practically hovering at a certain height. In the latter case, the linear control methods are adopted for the control of

the quadrotor. The classical proportional-integral-derivative (PID) controllers are proposed in (Bouabdallah *et al.*, 2004b; Erginer & Altug, 2007) to track a desired trajectory. The linear quadratic regulator (LQR) is another technique used to control the linearized dynamics due to its smooth implementation and satisfactory performance. In (Bouabdallah *et al.*, 2004b), the linearized quadrotor model was updated around each equilibrium point, and an adaptive LQR controller was developed to regulate the orientation of the quadrotor. In (Kim *et al.*, 2007), feedback linearization technique has been used to linearize the quadrotor input-output model, then the orientations of the quadrotor regulated using a proposed LQR controller. A model-free-control-based LQR controller is designed and implemented in (Younes *et al.*, 2014). The shortcoming of LQR occurs when the physical constraints of the quadrotor are enforced, e.g., the limited input voltage of motors and the restrained flying area. Therefore, the LQR becomes incapable to handle system constraints. To overcome these constraints, the model predictive control (MPC) can be a good alternative to solve this problem. The tracking control problem of quadrotor subjected to state and input constraints investigated using linear MPC technique by (Abdolhosseini *et al.*, 2013). A linear MPC algorithm combined with learning technique has been proposed by (Bouffard *et al.*, 2012).

1.2.2.2 Uncertain system control methods

If the external disturbances are small, the uncertainties are mainly caused by parameter perturbations, which can be solved by identifying the quadrotor dynamics. The translational position subsystem of the quadrotor is considered as a second-order linear system (Iskandarani *et al.*, 2013), whereas the trajectory tracking problem has been tackled using linear MPC according to the identified models. The step response can be used to obtain the unknown parameters. A similar methodology has been used by (Bouffard *et al.*, 2012) to identify the attitude subsystem. A piecewise affine representation of the linearized quadrotor dynamics has been rewritten around the equilibrium point, and updated around different operating points (Alexis *et al.*, 2010, 2012b).

To improve the control robustness of the quadrotor, enormous efforts have been made in recent

years in order to deal with external disturbances. Some adopted methods consider the sum of errors to deal with external disturbances. The integral-based method is one of these methods. An integral- prediction-based nonlinear H_∞ control algorithm has been proposed by (Raffo *et al.*, 2010) for tracking control of quadrotor. The drawback of these methods lies in the additional disturbances that might be caused by the integral-based actions if the nonlinear dynamics of the quadrotor are omitted. Therefore, when integral-based methods are used, it is required to consider the full dynamics of the quadrotor. Another integral backstepping control algorithm has been proposed by (Bouabdallah & Siegwart, 2007) to counteract external disturbances.
To overcome the problem of additional disturbances caused by the integral-based actions, the observer-based control algorithms have been adopted. Sliding mode and backstepping techniques are among the techniques that can be involved in observer-based algorithms. (Benallegue *et al.*, 2008) have proposed a high-order sliding mode observer for the estimation of state and the disturbance rejection. A sliding mode observer has been developed by (Besnard *et al.*, 2012) which depends on the boundaries of the disturbance. Other observers including feedback linearization technique combined with linear observer have been introduced by (Mokhtari *et al.*, 2006), a nonlinear symmetry- preserving observer has been given by (Mahony *et al.*, 2012). A modified observer-based will be adopted later in this dissertation.

1.3 Motivation

Many control methods have been proposed to deal satisfactorily with the control problems of UAVs. Most of them focused on the stabilization problem, which is the first step toward successful flights. Some also handled position tracking or velocity tracking in order to obtain certain maneuvers and thus full autonomous control. However, most of them relied on a complicated dynamic model that might be unavailable in certain situations and some control methods require intensive computation that might become a problem when applied on-board. Furthermore, only a few types of research have addressed disturbances in simulations or experiments, which should be a significant concern in real-world applications. Robust control of quadrotor have been proposed to deal with tasks that have model uncertainties and external

disturbances. Motivated by the aforementioned advantages of robust controller design against parameter uncertainties and external disturbances, this research will focus on the control system design of a quadrotor UAV for various maneuverings.

1.4 Objectives

This thesis intends to take advantage of mechanical simplicity and inexpensive construction of quadrotor to develop a robust control system for a quadrotor UAV in order to obtain a good trajectory tracking performance. The purpose of this thesis is to develop a robust nonlinear controller for the quadrotor UAV taking into account external disturbances and parameter uncertainties with the use of Kinect 2 for motion capture system. The validation and test have been done in an indoor laboratory on an area of four square meters. Only the quadrotor moves in the field of view of the Kinect. We will model at first the dynamics of the drone, then use this modeling to design a suitable controller for the position and attitude. For motion capture system, an algorithm based on the color detection is used to retrieve the position of the quadrotor from the Kinect. Due to the existing noise of the real systems, the current velocity of the quadrotor is estimated by Kalman filter. For the identification of parameters, three methods have been proposed to determine the parameters of the quadrotor. Ultimately, the validation of the designed controller by simulation and experimentation using the assembled quadrotor in our lab mounted with the well-known micro-controller, Pixhawk.
The main objectives of this thesis can be summarized as:

- Verify the capability, performance, and robustness against parameter uncertainties and external disturbances of the nonlinear dynamic model of a quadrotor UAV.
- Compare performance among robust control strategies for future development.
- Develop robust observer-based control approach on quadrotor trajectory tracking and obtain guidelines for further improvement.
- Implement experimentally the designed robust observer-based control in real-time applications.

Therefore, the practical objective of this thesis research is to implement the system model and controller design on pixhawk using px4.

1.5 Methodology Overview

The theoretical objectives mentioned previously are achieved in this thesis via simulations done in MATLAB by:

- Forming a nonlinear dynamic model of a quadrotor and derive the equations of motion from the mathematical model.
- Deriving the design of the robust position and attitude controllers for the quadrotor written in the Simulink software.
- Adding external disturbances into dynamic model of quadrotor in simulations to prove the robustness of the designed nonlinear controller.
- Implementing the designed controller for the quadrotor onto the PX4 autopilot. The commercial quadrotor S500 Glass Fiber Quadcopter Frame 480 mm - Integrated PCB assembled in our lab is selected to achieve this goal.
  Finally, the quadrotor's model and controller design is validated through a real autonomous flight test.

1.6 Thesis Contribution

As mentioned above, many efforts have been made to investigate the tracking problem of the quadrotor. Controlling the quadrotor is still a challenging problem in motion control. The detailed contributions of this dissertation are:

- Robust trajectory tracking: Based on the idea behind observer-based control, a robust control algorithm is proposed to provide good convergence and stability properties for the system with disturbances. The contribution lies in the extension of the controller to add robustness against external disturbances. The idea of extending an existing controller with an

observer to enhance disturbance rejection seems to be applicable to any trajectory-tracking controller (for underactuated systems).

- A backstepping-based sliding control algorithm is developed for quadrotor UAV with matched and unmatched uncertainties. To combine sliding mode control and backstepping control, the conventional Lyapunov based approach is used.
- The developed observer-based nonlinear control algorithm is realized on the real-time experimental platform.

1.7 Thesis Outline

The outline of this thesis is summarized as follows:

The first chapter provides an introduction to drones including the background of quadrotor technology and explains the motivation behind this thesis research; it also provides a general concept of quadrotor components and its parameter identification to implement an indoor flight.

The second chapter of this thesis describes the dynamic model of quadrotor and parameter identification.

The third chapter presents the first paper of this research work. It is called "Robust Observer-Based Dynamic Sliding Mode Controller for a Quadrotor UAV" and was published in IEEE Access Journal in October, 2018 (Nuradeen F. et al 2018)(online version).

The fourth chapter presents the second paper of this research work titled "Robust Sliding-Mode Tracking Control of a Quadrotor". It was submitted to Frankline institute Journal in December 2018.

The fifth chapter contains the third research paper titled "A Double-Sided Kernel Observer For Robust Trajectory Control Of Quadrotor". It was submitted to the International Journal of Control in March, 2018.

After, the conclusion and recommendation of the thesis based on the manuscripts described above are given. Finally, to present the additional content, Appendix I presents hardware set-up for experimental results of this research that were not encompassed in the third and fourth chapters.

CHAPTER 2

DYNAMIC MODEL OF QUADROTOR AND PARAMETER IDENTIFICATION

2.1 Theoretical concept of the quadrotor

The quadrotor is a flying machine that has four motors (M_1, M_2, M_3, M_4), to which are fixed four propellers (Fig. 2.1) mounted symmetrically on the crossbeam, and separated into two groups rotating in opposite directions. The rotary torque effectiveness is balanced because of the specific structure of the quadrotor due to the lightweight and powerful motors of quadrotor; it has higher accelerations than traditional helicopters. The quadrotor can conduct complicated tasks such as maneuvering, mapping, and navigation, etc. Since the quadrotor has 4 actuators with 6 degrees of freedom (DOF), it is an underactuated system. The system dynamics for the linear motions and the angular rotations of the quadrotor are coupled. As a first step in this research thesis, the modeling and simulation of the quadrotor must be performed to determine its flight characteristics and designing its robust position and attitude controllers.

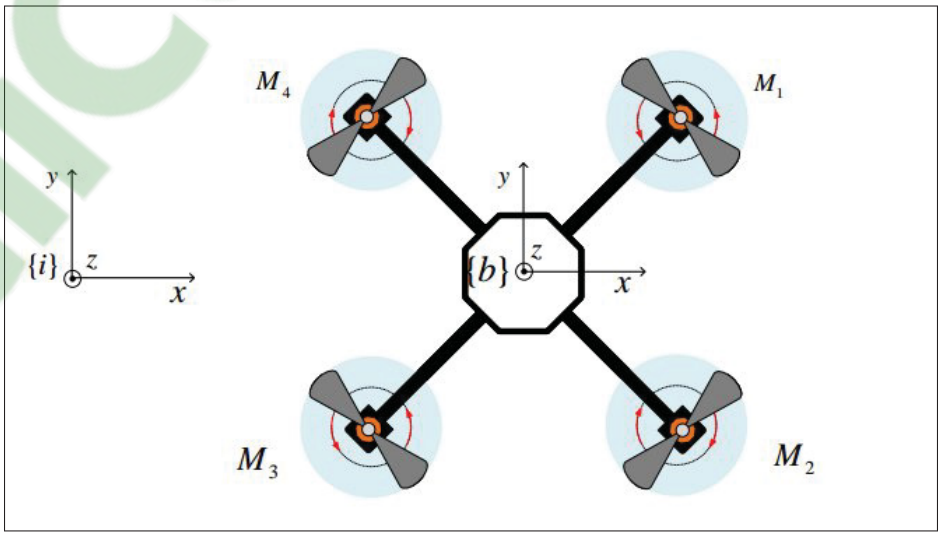

Figure 2.1 Principle representation of quadrotor

Along with the extraordinary simplicity of the mechanical design that eliminates the complexity of the main rotor control of the conventional helicopter, quadrotor UAVs become a different multirotor UAVs. They can be considered as Solid prototype UAVs. Due to their flight characteristics coupled with a low price of hardware, the number of applications has increased in both the military and commercial sectors. Furthermore, quadrotor is a popular platform widely used in military applications, where missions can be conducted using programmed quadrotors to fly into buildings to perform visual mapping and identify possible threats.

The motors M_1, M_3 rotate in counterclockwise direction with speed ω_1, ω_3 respectively. Likewise, the motors M_2, M_4 rotate in clockwise direction with speed ω_2, ω_4 respectively. The three orientation movements, roll, pitch, and yaw (ϕ, θ, ψ, see Fig. 2.2), can be achieved by the speed difference of the four engines. Increasing the engine speeds of motors M_1 and M_2 relative to the engine speeds of motors M_3 and M_4 will produce a positive rotation in the roll and vice versa for a negative rotation. An increase of the engine speeds of motors M_1 and M_4 relative to the engine speeds of motors M_2 and M_3 will produce a positive pitch rotation and vice versa for a negative rotation. The positive yaw rotation can be achieved by increasing the engine speeds of motors M_2 and M_4 relative to the engine speeds of motors M_1 and M_3. Likewise, increasing engine speeds of motors M_1 and M_3 relative to engine speeds M_2 and M_4 will produce a negative yaw rotation.

Two frames are used to describe the movement of the drone. The $\mathcal{I}$ frame represents the inertial frame. It is fixed in relation to the Earth. The $\mathcal{B}$ is the frame of the quadrotor's body. The z-axis of the $\mathcal{B}$ frame is always normal to the body of the quadrotor.

The orientation of the quadrotor can be described in different ways. We can indeed use quaternions (Jia, 2013b) or Euler angles. Unlike Euler angles, quaternions do not need to have auxiliary frames to be properly described. They can also avoid the so-called "gimbal lock" phenomenon, which removes two degrees of freedom from the quadrotor.

2.2 Transformation between the inertial frame and the body frame of the quadrotor

Three auxiliary frames have been used (r_i, r_ψ, r_θ) to describe the Euler angles. Namely, Yaw-Pitching-Roll convention will be used (see Fig. 2.2).

- The origin of the frame *ri* is at the center of quadrotor's body. Its orientation is the same as the orientation of the inertial frame $\mathcal{I}$;
- The frame r_ψ follows the rotation of angle ψ on the z-axis of the frame $\mathcal{I}$;
- The frame r_θ follows the rotation of angle θ on the y-axis of the frame r_ψ;
- The frame r_ϕ follows the rotation of angle ϕ on the x-axis of the frame r_θ and coincides with the reference frame $\mathcal{B}$.

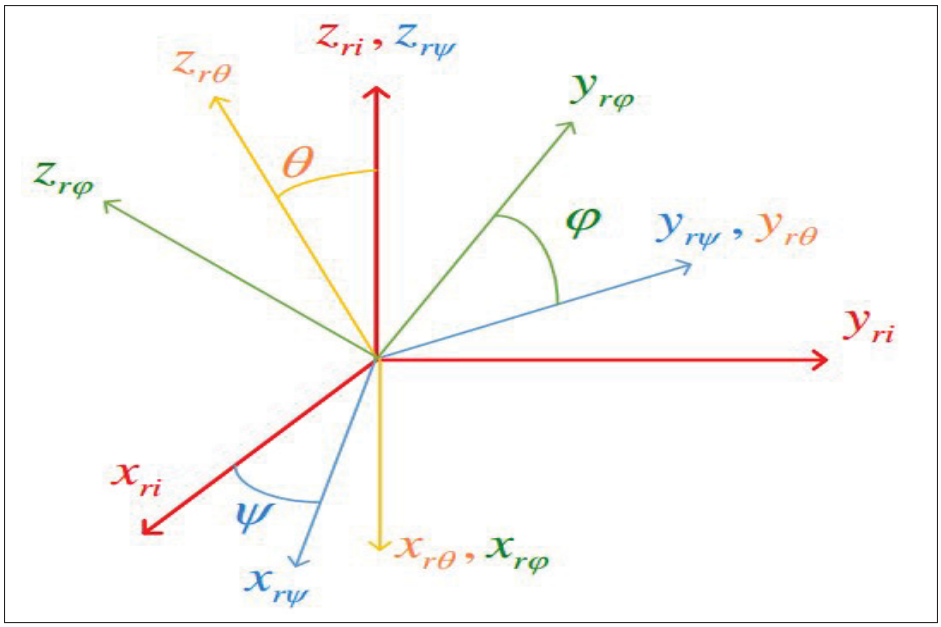

Figure 2.2 Auxiliary frames of the quadrotor

To describe the transformation between the frames, rotation matrices can be used. We define the rotation matrix ${}^x_y R$ to move from the frame $\{y\}$to the frame $\{x\}$. We then have the following rotation matrices:

$$ {}^{r_\theta}_{r_\psi}R = \begin{bmatrix} \cos(\theta) & 0 & -\sin(\theta) \\ 0 & 1 & 0 \\ \sin(\theta) & 0 & \cos(\theta) \end{bmatrix} \tag{2.1} $$

$$ {}^{\mathcal{B}}_{r_\theta}R = \begin{bmatrix} 1 & 0 & 0 \\ 0 & \cos(\phi) & \sin(\phi) \\ 0 & -\sin(\phi) & \cos(\phi) \end{bmatrix} \tag{2.2} $$

$$ {}^{r_\psi}_{r_i}R = \begin{bmatrix} \cos(\psi) & \sin(\psi) & 0 \\ -\sin(\psi) & \cos(\psi) & 0 \\ 0 & 0 & 1 \end{bmatrix} \tag{2.3} $$

From equations (2.3), (2.1) and (2.2), we can easily find the matrix of rotation ${}^{\mathcal{B}}_{r_i}R$ allowing transformation from the inertial frame r_i to the body frame $\mathcal{B}$:

$$ {}^{\mathcal{B}}_{r_i}R = {}^{\mathcal{B}}_{r_\theta}R \ {}^{r_\theta}_{r_\psi}R \ {}^{r_\psi}_{r_i}R \tag{2.4} $$

$$ {}^{\mathcal{B}}_{r_i}R = \begin{bmatrix} \cos(\theta)\cos(\psi) & \cos(\theta)\sin(\psi) & -\sin(\theta) \\ \sin(\phi)\sin(\theta)\cos(\psi)-\cos(\phi)\sin(\psi) & \sin(\phi)\sin(\theta)\sin(\psi)+\cos(\phi)\cos(\psi) & \sin(\phi)\cos(\theta) \\ \cos(\phi)\sin(\theta)\cos(\psi)+\sin(\phi)\sin(\psi) & \cos(\phi)\sin(\theta)\sin(\psi)-\sin(\phi)\cos(\psi) & \cos(\phi)\cos(\theta) \end{bmatrix} \tag{2.5} $$

In other words, a vector ${}^{\mathcal{I}}X$ expressed in the frame $\mathcal{I}$ can be expressed in the frame $\mathcal{B}$ by a vector ${}^{\mathcal{B}}X$ using the following expression:

$$ {}^{\mathcal{B}}X = {}^{\mathcal{B}}_{\mathcal{I}}R^{\mathcal{I}}X = {}^{\mathcal{B}}_{r_i}R^{\mathcal{I}}X \tag{2.6} $$

2.3 Angular Velocities

The quadrotor has a gyroscope to record its angular velocities relative to the reference $\mathcal{I}$ and expressed in the frame $\mathcal{B}$. These velocities can be defined by a vector ${}^{b}\Omega$. This vector is composed of three coordinates o, q, r describing the angular velocities respectively around the

x, y and z-axes in the body frame $\mathcal{B}$.

$$ {}^{b}\Omega = \begin{bmatrix} \rho \\ q \\ r \end{bmatrix} \tag{2.7} $$

To design a nonlinear controller for the orientation of the quadrotor, the angular velocities of Euler angles must be derived. Therefore, it is essential to find a relationship between the information obtained from the gyroscope and the orientation angles. It can be seen from (Craig (2005)) that the frames transformation of the angular velocity from one frame to another can be determined using the following relation:

$$ {}^{i+1}\Omega_{i+1} = {}^{i+1}_{i}R\Omega_i + \dot{\Theta}_{i+1}{}^{i+1}\hat{Z}_{i+1} \tag{2.8} $$

where ${}^{i+1}\Omega_{i+1}$ the angular velocity of the frame $\{i+1\}$ with respect to the inertial frame $\mathcal{I}$ expressed in the frame $\{i+1\}$, ${}^{i+1}_{i}R$ is the rotation transformation matrix passing from the old frame to the new one, $\dot{\Theta}_{i+1}$ the angular velocity of the rotation angle, and ${}^{i+1}\hat{Z}_{i+1}$ the unit vector associated with the axis of rotation in the new coordinate system. Hence, Eq.(2.8) leads to

$$ {}^{b}\Omega = \begin{bmatrix} \dot{\phi} \\ 0 \\ 0 \end{bmatrix} + {}^{b}_{r_\theta}R \begin{bmatrix} 0 \\ \dot{\theta} \\ 0 \end{bmatrix} + {}^{b}_{r_\theta}R^{r_\theta}_{r_\psi}R \begin{bmatrix} 0 \\ 0 \\ \dot{\psi} \end{bmatrix} \tag{2.9} $$

$$ {}^{b}\Omega = \begin{bmatrix} 1 & 0 & -\sin(\theta) \\ 0 & \cos(\phi) & \sin(\phi)\cos(\theta) \\ 0 & -\sin(\phi) & \cos(\phi)\cos(\theta) \end{bmatrix} \begin{bmatrix} \dot{\phi} \\ \dot{\theta} \\ \dot{\psi} \end{bmatrix} \tag{2.10} $$

$$ {}^{b}\Omega = J\dot{\eta} \tag{2.11} $$

where $\dot{\eta}$ is the angular velocity vector of Euler angles and J is the inverse of the Euler matrix.

2.4 Quadrotor Dynamics: Newton-Euler method

The forces exerted on the quadrotor can be expressed in the inertial frame $\mathcal{I}$ using Newton's laws:

$$m\ddot{p} = {}^{i}_{b}R\,{}^{b}F - mg\begin{bmatrix}0\\0\\1\end{bmatrix} - m\Delta \tag{2.12}$$

where m is the mass of the quadrotor in kg and $\ddot{p}$ is the acceleration vector of the quadrotor in $m.s^{-2}$ in the inertial frame $\mathcal{I}$ defined as:

$$\ddot{p} = \begin{bmatrix}\ddot{x}\\\ddot{y}\\\ddot{z}\end{bmatrix} \tag{2.13}$$

The vector ${}^{b}F$ represents the force (thrust) of lift expressed in the body frame $\mathcal{B}$ defined as:

$${}^{b}F = \begin{bmatrix}0\\0\\T\end{bmatrix} \tag{2.14}$$

where T is the total lift force along z-axis in N.

$m\Delta$ represents external forces acting on the quadrotor. These forces considered as external forces (wind gust, loads, etc.). Most likely, they are unknown. Δ is a vector in the form:

$$\Delta = \begin{bmatrix}\Delta_x\\\Delta_y\\\Delta_z\end{bmatrix} \tag{2.15}$$

It can be noted that the forces due to the resistance of the air were not included in the model. We assumed that the quadrotor will fly at low speed and the air resistance forces are too small

compared to other forces. The relations of Newton laws as well as the effects of Coriolis:

$$^{b}F_{t} = m(^{b}\dot{V} + ^{b}\Omega \times ^{b}V) \tag{2.16}$$

where $^{b}F_{t}$ the forces mentioned in the Eq. (2.12) expressed in the body frame $\mathcal{B}$ and ^{b}V is the linear velocity vector of the quadrotor relative to the inertial frame expressed in the frame $\mathcal{B}$ whose elements are:

$$^{b}V = \begin{bmatrix} u \\ v \\ w \end{bmatrix} \tag{2.17}$$

By modifying the equality in Eq. (2.16) and recall Eq. (2.7) and Eq. (2.17) yield:

$$\begin{bmatrix} \dot{u} \\ v \\ w \end{bmatrix} = \begin{bmatrix} rv - qw \\ pw - ru \\ qu - pv \end{bmatrix} + \frac{^{b}F_{t}}{m} \tag{2.18}$$

Using the equations of Euler's moment:

$$u_{\Theta} = I^{b}\dot{\Omega} + ^{b}\Omega \times (I^{b}\Omega) \tag{2.19}$$

with

$$u_{\Theta} = \begin{bmatrix} u_{\phi} \\ u_{\theta} \\ u_{\psi} \end{bmatrix} \tag{2.20}$$

And I is the moment of inertia of the quadrotor. The torques resulting from the rotation of the propellers due to a gyroscopic effect can be added to Eq. (2.19). These torques are expressed by the relation:

$$\tau_{g} = ^{b}\Omega \times \begin{bmatrix} 0 \\ 0 \\ J_{m}\Omega_{r} \end{bmatrix} \tag{2.21}$$

where J_m is the inertia of one of each rotor, Ω_r is the relative angular velocity of the propellers defined as:

$$\Omega_r = \omega_1 + \omega_3 - \omega_2 - \omega_4 \tag{2.22}$$

where ω_i (i=1,2,3,4) is the rotor speed.

For simplicity, it is assuming that the change in orientation of the quadrotor and its propellers is very small, therefore the influence of gyroscopic effects on the quadrotor can be considered small. Therefore they can be neglected. In addition, the quadrotor is considered to be a rigid body and symmetrical about the frame $\mathcal{B}$. The origin of the frame $\mathcal{B}$ is located in the center of the quadrotor. Therefore, the moment of inertia matrix is considered to be a diagonal matrix in the form:

$$I = \begin{bmatrix} I_{xx} & 0 & 0 \\ 0 & I_{yy} & 0 \\ 0 & 0 & I_{zz} \end{bmatrix} \tag{2.23}$$

The equations (2.11), (2.12), and (2.19) are involved to describe the dynamics of the quadrotor in the body frame state space as:

$$\dot{X} = f(X, U) \tag{2.24}$$

$$\begin{bmatrix} \ddot{x} \\ \dot{x} \\ \ddot{y} \\ \dot{y} \\ \ddot{z} \\ \dot{z} \\ \dot{\phi} \\ \dot{\theta} \\ \dot{\psi} \\ \dot{p} \\ \dot{q} \\ \dot{r} \end{bmatrix} = \begin{bmatrix} {}^{i}F_x/m - \Delta_x \\ \dot{x} \\ {}^{i}F_y/m - \Delta_y \\ \dot{y} \\ {}^{i}F_z/m - g - \Delta_z \\ \dot{z} \\ p + q\sin(\phi)\tan(\theta) + r\cos(\phi)\tan(\theta) \\ q\cos(\phi) - r\sin(\phi) \\ q\sin(\phi)\sec(\theta) + r\cos(\phi)\sec(\theta) \\ (I_{yy} - I_{zz})qr/I_{xx} + u_\phi/I_{xx} \\ (I_{zz} - I_{xx})pr/I_{yy} + u_\theta/I_{yy} \\ (I_{xx} - I_{yy})pq/I_{zz} + u_\psi/I_{zz} \end{bmatrix} \tag{2.25}$$

where

$$ {}^{i}F = \begin{bmatrix} {}^{i}F_x \\ {}^{i}F_y \\ {}^{i}F_z \end{bmatrix} = {}^{i}_{b}R\,{}^{b}F \tag{2.26} $$

$$ U = \begin{bmatrix} {}^{i}F \\ u_\Theta \end{bmatrix} \tag{2.27} $$

2.5 The Relationship between the forces and the torques of the quadrotor

The resulting forces and torques in the dynamics of the quadrotor will be determined to design the controller of the quadrotor. Therefore, the relationship between the forces and torques of the motors of the quadrotor were derived as: Let F_n and τ_n be the force and torque generated by the motor M_n. By taking l the length between the axis of a motor and the center of the quadrotor, we find the following relations in a cross configuration:

$$ \begin{aligned} u_\phi &= \frac{l(F_3 + F_4 - F_1 - F_2)}{\sqrt{2}} \\ u_\theta &= \frac{l(F_1 + F_4 - F_2 - F_3)}{\sqrt{2}} \\ u_\psi &= \tau_2 + \tau_4 - \tau_1 - \tau_3 \\ T &= F_1 + F_2 + F_3 + F_4 \end{aligned} \tag{2.28} $$

The velocity of the motors, their forces, and their torques are related by the following relations (Deters *et al.*, 2014)

$$ F_n = \rho D^4 C_T(\omega_n)\omega_n^2 \tag{2.29} $$

$$ \tau_n = \frac{\rho D^5}{2\pi} C_P(\omega_n)\omega_n^2 \tag{2.30} $$

where ρ is the density of the air and D is the diameter of a propeller. C_T and C_P are thrust and power factors respectively dependent on the motor speed. They also depend on the characteristics of the propellers. In practice, these factors are approximated by constants deduced experimentally. A measuring device will be used to measure the force and torque produced by each motor to derive these factors.

The equations (2.29) and (2.30) can be rearranged in one relation as

$$\tau_n = \frac{D}{2\pi}\frac{C_P}{C_T}F_n = f(\omega_n)F_n \tag{2.31}$$

Equation (2.28) can be re-written in the following form

$$\begin{bmatrix} T \\ u_\phi \\ u_\theta \\ u_\psi \end{bmatrix} = \begin{bmatrix} 1 & 1 & 1 & 1 \\ -\frac{l}{\sqrt{2}} & -\frac{l}{\sqrt{2}} & \frac{l}{\sqrt{2}} & \frac{l}{\sqrt{2}} \\ \frac{l}{\sqrt{2}} & -\frac{l}{\sqrt{2}} & -\frac{l}{\sqrt{2}} & \frac{l}{\sqrt{2}} \\ -f(\omega_n) & f(\omega_n) & -f(\omega_n) & f(\omega_n) \end{bmatrix} \begin{bmatrix} F_1 \\ F_2 \\ F_3 \\ F_4 \end{bmatrix} \tag{2.32}$$

and therefore

$$\begin{bmatrix} F_1 \\ F_2 \\ F_3 \\ F_4 \end{bmatrix} = \begin{bmatrix} \frac{1}{4} & -\frac{\sqrt{2}}{4l} & \frac{\sqrt{2}}{4l} & -\frac{1}{4f(\omega_n)} \\ \frac{1}{4} & -\frac{\sqrt{2}}{4l} & -\frac{\sqrt{2}}{4l} & \frac{1}{4f(\omega_n)} \\ \frac{1}{4} & \frac{\sqrt{2}}{4l} & -\frac{\sqrt{2}}{4l} & -\frac{1}{4f(\omega_n)} \\ \frac{1}{4} & \frac{\sqrt{2}}{4l} & \frac{\sqrt{2}}{4l} & \frac{1}{4f(\omega_n)} \end{bmatrix} \begin{bmatrix} T \\ u_\phi \\ u_\theta \\ u_\psi \end{bmatrix} \tag{2.33}$$

2.6 Parameters Identification

The previous section presented the dynamic model of the quadrotor in which the moments of inertia and the mass of the quadrotor must be known. The quadrotor can be weighed easily to find its mass. However, moments of inertia are more complicated to determine. A device measurement must also be used to determine the relationship between propeller speeds and exerted forces by each motor. In this section, the parameters of the S500 quadrotor will be determined. Three methods have been used to find these parameters; experimental method, the

software-based method, and theoretical method. The quadrotor platform used in this thesis is S500 (Fig.2.3). The equipments of the platform are

1. The electronic board which is the Pixhawk with PX4 firmware. It will be used to implement the controller and will control the motors;
2. The Odroid XU4 microcomputer equipped with a WI-FI dongle will establish the connection between the computer, where the trajectories and position information obtained by the Kinect will be sent, and the Pixhawk;
3. A 3300mAh Turnigy battery for an autonomy of about ten minutes;
4. A telecommunication DX6i Spectrum which has AR610 channel receiver;
5. Four 2216 KV920 brushless motors with speed controllers; Multistar SBEC4A Turnigy 20A.

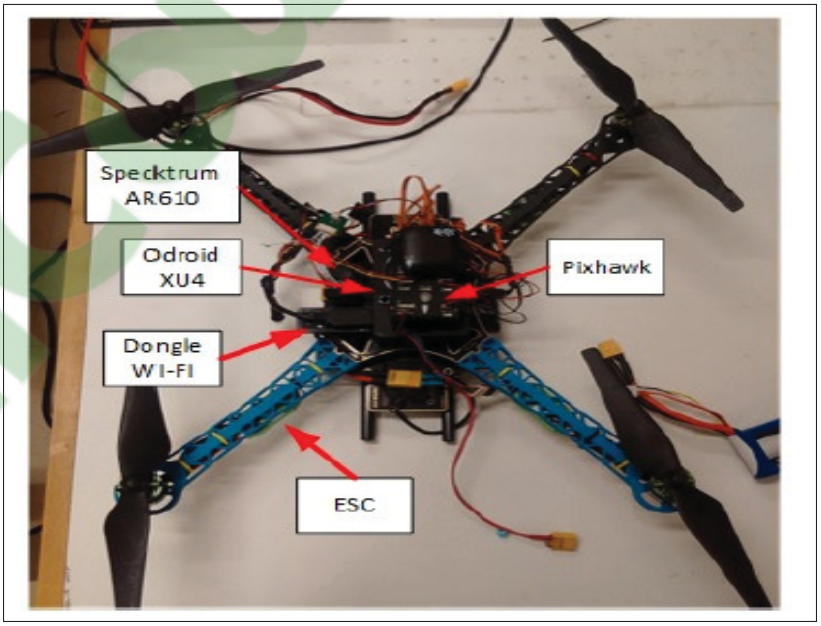

Figure 2.3 Auxiliary frames of the quadrotor

In this section, two methods, an experimental method and theoretical method, will be described respectively and the third one will be described in Chapter 3.

2.6.1 Experimental Method

The quadrotor tracking control design described above was tested by way of computer simulations as well as on a real quadrotor system in the Control System Laboratory of École de Technologie Supérieure (ETS), Montreal, Canada.
For the simulation and real flight trajectories to be comparable, the parameters of the real physical system had to be estimated first. To this end, we describe the estimation procedure in detail.
The mass of the quadrotor was simply obtained by weighing the device. However, obtaining the inertia moments was more complex. An RCbenchmark series 1580 dynamometer device (Robotics, 2018) was used to determine the relationship between the propellers' speeds and the forces exerted by the motors. A commercial quadrotor, S500 Glass Fiber Quadcopter Frame 480 mm - Integrated PCB was used as the experimental platform (see Figure 2.3). The measurements necessary for parameters identification were obtained by the use of an experimental method. In this method, the moment of inertia of quadrotor's mass is determined using the trifilar pendulum methodology. This methodology was introduced by (Piersol & Paez, 2009). To calculate the moment of inertia of quadrotor's mass , the quadrotor is held by the trifilar pendulum and rotated along the z-axis. The period of a single oscillation over three iterations will be measured. In the end, the average of measured values will be calculated. Ultimately, the period is used in a relation to calculate the moment of inertia of the quadrotor's mass. The trifilar pendulum setup comprises 3 wires fastened to the ceiling from one end and to a disc at an equal distance from each other (120°) from the other ends which make the disc hanging (see Figure 2.4).

Prior to determining the moment of inertia of the quadrotor using trifilar pendulum method, the disc's weight, its radius, and the wires' length have to be measured first. The results of the measurements for experimental setup are listed in Table 2.1. To figure out the moment of inertia of quadrotor's mass along any axis (i.e. I_{xx}, I_{yy} and I_{zz}), the trifilar pendulum's axis of oscillation was aligned with the axis of interest and the quadrotor was positioned on the disc. The moment of inertia of the quadrotor's mass (I) along the x-axis, y-axis and z-axis

measured via 3 configurations of displacement shown in Figure 2.5, Figure 2.6, and Figure 2.7 respectively. Thereafter, the trifilar pendulum will be rotated 10 rotations/oscillations for the period by applying a small angular displacement to the disc holding the quadrotor. For each period, the measurement was repeated three times. Three experimental rounds were tested and the average of the total period is considered in order to reduce random errors effects of experimental.

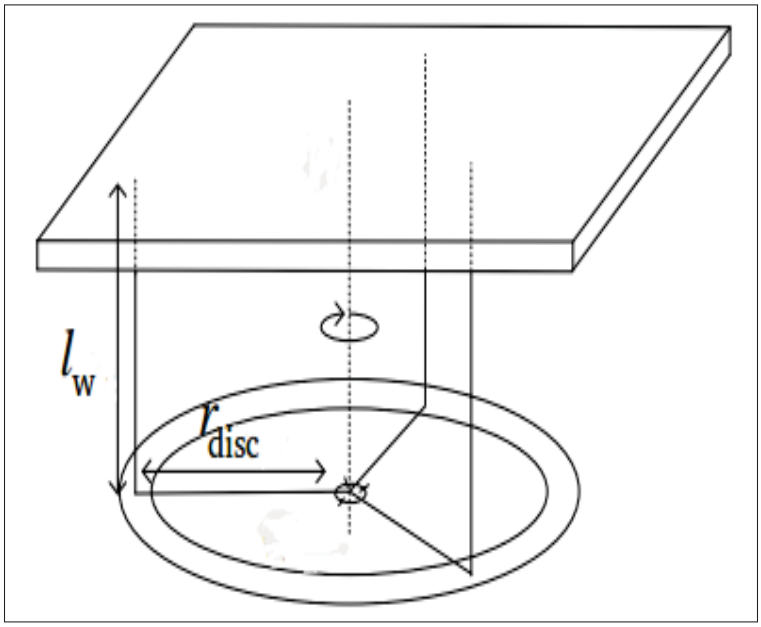

Figure 2.4 Wired Triangle Pendulum Method

Therefore, the moment of inertia along each base axis for the quadrotor's mass can be computed using equation 2.34:

$$I_{xx,yy,zz} = \frac{M r_{disc}^2 T_{x,y,z}}{4\pi^2 l_w} \tag{2.34}$$

where: $I_{xx,yy,zz}$ is moment of inertia of quadrotor in x,y, or z-axis, $T_{x,y,z}$ is period of one oscillation in s, M is the mass of the disc and quadrotor in kg, r_{disc} is radius of the disc in m, and l_w is length of wire suspending the disc from ceiling in m.

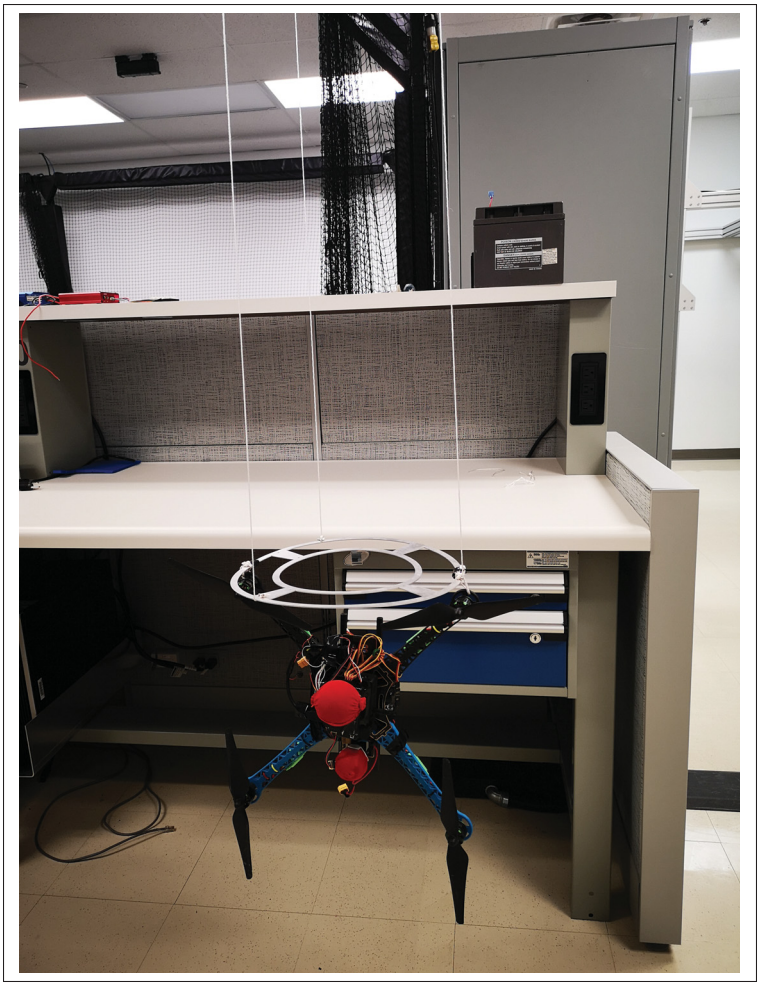

Figure 2.5 Measurement of Mass Moment of Inertia along x-axis

In order to calculate the moments of inertia I_{xx}, I_{yy} and I_{zz}, the quadrotor oscillated 10 oscillations using a timer in order to ensure the precision. The experiment was performed three times on the same axis to obtain the average of the measurements.

Table 2.1 Inertia moments of quadrotor S500 using experimental method.

	Reference	**Disc**	**Quadrotor**		
			$\mathbf{I}_{xx}$	$\mathbf{I}_{yy}$	$\mathbf{I}_{zz}$
Mass (kg)	0,2408	0,0908	1,354	1,354	1,354
Period,T (s)	2,708	2,68	1,856	1,85	2,452
Inertia (kg.m^2)	0,0052	negligible	0,0126	0,0125	0,0235

For simplicity, the contribution of the moment of inertia of the rotating disc to the equation (2.34) is omitted. The results from the measurement of the periods along each principal axis and the mass moment of inertia along each principal axis were calculated and summarized in Table 2.1.

Figure 2.6 Measurement of Mass Moment of Inertia along y-axis

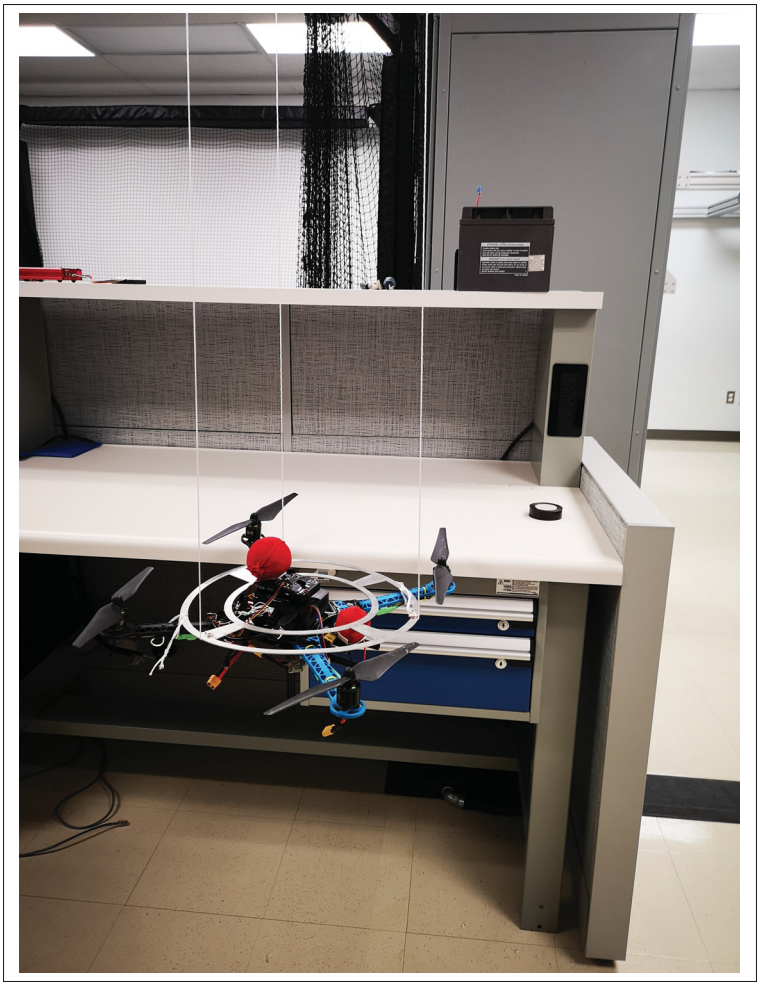

Figure 2.7 Measurement of Mass Moment of Inertia along z-axis.

2.6.2 Theoretical Method

In this method, the quadrotor is considered as a rigid body where the majority of the mass m_{base} distributed in a cylinder of radius r_{base} and height h_{base} located in the center of the drone. The arms are considered as rods of length l_{arm} and mass m_{arm}. The motors are modeled by cylinders of motor radius r_{motor}, motor height h_{motor} and motor mass m_{motor} (including the propellers mass). Figure 2.8 shows the model sketch. Therefore, from the theorem of parallel axes and the formulas of the moments of inertia of a rod and a cylinder, the relationships of the

moments of inertia can be written as

$$I_{zz} = 4(\frac{m_{motor}r_{motor}^2}{2} + m_{motor}l^2) + \frac{m_{base}r_{base}^2}{2} + \frac{m_{arm}l_{arm}^2}{3} + m_{arm}l_{arm}^2 \tag{2.35}$$

$$I_{xx} = I_{yy} = 4(\frac{m_{motor}(3r_{motor}^2 + h_{motor}^2)}{12} + \frac{m_{motor}l^2}{2}) + \frac{m_{base}(3r_{base}^2 + h_{base}^2}{12} + \frac{m_{arm}l_{arm}^2}{6} + \frac{m_{arm}l_{arm}^2}{2} \tag{2.36}$$

Table 2.2 shows the measurements of the S500 quadrotor.

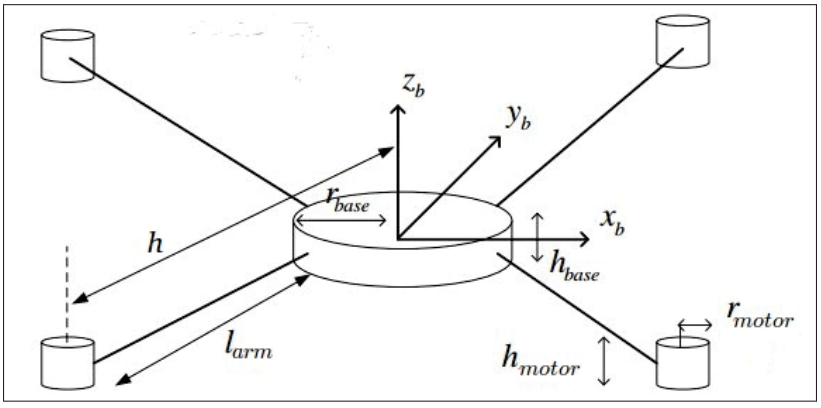

Figure 2.8 The theoretical model of a quadrotor.

Table 2.2 The Theoretical measurements of S500 quadrotor model.

m_{base} **(kg)**	0.7662	r_{base} **(m)**	0.08
m_{arm} **(kg)**	0.0704	l_{arm}**(m)**	0.0.18
m_{motor} **(kg)**	0.0766	h_{base} **(m)**	0.085
r_{motor} **(m)**	0.014	h **(m)**	0.225

therefore, the quadrotor's moments of inertia are calculated as
$I_{xx} = I_{yy} = 0.0122$ kg.m^2 and $I_{zz} = 0.0232$ kg.m^2

In practice, the outputs from the designed controller system are the calculated torques corresponding to the measured orientation of the quadrotor and the lift forces. These were then used to determine the forces exerted by each motor. However, the forces control the motors indirectly via PWM signals that regulate the motor speeds. Consequently, in order to find a motors' thrust coefficients, the relationships between the lifting force and the PWM signal for each motor had to be known. The aforementioned device (RCbenchmark Series 1580 Dynamometer, see Fig.2.9) was again used for this purpose. This measuring device generates more than four PWM output signals and can measure the speed of a motor.

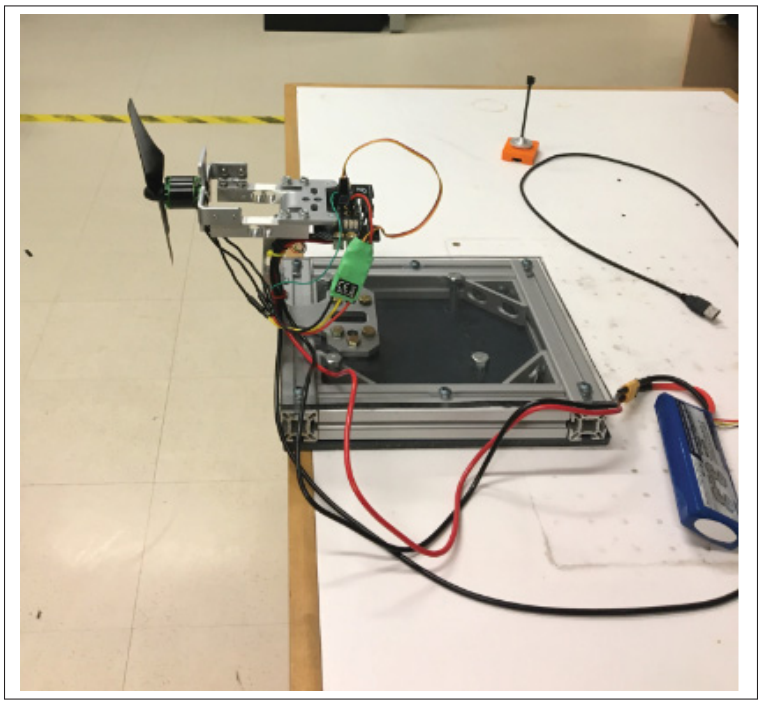

Figure 2.9 Motor force measuring device.

The force exerted by the motor can then be expressed as a function of the pulse width in μs. The obtained measurements are shown in Fig. 2.10. The obtained PWM has a duty cycle 50%.

Using the curve in Fig.2.10, the relation between the PWM signals and the lift force was approximated by a polynomial in the lift force f_i

$$\text{Pulse Width}(\mu s) = -13.0701 f_i^2 + 227.6249 f_i + 1036.3 \tag{2.37}$$

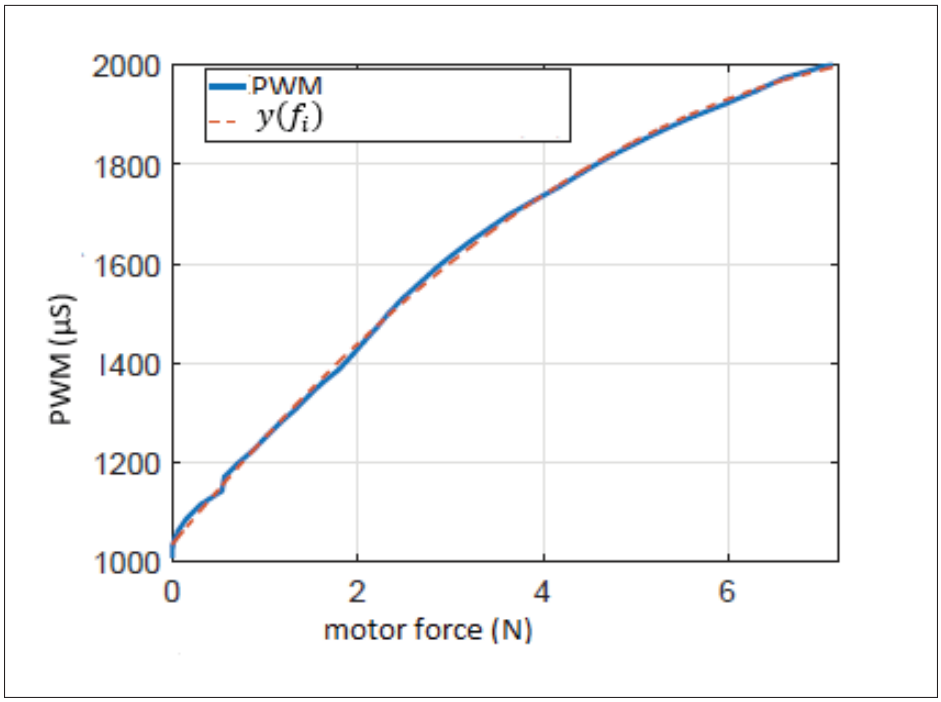

Figure 2.10 Motor force relative to PWM.

The relation between the torque and the force generated by each motor can be determined using the same device. The motor force and torque measurements are depicted in Fig.2.11.

The curve in Fig.2.11 was used to determine that the force was approximately a linear function of the torque τ_i.

$$f_i = 72.17\tau_i - 0.047 \tag{2.38}$$

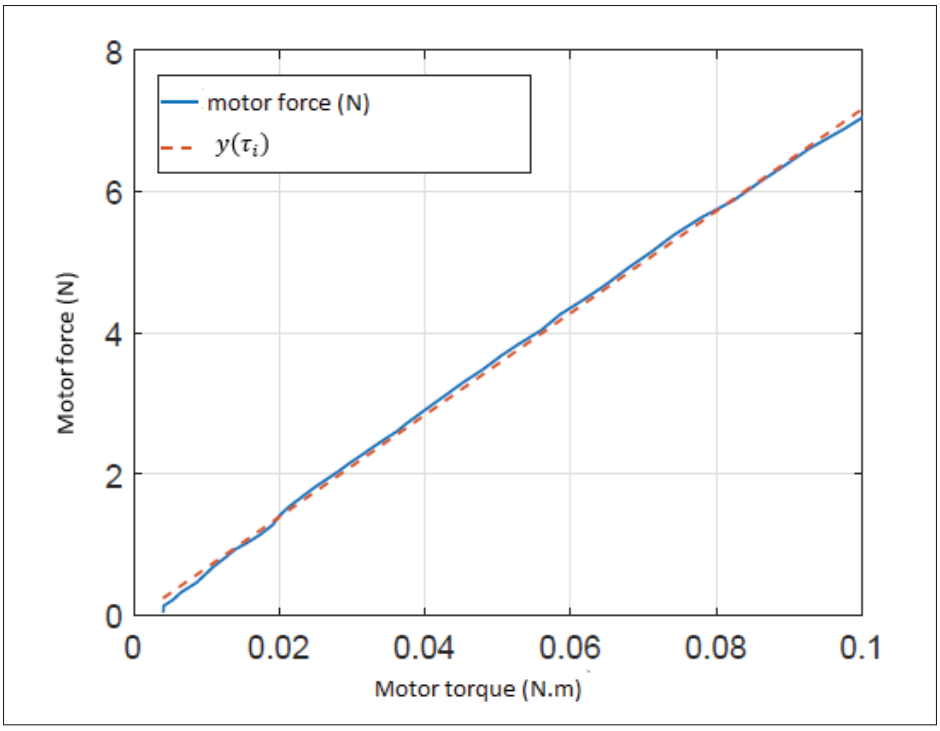

Figure 2.11 The relation between force and torque of the motor.

As will be seen later, the three methods used for determining the parameters of the quadrotor have given approximately the same values of moment of inertia.

CHAPTER 3

ROBUST OBSERVER-BASED DYNAMIC SLIDING MODE CONTROLLER FOR A QUADROTOR UAV

Nuradeen Fethalla [1], Maarouf Saad [2], Hannah Michalska [3], Jawhar Ghommam [4]

[1,2] Département de Génie électrique, École de Technologie Supérieure,
1100 Notre-Dame Ouest, Montréal, Québec, Canada H3C 1K3
[3] Electrical and computer engineering department McGill university, McConnell Eng. Bldg
3480 Rue University, Room 514, Montréal, QC H3A 0E9
[4]Department of Electrical and computer Engineering, Sultan Quaboos University,
P.O. Box 33, Al-Khod Muscat, 123 Sultanate of Oman

Accepted in IEEEAccess Journal August 12, 2018, date of publication August 20, 2018

3.1 Abstract

In this paper, a novel robust backstepping-based approach combined with sliding mode control is proposed for trajectory tracking of a quadrotor UAV subject to external disturbances and parameter uncertainties associated with the presence of aerodynamic forces and possible wind force. To enhance robustness, a nonlinear disturbance observer (NDO) is employed alongside the controller. A sliding surface is introduced which shares intermediate control goals with a conventional backstepping scheme. The closed-loop system comprising the sliding mode and backstepping controllers is finally combined with the NDO to track the desired position and attitude trajectories. Good tracking is achieved in the closed loop if the controller and observer gains are selected correctly. The system performance exhibits much better robustness than the existing backstepping control methods which are not equipped with nonlinear disturbance estimators. The simulation results are confirmed in terms of real laboratory experiments. Prior to the implementation of the control method the real system has been identified and calibrated.

keywords: Quadrotor UAV; Backstepping control; Sliding mode control; Nonlinear disturbance observer (NDO)

3.2 Introduction

Quadrotor UAVs have many important applications. It is hence not surprising that the control problem for quadrotors and other rotorcraft has recently received much attention. A vast literature exists on this topic in which both linear and nonlinear control schemes have been proposed for the attitude and position control of the quadrotor. Proportional-Integral-Derivative (PID) attitude control and Linear Quadratic Regulator (LQR) attitude control were studied by (Rinaldi *et al.*, 2014). Robustness properties of the conventional SMC are, however, limited to matched disturbances and uncertainties; see (Wadoo, 2013) for the definition of matched disturbances. Unfortunately, there are many important nonlinear system applications in which the matched disturbance property is invalid (Yu & Kaynak, 2009). The quadrotor UAV systems in (Bouabdallah & Siegwart, 2005; Besnard *et al.*, 2012) are leading examples of nonlinear systems that belong to this category. For this reason alone, most of the existing sliding mode controllers for quadrotor UAVs predominantly attenuate the uncertainties that are matched to the control input, i.e. uncertainties that can be instantaneously and directly compensated for by the system input; (Runcharoon & Srichatrapimuk, 2013; Ton & MacKunis, 2012).

The disturbance matching condition is restrictive and is not met in many practical UAV systems. In the case of a quadrotor UAV system, the uncertainties comprise perturbations of model parameters which are combined with the unknown aerodynamic forces and also possibly the external effects due to atmospheric winds. The latter act on the UAV system via different channels (enter different state equations of the system). Many of such disturbances affect state equations with no direct dependence on the control input; (Guo *et al.*, 2016). In this situation, the application of a conventional sliding mode control (SMC) leads to severe limitations in achieving asymptotic set point control; the closed loop system can only be stabilized to a neighborhood of a stationary point whose size is commensurate with the magnitude of the unmatched disturbance; (Yu & Kaynak, 2009). Many authors have hence made efforts of designing sliding surfaces with improved robustness properties; (Silva *et al.*, 2009; Polyakov & Poznyak, 2011). Classical backstepping and conventional sliding mode control designs presented in (Bouabdallah & Siegwart, 2005) and (Arellano-Muro *et al.*, 2013) offer

a robust backstepping control approach based on the concept of the Direction Cosine Matrix (DCM). The DCM method shown satisfactory robustness properties. A backstepping controller for complete stabilization of a quadrotor UAV was proposed in (Madani & Benallegue, 2006). However, the majority of existing control designs are still not sufficiently robust with respect to unknown dynamics or system perturbations which adversely affects flight control performance. In many quadrotor models available in the literature, it is assumed that the hover speed of the quadrotor during its mission is low, so the influence of the external aerodynamic forces and the torque disturbances can simply be neglected. However, in realistic flight conditions, the non-linear aerodynamic forces, the wind gusts, and torque disturbances can be powerful enough to destabilize the vehicle or knock it off the desired trajectory, (Xu *et al.*, 2015). Although the backstepping control approach, (Das *et al.*, 2009), is a powerful technique to deal with system nonlinearities, it applies to models of somewhat restricted structure. Moreover, the complexity of conventional backstepping control increases disproportionally with the dimension of the system to be steered. In this regard, robust versions of the backstepping are much better but need full state measurement (Sanca *et al.*, 2014). To simplify the implementation of robust backstepping, direct on-line differentiation of the measured output was proposed to recover the full state of the system, (Madani & Benallegue, 2007). A command filter was introduced in (Farrell *et al.*, 2009) to obviate the need to compute analytic derivatives and to create virtual signals to increase the degree of robustness of the backstepping controller.

Further attempts to increase the robustness of the quadrotor control schemes include a high order sliding mode controller developed by (Luque-Vega *et al.*, 2012) that is able to reject the influence of some of the uncertainties in the system. The robust controller of (Luque-Vega *et al.*, 2012) also attenuates chattering of the traditional sliding mode control approach. The NDO-SMC control is already widely used in robotics where it can achieve diverse objectives (Chen *et al.*, 2000). The SMC methods attempt to compensate for the unmatched uncertainties by utilizing bounds on the disturbances along with bounds on their first derivatives. The most restrictive requirement encountered in many nonlinear disturbance observers is that the time derivatives of the disturbances need to approach zero.

In this context, the consensus is that the best control approaches employ nonlinear distur-

bance observers in conjunction with nonlinear control. In our previous work, (Fethalla *et al.*, 2017a,b), the proposed UAV control approach employed an NDO in conjunction with two separated control blocks: using backstepping and SMC. In contrast, the approach presented here fully combines the actions performed by the NDO, backstepping, and SMC. Additionally, numerical simulation results are confirmed here by experimental results performed under laboratory conditions.

Recognizing the importance of robustness in practical control of UAVs, a novel observer-based feedback control design is proposed that comprises three concepts: (1) nonlinear sliding mode control, (2) robust backstepping as assisted by (3) a nonlinear disturbance observer. The systematic design procedure carefully combines the interacting translational and rotational control subsystems by the use of intermediate fictitious control variables. The task of the backstepping controller is predominantly to stabilize the translational subsystem while the SMC simultaneously steers the rotational subsystem. The NDO provides the estimates of all the disturbances both matched and unmatched insuring very good robustness of the combined feedback controls.

The novel contributions are hence summarized as follows:

- (i) The proposed approach yields the first combined SMC and backstepping controller that employs an NDO to compensate for all disturbances and model-system error. Although the same type of NDO was also used by (Yang *et al.*, 2013), its convergence properties were not assessed fully.
- (ii) In comparison with the work of (Luque-Vega *et al.*, 2012), our results show that the robustness of the closed-loop control system is increased by the presence of the NDO;
- (iii) Laboratory experiments were preceded by proper identification and calibration of the real system;
- (iv) The laboratory experiments reproduced the simulation results with high fidelity despite using a fan to simulate wind gusts.

The paper is organized as follows: the dynamic model of a quadrotor UAV is presented in section 3.3. The problem formulation and control objectives are stated in section 3.4. The design of the NDO and the associated backstepping-sliding mode controller for position and attitude subsystems are described in sections 3.5.1, 3.5.2, and 3.5.3 respectively. Section 3.6 delivers the stability analysis of the closed loop system. Model parameter identification of the real quadrotor is described in section 3.7. The performance of the proposed approach is assessed in simulations in section 3.8 as well as in the experimental laboratory setting in section 3.9 followed by the conclusions in section 3.10.

3.3 Dynamic modeling of a quadrotor

The dynamic model of the considered quadrotor UAV, shown in Fig.3.1, is originally described in (Hoffmann *et al.*, 2007b) and again employed in (Zheng *et al.*, 2014) and (Alexis *et al.*, 2012a).

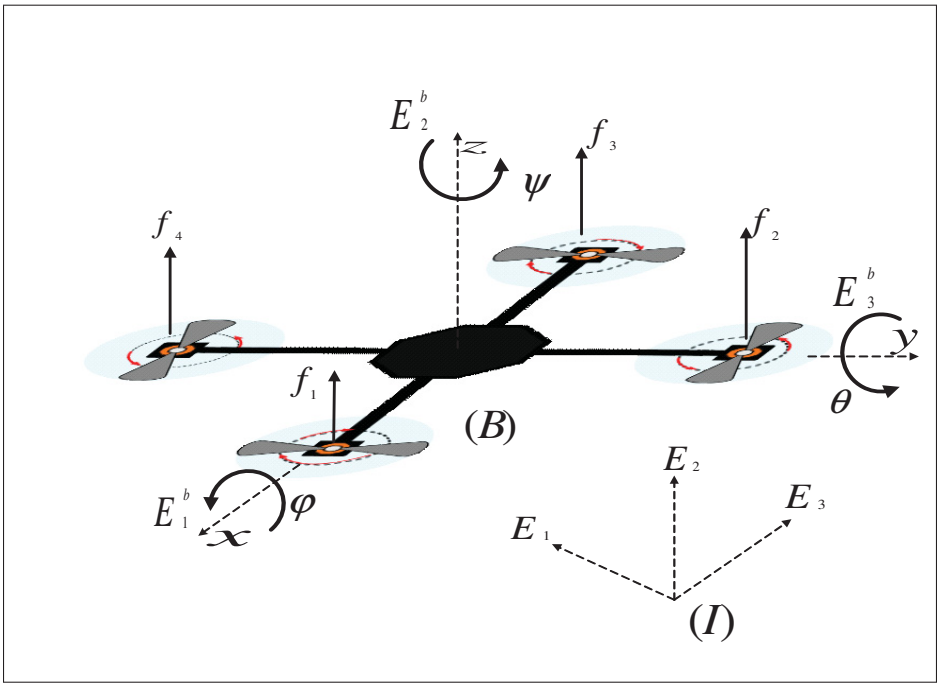

Figure 3.1 Quadrotor Airframe And Reference Frames configuration

Let us consider two main reference frames: the earth fixed frame ($\mathcal{I}$) associated with the unit vector basis (E_1, E_2, E_3) and body fixed frame ($\mathcal{B}$) associated with the unit vector basis (E_1^b, E_2^b, E_3^b) fixed at the center of mass of the quadrotor, as shown in Fig.3.1. The position of the center of the quadrotor's mass is denoted by the vector $p = [x, y, z]^T$. This position vector is expressed with respect to an inertial frame ($\mathcal{I}$) . The attitude is denoted by $\Theta = [\phi, \theta, \psi]$. These three angles are the Euler angles yaw ($-\pi < \psi < \pi$), pitch ($-\frac{\pi}{2} < \theta < \frac{\pi}{2}$), and roll ($-\frac{\pi}{2} < \phi < \frac{\pi}{2}$) that define the orientation vector of the quadrotor with respect to the inertial frame ($\mathcal{I}$). Define the angular velocity and acceleration of roll, pitch, and yaw as $\Omega = [\Omega_p, \Omega_q, \Omega_r]^T$ with respect to the body-fixed frame ($\mathcal{B}$), and $\ddot{\Theta} = [\ddot{\phi}, \ddot{\theta}, \ddot{\psi}]$ with respect to the inertia reference frame $\mathcal{I}$. The linear velocities and accelerations of the translational system are given respectively as $\dot{p} = [\dot{x}, \dot{y}, \dot{z}]$, and $\ddot{p} = [\ddot{x}, \ddot{y}, \ddot{z}]$. The transformation between the body-fixed reference frame $\mathcal{B}$ and the inertial reference frame $\mathcal{I}$ in the space orientation of the quadrotor is given by the rotation matrix R and Euler matrix $M(\Theta)$. These matrices are given by

$$R(\Theta) = \begin{bmatrix} C_\theta C_\psi & S_\phi S_\theta C_\psi - C_\phi S_\psi & C_\phi S_\theta C_\psi + S_\phi S_\psi \\ C_\theta S_\psi & S_\phi S_\theta S_\psi + C_\phi C_\psi & C_\phi S_\theta S_\psi - S_\phi c_\psi \\ -S_\theta & S_\phi C_\theta & C_\phi C_\theta \end{bmatrix}$$

$$M(\Theta) = \begin{bmatrix} 1 & 0 & -S_\theta \\ 0 & C_\phi & S_\phi C_\theta \\ 0 & -S_\phi & C_\phi S_\theta \end{bmatrix}$$

where the relationship between $\dot{\Theta}$ and Ω can be described as

$$\Omega = M(\Theta)\dot{\Theta} \tag{3.1}$$

An extended formulation of these transformations can be found in (Alexis *et al.*, 2012a).

The quadrotor dynamic equations will be written in the form of two subsystems corresponding to translational motion (referring to the position of the center of mass of the UAV) and angular

motion (referring to the attitude of the UAV). These equations can be stated in the reference frame ($\mathcal{I}$) as

$$\ddot{p} = \frac{1}{m}R(\Theta)F_{prop} - G + d_p(t) \tag{3.2a}$$

$$\begin{aligned}\ddot{\Theta} &= (IM(\Theta))^{-1}[T_{prop} - IN(\Theta,\dot{\Theta}) \\ &\quad - \Omega \times I\Omega - T_g] + d_\Theta(t) \\ &= \Phi(\Theta,\dot{\Theta}) + \Psi(\Theta)T_{prop} + d_\Theta(t)\end{aligned} \tag{3.2b}$$

where $N(\Theta,\dot{\Theta})$ is given by

$$N(\Theta,\dot{\Theta}) = \begin{bmatrix} -C_\theta\dot{\theta}\dot{\psi} \\ -S_\phi\dot{\phi}\dot{\theta} + C_\phi\dot{\phi}\dot{\psi} - S_\phi S_\theta\dot{\theta}\dot{\psi} \\ -C_\phi\dot{\phi}\dot{\theta} - S_\phi C_\theta\dot{\phi}\dot{\psi} - C_\phi S_\theta \end{bmatrix}$$

and T_g is the resultant torques due to the gyroscopic effects given as

$$T_d = \sum_{i=1}^{4} \Omega \times J_r[0,0,(-1)^{i+1}\omega_i]^T \tag{3.3}$$

where J_r is the moment of inertia of each rotor and $\omega_i, i = 1,2,3,4$ is the rotary speed of each motor.

$\Psi(\Theta)$ and $\Phi(\Theta,\dot{\Theta})$ are defined as

$$\Psi(\Theta) = (IM(\Theta))^{-1}$$

$$\Phi(\Theta,\dot{\Theta}) = -(IM(\Theta))^{-1}[IN(\Theta,\dot{\Theta}) - \Omega \times I\Omega - T_g]$$

The matrix $I = diag(I_x, I_y, I_z)$ is the inertia matrix of the quadrotor; $G = [0,0,-g]^T m/s^2$ is the gravitational force acting in the z-direction; m denotes the mass of the quadrotor. The terms $d_p = [d_x \;\; d_y \;\; d_z]^T$ and $d_\Theta = [d_\phi \;\; d_\theta \;\; d_\psi]^T$ model smooth and bounded external disturbances along with the aerodynamical disturbances. The functions $S_{(\cdot)}$ and $C_{(\cdot)}$ denote $\sin(\cdot)$ and $\cos(\cdot)$, respectively. Assuming that each motor produces thrust and drag that are proportional to the

square of the motor speed, the force generated by the ith motor is given by $f_i = b\omega_i^2 (i = 1,2,3,4)$ where b is the thrust factor. F_{prop} and T_{prop} are: the three-dimensional translational force vector and the three-dimensional reaction moment vector exerted by the propellers, respectively, as given by

$$F_{prop} = \begin{bmatrix} 0 \\ 0 \\ T \end{bmatrix} \quad T_{prop} = \begin{bmatrix} h(f_4 - f_2) \\ h(f_3 - f_1) \\ c\sum_{i=1}^{4}(-1)^i f_i \end{bmatrix}$$

where $T = \sum_{i=1}^{4} f_i$ is the total thrust, h is distance from the center of mass to the rotor, and c is the drag factor coefficient. It is easy to verify that equations (3.2a)-(3.2b) can actually be written as

$$\begin{aligned}
\ddot{\phi} &= r_1\dot{\theta}\dot{\psi} - r_2\dot{\theta}\omega + q_1 U_2 + d_\phi \\
\ddot{\theta} &= r_3\dot{\phi}\dot{\psi} + r_4\dot{\phi}\omega + q_2 U_3 + d_\theta \\
\ddot{\psi} &= r_5\dot{\theta}\dot{\phi} + q_3 U_4 + d_\psi \\
\ddot{x} &= (C_\phi S_\theta C_\psi + S_\phi S_\psi)\frac{1}{m}U_1 + d_x \\
\ddot{y} &= (C_\phi S_\theta S_\psi - S_\phi C_\psi)\frac{1}{m}U_1 + d_y \\
\ddot{z} &= -g + (C_\phi C_\theta)\frac{1}{m}U_1 + d_z
\end{aligned} \tag{3.4}$$

where $[U_1, U_2, U_3, U_4]^T = [T, T_{prop}]^T$ is the input vector, and

$$\begin{aligned}
r_1 &= \frac{I_y - I_z}{I_x}, r_2 = -\frac{J_r}{I_x}, r_3 = \frac{I_z - I_x}{I_y}, r_4 = \frac{J_r}{I_y}, \\
r_5 &= \frac{I_x - I_y}{I_z}, q_1 = \frac{h}{I_x}, q_2 = \frac{h}{I_y}, q_3 = \frac{1}{I_z}
\end{aligned}$$

are inertia related constants and $\omega = \omega_4 + \omega_3 - \omega_2 - \omega_1$.

The state vector X can thus be defined as

$$X = [p \;\; \dot{p} \;\; \Theta \;\; \dot{\Theta}]^T \in \mathbb{R}^{12}$$

3.4 Problem formulation

The dynamic model (3.4) of the quadrotor UAV is now conveniently viewed as a system composed of two subsystems, the position subsystem and the rotational subsystem. It can be noted that the disturbances d_Θ and d_z are matched while the rest of the disturbances d_x and d_y are unmatched. The idea is to apply a nonlinear disturbance observer to each subsystem separately, to remove the influence of matched and unmatched disturbances from the state variables in those subsystems. Considering (3.4), the objective is to design a controller that makes the state variables $[p, \psi]$ attain and follow their desired reference counterparts $[p_d, \psi_d]$. We make the following assumptions about the matched as well as the unmatched disturbances in the model (3.4).

Assumption 3.1. *For each subsystem, it is assumed that, the matched and unmatched perturbations are differentiable with bounded derivatives, i.e.*

$$\|\dot{d}_p(t)\| \leqslant D_p, \;\; \|\dot{d}_\Theta(t)\| \leqslant D_\Theta \quad t > 0 \tag{3.5}$$

for some positive constants D_p, D_Θ.

3.5 The combined NDO-based backstepping and sliding mode control

3.5.1 Nonlinear disturbance Observer design

In terms of flight performance, uncertainties cannot be neglected. To improve the robustness and stability of the overall control system, an NDO is employed to estimate the matched and unmatched external disturbances in the quadrotor system. The NDO is introduced by (Yang

et al., 2013) and can be employed in a similar form for both subsystems (position and orientation):

$$\begin{aligned} \dot{z}_p &= -L_p z_p - L_p[L_p\dot{p} + G + \frac{1}{m}U_p] \\ \hat{d}_p &= z_p + L_p\dot{p} \end{aligned} \tag{3.6a}$$

$$\begin{aligned} \dot{z}_\Theta &= -L_\Theta z_\Theta - L_\Theta[L_\Theta\dot{\Theta} + \Phi(\Theta,\dot{\Theta}) - U_\Theta] \\ \hat{d}_\Theta &= z_\Theta + L_\Theta\dot{\Theta} \end{aligned} \tag{3.6b}$$

where $U_p = R(\Theta)E_3U_1$, $U_\Theta = \Psi(\Theta)[U_2 \;\; U_3 \;\; U_4]^T$, and $\widehat{d_j}$ $(j = p,\Theta)$ is the estimation of the disturbance. The variable z_j is the state vector of the observer, and $L_j = L_j I_{3\times3}, L_j > 0$, $j = p,\Theta$, are the observer gain matrices to be tuned.

The following lemma will be helpful in proving convergence of the observer as well as the control scheme.

Lemma 3.1. *Let $\dot{x} = f(x)$ be a smooth multivariate dynamic system with $x \in \mathbb{R}^n$, with $f(0) = 0$. Let V be a Lyapunov function that is strictly positive definite, continuously differentiable, radially unbounded, with $V(0) = 0$. Let $C \subset \mathbb{R}^n$ be any given connected, compact set of initial conditions for the dynamic system. Finally, assume that along any trajectory of the system, $x : \mathbb{R}^+ \to \mathbb{R}^n$, starting in C , the following differential inequality*

$$\begin{aligned} &\frac{d}{dt}\{V(x(t))\} < -\alpha V(x(t)) + \beta \quad \textit{for all } t \geq 0 \\ &\qquad\qquad \textit{with } x(0) \in C \end{aligned} \tag{3.7}$$

is satisfied with $\beta > 0$ as a fixed positive constant and α as a positive parameter that can be tuned. Under these conditions: for every $\epsilon > 0$ there exist an $\alpha^* > 0$ such that for all $\alpha \geq \alpha^*$ all trajectories of the dynamic system starting in C are bounded by the selected value of ϵ, i.e.

$$\|x(t)\|^2 \leq \epsilon, \quad \textit{for all } t > T^*, \tag{3.8}$$

for a sufficiently large time T^*.

Proof. It is first convenient to define a function which is the composition of the Lyapunov function $V : \mathbb{R}^n \to \mathbb{R}^+$ with any given and admissible system trajectory function $x : \mathbb{R} \to \mathbb{R}^n$, $x(0) \in C$, i.e. a function $W : \mathbb{R}^+ \to \mathbb{R}^+$ such that

$$W(t) := V(x(t)); \quad t \geq 0 \tag{3.9}$$

It is obvious that inequality (3.7) re-writes as

$$\frac{d}{dt}W(t) < -\alpha W(t) + \beta \quad \text{for all } t \geq 0 \tag{3.10}$$

$$\text{for any } W(0) := W_0 = V(x_0) \in V(C) \tag{3.11}$$

where the image set $V(C)$ is compact as V is continuous hence maps compact sets into compact sets; in fact it is a compact interval in $\mathbb{R}^+$. The dependence of W on x is suppressed here as, by assumption, inequality (3.10) holds for any trajectory x of system $\dot{x} = f(x)$ passing through any initial condition $x(0) := x_0 \in C$.

Consider an equation for a different function $W^* : \mathbb{R}^+ \to \mathbb{R}^+$, given by

$$\frac{d}{dt}W^*(t) = -\alpha W^*(t) + \beta; \tag{3.12}$$

with the same parameters $\alpha > 0, \beta > 0$, but with an initial condition $W^*(0) := W_0^* \notin V(C)$ that satisfies

$$W_0^* > w \quad \text{for all } w \in V(C) \tag{3.13}$$

Its unique solution valid for all $t \geq 0$ is

$$W^*(t) = W_0^* \exp\{-\alpha t\} + \frac{\beta}{\alpha}[1 - \exp\{-\alpha t\}] \tag{3.14}$$
$$\text{so } W^*(t) \to \frac{\beta}{\alpha} \text{ as } t \to \infty$$

We shall now show that any system trajectory, $x(t); t \geq 0$, that implicitly satisfies (3.10) - (3.11) is majorized by the trajectory $W^*(t); t \geq 0$, i.e.

$$W(t) < W^*(t); \quad t \geq 0 \tag{3.15}$$

Clearly, $W(0) < W^*(0)$ by virtue of (3.13). The demonstration of (3.15) will be conducted by contradiction. To this end, if (3.15) were false then there would exist an initial condition $W_0 \in V(C)$ and a corresponding trajectory $W(t); t \geq 0$, for which the following set is nonempty:

$$Z := \{t \geq 0 \mid W(t) \geq W^*(t)\} \tag{3.16}$$

Defining $t_1 := \inf Z$, it is clear from (3.13) that $t_1 > 0$. Also

$$W(t_1) = W^*(t_1) \tag{3.17}$$
$$\text{and } W(t) < W^*(t) \text{ for } t \in [0, t_1) \tag{3.18}$$

By virtue of the above (3.17) - (3.18), for sufficiently small, but negative $h < 0$ the following inequality holds

$$\frac{W(t_1 + h) - W(t_1)}{h} > \frac{W^*(t_1 + h) - W^*(t_1)}{h} \tag{3.19}$$

which, in the limit as $h \to 0$, implies that

$$\frac{d}{dt} W(t_1) \geq \frac{d}{dt} W^*(t_1) \tag{3.20}$$

The assumption of the Lemma expressed in the form of (3.10) together with above (3.20) and (3.12) and (3.17) imply that there exists a trajectory $x(t); t \geq 0$, with $x(0) \in C$ such that, at some instant $t_1 > 0$:

$$\begin{aligned} -\alpha W(t_1) + \beta &> \frac{d}{dt} W(t_1) \\ &\geq \frac{d}{dt} W^*(t_1) = -\alpha W^*(t_1) + \beta \\ \text{so} \quad W(t_1) &< W^*(t_1) \quad \text{since} \quad -\alpha < 0. \end{aligned} \tag{3.21}$$

Inequality (3.21) is a clear contradiction of (3.17). So, Z is empty for all trajectories $W(t); t \geq 0$, starting in $V(C)$. Hence (3.15) holds true, as claimed. It then follows that all system trajectories that satisfy (3.10) - (3.11) are majorized by (3.14); i.e.

$$W(t) < W_0^* \exp\{-\alpha t\} + \frac{\beta}{\alpha}[1 - \exp\{-\alpha t\}]; \quad t \geq 0 \tag{3.22}$$

Now, it is easy to see that for any W_0^* satisfying (3.13)

$$W_0^* \exp\{-\alpha t\} \leq \frac{\beta}{\alpha} \quad \text{for all } t \geq T(\alpha) \tag{3.23}$$

$$\text{with} \quad T(\alpha) := \frac{1}{\alpha} \ln\left(\frac{W_0^* \alpha}{\beta}\right) \tag{3.24}$$

Combining (3.22) with (3.23) gives

$$W(t) < 2\frac{\beta}{\alpha} \quad \text{for all } t \geq T(\alpha) \tag{3.25}$$

along any trajectory of the system $x(t); t \geq 0$, with $x(0) \in C$, because the second term of (3.22) never exceeds β/α. Selecting an arbitrary positive constant $R > 0$, while setting

$$\alpha^* := \frac{2\beta}{R}; \quad T^* := T(\alpha^*) \tag{3.26}$$

gives

$$W(t) < 2\frac{\beta}{\alpha} \leq R \quad \text{for all } t \geq T^*, \alpha \geq \alpha^* \tag{3.27}$$

Denote a sublevel set of V by

$$V_R := \{x \mid V(x) \leq R\} \tag{3.28}$$

Since the Lyapunov function V is continuous and radially unbounded its sublevel sets are bounded so there exists a ball $B(0; \sqrt(\epsilon))$ which contains the sublevel set V_R. By virtue of (3.27) it follows that if $\alpha \geq \alpha^*$ then for all times $t \geq T^*$ any system trajectory starting from the set C satisfies $W(t) = V(x(t)) \leq R$. This is to say that all such $x(t); t \geq T^*$, remain in the sublevel set V_R , i.e. $x(t) \in V_R \subset B(0; \sqrt(\epsilon))$, which immediately implies that

$$\|x(t)\|^2 \leq \epsilon \quad \text{for all } t \geq T^* \tag{3.29}$$

as required.

Remark 3.1. *It should be noted that the assumption of Lemma 3.1 is stated as a sharp differential inequality entirely for the simplicity of the proof and thus can be replaced by a non-sharp inequality as long as* $\beta > 0$ *because any slightly tighter non-sharp inequality such as*

$$\frac{d}{dt}\{V(x(t))\} \leq -\alpha V(x(t)) + \frac{1}{2}\beta \quad \textit{for all } t \geq 0 \tag{3.30}$$

clearly implies a sharp inequality (3.7)*.*

We are now ready to show that the above observers can secure estimates with arbitrarily small observer errors.

Let estimation error vectors $e_{d_p}(t)$ and $e_{d_\Theta}(t)$ for the position and attitude subsystems be defined

as

$$e_{d_p} := \hat{d}_p - d_p \quad e_{d_\Theta} := \hat{d}_\Theta - d_\Theta \tag{3.31}$$

Proposition 3.1. *Under Assumption 3.1, there exist observer gains* $L_j > 0,\ j = p, \Theta$, *that are high enough to achieve any prescribed asymptotic estimation precision of the observers* (3.6a) - (3.6b)*; i.e. for every* $\epsilon > 0$ *there exist* $L_j^*, j = p, \Theta$, *such that for all* $L_j \geq L_j^*$ *the observer errors satisfy*

$$\|e_{d_j}(t)\|^2 \leq \epsilon, \quad \textit{for all } t > T^*, \quad j = p, \Theta \tag{3.32}$$

for a sufficiently large time T^*.

Proof. Note that the position and orientation equations in (3.4) can be compactly written as:

$$\begin{aligned} \ddot{p} &= G + \frac{U_p}{m} + d_p \\ \ddot{\Theta} &= \Phi(\Theta, \dot{\Theta}) + U_\Theta \end{aligned} \tag{3.33}$$

It follows from (3.6) that

$$\begin{aligned} \dot{\hat{d}}_p &= \dot{z}_p + L_p \ddot{p} = -L_p z_p - L_p[L_p \dot{p} + G + \frac{U_p}{m}] \\ &+ L_p[G + \frac{U_p}{m} + d_p] = -L_p[z_p + L_p \dot{p}] + L_p d_p \\ &= -L_p e_{d_p} \end{aligned} \tag{3.34}$$

It is shown similarly that

$$\dot{\hat{d}}_\Theta = -L_\Theta e_{d_\Theta} \tag{3.35}$$

The derivatives of the estimation errors e_{d_j}, $j = p, \Theta$ are hence given by

$$\dot{e}_{d_j} = -L_j e_{d_j} - \dot{d}_j \tag{3.36}$$

Since

$$-2e_{d_j}^T \dot{d}_j \leq \|e_{d_j}\|^2 + \|\dot{d}_j\|^2 \tag{3.37}$$

because

$$\begin{aligned} 0 \leq \|e_{d_j} + \dot{d}_j\|^2 &= e_{d_j}^T e_2 + 2e_{d_j}^T \dot{d}_j + \dot{d}_j{}^T \dot{d}_j \\ &= \|e_{d_j}\|^2 + \|\dot{d}_j\|^2 + 2e_{d_j}^T \dot{d}_j \end{aligned}$$

then, defining

$$V_{1j} := e_{d_j}^T e_{d_j} \quad j = p, \Theta \tag{3.38}$$

and multiplying (3.36) by $2e_{d_j}^T$ while using (3.37) together with Assumption 1 yields

$$\begin{aligned} \dot{V}_{1j} &= 2e_{d_j}^T \dot{e}_{d_j} = -2e_{d_j}^T L_j e_{d_j} - 2e_{d_j}^T \dot{d}_j \\ &\leq -2e_{d_j}^T L_j e_{d_j} + \|e_{d_j}\|^2 + \|\dot{d}_j\|^2 \\ &\leq -(2L_j + 1)e_{d_j}^T e_{d_j} + D_j^2 \\ &< -(2L_j + 1)V_{1j} + 2D_j^2 \quad j = p, \Theta \end{aligned} \tag{3.39}$$

Inequality (3.39) is clearly of the form (3.7). Hence invoking Lemma 3.1 basically ends the proof. For complete lucidity, note that in this case, it suffices to pick

$$L_j^* = \frac{2D_j^2}{\epsilon} - \frac{1}{2} \tag{3.40}$$

to secure that

$$V_{1j}(t) = \|e_{d_j}\|^2 \leq \epsilon \quad \text{for all } t \geq T^*;\ j = p, \Theta \tag{3.41}$$

as required.

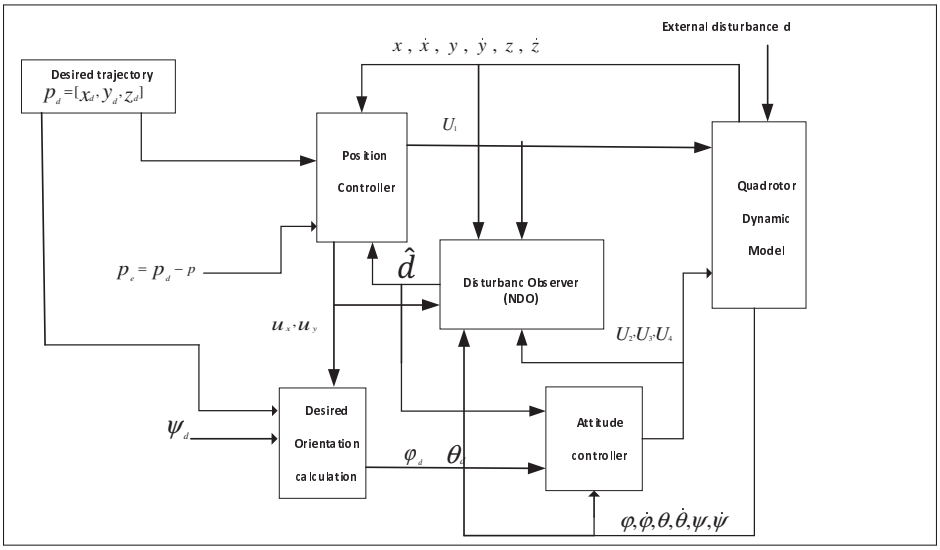

Figure 3.2 Block diagram of the proposed NDO based backstepping control design

3.5.2 Backstepping sliding mode control

This section first describes a regular backstepping technique for the position trajectory tracking control. The backstepping approach is known for its flexibility and capacity to control composite cascade nonlinear systems. With reference to the problem at hand, it will be shown to guarantee stability of translational and rotational subsystems. On the other hand, sliding mode control (SMC) can secure a degree of stability robustness of the closed loop. Such robustness is necessary to compensate for possible model errors and external disturbances so that high-tracking performance can be achieved. A combination of backstepping, SMC, and disturbance estimation performed by the NDO will be proved highly successful in achieving the control goals.

3.5.2.1 Position subsystem controller design

To design the backstepping control for the position subsystem let $p_1 = p$ and $p_2 = \dot{p}$, then the position subsystem in (3.2a) can be rewritten in a combined form as

$$\begin{aligned} \dot{p}_1 &= p_2 \\ \dot{p}_2 &= -ge_z + \frac{1}{m}U_p + d_p(t) \end{aligned} \tag{3.42}$$

Defining the position tracking error

$$e_1 = p_r - p_1 \tag{3.43}$$

its time derivative is

$$\dot{e}_1 = \dot{p}_{1r} - \dot{p}_1 = \dot{p}_{1r} - p_2 \tag{3.44}$$

Defining the velocity tracking error as

$$e_2 = p_{2r} - p_2,\ p_2 = p_{2r} - e_2 \tag{3.45}$$

and substituting (3.45) into (3.44) gives

$$\dot{e}_1 = \dot{p}_{1r} - p_{2r} + e_2 \tag{3.46}$$

where p_{2r} is the virtual control law designed to stabilize $\dot{e}_2$

$$p_{2r} = \dot{p}_{1r} + K_1 e_1,\ \ \dot{p}_{2r} = \ddot{p}_{1r} + K_1 \dot{e}_1 \tag{3.47}$$

where K_1 is positive definite matrix.

Substituting (3.47) into (3.46) yields

$$\dot{e}_1 = e_2 - K_1 e_1 \tag{3.48}$$

Choosing a Lyapunov function candidate as

$$V_{2p} = \frac{1}{2} e_1^T e_1 + \frac{1}{2} e_2^T e_2 \tag{3.49}$$

and taking time derivative of V_{2p}, while using (3.45) we obtain

$$\begin{aligned} \dot{V}_{2p} &= e_1^T \dot{e}_1 + e_2^T \dot{e}_2 \\ &= e_1^T (-K_1 e_1 + e_2) + e_2^T (\ddot{p}_{1r} + K_1 \dot{e}_1 - \dot{p}_2) \end{aligned} \tag{3.50}$$

Substituting (3.42) into (3.50), yields

$$\begin{aligned} \dot{V}_{2p} &= -e_1^T k_1 e_1 + e_1^T e_2 + e_2^T (\ddot{p}_{1r} + K_1 \dot{e}_1 - \\ &\quad (-g e_3 + \frac{1}{m} U_p + d_p)) \\ \dot{V}_{2p} &= -e_1^T K_1 e_1 + e_2^T (e_1 + \ddot{p}_{1r} + K_1 \dot{e}_1 - \\ &\quad g e_3 - \frac{1}{m} U_p - d_p) \end{aligned} \tag{3.51}$$

Now we defined the control input vector as

$$U_p = m[e_1 + K_1 \dot{e}_1 - g e_3 + \ddot{p}_{1r} - K_2 e_2 - \hat{d}_p] \tag{3.52}$$

where K_2 is another positive definite matrix. The position control law (3.52) has three components so $U_P = [U_x, U_y, U_z]^T$. Putting $U_p = R(\Theta) U_1 E_3$, the total thrust U_1 is obtained as

$$U_1 = \frac{U_z}{C_\phi C_\theta} \tag{3.53}$$

and

$$U_x = \frac{C_\phi s_\theta C_\psi + S_\phi S_\psi}{C_\phi C_\theta} U_1 \tag{3.54}$$

$$U_y = \frac{C_\phi S_\theta S_\psi - S_\phi C_\psi}{C_\phi C_\theta} U_1 \tag{3.55}$$

In order to implement the compensation for the disturbance d_p which is needed for improved robustness of the control, the nonlinear disturbance observer (3.6a) is employed.

Theorem 3.1. *Consider the position error subsystem* (3.43) *and* (3.45) *in closed loop with the disturbance observer designed as in* (3.6a)-(3.6b) *and the control law designed according to* (3.52) - (3.53)*. There exist positive definite gain matrices K_1, K_2 and L_p, such that the closed loop position error satisfies*

$$\|e_1\|^2 + \|e_2\|^2 \leq \epsilon \ \ for\ all\ t \geq T^* \tag{3.56}$$

with any pre-selected precision $\epsilon > 0$ where T^* is sufficiently large.

Proof. Define a Lyapunov function candidate as

$$V_1 = V_{1p} + V_{2p} \tag{3.57}$$

Considering (3.52), (3.53), and taking the time derivative of (3.57), yields

$$
\begin{aligned}
\dot{V}_1 &= \dot{V}_{1p} + \dot{V}_{2p} \\
&= -e_1^T K_1 e_1 + e_1^T e_2 + e_2^T (\ddot{p}_{1r} + K_1 \dot{e}_1 - \\
&ge_3 + \frac{1}{m} U_p + d_p)) \\
&- e_{d_p}^T (L_p - \frac{1}{2} I_{3x3}) e_{d_p} + \frac{1}{2} D_p^2 \\
&= -e_1^T K_1 e_1 - e_2^T K_2 e_2 + e_2^T (d_p - \hat{d}_p) \\
&- e_{d_p}^T (L_p - \frac{1}{2} I_{3x3}) e_{d_p} + \frac{1}{2} D_p^2 \\
&= -e_1^T K_1 e_1 - e_2^T K_2 e_2 - e_2^T e_{d_p} \\
&- e_{d_p}^T (L_p - \frac{1}{2} I_{3x3}) e_{d_p} + \frac{1}{2} D_p^2 \\
&\leq -e_1^T K_1 e_1 - e_2^T K_2 e_2 - \frac{1}{2} e_2^T e_2 - \frac{1}{2} e_{d_p}^T e_{d_p} \\
&- e_{d_p}^T L_p e_{d_p} + \frac{1}{2} e_{d_p}^T e_{d_p} + \frac{1}{2} D_p^2 \\
&\leq -e_1^T K_1 e_1 - e_2^T (K_2 + \frac{1}{2} I_{3x3}) e_2 \\
&- e_{d_p}^T (L_p - I_{3x3}) e_{d_p} + \frac{1}{2} D_p^2 \\
&< -\delta_1 V_1 + D_p^2
\end{aligned}
\tag{3.58}
$$

where

$$
\delta_1 = min\{2\lambda_{min}(K_1), 2(\lambda_{min}(K_2) - \frac{1}{2}), 2(\lambda_{min}(L_p - 1))\}
$$

It can be seen that the above gains can be chosen to deliver any magnitude of the tunable coefficient $\delta_1 > 0$. The result of Theorem 3.1 then follows directly from Lemma 3.1.

3.5.3 Attitude controller design

In this section, the NDO, the backstepping, and sliding control strategies are again combined to deliver attitude control.

In practice, whenever the position of the center of mass of the quadrotor deviates from its

reference x_r or y_r the angular position ϕ_r and θ_r also deviate.

The position and attitude control systems are coupled in such a way as to permit the desired attitude angles ϕ_r and θ_r to be tracked by the attitude controller (see Fig. 3.2) implicitly using the position control law (3.52). We define the reference trajectory for the attitude subsystem as $\Theta_r = [\phi_r, \theta_r, \psi_r]^T$ where it is assumed that ψ_r is measured directly by a sensor.

The reference angles ϕ_r and θ_r are obtained as follows. Multiplying (3.54) by $C_\phi C_\theta C_\psi$ and (3.55) by $C_\phi C_\theta S_\psi$, respectively, yields

$$U_x C_{\phi_r} C_{\theta_r} C_{\psi_r} = (C_{\phi_r} S_{\theta_r} C_{\psi_r}^2 + S_{\phi_r} S_{\psi_r} C_{\psi_r}) U_1 \tag{3.59}$$

$$U_y C_{\phi_r} C_{\theta_r} S_{\psi_r} = (C_{\phi_r} S_{\theta_r} S_{\psi_r}^2 - S_{\phi_r} S_{\psi_r} C_{\psi_r}) U_1 \tag{3.60}$$

Adding (3.59) to (3.60) and dividing by $C_{\phi_r} C_{\theta_r}$ yields,

$$U_x C_{\psi_r} + U_y S_{\psi_r} = \tan(\theta_r) U_1 \tag{3.61}$$

Then θ_r and ϕ_r are obtained from (3.59) - (3.60), and (3.61) as

$$\theta_r = \arctan \frac{(U_x C_{\psi_r} + U_y S_{\psi_r})}{U_1} \tag{3.62}$$

$$\phi_r = \arctan \frac{C_{\theta_r}(U_x S_{\psi_r} - U_y C_{\psi_r})}{U_1} \tag{3.63}$$

Let $\Theta_1 = \Theta$ and $\Theta_2 = \dot{\Theta}$. Then the rotational subsystem of (3.2) can be rewritten in a combined form as

$$\begin{aligned} \dot{\Theta}_1 &= \Theta_2 \\ \dot{\Theta}_2 &= \Phi(\Theta, \dot{\Theta}) + U_\Theta + d_\Theta(t) \end{aligned} \tag{3.64}$$

Defining the tracking error

$$e_3 = \Theta_{1r} - \Theta_1 \tag{3.65}$$

its time time derivative is written as

$$\dot{e}_3 = \dot{\Theta}_{1r} - \dot{\Theta}_1 = \dot{x}_{3r} - \Theta_2 \tag{3.66}$$

Defining a sliding surface in terms of the error such as:

$$s = e_4 = \Theta_{2r} - \Theta_2,\ \Theta_2 = \Theta_{2r} - e_4 \tag{3.67}$$

and substituting (3.67) into (3.66) gives

$$\dot{e}_3 = \dot{\Theta}_{1r} - \Theta_{2r} + s \tag{3.68}$$

where Θ_{2r} is the virtual control law designed to stabilize $\dot{e}_4$:

$$\Theta_{2r} = \dot{\Theta}_{1r} + K_3 e_3,\ \ \dot{\Theta}_{2r} = \ddot{\Theta}_{1r} - K_3 \dot{e}_3 \tag{3.69}$$

where K_3 is a positive definite matrix.
Substituting (3.69) into (3.68) yields

$$\dot{e}_3 = s - K_3 e_3 \tag{3.70}$$

Choosing a Lyapunov function candidate as

$$V_{2\Theta} = \frac{1}{2} e_3^T e_3 + \frac{1}{2} s^T s \tag{3.71}$$

and taking time derivative of $V_{2\Theta}$, gives

$$\begin{aligned} \dot{V}_{2\Theta} &= e_3^T \dot{e}_3 + s^T \dot{s} \\ &= e_3^T (-K_3 e_3 + s) + s^T (\ddot{\Theta}_{1r} + K_3 \dot{e}_3 - \dot{\Theta}_2) \end{aligned} \tag{3.72}$$

Substituting (3.64) into (3.72), yields

$$\begin{aligned}\dot{V}_{2\Theta} &= -e_3^T K_3 e_3 + e_3^T s + s^T(\ddot{\Theta}_{1r} + K_3\dot{e}_3 - \\ &(\Phi(\Theta,\dot{\Theta}) + U_\Theta) - d_\Theta) \\ &= -e_3^T K_3 e_3 + s^T(e_3 + \ddot{\Theta}_{1r} + K_3\dot{e}_3 - \\ &\Phi(\Theta,\dot{\Theta}) - U_\Theta - d_\Theta)\end{aligned} \tag{3.73}$$

Thus the control input vector U_Θ can be defined as

$$\begin{aligned}U_\Theta = [&e_3 + K_3\dot{e}_3 - \Phi(\Theta,\dot{\Theta}) + \ddot{\Theta}_{1r} - \\ &\hat{d}_\Theta + K_4 s + A\text{sign}(s)]\end{aligned} \tag{3.74}$$

where K_4 and A are positive definite matrices.

To compensate for d_Θ, the same nonlinear disturbance observer (3.6b) is used in the attitude system.

The discontinuous function sign(.) in the control law (3.74) is replaced by a continuous function to reduce the effect of the chattering in the control signal. For instance, the signum function sign(.) can be replaced by the following function (O'Toole *et al.*, 2010b)

$$\text{sign}(s) = \frac{s}{\|s\| + \varsigma} \tag{3.75}$$

where ς is a positive tuning parameter that smoothes the discontinuity. It is tuned manually to attenuate the chattering problem.

We prove the following attitude counterpart of Theorem 3.1.

Theorem 3.2. *Consider the attitude error subsystem* (3.65) *and* (3.67) *in closed loop with the disturbance observer designed as in* (3.6a)-(3.6b) *and the control law designed according to* (3.74). *There exist positive definite gain matrices K_3, K_4, A, and L_Θ, such that the closed loop*

attitude error satisfies

$$\|e_3\|^2 + \|e_4\|^2 \leq \epsilon \ \textit{for all } t \geq T^* \tag{3.76}$$

with any pre-selected precision $\epsilon > 0$ *where* T^* *is sufficiently large.*

Proof. Define a Lyapunov function candidate as:

$$V_2 = V_{1\Theta} + V_{2\Theta} \tag{3.77}$$

Considering (3.74), (3.53), and taking the time derivative of (3.77), yields

$$\begin{aligned}
\dot{V}_2 &= \dot{V}_{1\Theta} + \dot{V}_{2\Theta} \\
&= -e_3^T K_3 e_3 + e_3^T s + s^T(\ddot{\Theta}_{1r} + K_3 \dot{e}_3 - \Phi(\Theta, \dot{\Theta}) \\
&+ U_\Theta - \hat{d_\Theta}) + e_{d_\Theta}^T (L_\Theta - \frac{1}{2} I_{3x3}) e_{d_\Theta} + \frac{1}{2} D_\Theta^2 \\
&= -e_3^T K_3 e_3 - s^T K_4 s - s^T e_{d_\Theta} - s^T A \ \text{sign}(s) \\
&- e_{d_\Theta}^T (L_\Theta - \frac{1}{2} I_{3x3}) e_{d_\Theta} + \frac{1}{2} D_\Theta^2 \\
&\leq -e_3^T K_3 e_3 - s^T K_4 s - \frac{1}{2} s^T s + \frac{1}{2} e_{d_\Theta}^T e_{d_1} \\
&- s^T A \ \text{sign}(s) - e_{d_\Theta}^T (L_\Theta) e_{d_1} \\
&+ \frac{1}{2} e_{d_\Theta}^T e_{d_\Theta} + \frac{1}{2} D_\Theta^2 \\
&\leq -e_3^T K_3 e_3 - s^T (K_4 + \frac{1}{2} I_{3x3}) s - s^T A \ \text{sign}(s) \\
&- e_{d_\Theta}^T (L_\Theta - I_{3x3}) e_{d_\Theta} + \frac{1}{2} D_\Theta^2 \\
&\leq -e_3^T K_3 e_3 - s^T ((K_4 + A \ \text{sign}(s)) + \frac{1}{2} I_{3x3}) s \\
&- e_{d_\Theta}^T (L_\Theta) e_{d_\Theta} + \frac{1}{2} D_\Theta^2 \\
&< -\delta_2 V_2 + D_\Theta^2
\end{aligned} \tag{3.78}$$

where

$$\delta_2 = min\{2\lambda_{min}(K_3), 2(\lambda_{min}(K_4 + A\ \text{sign}(s)) - \frac{1}{2}),$$
$$2(\lambda_{min}(L_\Theta - 1)\}$$

It can be seen that the above gains can be chosen to deliver any magnitude of the tunable coefficient $\delta_2 > 0$. The result of Theorem 3.2 then follows directly from Lemma 3.1.

3.6 Stability analysis of the overall closed loop system

In view of the results presented in Theorems 3.1 and 3.2, it is now straightforward to prove stability for the overall closed loop tracking control system.

Theorem 3.3. *Let the position error subsystem* (3.43) *and* (3.45) *in closed loop with the disturbance observer designed as in* (3.6a)-(3.6b) *be controlled according to* (3.52) - (3.53)*. Also, let the attitude error subsystem* (3.65) *and* (3.67) *in closed loop with the disturbance observer designed as in* (3.6a)-(3.6b) *be controlled according to* (3.74)*. Under these conditions, there exists an ensemble of gain matrices* K_1, K_2, K_3, K_4, A *and* L_p, L_Θ *such that the overall closed loop control error vector* $[e_1, e_2, e_3, e_4]$ *is bounded as follows*

$$\|e\|^2 \leq \epsilon \ \textit{for all}\ t \geq T^* \tag{3.79}$$

with any pre-selected precision $\epsilon > 0$ *where* T^* *is sufficiently large.*

Proof. Choose the Lyapunov function candidate for the overall closed loop system to be

$$V = V_1 + V_2 \tag{3.80}$$

Differentiating (3.80) and using (3.58) and (3.78) gives

$$\begin{aligned} \dot{V} &= \dot{V}_1 + \dot{V}_2 \\ &\leq -\delta_1 V_1 + \frac{1}{2} D_2^2 - \delta_2 V_2 + \frac{1}{2} D_1^2 \quad < -\delta V + \gamma \end{aligned} \tag{3.81}$$

where $\delta = \min\{\delta_1, \delta_2\}$ and $\gamma = \frac{1}{2} D_1^2 + D_2^2$.

Since the coefficients δ_1 and δ_2 are both tunable in their respective position and attitude control subsystems, the δ is also tunable. Hence it again follows from Lemma 3.1, that for any desired tracking precision $\epsilon > 0$ there exists an ensemble of gain matrices $K_1, K_2, K_3, K_4, A, L_p, L_\Theta$ such that the magnitude of both the position and attitude errors do not exceed ϵ on sufficiently long control horizons. The quadrotor tracking control design is hence complete.

3.7 Parameter Identification for the Quadrotor Prototype

The quadrotor tracking control design described above was tested by way of computer simulations as well as on a real quadrotor system in the Control System Laboratory of École de Technologie Supérieure (ETS), Montreal, Canada.

For the simulation and real flight trajectories to be comparable, the parameters of the real physical system (see (3.4)) had to be estimated first. To this end we describe the estimation procedure in detail. The mass of the quadrotor was simply obtained by weighing the device. However, obtaining the inertia moments was more complex. An RCbenchmark series 1580 dynamometer device was used to determine the relationship between the propellers' speeds and the forces exerted by the motors. A commercial quadrotor, S500 Glass Fiber Quadcopter Frame 480 mm - Integrated PCB was used as the experimental platform (see Figure 3.3).

The measurements necessary for parameter identification were obtained by the use of the solid modeling CAD software (Solidworks 2017) (see Fig. 3.4). Table 3.1 shows the resulting estimates of the inertia moments for the quadrotor S500.

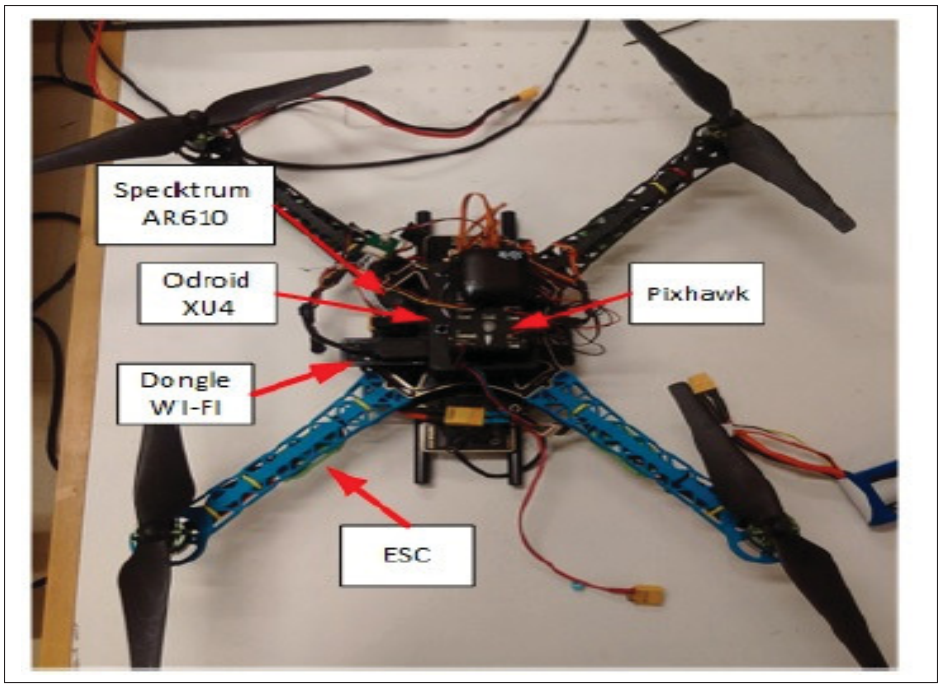

Figure 3.3 The quadrotor used in real flight tests

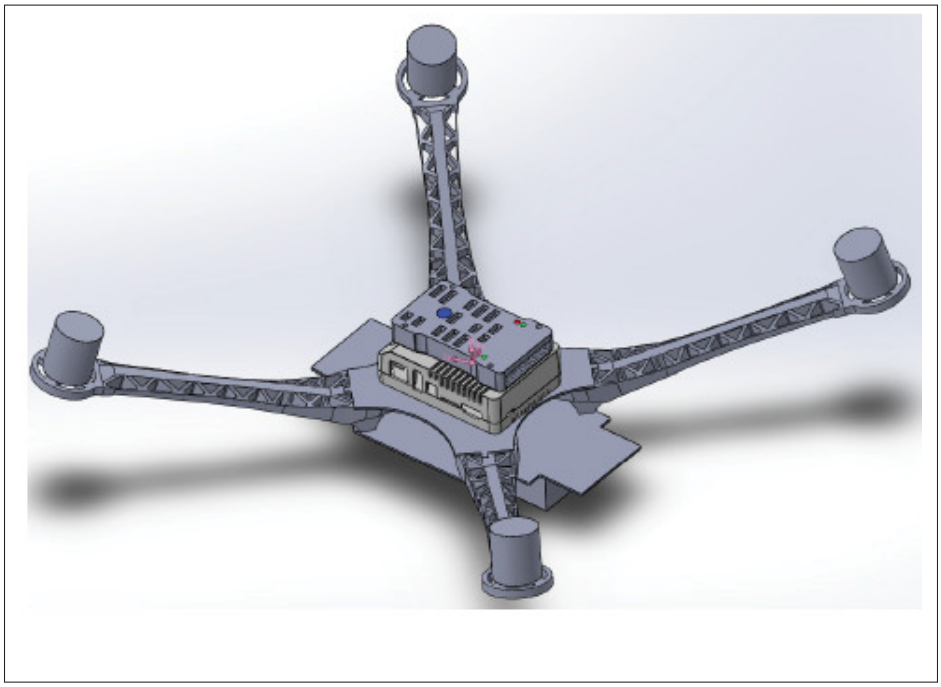

Figure 3.4 Sildworks 3-D model of quadrotor S500

In practice, the outputs from the designed controller system are the calculated torques corresponding to the measured orientation of the quadrotor and the lift forces. These were then used to determine the forces exerted by each motor. However, the forces control the motors indirectly via PWM signals that regulate the motor speeds. Consequently, in order to find a motor's thrust coefficients, the relationships between the lifting force and the PWM signal for each motor had to be known. The aforementioned device (RCbenchmark Series 1580 Dynamometer, see Fig.3.5) was again used for this purpose. This measuring device generates more than four PWM output signals and can measure the speed of a motor.

Table 3.1 Inertia moments of quadrotor S500 using Solidworks

m (kg)	$\mathbf{I}_{xx}$ **(kg· m^2)**	$\mathbf{I}_{xx}$ **(kg· m^2)**	$\mathbf{I}_{xx}$ **(kg· m^2)**
1,354	0.01275	0.01278	0.02271

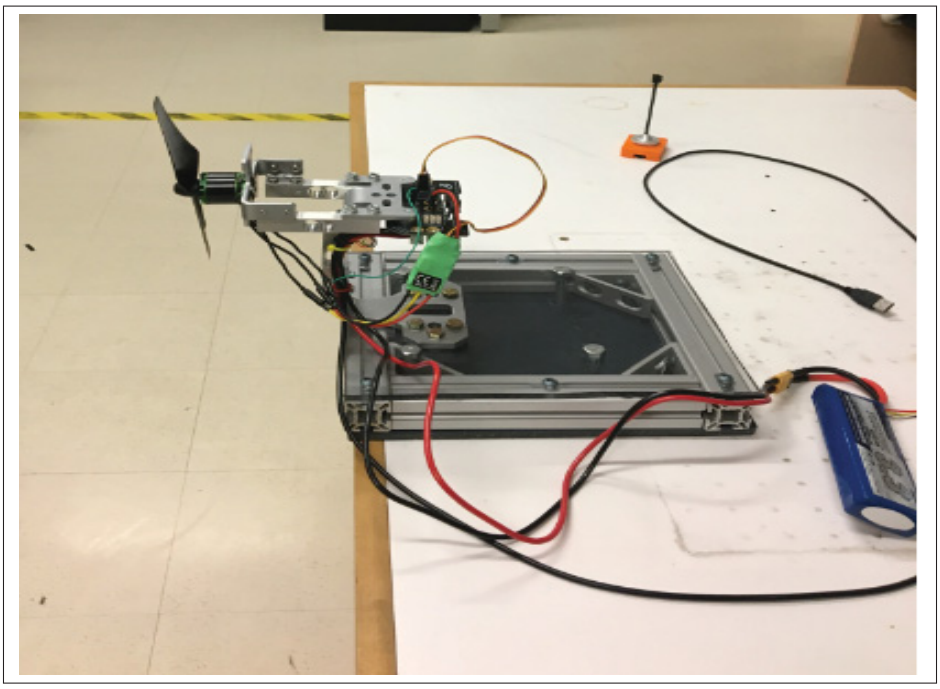

Figure 3.5 Motor force measuring device

The force exerted by the motor can then be expressed as a function of the pulse width in μs. The obtained measurements are shown in Fig. 3.6 Using the curve in Fig.3.6, the relation between the PWM signals and the lift force was approximated by a polynomial in the lift force f_i

$$\text{Pulse Width}(\mu s) = -13.0701 f_i^2 + 227.6249 f_i + 1036.3$$
$$f_i = 72.17\tau_i - 0.047 \tag{3.82}$$

The relation between the torque and the force generated by each motor can be determined using the same device. The motor force and torque measurements are depicted in Fig.3.7. The curve in Fig.3.7, was used to determine that the force was approximately a linear function of the torque τ_i.

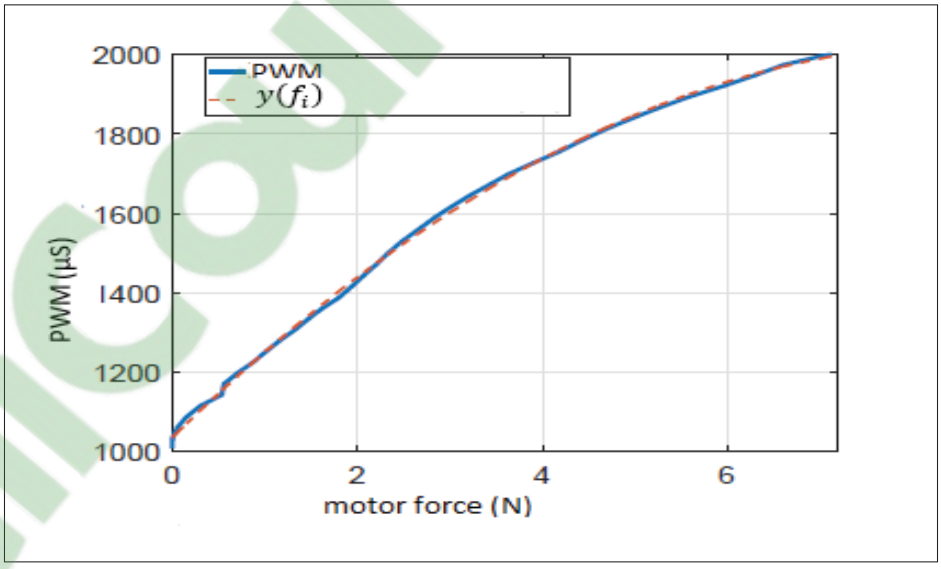

Figure 3.6 Motor force relative to PWM

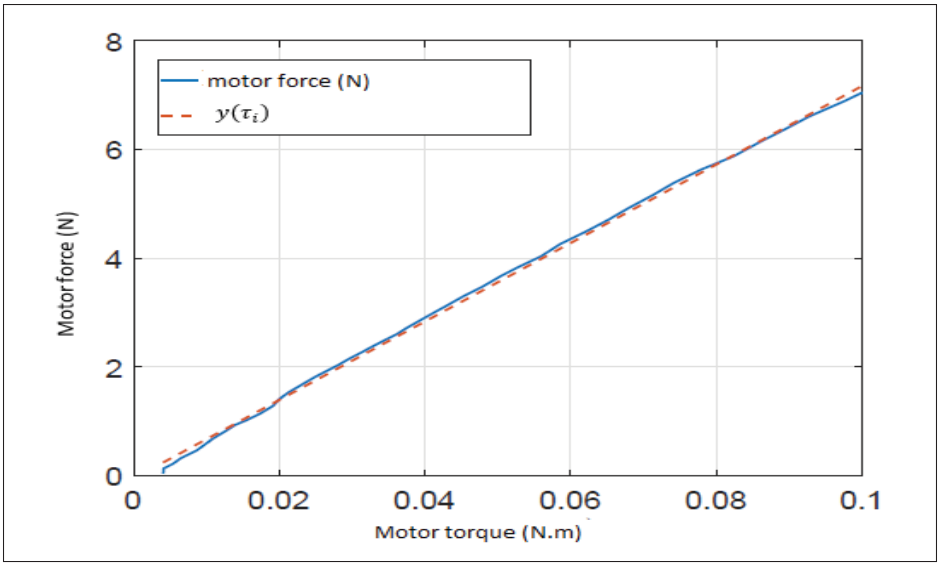

Figure 3.7 The relation between force and torque of the motor

3.8 Simulation results

In order to verify the effectiveness of the proposed method, the simulation results were obtained considering the physical parameters described in the previous section, where the remaining constants were set as follows: $h = 0.225m, J_R = 3.357 \times 10^{-5} Kgm^2$, and $g = 9.81m/s^2$. The quadrotor was required to follow the desired trajectory defined for $t \geq 0$:

$$[x_d, y_d, z_d] = [0.5\sin(2\pi t/40), 0.5\cos(2\pi t/40), 1] \tag{3.83}$$

Furthermore, the yaw angle reference trajectory was set at $x_{5r} = 0$ rad over the entire simulation horizon. For the purpose of the simulation, the external disturbance vector was considered as a "gust of wind" given by the functions

$$\begin{aligned} d_1 &= [d_x, d_y, d_z]^T \\ &= [1.5 + 2.5\sin(4t), 1.5 + 2.5\ \sin(4t), 1.5]N \\ d_2 &= [d_\phi, d_\theta, d_\psi]^T \\ &= [2.5\sin(4t), \sin(0.1t), \sin(0.1t)]^T Nm \end{aligned}$$

The position and attitude controller gains are 3×3 matrices: $K_1 = \text{diag}[k_x, k_y, k_z]$, $K_2 = \text{diag}[k_{xx}, k_{yy}, k_{zz}]$, $K_3 = \text{diag}[k_\phi, k_\theta, k_\psi]$, $K_4 = \text{diag}[k_{\phi\phi}, k_{\theta\theta}, k_{\psi\psi}]$, and $A = \text{diag}[A_\phi, A_\theta, A_\psi]$. Likewise, the nonlinear observer gains are 3×3 matrices: $L_p = \text{diag}[l_x, l_y, l_z]$ and $L_\Theta = \text{diag}[l_\phi, l_\theta, l_\psi]$. All gains were tuned manually by trial and error in computer simulations. The best values of all gains, which secure the smallest tracking errors, are shown in Table 2.

Table 3.2 Controller gains.

Gain	**Value**	**Gain**	**Value**	**Gain**	**Value**
k_x	2.0313	l_y	15	$k_{\psi\psi}$	10.861
k_y	2.0313	l_z	15	l_ϕ	20
k_z	2.216	$k\phi$	12.861	l_ψ	20
k_{xx}	0.0313	k_θ	12.861	l_θ	20
k_{yy}	0.0313	k_ψ	12.861	A_ϕ	0.7
k_{zz}	0.216	$k_{\phi\phi}$	10.861	A_ψ	0.7
l_x	15	$k_{\theta\theta}$	10.861	A_θ	0.7

The simulation results are shown in Fig. 3.8 - Fig. 3.13. It can be seen from Fig.3.8 and Fig. 3.9 that the quadrotor can track the desired flight path correctly while compensating for the disturbances. Fig.3.11 also shows good tracking of the attitude reference trajectory. Furthermore, Fig.3.8 and Fig.3.11 provide the comparison between the tracking results in position and attitude subsystems obtained using the proposed controller versus the standard backstepping controller. The proposed control-observer scheme is clearly performing better.

The plots of the errors in the position and attitude subsystems are presented in Fig.3.10 and Fig. 3.12. It can be seen that the nonlinear disturbance observer can estimate the disturbances quickly and accurately. The control inputs of rotors are presented in Fig. 3.13.

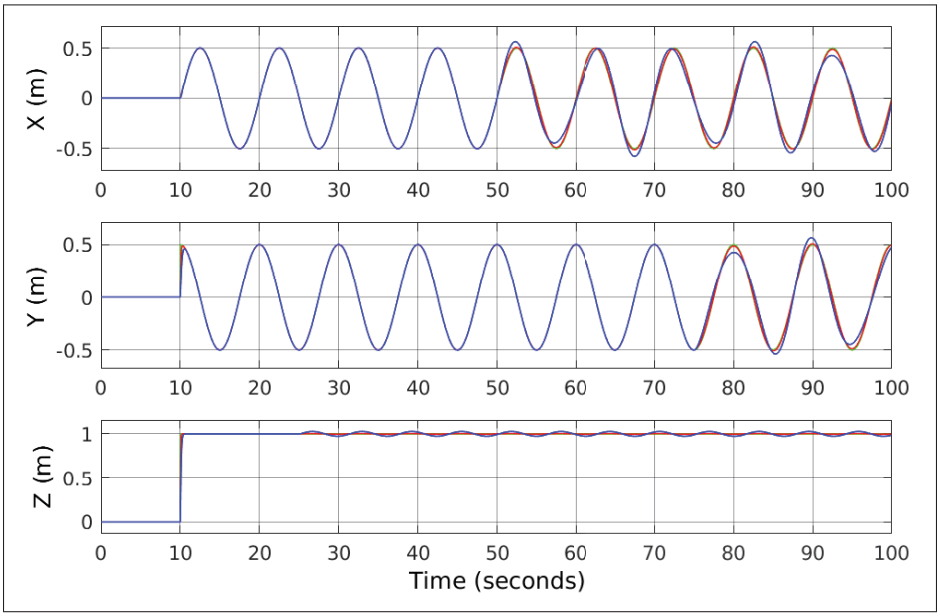

Figure 3.8 Position tracking in coordinates (x, y, z). Graph legend: Green - Reference Trajectory ; Red - Trajectory Obtained Using the Proposed Controller; Blue - Trajectory Obtained Using the Standard Backstepping Controllers

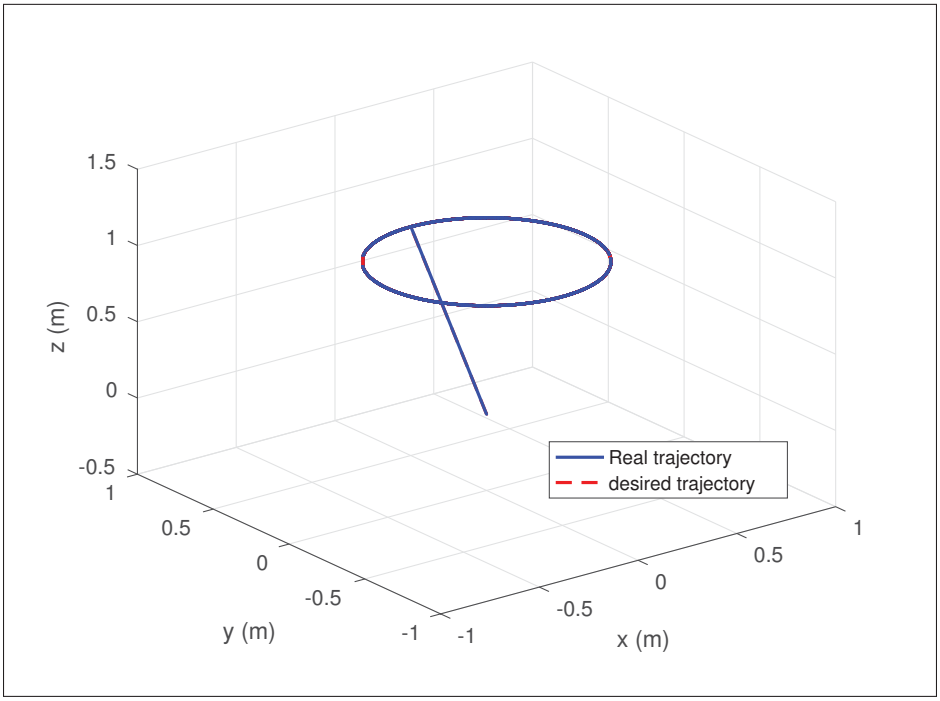

Figure 3.9 3D Position tracking in simulation

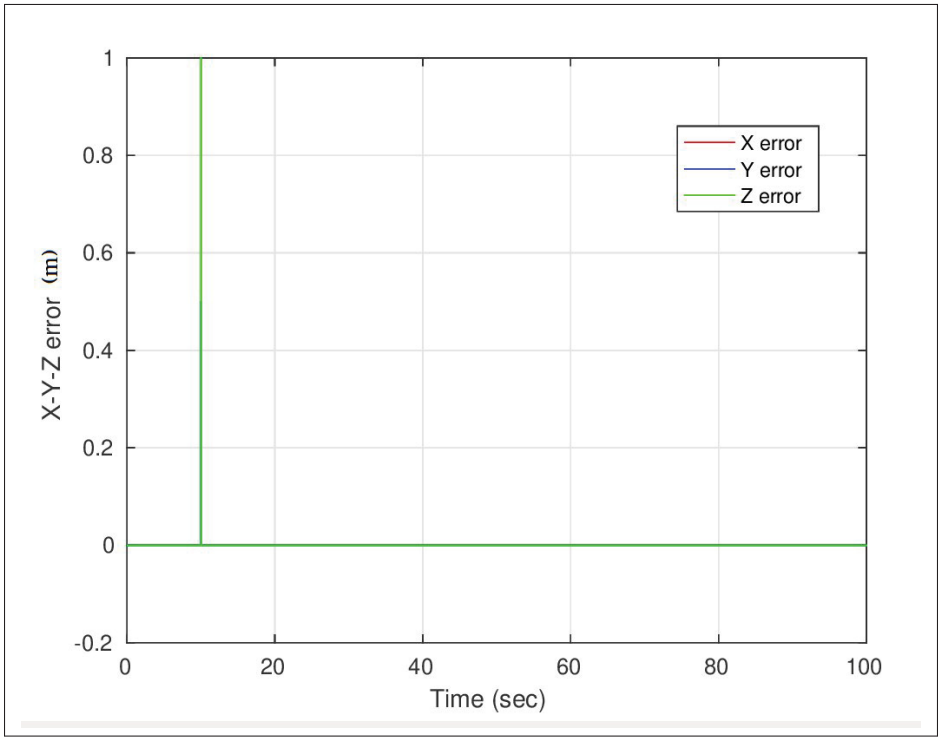

Figure 3.10 Position tracking errors in the (x, y, z) coordinates

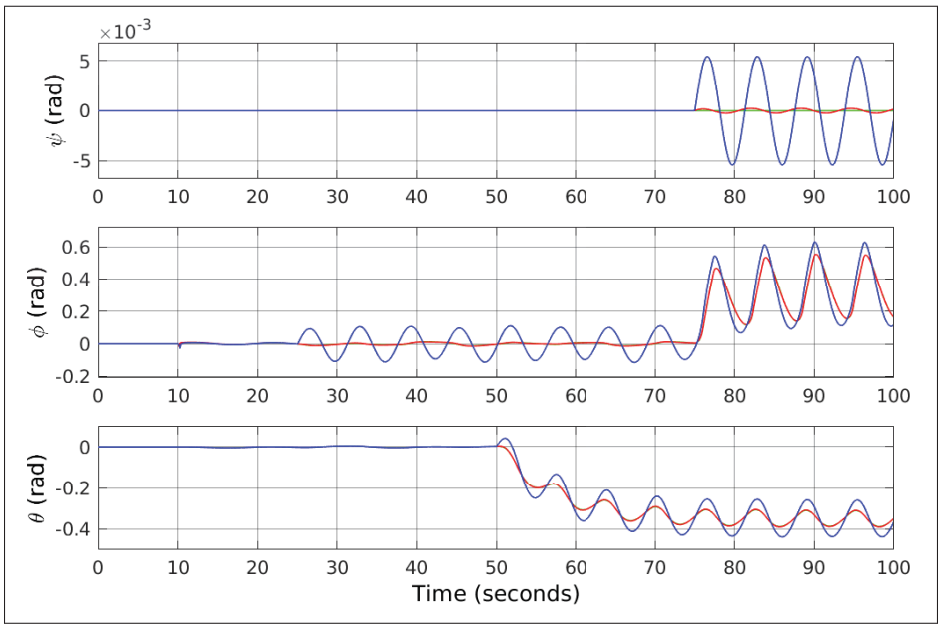

Figure 3.11 Attitude tracking (ϕ, θ, ψ). Graph legend: Green - Reference Trajectory ; Red - Trajectory Obtained Using the Proposed Controller; Blue - Trajectory Obtained Using the Standard Backstepping Controllers

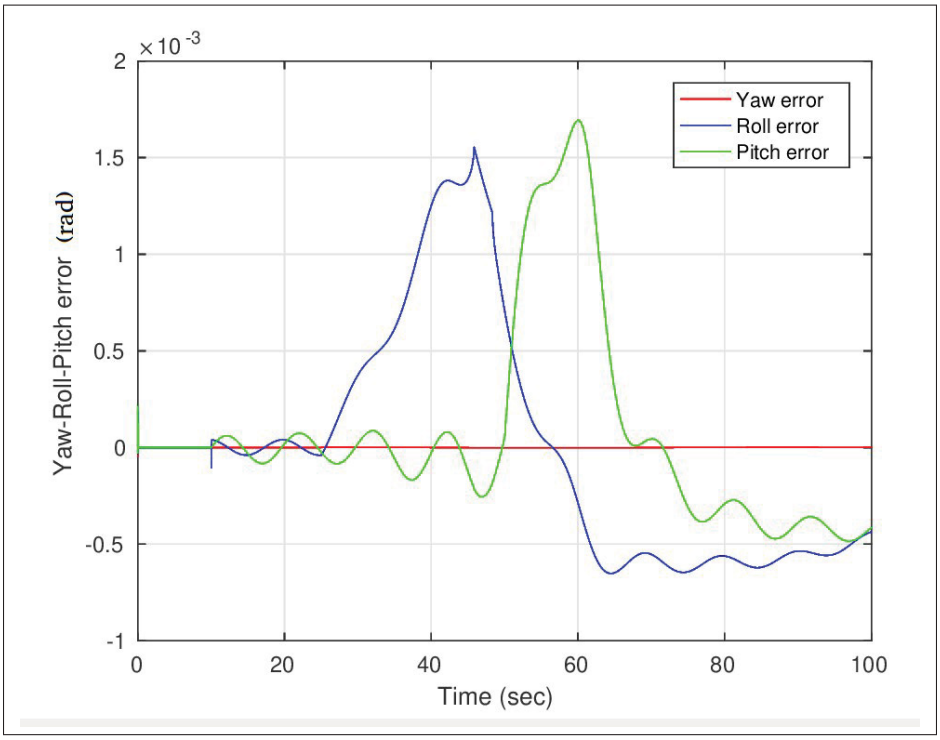

Figure 3.12 Attitude tracking errors

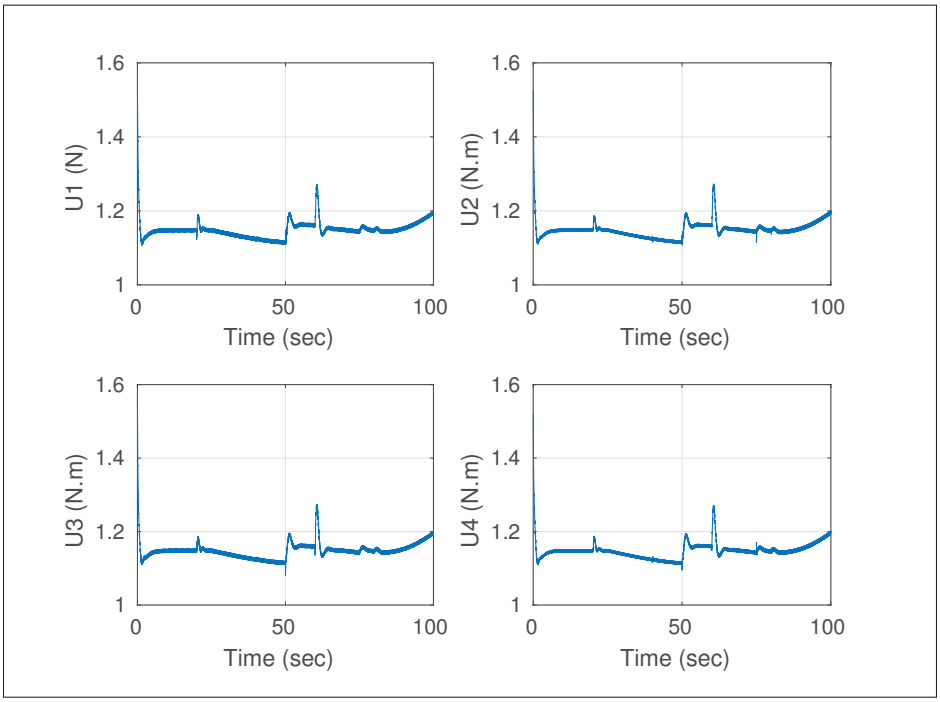

Figure 3.13 Inputs generated by controllers during simulation

3.9 Experimental results

The Pixhawk autopilot was employed as the onboard flight controller to implement the data fusion algorithm and the proposed flight control strategy. For positioning system, a special localization sensor/algorithm (Kinect) is used to capture the position of the quadrotor during the flight. A companion computer (Odroid XU4) is used to interface and communicate with the pixhawk flight controller using the MAVLink protocol over a serial connection. A connection is established for the communication between the companion computer and the ground station. By doing this, the companion computer gets all the MAVLink data produced by the autopilot and the positioning sensor (Kinect). The controller and estimator parameters employed in the experiment were those listed in Table 2. In practical applications, the attitude gains are usually tuned first, followed by the position gains. Based on the permitted overshoot, settling time, the steady-state error requirements, these gains can be tuned by trial and error in hovering conditions.

The goal of the laboratory experiment was to demonstrate that the designed controller achieves good tracking in the presence of external wind gusts. An electrical fan was used to generate the wind gusts that affect the quadrotor during flight, as shown in Fig. 3.14. It was required that the quadrotor follows the same trajectory as the one used in computer simulations.The responses of the position and attitude subsystem under wind gusts are depicted in Fig. 3.15 - Fig. 3.19 together with the respective tracking errors. The results clearly confirm that the proposed controller is capable of compensating for wind gusts as additional unknown disturbances. The quadrotor tracks the given trajectory with tracking errors that do not exceed 0.2 m.

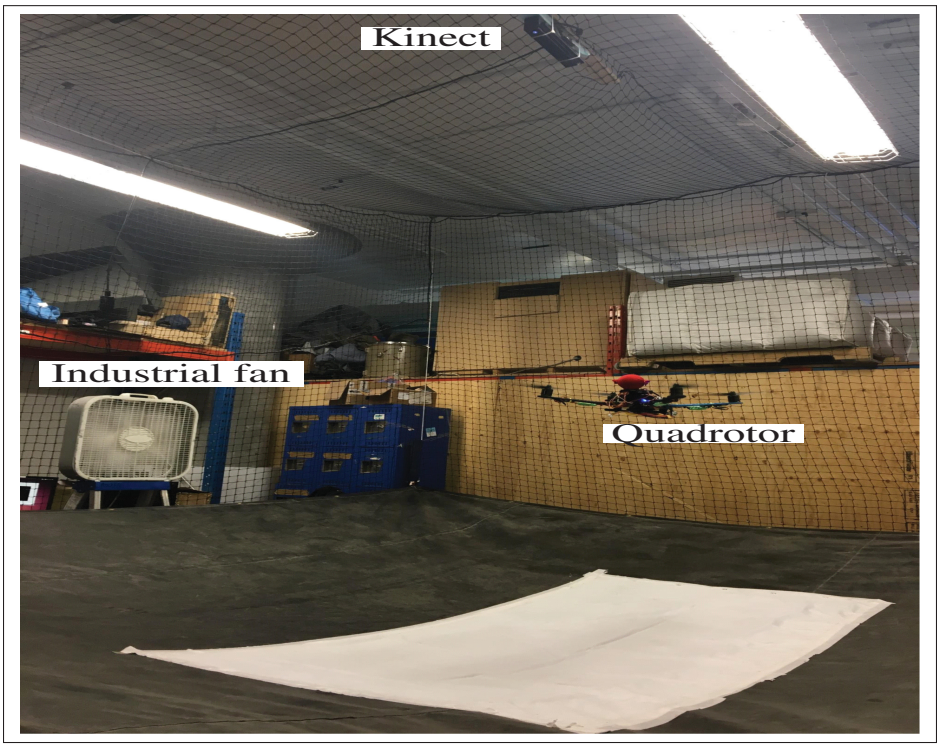

Figure 3.14 The experimental setup used in real flight tests

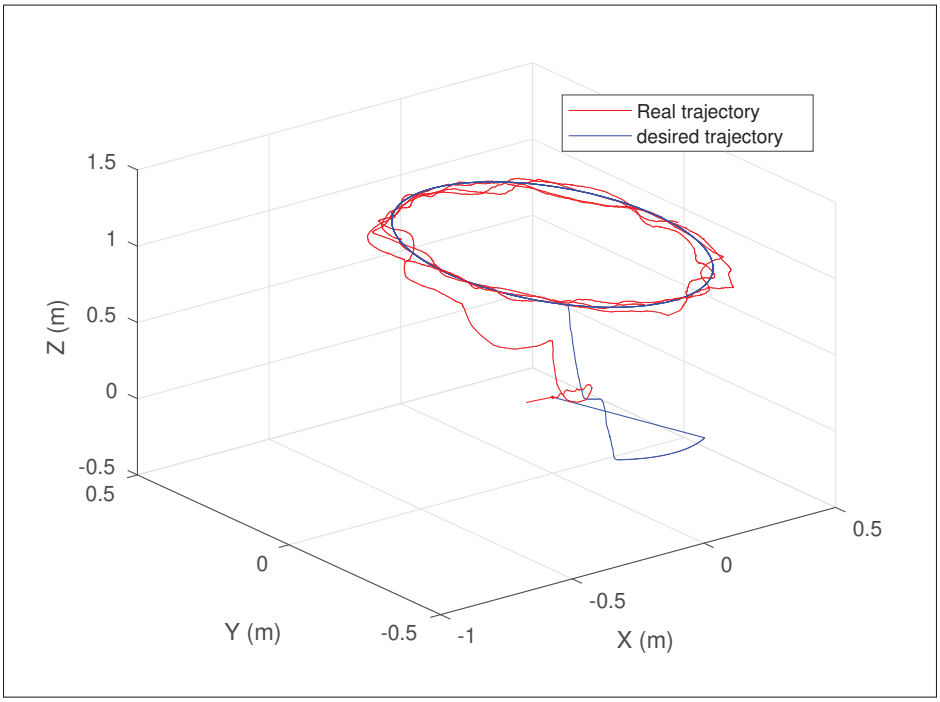

Figure 3.15 Real flight test of 3D position tracking by the proposed controller under the effect of wind gusts

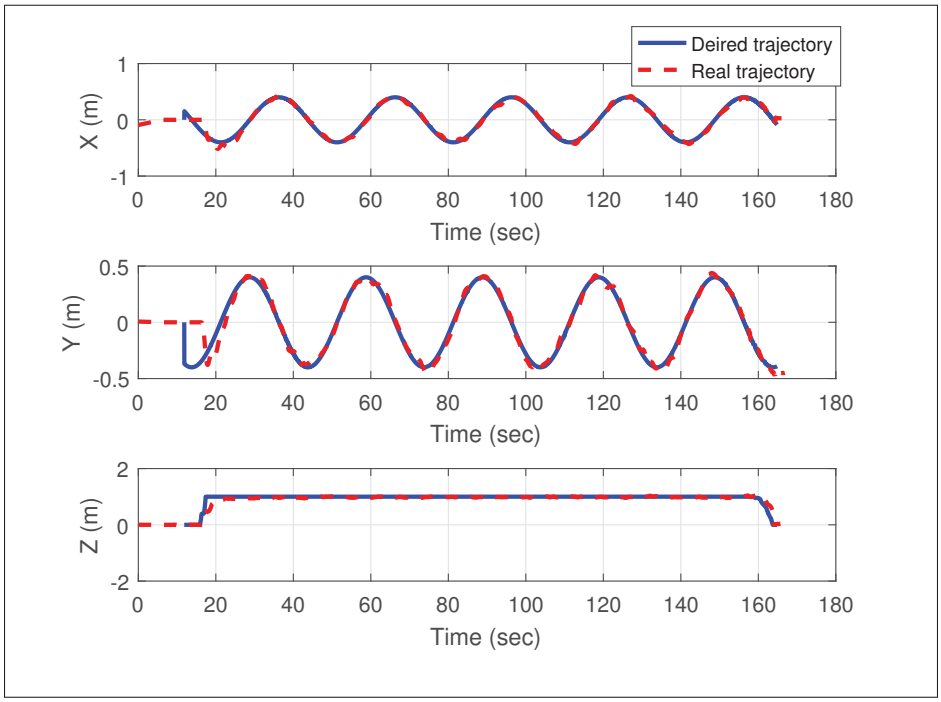

Figure 3.16 Real flight tracking of three position coordinates by proposed controller under the effect of wind gusts

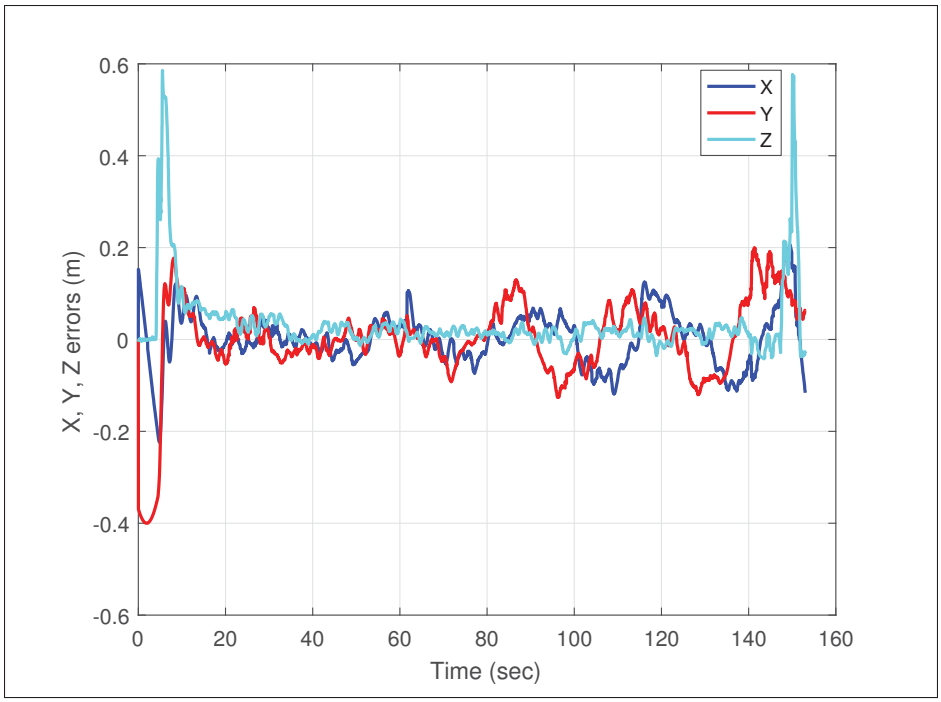

Figure 3.17 The position tracking errors under the effect of wind gusts

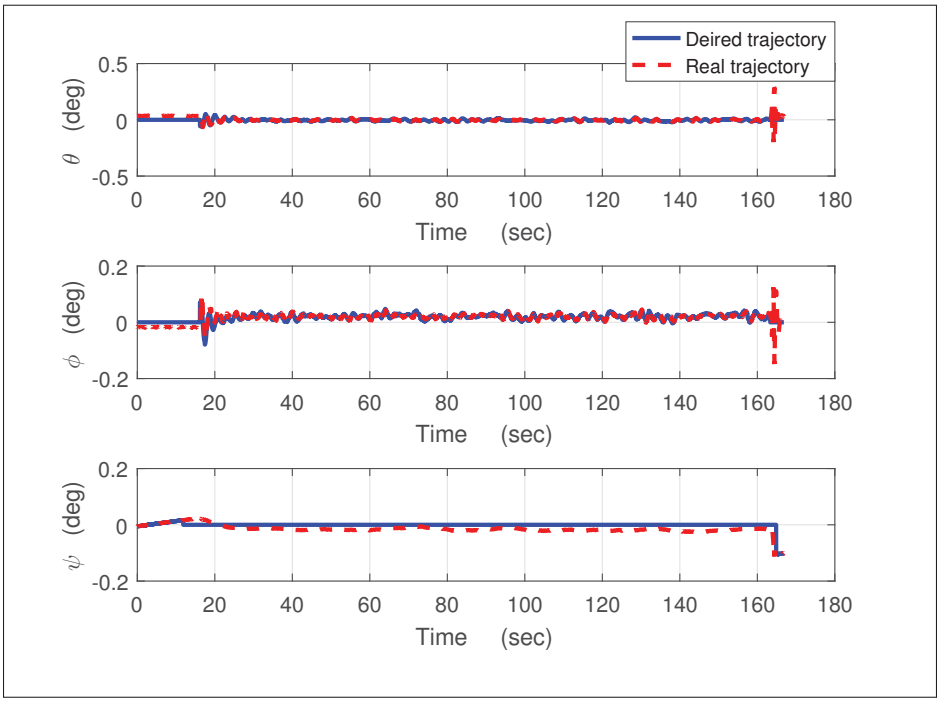

Figure 3.18 Real flight tracking of three attitude angles by proposed controller under the effect of wind gusts

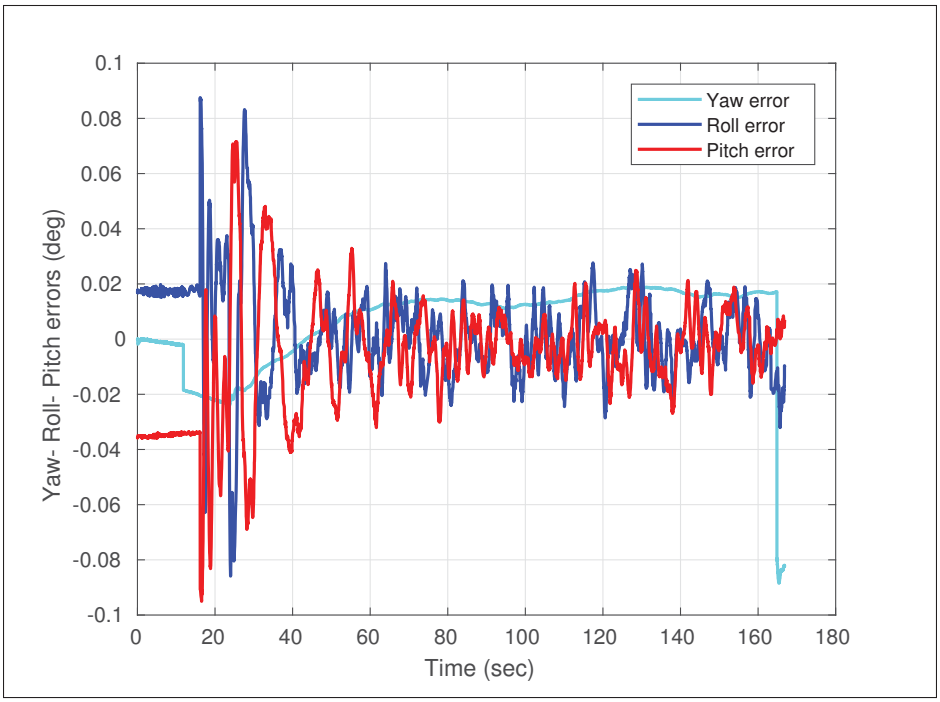

Figure 3.19 The attitude tracking errors under the effect of wind gusts

3.10 Conclusion

This paper explores a novel approach to robust trajectory tracking control of a quadrotor UAV. A bank of nonlinear disturbance observers is employed in conjunction with a matching set of generalized backstepping and sliding mode controllers to compensate the influence of the unmatched uncertainties affecting the system during the flight.The stability of the system is guaranteed by designing the backstepping-sliding mode controller combined with the NDO as demonstrated employing a direct Lyapunov analysis. The validity of the developed approach was first confirmed by computer simulations. The performance of the observer-based backstepping-sliding mode control strategy was next extensively validated in real time flight tests using an experimental platform setup. Furthermore, the localization algorithm (Kinect) will be extended to use a precise position measurement from a motion capture system to upgrade the experimental UAV setup. This will enable much better performance of the implemented nonlinear controller.

CHAPTER 4

ROBUST SLIDING-MODE TRACKING CONTROL OF QUADROTOR

Nuradeen Fethalla [1], Maarouf Saad [2], Hannah Michalska [3]

[1,2] Département de Génie électrique, École de Technologie Supérieure,
1100 Notre-Dame Ouest, Montréal, Québec, Canada H3C 1K3
[3] Electrical and computer engineering department McGill university, McConnell Eng. Bldg
3480 Rue University, Room 514, Montréal, QC H3A 0E9

Submitted to Journal of The Franklin Institute, January,2019

4.1 Abstract

This paper presents a novel robust non-linear controller which is inspired from sliding mode control. To attain a trajectory tracking capability of a quadrotor UAV in the presence of external disturbances and parameter uncertainties associated with the presence of aerodynamic forces and possible wind force, the structure of the proposed technique is composed of a super-twisting sliding mode observer (STO) alongside the sliding mode control (SMC). A conventional sliding mode scheme shares intermediate control goals by an introduced sliding surface. The closed-loop system including the sliding mode controller is finally linked with the STO to track the desired position and attitude trajectories. The controller and observer gains are selected properly to achieve good tracking. The system performance exhibits much better robustness than the existing sliding mode control methods which are not equipped with super-twisting estimators. Real-time laboratory experiment results performed on hardware testbed are presented to confirm the simulation results.

keywords: Tracking control, Sliding mode control,Observer, Quadrotor.

4.2 Introduction

Numerous types of non-linear control methods have been developed and applied to the UAV trajectory tracking problem. The review considered in this section does not claim to be ex-

haustive. One of the researches that have been extensively studied within UAV control deals with the development of position and attitude controls for the UAV trajectory tracking problems. In practice, there are various technical challenges in the control of a quadrotor UAV that is subjected to unknown external disturbances and model uncertainties. The unknown disturbances in practical aerospace environments include wind gust, noises and etc. The model uncertainties of a quadrotor UAV are usually induced by the imprecise hydrodynamic coefficients which arise in the mathematical model of the quadrotor. To tackle the technical issues of external disturbances and model uncertainties, several methods have been introduced. Among these introduced methods, adaptive control (Dydek *et al.*, 2013; Bouadi *et al.*, 2015), robust control (Ramirez-Rodriguez *et al.*, 2014; Zheng *et al.*, 2014), and disturbance observer-based control (Fethalla *et al.*, 2018; Rashad *et al.*, 2016). In (Dydek *et al.*, 2013), the parametric uncertainties have been compensated using the adaptive nonlinear control method based on Lyapunov stability arguments, that has been widely used as a suitable choice. However, a linear parametrization (LP) condition always required for the classic adaptive control method, and sometimes, the singularities will accompany the controller (Bouadi *et al.*, 2015). In (Ramirez-Rodriguez *et al.*, 2014), an integral sliding-mode incorporated with backstepping control to propose a novel robust controller that is a robust backstepping-based approach for a quadrotor UAV. Despite the design of backstepping scheme is a very clear procedure and has a standardized proof of the stability, the gains of the controller are not easy for tuning. Sliding mode control (SMC) scheme is advantageous as it captures the robust nature among the existing nonlinear approaches. SMC has a chattering phenomenon drawback, which reduces the trajectory tracking smoothness and causes energy losses. To reduce the effect of this phenomenon, some methods, such as the high-order sliding-mode controller (Zheng *et al.*, 2014) have proposed. In (Xiong & Zheng, 2014), a terminal sliding mode control designed for fully actuated subsystem while a sliding mode control designed for the under-actuated subsystem. The feasibility of the terminal sliding mode approach has been shown via simulations. However, this control approach is known to be very robust, which is a huge benefit. An integral sliding mode controller (ISMC) is proposed in (Mu *et al.*, 2017) for trajectory tracking of the quadrotor. Due

to the effect of the induced additional error integral term of the ISMC, the trajectory tracking performance of ISMC is more accurate than the conventional SMC.

The alternative approach to overcome the effect of the external disturbance and uncertainties is to design an observer to estimate these external disturbances and uncertainties, followed by the designed controller. Such disturbance observers include a nonlinear disturbance observer introduced in (Fethalla *et al.*, 2018; Rashad *et al.*, 2016). The validated results have shown that non-linear disturbance observer (NDO) control can handle disturbances through a faster dynamic response. In (Besnard *et al.*, 2007), a sliding mode controller based on a sliding mode observer is proposed for a quadrotor UAV. The observer is introduced to estimate the external disturbances and to reduce the control gain. Furthermore, many researchers have exploited the augmentation of integral control with the backstepping technique to limit the effects of parametric uncertainties and external disturbances for the trajectory tracking control of quadrotors (Bouabdallah & Siegwart, 2007), (Raffo *et al.*). However, the limitation of the integral action is that the uncertainties or disturbances that could be effectively rejected are exclusive ones, such as a constant or lumped disturbance. In (Wang *et al.*, 2016), uncertain non-linear systems considered and a backstepping-based control approach with the help of generalized disturbance observer (GDOB) has been proposed. An asymptotic rejection of unmatched general periodic disturbances as the output feedback form is considered. The unmatched disturbances are rejected and the asymptotic stability of the system ensured using the proposed disturbance estimation based scheme. In (Shao *et al.*, 2018), a robust backstepping approach based on extended state observer (ESO) is introduced. The extended state observer (ESO) combined with a backstepping controller is derived to estimate the lumped disturbances and the unmeasurable states in a rotational subsystem simultaneously. However, the proposed scheme has the main limitation which is the lack of the robustness to various types of the disturbances applied to the system as it is restrictive to lumped disturbances. The authors in (Aguiar & Hespanha, 2007) presented a backstepping approach for one kind of under-actuated autonomous vehicles. Based on Lyapunov theory, the problem of global stability is discussed and the tracking error is guaranteed to converge to a neighborhood of the origin that can be made arbitrarily small.

The novel contributions are hence summarized as follows: (i) The proposed approach yields the first SMC and controller that employs a super-twisting observer (STO) to compensate for matched and unmatched disturbances and model-system error. Although the same type of STO was also used in (Besnard *et al.*, 2012), its convergence properties were not assessed fully; (ii) The proof of asymptotic stability for the closed-loop system via the Lyapunov based stability analysis; (iii) the requirements of the model knowledge for the proposed nonlinear a robust controller is very limited and it can be implemented easily; its performance is verified via real-time experiments on quadrotor platform, where the laboratory experiments were preceded by proper identification and calibration of the real system; (iv) The laboratory experiments reproduced the simulation results with high fidelity despite using a fan to simulate wind gusts.

The rest of this paper is organized in the following manner. In Section 4.3, we describe the nonlinear dynamic model of the quadrotor and present the control objective. The super-twisting observer development is stated in Section 4.4. The tracking control laws for the second-order systems in vector forms are developed in Section 4.5, the tracking control design development for quadrotor is provided in Section 4.6, and the observer based tracking control analysis and the stability of the closed-loop system are proven in Section 4.7. The performance of the proposed approach is assessed in simulations as well as in the experimental laboratory setting in section 4.8 followed by the conclusions in section 4.9.

4.3 Dynamical model of a quadrotor

The dynamical model of a quadrotor employed here was originally described in (Hoffmann *et al.*, 2007b) and used extensively in the literature; see e.g. (Zheng *et al.*, 2014) and (Alexis *et al.*, 2012a). It is cited here for completeness of exposition. Consider two reference frames: the earth fixed frame ($\mathcal{I}$) associated with the unit vector basis (E_1, E_2, E_3) and body fixed frame ($\mathcal{B}$) associated with the unit vector basis (E_1^b, E_2^b, E_3^b) fixed at the center of mass of the quadrotor, as shown in Fig.4.1.

The position of the center of the quadrotor's mass is denoted by the vector $p = [x, y, z]^T$. This position vector is expressed with respect to an inertial frame ($\mathcal{I}$). The attitude of the quadrotor in frame ($\mathcal{I}$) is denoted by $\Theta = [\phi, \theta, \psi]$. These three angles are the Euler angles: yaw ($-\pi < \psi < \pi$), pitch ($-\frac{\pi}{2} < \theta < \frac{\pi}{2}$), and roll ($-\frac{\pi}{2} < \phi < \frac{\pi}{2}$). The angular velocity vector of the quadrotor in the body-fixed frame ($\mathcal{B}$) is denoted by $\Omega = [\Omega_p, \Omega_q, \Omega_r]^T$. The acceleration vector, with the acceleration components of roll, pitch, and yaw, respectively, is expressed in the inertial frame $\mathcal{I}$ as $\ddot{\Theta} = [\ddot{\phi}, \ddot{\theta}, \ddot{\psi}]$. The linear velocities and accelerations of the translational system are given respectively as $\dot{p} = [\dot{x}, \dot{y}, \dot{z}]$, and $\ddot{p} = [\ddot{x}, \ddot{y}, \ddot{z}]$.

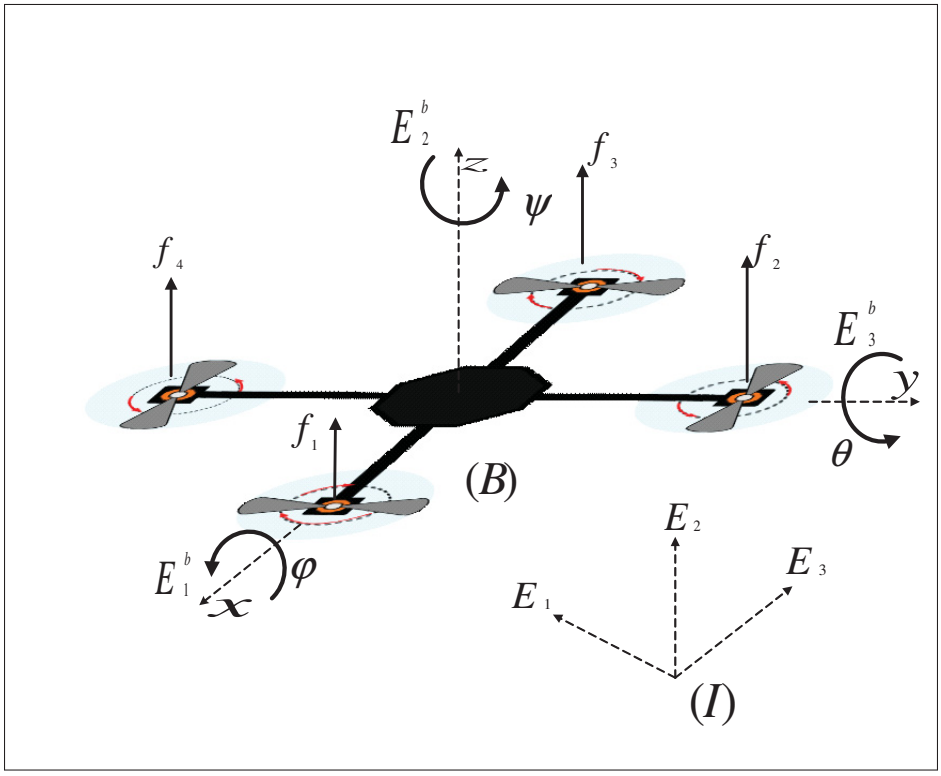

Figure 4.1 Quadrotor Airframe And Reference Frames.

The transformation between the body-fixed frame $\mathcal{B}$ and the inertial frame $\mathcal{I}$ is carried out by the use of the rotation matrix $R(\Theta)$ and Euler matrix $M(\Theta)$ respectively, computed as

$$R(\Theta) = \begin{bmatrix} C_\theta C_\psi & S_\phi S_\theta C_\psi - C_\phi S_\psi & C_\phi S_\theta C_\psi + S_\phi S_\psi \\ C_\theta S_\psi & S_\phi S_\theta S_\psi + C_\phi C_\psi & C_\phi S_\theta S_\psi - S_\phi c_\psi \\ -S_\theta & S_\phi C_\theta & C_\phi C_\theta \end{bmatrix}$$

$$M(\Theta) = \begin{bmatrix} 1 & 0 & -S_\theta \\ 0 & C_\phi & S_\phi C_\theta \\ 0 & -S_\phi & C_\phi S_\theta \end{bmatrix}$$

where the relationship between $\dot{\Theta}$ and Ω is

$$\Omega = M(\Theta)\dot{\Theta} \tag{4.1}$$

The functions $S_{(\cdot)}$ and $C_{(\cdot)}$ denote $\sin(\cdot)$ and $\cos(\cdot)$, respectively. Detailed derivation of these transformations can be found in (Alexis *et al.*, 2012a). The quadrotor dynamic equations are written in the form of two subsystems corresponding to translational motion (referring to the position of the center of mass of the UAV) and angular motion (referring to the attitude of the UAV). These equations can be stated in the inertial frame ($\mathcal{I}$) as

$$\ddot{p} = \frac{1}{m} R(\Theta) F_{prop} - G + d_p \tag{4.2a}$$

$$\begin{aligned} \ddot{\Theta} &= (IM(\Theta))^{-1}[T_{prop} - IN(\Theta, \dot{\Theta}) \\ &\quad - \Omega \times I\Omega - T_g] + d_\Theta \\ &= \Phi(\Theta, \dot{\Theta}) + \Psi(\Theta) T_{prop} + d_\Theta \end{aligned}$$

$$G := [0, 0, g]^T = g e_z; \tag{4.2b}$$

The matrix $I = diag(I_x, I_y, I_z)$ is the inertia matrix of the quadrotor, G is the acceleration due to gravity, and m denotes the mass of the quadrotor. The terms $d_p = [d_x \;\; d_y \;\; d_z]^T$ and $d_\Theta =$

$[d_\phi \;\; d_\theta \;\; d_\psi]^T$ represent time-varying unknown disturbance vectors which are assumed smooth and bounded and include the aerodynamical disturbances. The vector $N(\Theta, \dot{\Theta})$ is

$$N(\Theta, \dot{\Theta}) = \begin{bmatrix} -C_\theta \dot{\theta}\dot{\psi} \\ -S_\phi \dot{\phi}\dot{\theta} + C_\phi \dot{\phi}\dot{\psi} - S_\phi S_\theta \dot{\theta}\dot{\psi} \\ -C_\phi \dot{\phi}\dot{\theta} - S_\phi C_\theta \dot{\phi}\dot{\psi} - C_\phi S_\theta \end{bmatrix}$$

and the matrices $\Psi(\Theta)$ and $\Phi(\Theta, \dot{\Theta})$ are given as

$$\Psi(\Theta) = (IM(\Theta))^{-1}$$
$$\Phi(\Theta, \dot{\Theta}) = -(IM(\Theta))^{-1}[IN(\Theta, \dot{\Theta}) - \Omega \times I\Omega - T_g]$$

where T_g models the gyroscopic effects as

$$T_g = \sum_{i=1}^{4} \Omega \times J_r[0, 0, (-1)^{i+1}\omega_i]^T \tag{4.3}$$

where J_r is the moment of inertia of each rotor and $\omega_i, i = 1, 2, 3, 4$ is the rotary speed of each motor. Assuming that each motor produces thrust and drag that are proportional to the square of the motor speed, the force generated by the ith motor is given by $f_i = b\omega_i^2 (i = 1, 2, 3, 4)$ where b is the thrust factor. F_{prop} and T_{prop} are: the three-dimensional translational force vector and the three-dimensional reaction moment vector exerted by the propellers, respectively, as given by

$$F_{prop} = \begin{bmatrix} 0 \\ 0 \\ T \end{bmatrix} \quad T_{prop} = \begin{bmatrix} h(f_4 - f_2) \\ h(f_3 - f_1) \\ c\sum_{i=1}^{4}(-1)^i f_i \end{bmatrix}$$

where $T = \sum_{i=1}^{4} f_i$ is the total thrust, h is the distance from the center of mass to the rotor, and c is the drag factor coefficient. It is easy to verify that equations (4.2a)-(4.2b) can actually be written as

$$
\begin{aligned}
\ddot{\phi} &= r_1\dot{\theta}\dot{\psi} - r_2\dot{\theta}w + q_1U_2 + d_\phi \\
\ddot{\theta} &= r_3\dot{\phi}\dot{\psi} + r_4\dot{\phi}w + q_2U_3 + d_\theta \\
\ddot{\psi} &= r_5\dot{\theta}\dot{\phi} + q_3U_4 + d_\psi \\
\ddot{x} &= (C_\phi S_\theta C_\psi + S_\phi S_\psi)\frac{1}{m}U_1 + d_x \\
\ddot{y} &= (C_\phi S_\theta S_\psi - S_\phi C_\psi)\frac{1}{m}U_1 + d_y \\
\ddot{z} &= -g + \frac{1}{m}(C_\phi C_\theta)U_1 + d_z
\end{aligned}
\tag{4.4}
$$

where $[U_1, U_2, U_3, U_4]^T = [T, T_{prop}]^T$ is the control input vector.

$$
\begin{aligned}
r_1 = \frac{I_y - I_z}{I_x}, r_2 = -\frac{J_r}{I_x}, r_3 = \frac{I_z - I_x}{I_y}, r_4 = \frac{J_r}{I_y}, \\
r_5 = \frac{I_x - I_y}{I_z}, q_1 = \frac{h}{I_x}, q_2 = \frac{h}{I_y}, q_3 = \frac{1}{I_z}
\end{aligned}
$$

are inertia related constants and $\omega = \omega_4 + \omega_3 - \omega_2 - \omega_1$.

The entire state vector X of the quadrotor model is defined as

$$
X = [p \;\; \dot{p} \;\; \Theta \;\; \dot{\Theta}]^T \in \mathbb{R}^{12}
$$

For transparency of further derivations, it is finally convenient to re-write equations (4.2a)-(4.2b) (or equivalently those in (4.4)) in the following block compact form

$$
\ddot{p} = -G + U_p + d_p \tag{4.5}
$$

$$
\ddot{\Theta} = \Phi(\Theta, \dot{\Theta}) + U_\Theta + d_\Theta \tag{4.6}
$$

with

$$
U_p := \frac{1}{m}R(\Theta)U_1 e_z; \tag{4.7}
$$

$$
U_\Theta := \Psi(\Theta)[U_2 \;\; U_3 \;\; U_4]^T \tag{4.8}
$$

4.3.1 Problem statement

The control objective in steering the quadrotor is stated as follows:

Control Objective for the Quadrotor

The goal is to design and analyze the performance of a bank of controllers that enable asymptotic tracking of the position of the center of mass and the yaw angle of the quadrotor: (p, ψ) to prescribed reference trajectories $p_r(t), \psi_r(t); t \geq 0$. The designed controllers are required to be robust with respect to the unknown force and torque disturbances d_p, d_Θ. The unknown disturbances are assumed to be uniformly bounded.

For the purpose of control design, the dynamic model (4.4) of the quadrotor is viewed as a system composed of two subsystems, the position subsystem (4.5), and the rotational subsystem (4.6). It is seen that the attitude subsystem is decoupled from the position subsystem and that it is fully input-output actuated, with the output defined as the attitude vector Θ. Also, its disturbances d_Θ are matched to the three components of the propeller torque vector. By contrast, the position subsystem is underactuated as its only control variable is the thrust force which can be used to attenuate the disturbance component d_z while leaving the disturbances d_x, d_y unmatched by the thrust control.

4.4 Super-twisting Sliding Mode Observer

In terms of flight performance, uncertainties cannot be neglected. The disturbance rejection task of tracking controllers may be much facilitated if the disturbances can be estimated online. Nonlinear disturbance observers will thus be employed that effectively allow decomposing d_p and d_Θ into

$$d_p = \hat{d}_p + e_{d_p}; \;\; d_\Theta = \hat{d}_\Theta + e_{d_\Theta} \tag{4.9}$$

where $\hat{d}_p$, $\hat{d}_\Theta$ represent the disturbances estimates while e_{d_p}, e_{d_Θ} are the observer errors to be attenuated by the controllers.

The high gain type observers suggested requiring strict assumptions about the matched as well as the unmatched disturbances in the model (4.4).

Assumption 4.1. *The disturbances d_p and d_Θ are assumed to be limited to the class of bounded differentiable functions with bounded derivatives, i.e.*

$$\|\dot{d}_p(t)\| \leqslant D_p, \;\; \|\dot{d}_\Theta(t)\| \leqslant D_\Theta \quad t > 0 \tag{4.10}$$

for some positive constants D_p, D_Θ.

$$\hat{\dot{p}} = f_p(X, T) + v_p \tag{4.11a}$$

$$\hat{\dot{\Theta}} = f_\Theta(X, T_{prop}) + v_\Theta \tag{4.11b}$$

where $\hat{\dot{p}}$, and $\hat{\dot{\Theta}}$ are the estimate of $\dot{p}$ and $\dot{\Theta}$ respectively. v_p and v_Θ are the injection terms that are defined below. The dynamics of estimation errors are derived as

$$\dot{e}_p = \ddot{p} - \hat{\ddot{p}} = d_p - v_p, \quad \dot{e}_\Theta = \hat{\ddot{\Theta}} - \ddot{\Theta} = d_\Theta - v_\Theta \tag{4.12}$$

Therefore, the auxiliary (observer) sliding variables, which dynamics are given by Eq. 4.12 can be stabilized by the second order sliding mode differentiators (Levant, 1998) that are introduced for each subsystem as follows:

$$\begin{aligned} v_p &= -\lambda_p |e_p|^{1/2} \mathrm{sign}(e_p) + u_p \\ \dot{u}_p &= -\alpha_p \mathrm{sign}(e_p) \end{aligned} \tag{4.13a}$$

$$\begin{aligned} v_\Theta &= -\lambda_\Theta |e_\Theta|^{1/2} \mathrm{sign}(e_\Theta) + u_\Theta \\ \dot{u}_\Theta &= -\alpha_\Theta \mathrm{sign}(e_\Theta) \end{aligned} \tag{4.13b}$$

where $\mathrm{sign}(e_p)$, $\mathrm{sign}(e_\Theta)$ are the extension of the signum function to vectors.
With sufficiently large gains λ_p, α_p, λ_Θ, and α_Θ, the estimation errors e_p and e_Θ converge to

zero in finite time. Therefore, the continuous super-twist control injection terms v_p and v_Θ will estimate exactly the disturbances d_p and d_Θ respectively.

$$\hat{d}_p = v_p, \quad \hat{d}_\Theta = v_\Theta \tag{4.14}$$

The proposed Lyapunov function of the super-twisting observer written in its quadratic form is $V_{sj} = \zeta_j^T P_j \zeta_j$, where $\zeta_j = [|e_j|^{\frac{1}{2}} sign(e_j), v_j]^T$ and P_j is a positive definite matrix defined as

$$P = \frac{1}{2}\begin{bmatrix} 4\alpha_j + \lambda_j^2 & -\lambda_j \\ -\lambda_j & 2 \end{bmatrix} \tag{4.15}$$

where $j = p, \Theta$. Notice that $V_{S\,j}(\zeta_j, t)$ is continuous but not differentiable at $e_j = 0$. In fact it is positive definite but radially unbounded if $\varrho_j > 0$, i.e.

$$\lambda_{min}(P_j) \parallel \zeta_j \parallel^2 \leq V_{S\,j}(e_j, v_j) \leq \lambda_{max}(P_j) \parallel \zeta_j \parallel^2 \tag{4.16}$$

where the Euclidean norm $\parallel \zeta_j \parallel^2$ of ζ_j is defined as $\parallel \zeta_j \parallel^2 = |e_j| + v_j^2$. The time derivative of the Lyapunov function defined above is

$$\dot{V}_{S\,j} = -\frac{1}{|e_j|^{\frac{1}{2}}} \zeta_j^T Q_j \zeta_j \tag{4.17}$$

where

$$Q_j = \frac{\lambda_j}{2}\begin{bmatrix} 2\alpha_j + \lambda_j^2 - (\frac{4\alpha_j}{\lambda_j} + \lambda_j)\iota_j & -\lambda_j - 2\iota_j \\ -\lambda_j - 2\iota_j & 1 \end{bmatrix} \tag{4.18}$$

where ι_j is positive constant. It can be noted that $\dot{V}_{S\,j}$ is negative definite if $Q_j > 0$. Furthermore, from Eq. 4.16, we deduce the following inequality:

$$|e_j|^{\frac{1}{2}} \leq \parallel \zeta_j \parallel \leq \frac{V_{S\,j}(\zeta_j)^{\frac{1}{2}}}{\lambda_{min}^{\frac{1}{2}}(P)} \tag{4.19}$$

We can then conclude that $\dot{V}_{S\,j}$ satisfies

$$\dot{V}_{S\,j} \leq -\varsigma_j V_{S\,j}^{\frac{1}{2}}(\zeta_j) \tag{4.20}$$

where $\varsigma_j = (\lambda_{min}^{\frac{1}{2}}(P)\lambda_{min}(Q)/\lambda_{max}(P)$.
The previous result guarantees the finite time convergence of e_j to zero and reaches this value at the bounded time $T = (2V_{S\,j}^{\frac{1}{2}}(\zeta(0))/\varsigma_j$, where $\zeta_j(0)$ is the initial value of ζ_j for $j = p, \Theta$. Eq.4.20 can be re-written for both subsystems as

$$\begin{aligned} \dot{V}_{S\,p} &\leq -\varsigma_p V_{S\,p}^{\frac{1}{2}}(\zeta_p) \\ \dot{V}_{S\,\Theta} &\leq -\varsigma_\Theta V_{S\,\Theta}^{\frac{1}{2}}(\zeta_\Theta) \end{aligned} \tag{4.21}$$

4.5 Tracking control laws for second order systems in vector form

Towards the design of the tracking control, it is first noted that the attitude and position subsystems (4.5) and (4.6) are only coupled by the attitude vector Θ. It is also easy to verify that the mapping of the four motor forces to the propeller torques and thrust force: $[f_1, \cdots, f_4] \mapsto [T_{prop}; T]$ is invertible, thus it can be assumed that the position and attitude controls, U_1 and $[U_2, U_3, U_4]$, are acting independently. The attitude subsystem (4.6) is an uncertain second order system in vector form whose output, the attitude vector Θ, is fully actuated by its three-dimensional control U_Θ. A fortunate property of this subsystem is that the unknown disturbances that affect it are fully matched by the controls U_Θ. What is implied is that, if known, the disturbances d_Θ can be instantaneously canceled by the action of the control U_Θ.

Prior to approaching the tracking control design for the whole quadrotor system, it is hence justified to present a few results pertaining to the construction of tracking control laws for general, fully actuated, but uncertain second order systems in vector form. This general system is important because the Lagrangian equations for the motion of a fully actuated rigid body are one example of this class. Other, possibly more robust and more flexible methods for

the solution of the same problem can be derived adapting the vector stabilization approaches presented in (Adegas & Stoustrup; Henrion *et al.*, 2003).

The uncertain second order systems considered here are assumed to take the form of a vector double integrator

$$\begin{bmatrix} \dot{x}_1 \\ \dot{x}_2 \end{bmatrix} = \begin{bmatrix} 0 & I \\ 0 & 0 \end{bmatrix} \begin{bmatrix} x_1 \\ x_2 \end{bmatrix} + \begin{bmatrix} 0 \\ U \end{bmatrix} + \begin{bmatrix} 0 \\ \hat{d} \end{bmatrix} + \begin{bmatrix} 0 \\ e_d \end{bmatrix} \tag{4.22}$$

$$y = x_1 \tag{4.23}$$

with, generally, n-dimensional control, disturbance, state and output vectors, i.e. $U, \hat{d}, e_d, y, x_i \in \mathbb{R}^n$; $i = 1, 2$. It is seen that the above system is fully actuated as an input-output mapping: $U \mapsto y$, and that all disturbances are matched to the controls U. The following will be used :

Lemma 4.1. *For all vectors* $x, y \in \mathbb{R}^n$

$$|x^T y| \leq \frac{1}{2}||x||^2 + \frac{1}{2}||y||^2 \tag{4.24}$$

Proof. It suffices to prove the inequality for the case when $x^T y > 0$. The result follows immediately by rearranging the quadratic inequality

$$0 \leq (x-y)^T (x-y) = x^T x - 2x^T y + y^T y \tag{4.25}$$

Assumption 4.2.

- *The disturbance* $\hat{d}$ *is considered known while the disturbance* e_d *is an unknown function of time, which is, however, assumed bounded by a known constant D, i.e.*

$$||e_d(t)|| \leq D \ \ for\ all \quad t \in [0, \infty) \tag{4.26}$$

- *The reference trajectory to be tracked, denoted by:* $x_{1r}(t); t \geq 0,\ x_{1r}(t) \in \mathbb{R}^n$*, is required to be a twice continuously differentiable vector function of time.*

- *The full system state* $[x_1(t), x_2(t)]; t \geq 0$*, is available for feedback control and the control* U *is unconstrained.*

Remark 4.1. *The known disturbance* $\hat{d}$ *can include known nonlinear functions of time and system states, possibly combined with on-line estimates of unknown system disturbances, if the latter are available. The unknown disturbance functions* e_d *can represent remaining uncertainties in the system such as estimation errors of any nonlinear disturbance observers employed. It is also seen that the integrator chains of* (4.22) *are fully actuated and that the functions* $\hat{d}$ *and* e_d *can both be considered as "matched disturbances" in* (4.22) *controlled by* U*.*

With the control goal of tracking the prescribed reference trajectory $x_{1r}(t); t \geq 0$, the following results analyze basic closed-loop tracking control methods, with and without the effect of the unknown disturbances. The first method, analyzed in Proposition 4.1, relies exclusively on the magnitude of the gains to ensure the desired precision of tracking and robustness to disturbances (i.e. attenuation of unknown disturbances). The advantage is smooth tracking control. The second method, analyzed in Proposition 4.2, employs a variant of sliding mode control in combination with gain tuning to achieve finite time convergence to the second order tracking manifold, simultaneously featuring stronger robustness properties in asymptotic tracking.

Proposition 4.1. *(Smooth high gain tracking control)*
Consider a system in vector form (4.22) *under Assumptions 4.2.*

Part A (Unknown disturbances are absent i.e. $e_d \equiv 0$)
Assuming that the disturbance vector $\hat{d}$ is known, the unknown disturbances are absent, $e_d \equiv 0$, and the control vector U is unconstrained, the closed loop system (4.22) with the control law employing any strictly positive gain matrices $K_1, K_2 \in \mathbb{R}^{n \times n}$, $K_1 > 0.5I$, $K_2 > 0.5I$,

$$\begin{aligned} U^H(x_1, x_2, x_{1r}, \hat{d}) &:= (K_2 + K_1)(\dot{x}_{1r} - x_2) \\ &+ K_2 K_1 (x_{1r} - x_1) + \ddot{x}_{1r} - \hat{d} \end{aligned} \tag{4.27}$$

achieves asymptotic tracking of any prescribed vector reference trajectory $x_{1r}(t), t \geq 0$, in the sense that

$$\|x_1 - x_{1r}\| \to 0 \text{ and } \|\dot{x}_1 - \dot{x}_{1r}\| \to 0 \quad \text{as } t \to \infty \tag{4.28}$$

Part B (Unknown disturbances are present)
Assuming that the disturbance vector $\hat{d}$ is known, the unknown disturbances are bounded by (4.26), and the control vector U is unconstrained, then for any constant $\epsilon > 0$, there exist control gains $K_1, K_2 \in \mathbb{R}^{n \times n}$ such that the tracking error for system (4.22) in closed loop with the control law (4.27) is asymptotically bounded as follows

$$\|x_1(t) - x_{1r}(t)\|^2 + \|x_2(t) - \dot{x}_{1r}(t)\|^2 \leq \epsilon \tag{4.29}$$

for all $t \geq T^*$, for a sufficiently large time $T^* > 0$.

Proof. (*Part A) Define two new vector variables as functions of the state vectors x_1, x_2 and the vector reference trajectory x_{1r} with time derivative $\dot{x}_{1r}$:*

$$e_1 := x_{1r} - x_1 \tag{4.30}$$

$$e_2 := \dot{x}_{1r} - x_2 + K_1 e_1 = \dot{x}_{1r} - \dot{x}_1 + K_1 e_1 \tag{4.31}$$

$$= \dot{x}_{1r} - x_2 + K_1(x_{1r} - x_1) \tag{4.32}$$

for any given strictly positive definite matrix $K_1 > 0$. The following implications then clearly hold as $t \to \infty$:

$$\{e_1 \to 0\} \implies \{x_1 \to x_{1r}\} \tag{4.33}$$

$$\{e_2 \to 0\} \implies \{\dot{x}_1 \to \dot{x}_{1r}\} \tag{4.34}$$

as is required. To construct a control that results in the above, consider the Lyapunov function

$$V_e := \frac{1}{2}[e_1^T e_1 + e_2^T e_2] \tag{4.35}$$

Definitions (4.30) - (4.31) *combined with the system equations* (4.22) *imply the following expressions for the derivatives*

$$\begin{aligned} \dot{e}_1 &= \dot{x}_{1r} - \dot{x}_1 = -K_1 e_1 + e_2 \qquad (4.36)\\ &= -K_1 e_1 + (\dot{x}_{1r} - x_2 + K_1 e_1) = \dot{x}_{1r} - x_2 \\ \dot{e}_2 &= \ddot{x}_{1r} - \dot{x}_2 + K_1 \dot{e}_1 \\ &= \ddot{x}_{1r} + K_1 \dot{e}_1 - U - \hat{d} \qquad (4.37) \end{aligned}$$

Hence, using (4.36) - (4.37)*, gives*

$$\begin{aligned} \dot{V}_e &= e_1^T \dot{e}_1 + e_2^T \dot{e}_2 \\ &= -e_1^T K_1 e_1 + e_1^T e_2 + e_2^T (\ddot{x}_{1r} + K_1 \dot{e}_1 - U - \hat{d}) \qquad (4.38) \end{aligned}$$

Let the control U solve

$$-K_2 e_2 = +\ddot{x}_{1r} + K_1 \dot{e}_1 - U - \hat{d} \tag{4.39}$$

By virtue of (4.30) - (4.32)*, and* (4.36) - (4.37)*, the solution is*

$$\begin{aligned} U^H &:= K_2 e_2 + K_1 \dot{e}_1 + \ddot{x}_{1r} - \hat{d} \\ &= K_2[(\dot{x}_{1r} - x_2) + K_1(x_{1r} - x_1)] + K_1[\dot{x}_{1r} - x_2] \\ &\quad + \ddot{x}_{1r} - \hat{d} \qquad (4.40) \\ &= (K_2 + K_1)(\dot{x}_{1r} - x_2) + K_2 K_1 (x_{1r} - x_1) \\ &\quad + \ddot{x}_{1r} - \hat{d} \qquad (4.41) \end{aligned}$$

From Lemma 4.1

$$e_1^T e_2 \leq \frac{1}{2}\|e_1\|^2 + \frac{1}{2}\|e_2\|^2 \tag{4.42}$$

Using this fact in (4.38) *with control* U^H *yields*

$$\begin{aligned} \dot{V}_e &= -e_1^T K_1 e_1 + e_1^T e_2 - e_2^T K_2 e_2 \\ &\leq -e_1^T (K_1 - 0.5I) e_1 - e_2^T (K_2 - 0.5I) e_2 < 0 \quad \textit{for } t \geq 0 \end{aligned} \tag{4.43}$$

provided that $K_1, K_2 > 0.5I$. *Inequality* (4.43) *then proves* (4.33) - (4.34) *and thus* (4.28) *with the tracking control as in* (4.27).

Proof. (*Part B) If the unknown disturbance is nonzero then equation* (4.37) *becomes*

$$\begin{aligned} \dot{e}_2 &= \ddot{x}_{1r} + K_1 \dot{e}_1 - \dot{x}_2 \\ &= \ddot{x}_{1r} + K_1 \dot{e}_1 - U - \hat{d} - e_d \end{aligned} \tag{4.44}$$

With the control law still satisfying (4.39)*, the inequality* (4.38) *involves an additional term*

$$\begin{aligned} \dot{V}_e &= -e_1^T K_1 e_1 + e_1^T e_2 + e_2^T (\ddot{x}_{1r} + K_1 \dot{e}_1 - U - \hat{d} - e_d) \\ &\leq -e_1^T (K_1 - 0.5I) e_1 - e_2^T (K_2 - 0.5I) e_2 - e_2^T e_d \end{aligned} \tag{4.45}$$

By Lemma 4.1

$$-e_2^T e_d \leq \frac{1}{2}\|e_2\|^2 + \frac{1}{2}\|e_d\|^2 \tag{4.46}$$

Letting $K_i, i = 1,2$ *satisfy* $K_i - 0.5I \geq k_i I_{n\times n}$*, for some constants* $k_1 > 0, k_2 > 0.5$*, inequality* (4.45) *combines with* (4.46) *and the bound* (4.26) *to yield*

$$\begin{aligned}\dot{V}_e &\leq -k_1 e_1^T e_1 - (k_2 - \frac{1}{2}) e_2^T e_2 + \frac{D^2}{2} \\ &\leq -\alpha V_e + \frac{D^2}{2} \end{aligned} \tag{4.47}$$

for $\alpha := 2\ min\{k_1, k_2 - 0.5\}$. *Invoking Proposition 4.1 proves* (4.29).

When the initial conditions of the system (4.22) are far from the reference trajectory the tracking control of Proposition 4.1 can be enhanced by introducing an additional sliding mode control term, as presented and analyzed below. This result does not require separate consideration of the case with unknown disturbances as the latter can be attenuated by the power of the sliding mode control alone.

Proposition 4.2. *(First order sliding mode tracking control)*
Consider a system in vector form (4.22) *under Assumptions 4.2. Let the tracking error variables be defined as in Proposition 4.1.*

For simplicity of analysis it will be assumed that the tunable controller gains K_1, K_2 in the control law proposed below will take, or else be majorized by, the respective simple forms: $K_1 := k_1 I_{n\times n}$, $K_2 := k_2 I_{n\times n}$ for some constants $k_1 > 0.5$, $k_2 > 0$ to be selected in specific applications. Defining a sliding surface as

$$S(x_1, x_2) := e_2 = 0 \tag{4.48}$$

the tracking control (4.27) of Proposition 4.2 is augmented by a sliding mode control term as follows:

$$\begin{aligned} U^S(x_1, x_2, x_{1r}, \hat{d}) &:= (K_2 + K_1)(\dot{x}_{1r} - x_2) \\ &+ K_2 K_1 (x_{1r} - x_1) + \ddot{x}_{1r} - \hat{d} \\ &+ A\ \text{sign}[(\dot{x}_{1r} - x_2) + K_1 (x_{1r} - x_1)] \end{aligned} \tag{4.49}$$

where $A := \text{diag}\{a_1, a_2, \cdots, a_n\}$, $a_i > D, i = 1, \cdots, n$, and for any vector $v \in \mathbb{R}^n$, the term A sign(v) represents a column vector whose components are: $a_i \text{sign}(v_i), i = 1, \cdots, n$.

Under these assumptions, for any initial conditions $[x_1(0), x_2(0)]$ of the system at $t = 0$, the trajectories of the closed loop system using the control law U^S reach the sliding surface $e_2 = 0$ in finite time t^* bounded by

$$t^* \leq 2 \max_i \left\{ \frac{|e_{2i}(0)|}{(a_i - D)} \right\} \tag{4.50}$$

In the absence of unknown disturbances the closed loop system trajectories remain on the sliding surface $e_2 \equiv 0$ for all times $t \geq t^*$. The system trajectories converge asymptotically to the desired reference trajectory, i.e. as $t \to \infty$:

$$\{e_1 \to 0\} \implies \{x_1 \to x_{1r}\} \tag{4.51}$$

$$\{e_2 \to 0\} \implies \{\dot{x}_1 \to \dot{x}_{1r}\} \tag{4.52}$$

The equivalent control in sliding mode is derived from the equality $\dot{S} = 0$ (with the disturbance $e_d = 0$ set to zero) thus

$$\begin{aligned} U_{eq}^S &= \ddot{x}_{1r} + K_1 \dot{e}_1 - \hat{d} \\ &= \ddot{x}_{1r} + K_1[\dot{x}_{1r}(t) - x_2(t)] - \hat{d} \end{aligned} \tag{4.53}$$

The system dynamics in sliding regime is

$$\begin{aligned} &\frac{d}{dt} x_1(t) = \dot{x}_{1r}(t) - K_1[x_1(t) - x_{1r}(t)]; \\ &\text{i..e.} \quad \frac{d}{dt} e_1(t) = -K_1 e_1(t); \quad t \geq t^* \end{aligned} \tag{4.54}$$

Proof. Employing the same definitions for the variables e_1 and e_2 as in (4.30) - (4.31), and the same Lyapunov function as that in (4.35), its derivative is

$$\dot{V}_e = e_1^T \dot{e}_1 + e_2^T \dot{e}_2 \tag{4.55}$$

$$= -e_1^T K_1 e_1 + e_1^T e_2 \tag{4.56}$$

$$+ e_2^T (\ddot{x}_{1r} + K_1 \dot{e}_1 - U^S - \hat{d} - e_d)$$

$$\text{with} \quad \dot{e}_2 = \ddot{x}_{1r} + K_1 \dot{e}_1 - U^S - \hat{d} - e_d \tag{4.57}$$

Let U^S satisfies

$$-A \text{ sign}(e_2) - K_2 e_2 = \ddot{x}_{1r} + K_1 \dot{e}_1 - U^S - \hat{d} \tag{4.58}$$

It follows that

$$U^S := K_2 e_2 + A \text{ sign}(e_2) + K_1 \dot{e}_1 + \ddot{x}_{1r} - \hat{d}$$

$$= K_2[(\dot{x}_{1r} - x_2) + K_1(x_{1r} - x_1)] + K_1(\dot{x}_{1r} - x_2)$$

$$+ \ddot{x}_{1r} - \hat{d} + A \text{ sign}(e_2) \tag{4.59}$$

$$= (K_2 + K_1)(\dot{x}_{1r} - x_2) + K_2 K_1 (x_{1r} - x_1)$$

$$+ \ddot{x}_{1r} - \hat{d}$$

$$+ A \text{ sign}[(\dot{x}_{1r} - x_2) + K_1(x_{1r} - x_1)] \tag{4.60}$$

which confirms (4.49). After substituting U^S into (4.57)

$$\dot{e}_2 = -K_2 e_2 - A \text{ sign}(e_2) - e_d \tag{4.61}$$

With $e_{2i}, e_{di}; i = 1, \cdots, n$, denoting the entries of the vectors e_2 and e_d, respectively, (4.61) rewrites componentwise as

$$\dot{e}_{2i} = -k_2 e_{2i} - a_i \text{ sign}(e_{2i}) - e_{di}; \quad i = 1, \cdots n \tag{4.62}$$

Multiplying by e_{2i} gives

$$e_{2i}\dot{e}_{2i} = \frac{1}{2}\frac{d}{dt}e_{2i}^2 = -k_2 e_{2i}^2 - a_i|e_{2i}| - e_{2i}e_{di};$$
$$\leq -k_2 e_{2i}^2 - (a_i - D)|e_{2i}| \tag{4.63}$$
$$\leq -(a_i - D)|e_{2i}| \quad i = 1, \cdots n \tag{4.64}$$

because $k_2 > 0$ and

$$-e_{2i}e_{di} \leq |e_{2i}e_{di}| \leq D|e_{2i}| \tag{4.65}$$
$$\text{with } |e_{di}| \leq \|e_d\| \leq D \quad \text{for all } \ i = 1, \cdots, n. \tag{4.66}$$

From Lemma 4.1

$$e_1^T e_2 \leq \frac{1}{2}\|e_1\|^2 + \frac{1}{2}\|e_2\|^2 \tag{4.67}$$

so, using (4.63) in (4.56), yields

$$\dot{V}_e = -k_1 e_1^T e_1 + e_1^T e_2 + e_2^T \dot{e}_2$$
$$\leq -(k_1 - 0.5)e_1^T e_1 - (k_2 - 0.5)e_2^T e_2 \tag{4.68}$$
$$-(a_i - D)|e_{2i}| < 0 \quad t \geq 0 \tag{4.69}$$

provided that $a_i > D$ for all $i = 1, \cdots, n$ and $k_1 > 0.5$, $k_2 > 0.5$.

Without the loss of generality assume that $e_{2i}(0) > 0$; then (4.63) implies

$$2e_{2i}\frac{d}{dt}e_{2i} \leq -(a_i - D)e_{2i}$$
$$\text{i.e} \quad \frac{d}{dt}e_{2i} \leq -\frac{1}{2}(a_i - D) \tag{4.70}$$

Integrating the above on the interval $[0, t_i^*]$ where t_i^* is the finite reaching time for component e_{2i} renders the bound

$$
\begin{aligned}
e_{2i}(t_i^*) - e_{2i}(0) &\leq -\frac{1}{2}(a_i - D)(t_i^* - 0) \\
\implies t_i^* &\leq 2\frac{e_{2i}(0)}{(a_i - D)}
\end{aligned} \tag{4.71}
$$

as $e_{2i}(t_i^*) = 0$. Generalizing to the case of $e_{2i}(0) < 0$ and taking a maximum over i yields the total bound (4.50).

Inequality (4.68) then immediately implies the validity of (4.51) - (4.52). The dynamics in the sliding mode (4.54) is obtained by setting $e_2 = 0$ in (4.32) and the equivalent control (4.53) is calculated by assuming that $\dot{e}_2 = 0$ and $e_d = 0$ in (4.57).

Remark 4.2. *In terms of the tracking errors e_1 and e_2 as defined by* (4.30) - (4.31)*, and with the $\dot{e}_1$ given in* (4.36)*, the expressions for the control laws U^H and U^S of Propositions 4.1 and 4.2, respectively, are given by*

$$
\begin{aligned}
U^H &= K_2 e_2 + K_1 \dot{e}_1 + \ddot{x}_{1r} - \hat{d} \\
&= K_2 e_2 + K_1(-K_1 e_1 + e_2) + \ddot{x}_{1r} - \hat{d} \\
&= (K_1 + K_2) e_2 + (1 + K_1^2) e_1 + \ddot{x}_{1r} - \hat{d}
\end{aligned} \tag{4.72}
$$

$$
\begin{aligned}
U^S &= K_2 e_2 + A\ sign(e_2) + K_1 \dot{e}_1 + \ddot{x}_{1r} - \hat{d} \\
&= (K_1 + K_2) e_2 + (1 + K_1^2) e_1 \\
&\quad + A\ sign(e_2) + \ddot{x}_{1r} - \hat{d}
\end{aligned} \tag{4.73}
$$

There are several practical implementations of the signum function in the sliding mode control (4.49) that allows attenuating the undesirable phenomenon of chattering; (O'Toole *et al.*, 2010b). Here, a simple saturation function with constant boundary layer was employed.
The output of the sliding mode controller is additionally smoothed by the presence of the inertial term $-K_2 e_2$ in the sliding mode equation (4.61). This explains the absence of chattering behavior in simulation results.

Remark 4.3. *The result of Proposition 4.3 indicates that the adverse effect of the unknown system disturbances can be effectively eliminated by the inherent robustness properties of the sliding mode control. This can be achieved because the disturbance and control variables in system* (4.22) *are fully matched and the disturbances are bounded in magnitude. Similar disturbance robustness properties are not shared by the smooth high gain tracking control of Proposition 2 as the disturbances cannot be dominated by any component of that control. By contrast, such domination is accomplished by the scaled signum function in the sliding mode. Additionally, the sliding mode control provides a very effective means of adjusting the speed of convergence to the desired reference trajectory by increasing the gains A and* K_1*, see equations* (4.50) *and* (4.54).

When smooth control is a priority, the tracking control quality must be traded for limited tracking precision and speed of convergence unless the system disturbances are fully known or else can be estimated with zero asymptotic error.
The disturbance observer developed in the preceding section can prove the following useful characteristics:

- provide disturbance estimates with a desired bound on the estimation error, hence securing "double tracking precision" in a closed loop with the smooth control law if its gains are limited in magnitude ;
- indirectly decrease the bound on the unknown disturbances in a closed loop with the sliding mode controller; see the decompositions (4.9), thus reducing the control effort (decreasing the magnitude of the gains) and increasing the speed of convergence.

4.6 Tracking control design for the quadrotor

The position subsystem (4.5) is clearly not in the form of (4.22). Specifically, this is because the components of the control vector $U \in \mathbb{R}^3$ of (4.22), now considered as a member of $\mathbb{R}^3$, are explicitely assumed to be functionally independent and unconstrained. By contrast, if the position subsystem (4.5) were to match the form and assumptions of (4.22), then it would have

to hold that

$$U(t) = \frac{1}{m} R(\Theta(t)) T(t) e_z \quad \text{for all } t \geq 0 \tag{4.74}$$

for any desired value of the control vector $U(t)$ and any value of the attitude state vector $\Theta(t)$ of the evolving attitude subsystem. As the value of $T(t)$ is a scalar, this is impossible as the control vector $U(t)$ is clearly aligned with the vector $R(\Theta(t))e_z$ for all times t. Implied is also the fact that in the position subsystem the disturbances are not matched with the control (the disturbances cannot be cancelled instantaneously by the choice of the thrust force alone).

To find a way in which to resolve these difficulties, hypothesize that the control constraint in the position subsystem can somehow be relaxed by way of substituting it with

$$U(t) = \frac{1}{m} R(\Theta_r(t)) T(t) e_z \quad \text{for all } t \geq 0 \tag{4.75}$$

where $\Theta_r(t) := (\psi_r(t), \theta_r(t), \phi_r(t))$, with the yaw angle trajectory imposed as a reference $\psi_r(t)$ and the trajectories $\theta_r(t), \phi_r(t)$ to be chosen freely together with the value of the thrust force $T(t)$ to match any desired value of the right hand side control vector $U(t)$. Then, the position control law of Proposition 4.2 could be applied to steer the position system as required. By making the following variable substitutions in the generic second order tracking system (4.22) with $n = 3$:

$$\begin{aligned} &x_1 := p;\ x_2 := \dot{p};\ x_{1r} := p_r; \\ &\hat{d} := \hat{d}_p + G;\ U^H := U_p \end{aligned} \tag{4.76}$$

the control law for tracking a given spatial reference position p_r would be given by

$$\begin{aligned} U_p := &(K_{1p} + K_{2p})(\dot{p}_r - \dot{p}) + K_{2p} K_{1p} (p_r - p) \\ &+ \ddot{p}_r - \hat{d}_p - G \end{aligned} \tag{4.77}$$

where it is assumed that the actual position and velocity vectors p and $\dot{p}$ would be available from on-line measurement. The control law U_p (4.77) will henceforward be referred to as the "desired" position control because it would have to be "reconciled" with the U of (4.75) as, generally, $\Theta(t) \neq \Theta_r(t)$.

On the other hand, the attitude subsystem is fully actuated. As will become clear, the precision, robustness, and speed of the tracking attitude control will prove primordial towards achieving the overall tracking goal of combined position and yaw angle of the rotorcraft. Sliding mode control is hence better suited to attain tracking of the attitude. To this end the disturbance vector d_Θ is considered estimated and the following variable substitutions are made in (4.22) with $n = 3$:

$$\begin{aligned} &x_1 := \Theta;\ x_2 := \dot{\Theta};\ x_{1r} := \Theta_r; \\ &\hat{d} := \hat{d}_\Theta + \Phi(\Theta, \dot{\Theta});\ U^S := U_\Theta \end{aligned} \tag{4.78}$$

to deliver the sliding mode tracking law for the entire Θ_r with suitably chosen gain matrices A, $K_3 > 0.5I, K_4 > 0.5I$ as in Proposition 4.3.

$$\begin{aligned} U_\Theta := &(K_{1\Theta} + K_{2\Theta})(\dot{\Theta}_r - \dot{\Theta}) + K_{2\Theta}K_{1\Theta}(\Theta_r - \Theta) \\ &+ \ddot{\Theta}_r - \hat{d}_\Theta - \Phi(\Theta, \dot{\Theta}) \\ &+ A_\Theta \ \text{sign}[(\dot{\Theta}_r - \dot{\Theta}) + K_{1\Theta}(\Theta_r - \Theta)] \end{aligned} \tag{4.79}$$

It is again assumed that the angular position and velocity vectors Θ and $\dot{\Theta}$ are available from on-line measurement.

The discontinuous function sign(.) in the control law (4.79) is replaced by a continuous function to reduce the effect of the chattering in the control signal. For instance, the signum function sign(.) can be replaced by the following function (O'Toole *et al.*, 2010b)

$$\text{sign}(s) = \frac{s}{\|s\| + \varsigma} \tag{4.80}$$

where ς is a positive tuning parameter that smoothes the discontinuity. It is tuned manually to attenuate the chattering problem.

The above control laws are abstract in the sense that they cannot be applied directly to achieve the tracking goal as stated in section 4.4, if only for the reason that the "decoupling" virtual attitude needed in (4.75) is yet undefined. However, the idea is now clear as the number of the system variables to be tracked (x_r, y_r, z_r, ψ_r) matches the number of "free" control variables (U_1, U_2, U_3, U_4) so, indirectly, the tracking problem is fully actuated. The "virtual reference trajectories" $\theta_t(t), \phi_r(t); t \geq 0$, for the "free" attitude angles θ and ϕ can be imposed as to emulate independence of the three "desired" position control components (U_{xd}, U_{yd}, U_{zd}) of U_p in (4.77). Exact tracking of full attitude in $\mathbb{R}^3$ is feasible because the components of the attitude control $U_\Theta = [U_2, U_3, U_4]$ are unconstrained and matched to the unknown disturbances thus permitting simultaneous tracking of all the three attitude reference trajectories $(\psi_r, \theta_r, \phi_r)$.

To generate the aforementioned reference trajectories θ_r and ϕ_r, it is first convenient to re-state the explicit parametrization of the desired control $U_p = (U_{xd}, U_{yd}, U_{zd})$ as given by (4.77):

$$U_{xd} = (C_{\phi_r} S_{\theta_r} C_{\psi_r} + S_{\phi_r} S_{\psi_r}) \frac{U_{1d}}{m} \tag{4.81}$$

$$U_{yd} = (C_{\phi_r} S_{\theta_r} S_{\psi_r} - S_{\phi_r} C_{\psi_r}) \frac{U_{1d}}{m} \tag{4.82}$$

$$U_{zd} = (C_{\phi_r} C_{\theta_r}) \frac{U_{1d}}{m} \tag{4.83}$$

where, at this point, U_{1d} has the interpretation of a desired thrust force to be applied to the system. Multiplying (4.81) and (4.82) by C_{ψ_r} and S_{ψ_r}, respectively, and adding the result side by side yields

$$C_{\psi_r} U_{xd} + S_{\psi_r} U_{yd} = (C_{\phi_r} S_{\theta_r}) \frac{U_{1d}}{m} = \tan(\theta_r) U_{zd} \tag{4.84}$$

Similarly, multiplying (4.81) and (4.82) by S_{ψ_r} and $-C_{\psi_r}$, respectively, and adding the result side by side yields

$$S_{\psi_r} U_{xd} - C_{\psi_r} U_{yd} = S_{\phi_r} \frac{U_{1d}}{m} = \tan(\phi_r) \frac{U_{zd}}{C_\theta} \tag{4.85}$$

Hence, it follows that, given any desired values of U_{xd}, U_{yd} and $U_{zd} \neq 0$, that satisfy (4.77), and any reference value of the yaw angle ψ_r, one can impose corresponding "desired values" of the roll and pitch angles :

$$\theta_r = \arctan \frac{(C_{\psi_r} U_{xd} + S_{\psi_r} U_{yd})}{U_{zd}} \tag{4.86}$$

$$\phi_r = \arctan \frac{C_{\theta_r} (S_{\psi_r} U_{xd} - C_{\psi_r} U_{yd})}{U_{zd}} \tag{4.87}$$

so that any desired (U_{xd}, U_{yd}, U_{zd}) controls are replaced, albeit indirectly, by the "virtual controls" $(\theta_r, \phi_r, U_{1d})$.

The position and attitude control systems are coupled in such a way as to permit the desired attitude angles ϕ_r and θ_r and to be tracked by the attitude controller (see Fig. 4.2 implicitly using the position control law (4.77)).

Remark 4.4. *It should be noted that the four-quadrant inverse of the tangent function is a multivalued function comprising three separate branches. The reference angles in* (4.86) - (4.87) *will be computed from the principal branch of the arctan function only if the desired value of U_{zd} is strictly positive. In that case, the reference angles will lie in the set*

$$\mathcal{R} := \{(\phi_r, \theta_r) | \phi_r \in (-\frac{\pi}{2}, \frac{\pi}{2}); \theta_r \in (-\frac{\pi}{2}, \frac{\pi}{2})\} \tag{4.88}$$

which corresponds to the singularity free situation in which $C_{\phi_r} > 0, C_{\theta_r} > 0$ that also implies that:

- *the virtual reference trajectories $\phi_r(t), \theta_r(t); t \geq 0$, are twice continuously differentiable functions, as required by Propositions 4.1 and 4.2;*
- *the control thrust force applied to the quadrotor, denoted here by $T^A(t)$, is well defined and takes positive values for all $t > 0$.*

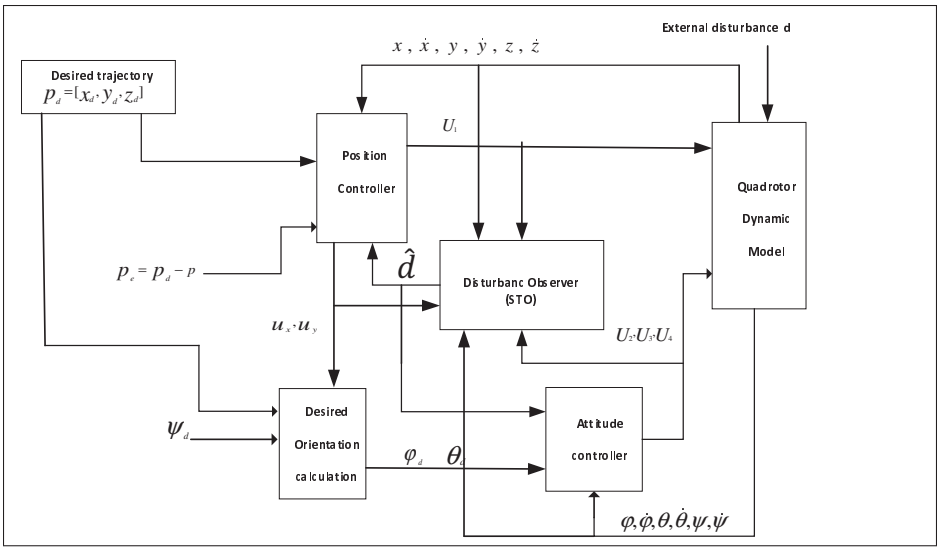

Figure 4.2 Block diagram of the proposed slidng mode control driven by STO design.

As the above conditions need to hold for the tracking control to be implementable, restrictions need to be imposed on the reference trajectories to be tracked, initial conditions of the system, as well as the control gains. This will be addressed in the next section.

The structure of the disturbance observer used here was introduced in (Yang *et al.*, 2013), but its analysis is much more detailed leading to a stronger property. The implementation of the combined tracking control law for the quadrotor is carried out as follows

Tracking control for the quadrotor

- Given the desired reference vector $(p_r(t), \psi_r(t))$ and the measured state $(p(t), \dot{p}(t))$ at any time instant t, the right hand side of (4.77) is first computed to yield the value of the desired control vector $(U_{xd}, U_{yd}, U_{zd})(t)$ for the position subsystem to track the given reference p_r.
- The corresponding virtual reference angles $(\theta_r(t), \phi_r(t))$ are next computed from the arctan functions in (4.86) - (4.87).

- Provided that $(\theta_r(t), \phi_r(t)) \in \mathcal{R}$, the actual position tracking control to be applied to the system, here denoted by U_p^A, is then given by; see (4.4):

$$U_p^A(t) = \frac{1}{m} R(\Theta(t)) T^A(t) e_z \tag{4.89}$$

where the thrust force function is calculated as

$$U_{1d}(t) := T^A(t) = m \frac{U_{zd}(t)}{C_{\phi_r(t)} C_{\theta_r(t)}} > 0 \tag{4.90}$$

- The attitude control U_Θ is computed as in (4.79) with its reference attitude trajectory

$$\Theta_r(t) = (\psi_r, \theta_r, \phi_r)(t) \tag{4.91}$$

and is applied to the system in the form of the torque vector

$$[U_2, U_3, U_4](t) = \Psi(\Theta(t))^{-1} U_\Theta(t); \quad t \geq 0 \tag{4.92}$$

Clearly, the applied position tracking control U_p^A is a function of both the measured attitude Θ and the virtual angles (θ_r, ϕ_r) and also U_{zd}.

Remark 4.5. *Note that U_p and U_p^A differ as the correct thrust force in U_p would be, as required by Proposition 4.2*

$$T(t) = m \frac{U_{zd}(t)}{C_{\phi(t)} C_{\theta(t)}} \tag{4.93}$$

rather than that of (4.90).

The difference of the control values $U_p^A(t)$ and $U_p = (U_{xd}, U_{yd}, U_{zd})(t)$ is then dependent on the convergence of the attitude subsystem trajectories to their full attitude reference $\Theta_r(t)$. By the results of Proposition 4.3, convergence rate to the attitude reference trajectory can be regulated as desired if the control gains are not limited in magnitude.

4.7 Observer based tracking control analysis

If the unknown disturbances d_p and d_Θ are estimated by their respective observers (4.11a)-(4.11b), the position and attitude closed loop subsystems with all their inaccuracies can be written as

$$\ddot{p} = G + U_p^A + \hat{d}_p + e_{d_p} + (U_p - U_p^A) \tag{4.94}$$

$$\ddot{\Theta} = \Phi(\Theta, \dot{\Theta}) + U_\Theta + \hat{d}_\Theta + e_{d_\Theta} \tag{4.95}$$

with the control laws U_p^A and U_Θ employing the estimates $\hat{d}_p$ and $\hat{d}_\Theta$ as in (4.89), (4.79), with the total unknown disturbances in the position and atttude subsystems defined as

$$e_p := e_{d_p} + (U_p - U_p^A) \tag{4.96}$$

$$e_\Theta := e_{d_\Theta} \tag{4.97}$$

For simplicity of the convergence analysis and without much loss of generality it will henceforth be assumed that all the controller gains are diagonal as given by:

$$\begin{aligned} &K_{ip} := k_{ip} I_{3\times 3};\ K_{i\Theta} := k_{i\Theta} I_{3\times 3};\ \ i = 1,2 \\ &A_\Theta := \text{diag}\{a_1, a_2, a_3\} \end{aligned} \tag{4.98}$$

for some positive constants $k_{ip}, k_{i\Theta}, a_k;\ i = 1,2, k = 1,2,3$.

As pointed out in Remark 4.4, the tracking control for the quadrotor is implementable only when the computed, desired altitude control component U_{zd} of U_p is strictly positive for all times.

Definition 4.1. *(Tracking control feasibility)*
The tracking control is feasible if the intial conditions of the system, the reference trajectories to be tracked $p_r(t), \psi_r(t); t \geq 0$, the ensemble of system disturbances, and the position controller

gains $k_{ip}, i = 1,2$*, are such that the computed attitude control component, and consequently the control thrust force satisfy*

$$U_{zd}(t) > 0,\ T^A(t) > 0; \quad \textit{for all } t \geq 0 \tag{4.99}$$

A brief discussion of sufficient conditions for the tracking control feasibility is in place. Since the position controller gains are assumed diagonal, the instantaneously desired altitude control component of U_p is computed as

$$\begin{aligned} U_{zd} &= (k_{1p} + k_{2p})e_{2p}(3) + (1 + k_{1p}^2)e_{1p}(3) + \ddot{z}_r \\ &\quad - \hat{d}_z + g \\ e_{1p}(3) &= z_r - z; \quad e_{2p}(3) = \dot{z}_r - \dot{z} + k_{1p}(z_r - z) \end{aligned} \tag{4.100}$$

see also (4.72), where $e_{ip}(3), i = 1,2$, denote the altitude i.e. z-components of the respective tracking errors. It is clear that a sufficient condition for U_{zd} to be positive is that the gravity term g defined in (4.2b) dominates the sum of all other terms in (4.100) at all times. Such a condition is clearly too conservative as some of the terms in (4.100) can be positive during tracking and especially during sustained ascent when $e_{1p}(3) > 0, \dot{e}_{1p}(3) > 0$ and $\ddot{z}_r > 0$. The same terms are, however, equally likely to be negative during descent and then the dominance of g might require reduction of the controller gains to preserve positivity of the thrust force during flight. In the case when the vertical disturbance d_z is estimated without any error (i.e. when $e_{d_p}(3) \equiv 0$) the vertical component of the tracking error eventually converges to zero, so

$$U_{zd} \to \ddot{z}_r - \hat{d}_z + g \quad \text{as } t \to \infty \tag{4.101}$$

If, additionally, the reference accelerations in altitude are asymptotically zero, the necessary condition for tracking control feasibility is the dominance of the vertical disturbance accelera-

tion by the gravitational one.

$$g > |\hat{d}_z(t)| \quad \text{for all } t \geq 0 \tag{4.102}$$

Clearly, this condition is generally not sufficient for control feasibility.

Remark 4.6. *In conclusion, the feasibility of the tracking control hinges entirely on the altitude control of the quadrotor. The vertical disturbance force must not exceed the gravitational force for the tracking control to be feasible, which is obvious from a practical point of view. Control feasibility is more likely to be lost during descent thus the sign of the calculated desired vertical component of the position control U_{zd} can be monitored and corrected by decreasing the controller gains adaptively during descent, if necessary.*

It is now straightforward to characterize the stability of the overall closed-loop tracking control system.

Theorem 4.1. *The quadrotor system in closed loop with the control laws of the form* (4.89) - (4.91)*,* (4.79)*, and indirectly by the desired law* (4.77)*, when coupled with the nonlinear estimators* (4.11a) - (4.11b) *of the unknown disturbances d_p and d_Θ, achieves the tracking goal as specified below.*

With the assumption that the tracking control problem is feasible as defined in Definition 4.1, with disturbances limited as in (4.102) *, let $p_r(t) \in \mathbb{R}^3$, $\psi_r(t) \in \mathbb{R}$, $t \geq 0$, be the twice continuously differentiable position and yaw angle reference trajectories to be tracked asymptotically. Given an admissible tolerance $\epsilon_{tol} > 0$ for the total asymptotic tracking error in the position and yaw angle (p, ψ), there exist position controller gains K_{1p}, K_{2p}, attitude controller gains $K_{1\Theta}, K_{2\Theta}, A_\Theta$, and a time $T^* > 0$ such that*

$$||p(t) - p_r(t)||^2 + |\psi(t) - \psi_r(t)|^2 \leq \epsilon_{tol} \ \textit{for } t \geq T^* \tag{4.103}$$

Proof. Since the disturbance observers do not depend directly on the action of the tracking controllers, let $T_E^* > 0$ be a time such that both disturbance observer estimation errors satisfy

$$\max\{\|e_{d_p}(t)\|^2, \|e_{d_\Theta}(t)\|^2\} \leq 0.25\epsilon_{tol}; \;\; t \geq T_E^* \tag{4.104}$$

By construction of the virtual attitude trajectory $\Theta_r(t); t \geq 0$, if the tracking control problem is feasible then θ_r, ϕ_r are analytic functions of their arguments, and since the reference trajectory ψ_r is twice differentiable, the following bound holds for the difference between the desired and applied position controls

$$\begin{aligned} &|U_p^A(t) - U_p(t)| \\ &\leq U_{zd}\|R(\Theta(t))e_z\| \left| \frac{1}{C_{\phi_r(t)}C_{\theta_r(t)}} - \frac{1}{C_{\phi(t)}C_{\theta(t)}} \right| \end{aligned} \tag{4.105}$$

for all $t \geq 0$. By continuity of trajectory $\Theta(t); t \geq 0$, there exists a constant $\delta_\Theta > 0$ such that

$$\begin{aligned} &|U_p^A(t) - U_p(t)| < \sqrt{0.25\epsilon_{tol}} \;\; \text{for all } t \text{ such that} \\ &\|\Theta(t) - \Theta_r(t)\| < \delta_\Theta \end{aligned} \tag{4.106}$$

where, without the loss of generality it can be assumed that $\delta_\Theta < \sqrt{0.5\epsilon_{tol}}$.

As already pointed out, convergence in the attitude tracking is completely independent of the performance of the position tracking control as the attitude subsystem is decoupled from the position subsystem and hence can be controlled independently. Given any attitude reference trajectory Θ_r the sliding mode attitude controller (4.79) in closed loop of the attitude subsystem dynamics can be tuned to deliver asymptotic tracking, in spite of its unknown disturbances e_Θ as in (4.97)

$$\|\Theta(t) - \Theta_r(t)\| \to 0 \;\; \text{as } t \to \infty \tag{4.107}$$

with any desired convergence rate provided the choice of controller gains $K_{1\Theta}, K_{2\theta}$ and A_Θ are unrestricted to permit full compensation of unknown disturbances. Then let $T^*_\Theta > 0$ be such that

$$\|\Theta(t) - \Theta_r(t)\|^2 \leq \delta_\Theta \leq 0.5\epsilon_{tol} \quad \text{for all } t \geq T^*_\Theta \tag{4.108}$$

It then follows from (4.104) - (4.105) that the total unknown disturbances (4.96) to be compensated for in the position subsystem are bounded by

$$\begin{aligned} \|e_p\|^2 \leq \|e_{d_p}\|^2 + |U^A_p(t) - U_p(t)|^2 \leq 0.5\epsilon_{tol} \\ \text{for all } t \geq \max\{T^*_E, T^*_\Theta\} \end{aligned} \tag{4.109}$$

By virtue of Proposition 4.2 there exist controller gains K_{1p}, K_{2p} and a time $T^*_p > 0$ such that

$$\|p(t) - p_r(t)\| \leq 0.5\epsilon_{tol} \quad \text{for all } t \geq T^*_p \tag{4.110}$$

in spite of the total unknown disturbances e_p as in (4.96). The inequality (4.103) then holds for

$$T^* := \max\{T_E, T^*_\Theta; T^*_p\} \tag{4.111}$$

This completes the convergence analysis of the observer-based tracking control for the quadrotor.

Remark 4.7. *The control design has so far disregarded constraints. Respecting constraints on actuators is critical in real flight conditions. Hence, it is imperative that future work focuses on more realistic and implementable control strategies.*

4.8 Results discussion

The quadrotor tracking control design described above was tested by way of computer simulations as well as on a real quadrotor system in the Control System Laboratory of École de

Technologie Supérieure (ETS), Montreal, Canada.

For the simulation and real flight trajectories to be comparable, the parameters of the real physical system (see Eq. (4.4)) had to be estimated first. To this end, we describe the estimation procedure in detail.

The mass of the quadrotor was simply obtained by weighing the device. However, obtaining the inertia moments was more complex. An RCbenchmark series 1580 dynamometer device was used to determine the relationship between the propellers' speeds and the forces exerted by the motors. A commercial quadrotor, S500 Glass Fiber Quadcopter Frame 480 mm - Integrated PCB was used as the experimental platform (see Figure 4.3). In order to verify the effectiveness of the proposed method, the physical parameters for the quadrotor UAV are summarized as :h= 0.225 m, $J_R = 3.357 \times 10^{-5}$ kg m^2, g= 9.81m/s^2, I_{xx} =0,0126 $kg.m^2$, I_{yy} =0,0125 $kg.m^2$, and I_{zz} =0,0235 $kg.m^2$.

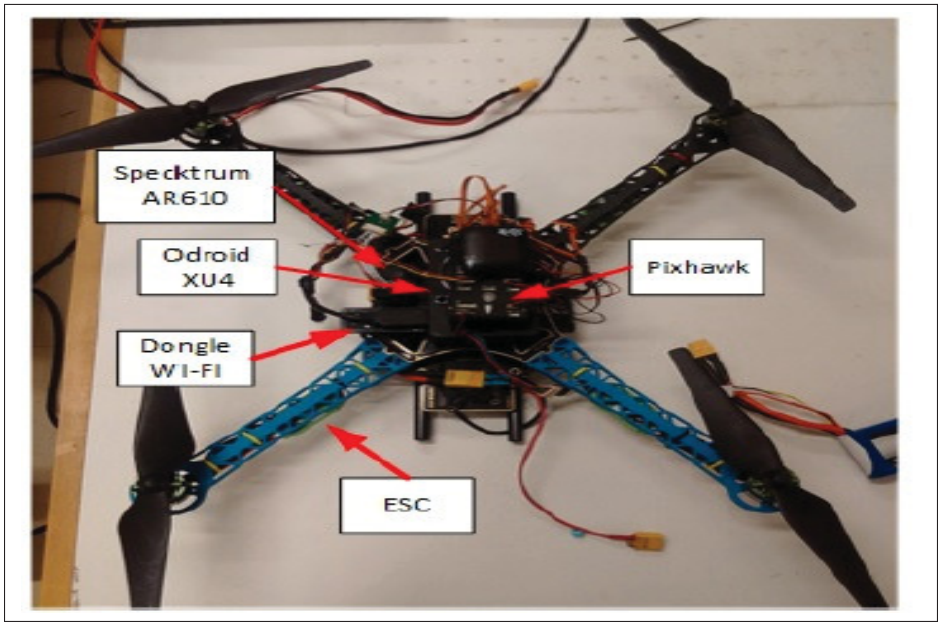

Figure 4.3 The quadrotor used in real flight tests.

4.8.1 Numerical Results

In the simulation, the quadrotor was required to follow the desired trajectory defined in Fig.4.4 for $t \geq 0$. Furthermore, the yaw angle reference trajectory was set at $x_{5r} = 0$ rad over the entire simulation horizon. For the purpose of the simulation, the external disturbance vector was considered as a "gust of wind" given by the functions

$$\begin{aligned} d_1 &= [d_x, d_y, d_z]^T \\ &= [1.5 + 2.5\sin(4t), 1.5 + 2.5\,\sin(4t), 1.5]N \\ d_2 &= [d_\phi, d_\theta, d_\psi]^T \\ &= [2.5\sin(4t), \sin(0.1t), \sin(0.1t)]^T Nm \end{aligned}$$

The position and attitude controller gains are 3×3 matrices: $K_{1p} = \text{diag}[k_{1x}, k_{1y}, k_{1z}]$, $K_{2p} = \text{diag}[k_{2x}, k_{2y}, k_{2z}]$, $K_{1\Theta} = \text{diag}[k_{1\phi}, k_{1\theta}, k_{1\psi}]$, $K_{2\Theta} = \text{diag}[k_{2\phi}, k_{2\theta}, k_{2\psi}]$, and $A = \text{diag}[A_\phi, A_\theta, A_\psi]$. Likewise, the super-twisting observer gains are 3×3 matrices: $\lambda_p = \text{diag}[\lambda_x, \lambda_y, \lambda_z]$, $\lambda_\Theta = \text{diag}[\lambda_\phi, \lambda_\theta, \lambda_\psi]$, $\alpha_p = \text{diag}[\alpha_x, \alpha_y, \alpha_z]$, and $\alpha_\Theta = \text{diag}[\alpha_\phi, \alpha_\theta, \alpha_\psi]$

All gains were tuned manually by trial and error in computer simulations. The best values of all gains, which secure the smallest tracking errors, are shown in Table 4.1.

Table 4.1 Used gains of the controller and observer

Gain	Value	Gain	Value	Gain	Value
k_{1x}	2.0313	λ_y	15	$k_{2\psi}$	10.861
k_{1y}	2.0313	λ_z	15	λ_ϕ	20
k_{1z}	2.216	$k_{1\phi}$	12.861	λ_ψ	20
k_{2x}	0.0313	$k_{1\theta}$	12.861	λ_θ	20
k_{2y}	0.0313	$k_{1\psi}$	12.861	A_ϕ	0.7
k_{2z}	0.216	$k_{2\phi}$	12.861	A_ψ	0.7
λ_x	15	$k_{2\theta}$	12.861	A_θ	0.7
α_x	15	α_y	12.861	α_z	0.7
α_ϕ	15	α_θ	12.861	α_ψ	0.7

The simulation results are shown in Fig. 4.4 - Fig. 4.8. It can be seen from Fig. 4.4 that the quadrotor can track the desired flight path correctly while compensating for the disturbances. Fig. 4.6 also shows good tracking of the attitude reference trajectory.

The plots of the errors in the position and attitude subsystems are presented in Fig. 4.5 and Fig. 4.7. It can be seen that the nonlinear disturbance observer can estimate the disturbances quickly and accurately. The control inputs of rotors are presented in Fig. 4.8. The obtained control inputs commands could easily be applied to the real model. Furthermore Fig. 4.9-Fig. 4.12 provide the estimation of disturbances and their errors for position and attitude systems.

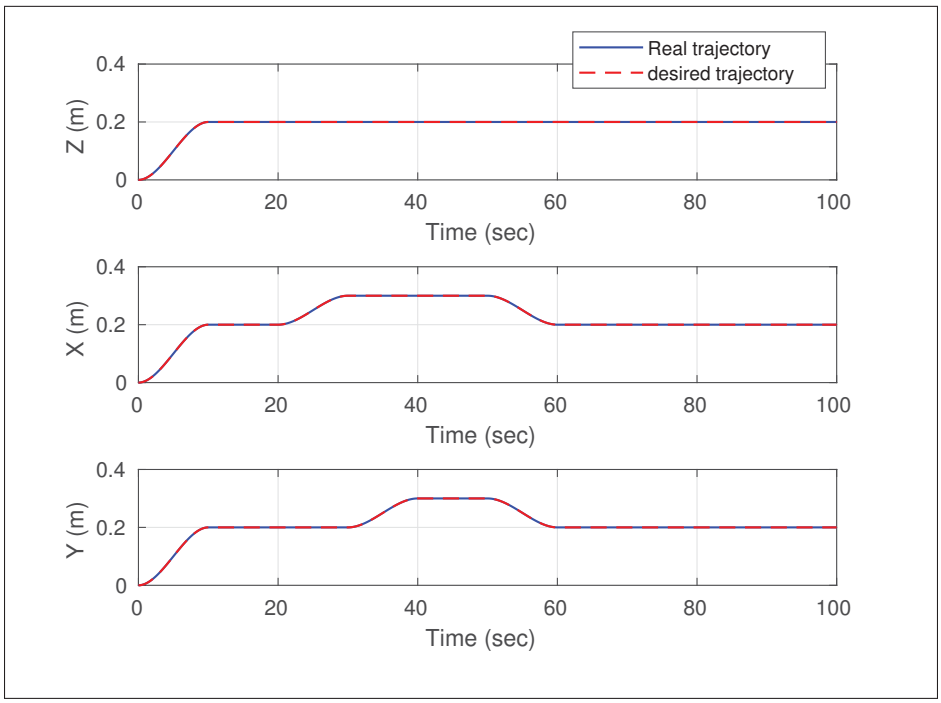

Figure 4.4 Position tracking in coordinates (x, y, z)

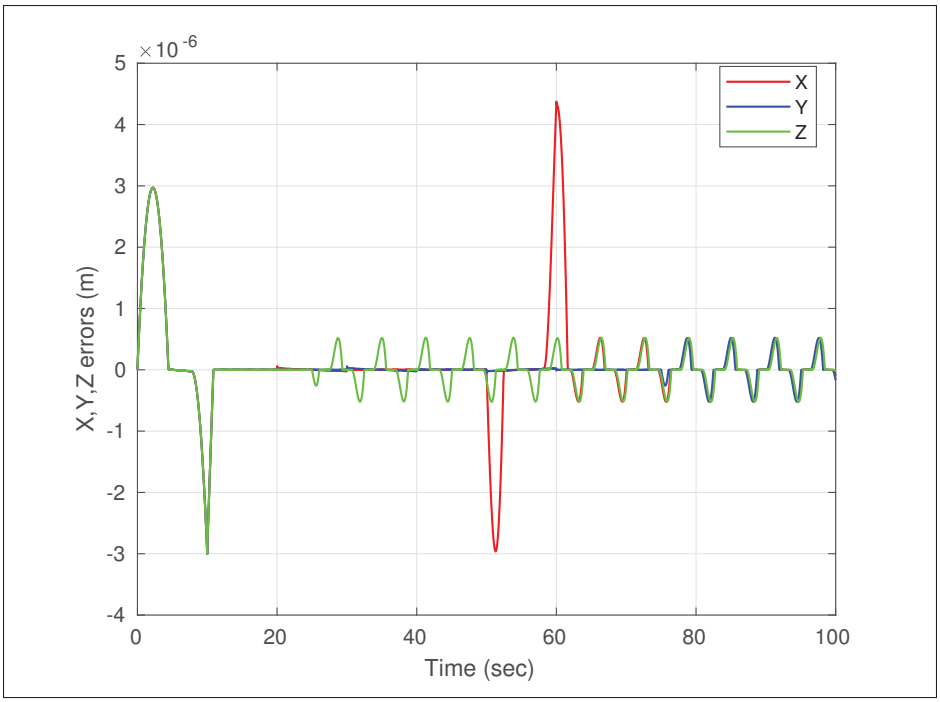

Figure 4.5 Position tracking errors in the (x, y, z) coordinates

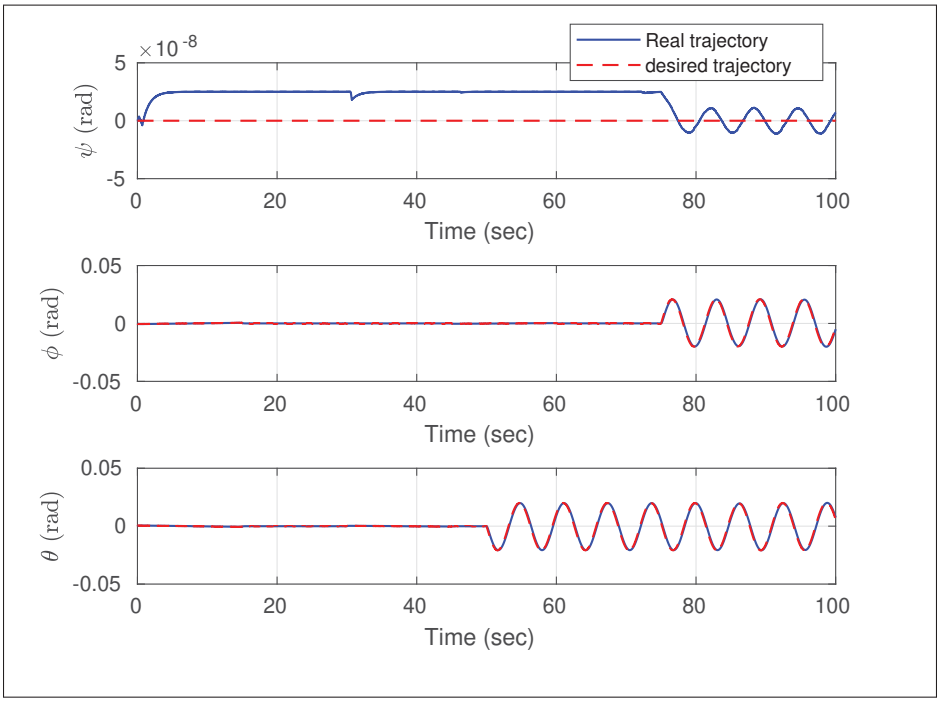

Figure 4.6 Attitude tracking (ϕ, θ, ψ)

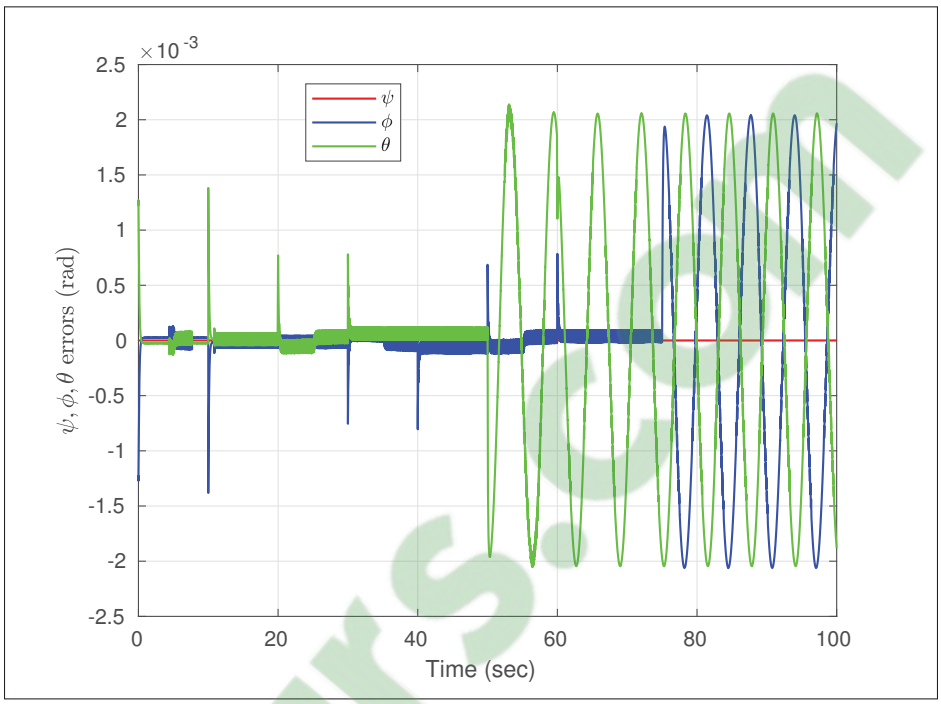

Figure 4.7 Attitude tracking errors in (ϕ, θ, ψ) coordinates

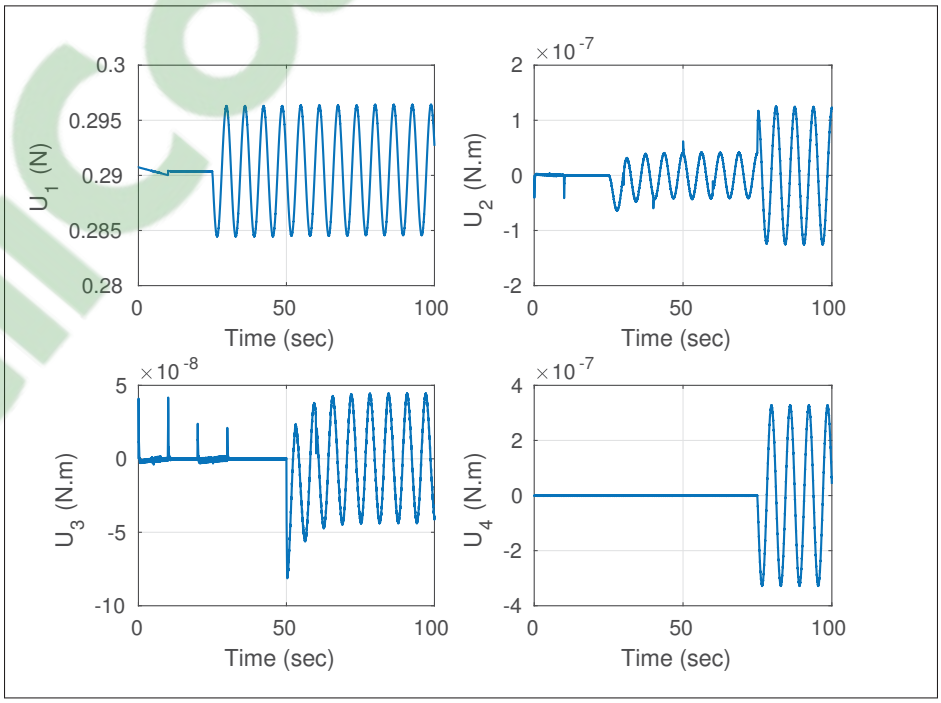

Figure 4.8 Input signals generated by controllers during simulation

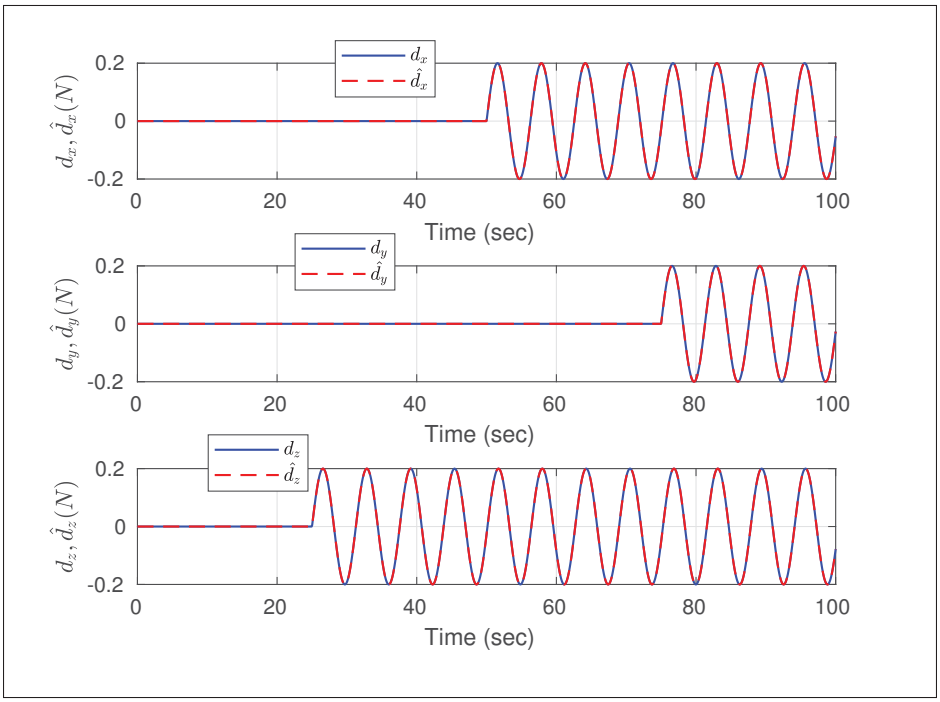

Figure 4.9 Disturbance estimation in coordinates x, y, z

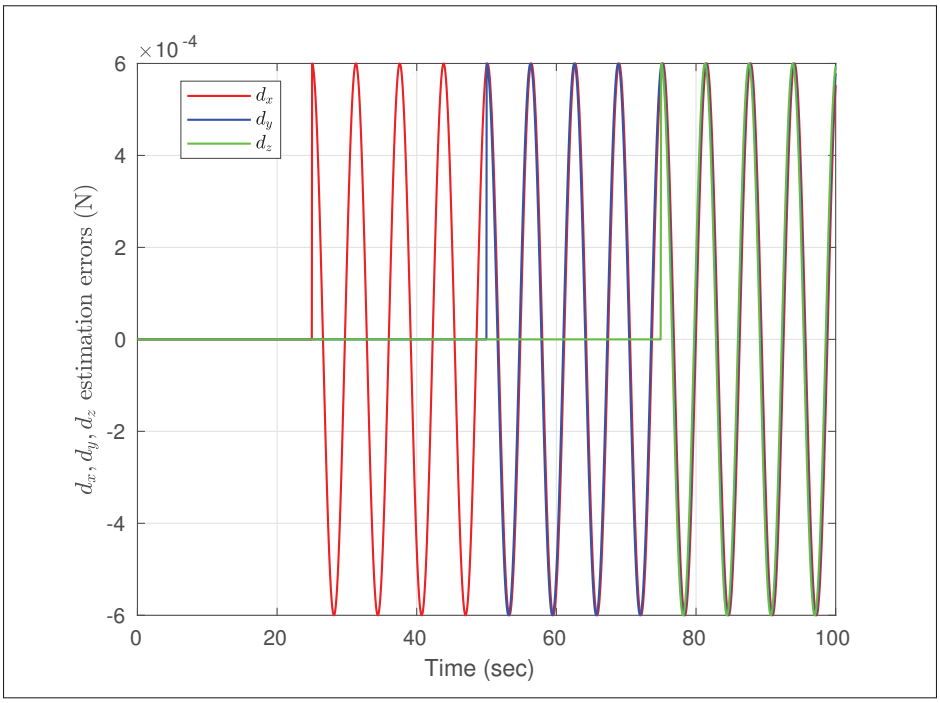

Figure 4.10 Disturbance estimation errors in coordinates x, y, z

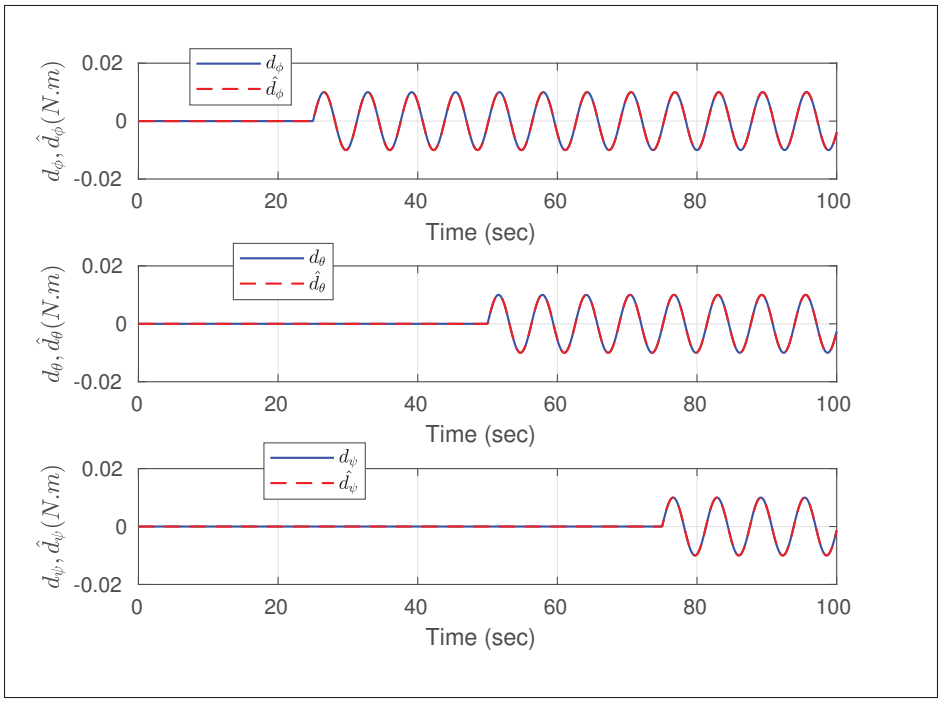

Figure 4.11 Disturbance estimation in coordinates (ϕ, θ, ψ)

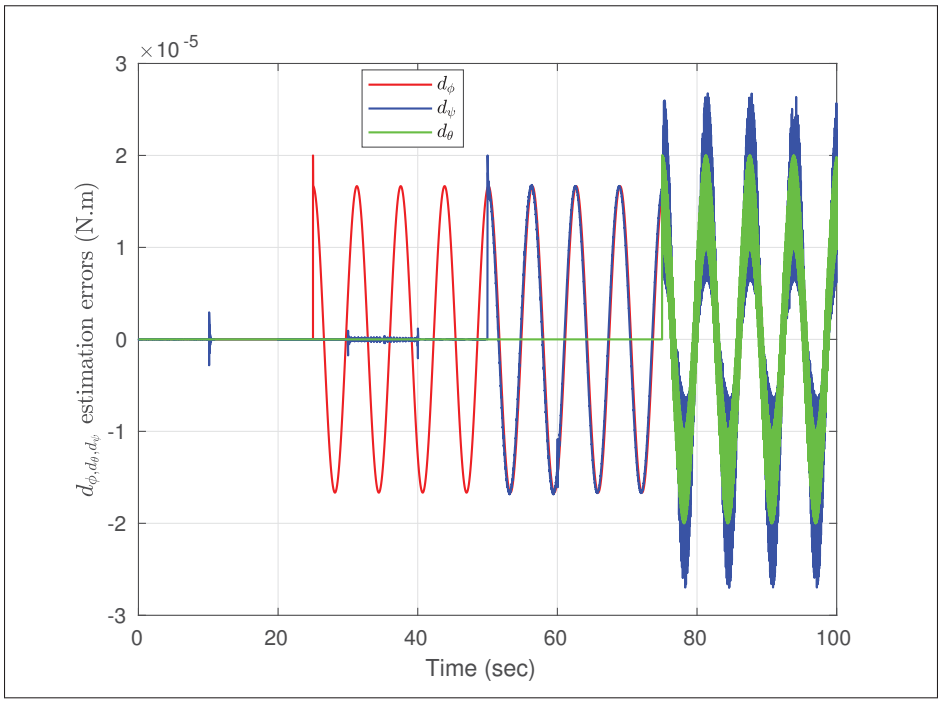

Figure 4.12 Disturbance estimation errors in coordinates (ϕ, θ, ψ)

4.8.2 Experimental Results

The Pixhawk autopilot was employed as the onboard flight controller to implement the data fusion algorithm and the proposed flight control strategy. For positioning system, a special localization sensor/algorithm (Kinect) is used to capture the position of the quadrotor during the flight. A companion computer (Odroid XU4) is used to interface and communicate with the pixhawk flight controller using the MAVLink protocol over a serial connection. A connection is established for the communication between the companion computer and the ground station. By doing this, the companion computer gets all the MAVLink data produced by the autopilot and the positioning sensor (Kinect). The controller and estimator gains employed in the experiment were those listed in Table 4.1. In practical applications, the attitude gains are usually tuned first, followed by the position gains. Based on the permitted overshoot, settling time, the steady state error requirements, these gains can be tuned by trial and error in hovering conditions.

Figure 4.13 The experimental setup used in real flight tests.

The goal of the laboratory experiment was to demonstrate that the designed controller achieves good tracking in the presence of external wind gusts. An electrical fan was used to generate the wind gusts that affect the quadrotor during flight, as shown in Fig. 4.13. It was required that the quadrotor follows the same trajectory as the one used in computer simulations. The responses of the position and attitude subsystem under wind gusts are depicted in Fig. 4.14 - Fig. 4.17 together with the respective tracking errors. The results clearly confirm that the proposed controller is capable of compensating for wind gusts as additional unknown disturbances. From Figure 4.15, it can be seen that quadrotor tracks the given trajectory with position tracking errors that do not exceed 0.1 m. From Figure 4.17, it is shown that the attitude tracking errors are smaller than 0.08°. It is obvious that both the position errors and attitude errors are driven within a small range quickly.

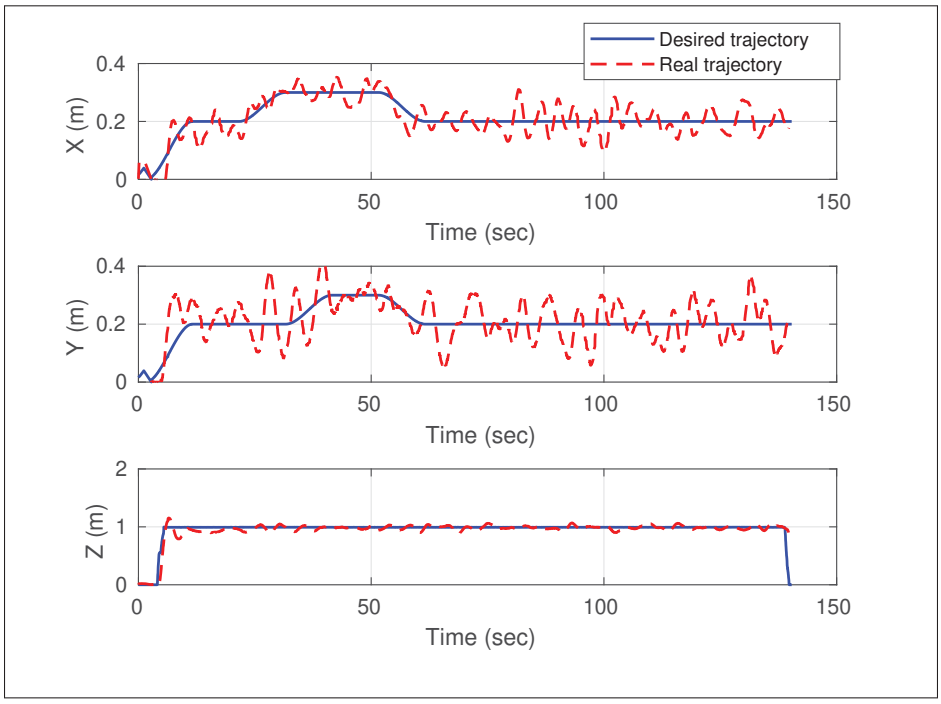

Figure 4.14 Real flight tracking of three position coordinates by proposed controller under the effect of wind gusts

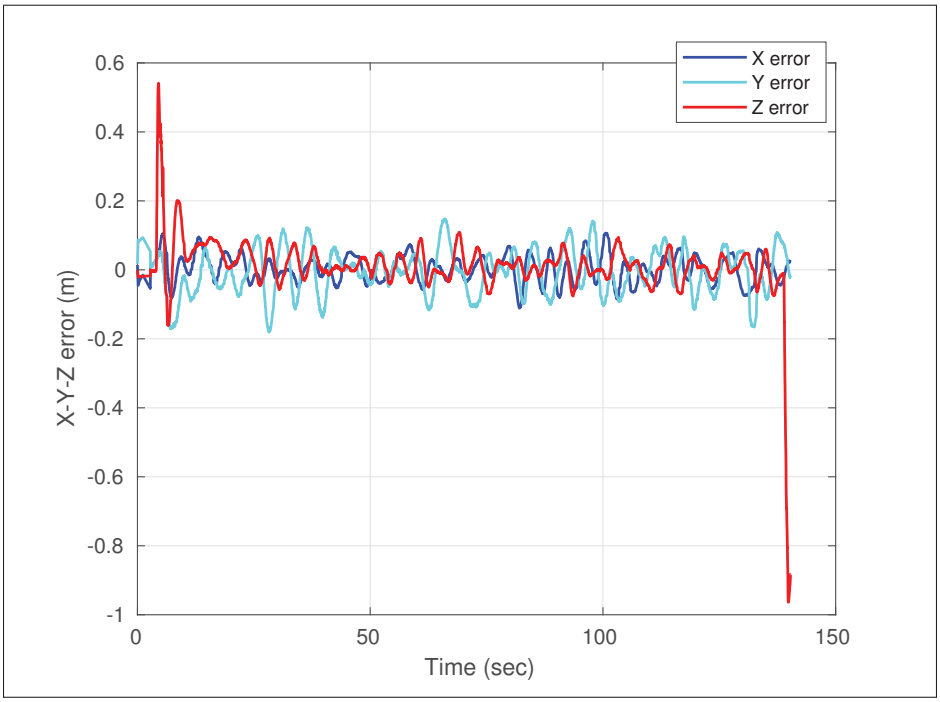

Figure 4.15 The position tracking errors under the effect of wind gusts

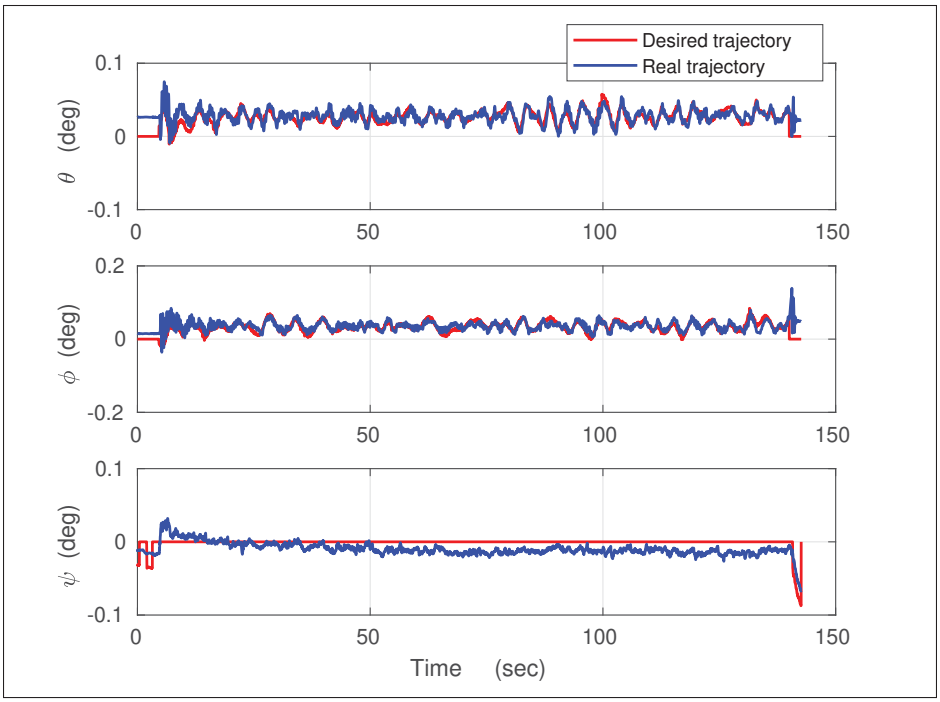

Figure 4.16 Real flight tracking of three attitude angles by proposed controller under the effect of wind gusts

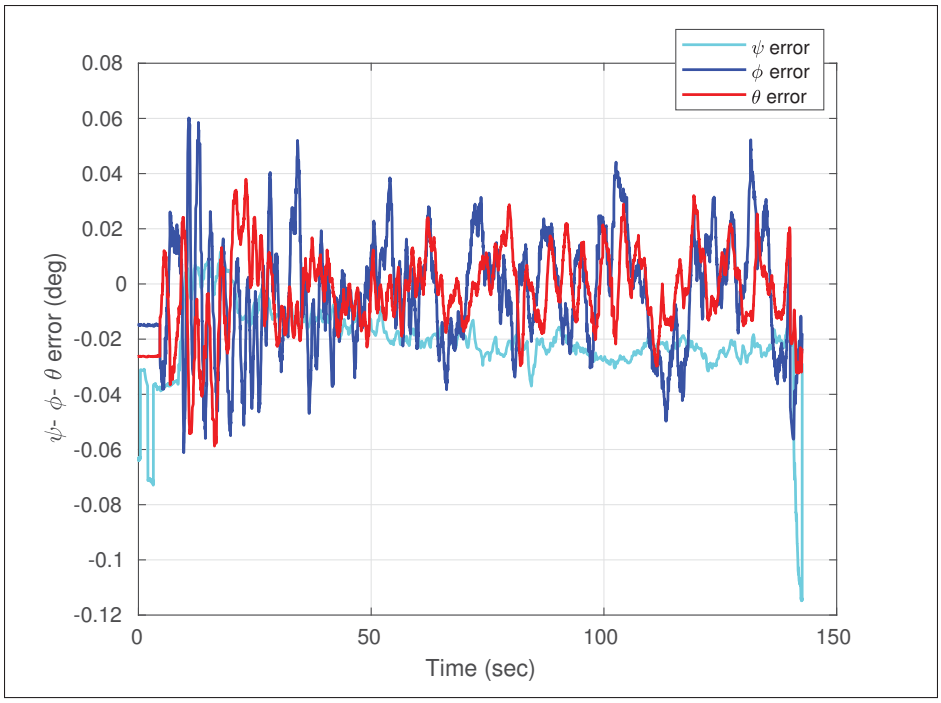

Figure 4.17 The attitude tracking errors under the effect of wind gusts

4.9 Conclusion

This paper explores a novel approach to robust trajectory tracking control of a quadrotor UAV. A bank of the super-twisting observer (STO) is employed in conjunction with a matching set of generalized sliding mode controller to compensate the influence of the unmatched uncertainties affecting the position and attitude systems during the flight. The stability of the system is guaranteed by designing the sliding mode controller combined with the super-twisting observer as demonstrated employing a direct Lyapunov analysis. The validity of the developed approach was first confirmed by computer simulations. The performance of the observer-based sliding mode control strategy was next extensively validated in real time flight tests using an experimental platform setup. The analysis of the tracking control approach, for the first time carried out with full rigor, leads to the following useful conclusions; (i) The disturbance observer employs excessively restrictive assumptions and cannot be shown to converge to the correct estimates; more precise estimates can be obtained only by using high gains. (ii) The

smooth tracking controller employed to achieve tracking in the position subsystem has similar flaws: it cannot fully compensate for unknown disturbances in the position subsystem, thus its robustness and precision may be questioned. (iii) The first order sliding mode controller proves to have superior properties as it is fast and able to reject bounded unknown disturbances. Furthermore, the localization algorithm (Kinect) will be extended to use a precise position measurement from a motion capture system to upgrade the experimental UAV setup. This will enable much better performance of the implemented nonlinear controller.

CHAPTER 5

DOUBLE-SIDED OBSERVER FOR ROBUST TRAJECTORY TRACKING CONTROL OF QUADROTOR UAV

Nuradeen Fethalla[1], Bashar Khan[2], Maarouf Saad[3], Hannah Michalska[4], Jawhar Ghommam[5]

[1,2,3] Département de Génie électrique, École de Technologie Supérieure,
1100 Notre-Dame Ouest, Montréal, Québec, Canada H3C 1K3
[4] Electrical and computer engineering department McGill university,
3480 Rue University, Montréal, QC H3A 0E9
[5]Department of Electrical and computer Engineering, Sultan Quaboos University,
P.O. Box 33, Al-Khod Muscat, 123 Sultanate of Oman

Submitted to International Journal of Control, March 15, 2019

5.1 Abstract

The aim of this article is to present a kernel-based disturbance observer trajectory tracking controller for quadrotor UAV. To assess the performance of the proposed observer in a comparison manner, two other observer-based feedback control designs in an application of robust trajectory tracking for a quadrotor are introduced. Specifically, the study investigates the utility of three different disturbance observers: a kernel disturbance observer (KDO), a super twisting sliding mode observer (STO), and a nonlinear disturbance observer (NDO) in feedback with a robust sliding mode tracking control. It is assumed that the quadrotor is subject to large but unknown aero-dynamic disturbances during its flight. The analysis shows that asymptotic tracking of the full position and the yaw orientation angle is achieved during flight with each of the disturbance observers. However, the kernel-based observer delivers the fastest convergence to the desired trajectory and hence is superior despite its heigh computational cost.

5.2 Introduction

Robust control design for quadrotors has attracted much research attention as it has many important applications. Realistic flight conditions imply the need to compensate for unknown

disturbances such as wind gusts that may be powerful enough to justify the incorporation of fast and accurate observers of the aero-dynamical forces involved.

Most of the existing control strategies are designed based on simplified models without compensation for modeling errors or external disturbances; see e.g. (Bouabdallah *et al.*, 2004a; Herissé *et al.*, 2012). Works that incorporate disturbance observers as a component of the tracking control system fall into two groups based on the type of the disturbance estimation employed: (i) continuous time and nonlinear; (ii) hybrid or discontinuous in time. The first group is represented by observer-based tracking control schemes in which the observers (here referred to as NDO) are smooth systems that converge rather slowly and necessitate additional assumptions to be made about the disturbance signals; see (Fethalla *et al.*, 2017b; Cheng *et al.*, 2018; Yang *et al.*, 2012; Ginoya *et al.*, 2014; Obaid *et al.*, 2016; Zhao *et al.*, 2015) who proposes an integrated adaptive tracking control approach.

When the disturbances are known to be powerful, however, a natural choice is to employ discontinuous or hybrid estimation approaches, notably sliding mode observers (SMO) that are valued for their powerful attributes, such as finite time convergence and low sensitivity to sensor noise; see (Edwards & Spurgeon, 1994; Drakunov & Utkin, 1995; Edwards *et al.*, 2002). A first order sliding mode observers have been employed in (Besnard *et al.*, 2007, 2012) in conjunction with regular sliding mode control (SMC); both featuring uncompensated chatter. An asymptotic super-twisting observer was introduced in (Levant, 2003),(Davila *et al.*, 2005) while a super-twisting second order disturbance observer (STO) has also been employed in (Luque-Vega *et al.*, 2012). More powerful higher order sliding mode disturbance observers have been proposed in (Derafa *et al.*, 2012) that are also combined with on-line differentiators and exhibit finite time convergence with robustness to measurement noise. A real-time implementation of a super-twisting scheme for attitude tracking of quadrotor is implemented in (Gonzalez-Hernandez *et al.*, 2017).

Many more contributions can be listed that rely on the combination of disturbance observation to assist feedback controllers to achieve accuracy and robustness in trajectory tracking applica-

tions. To the best of our knowledge, however, there are no studies that attempt to compare and evaluate the attributes of diverse disturbance estimation approaches in integration with feedback control of rotorcraft. This being the main motivation for the present contribution, three different disturbance observers are presented and analyzed here while functioning in tandem with a dual backstepping-sliding mode tracking control for a quadrotor. While the NDO and STO have been presented before; see (Fethalla *et al.*, 2017b; Cheng *et al.*, 2018), and (Levant, 1998), the kernel-based disturbance observer (KDO) is new. Although the kernel system representation for both LTI and LTV systems has been presented and employed for the purpose of "almost instantaneous" joint parameter and state estimation in (Ghoshal *et al.*, 2017) and further discussed with reference to LPV and nonlinear systems (Sinha; Ravichandran, 2018), it has never been exploited in the context of any specific practical application.

Simulation results presented here demonstrate that although all three observers, the KDO, STO, and NDO, are able to deliver good matched and unmatched disturbance estimates during the flight of a quadrotor, the KDO is the fastest of them. However, the KDO is also very computationally demanding. The next best, as far as speed and robustness to measurement noise is concerned, is the STO. It is worth mentioning that the robustness properties (with respect to measurement noise) of the KDO can still be significantly improved as will be demonstrated elsewhere. The NDO is perhaps the least desired solution as it requires making additional assumptions about the estimated signal and relies on employing very high gains to achieve desired asymptotic accuracy and speed.

The paper is organized as follows: the dynamic model of a quadrotor UAV is presented in Section 5.3. The robust tracking control objective is described in Section 5.4. The KDO, NDO, and STO disturbance observers are presented and developed in Section 5.5. The associated backstepping-sliding mode controller for position and attitude subsystems are described in Section 5.6. Section 5.7 delivers the stability analysis of the observer-based tracking control. The performance of the three observers: the KDO, NDO, and STO is then assessed in simulations in Section 5.8 with reference to some challenging chaotic type disturbances. The KDO, NDO, and STO observer-based feedback control structures are also evaluated in the

same section of the paper. The attributes of the compared scheme are discussed and followed by conclusion in Section 5.9.

5.3 Dynamic modeling of a quadrotor

A dynamic model of a quadrotor UAV, shown in Fig.5.1, was originally adopted in (Hoffmann *et al.*, 2007b), and subsequently employed in (Zheng *et al.*, 2014) and (Alexis *et al.*, 2012a). It is again cited here for completeness of exposition.

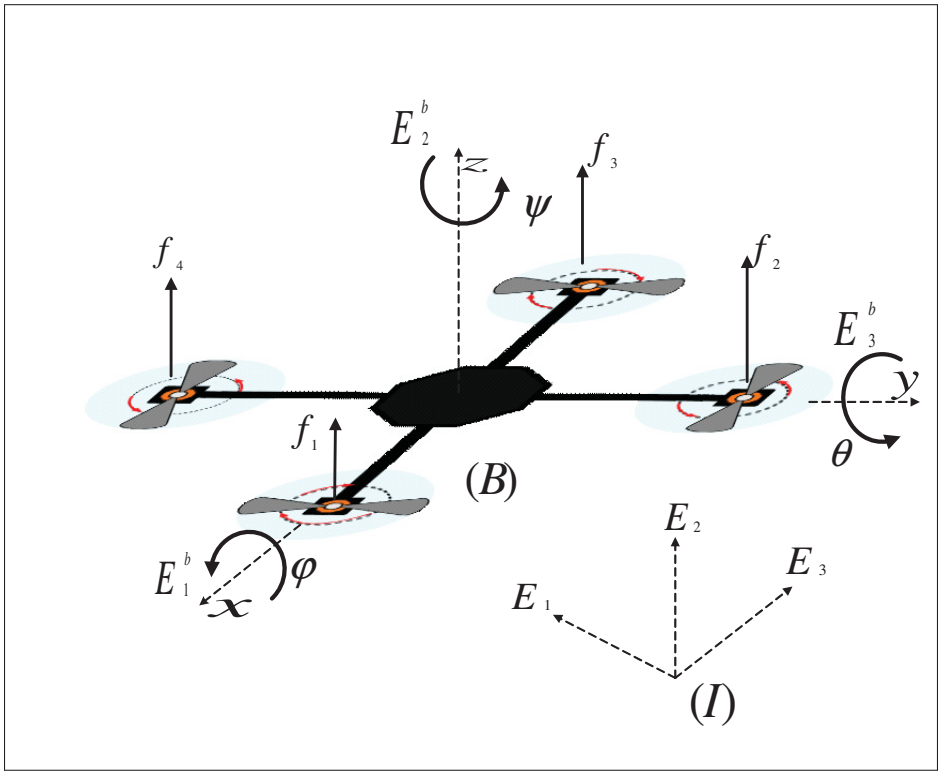

Figure 5.1 Quadrotor Airframe And Reference Frames

Consider two reference frames: the earth fixed frame ($\mathcal{I}$) associated with the unit vector basis (E_1, E_2, E_3) and body fixed frame ($\mathcal{B}$) associated with the unit vector basis (E_1^b, E_2^b, E_3^b) fixed at the center of mass of the quadrotor, as shown in Fig.5.1. The position of the center of the quadrotor's mass is denoted by the vector $p = [x, y, z]^T$. This position vector is expressed with respect to an inertial frame ($\mathcal{I}$). The attitude is denoted by $\Theta = [\phi, \theta, \psi]$. These three angles are

the Euler angles: yaw ($-\pi < \psi < \pi$), pitch ($-\frac{\pi}{2} < \theta < \frac{\pi}{2}$), and roll ($-\frac{\pi}{2} < \phi < \frac{\pi}{2}$) that define the orientation vector of the quadrotor with respect to the inertial frame ($\mathcal{I}$). The angular velocity and acceleration of roll, pitch, and yaw defined with respect to the body-fixed frame ($\mathcal{B}$) and the inertial reference frame $\mathcal{I}$ respectively as $\Omega = [\Omega_p, \Omega_q, \Omega_r]^T$, and $\ddot{\Theta} = [\ddot{\phi}, \ddot{\theta}, \ddot{\psi}]$. $\dot{p} = [\dot{x}, \dot{y}, \dot{z}]$ and $\ddot{p} = [\ddot{x}, \ddot{y}, \ddot{z}]$ represent the linear velocities and accelerations of the translational system respectively. The rotation matrix R and Euler matrix $M(\Theta)$ denote the transformation between the body-fixed reference frame $\mathcal{B}$ and the inertial reference frame $\mathcal{I}$ in the space orientation of the quadrotor and are given by

$$R(\Theta) = \begin{bmatrix} C_\theta C_\psi & S_\phi S_\theta C_\psi - C_\phi S_\psi & C_\phi S_\theta C_\psi + S_\phi S_\psi \\ C_\theta S_\psi & S_\phi S_\theta S_\psi + C_\phi C_\psi & C_\phi S_\theta S_\psi - S_\phi c_\psi \\ -S_\theta & S_\phi C_\theta & C_\phi C_\theta \end{bmatrix}$$

$$M(\Theta) = \begin{bmatrix} 1 & 0 & -S_\theta \\ 0 & C_\phi & S_\phi C_\theta \\ 0 & -S_\phi & C_\phi S_\theta \end{bmatrix}$$

where $\dot{\Theta}$ and Ω are related by the following relationship

$$\Omega = M(\Theta)\dot{\Theta} \tag{5.1}$$

These transformations cab found in a detailed formulation (Alexis *et al.*, 2012a).

The equations of motion of the quadrotor can be divided into two subsystems; equations of motion of the translational subsystem (referring to the position of the center of mass of the UAV) and equations of motion of the angular subsystem (referring to the attitude of the UAV). These equations can be stated in the reference frame ($\mathcal{I}$) as

$$\ddot{p} = \frac{1}{m} R(\Theta) F_{prop} - G + d_p(t) \tag{5.2a}$$

$$\begin{aligned} \ddot{\Theta} &= (IM(\Theta))^{-1} [T_{prop} - IN(\Theta, \dot{\Theta}) \\ &\quad - \Omega \times I\Omega - T_g] + d_\Theta(t) \\ &= \Phi(\Theta, \dot{\Theta}) + \Psi(\Theta) T_{prop} + d_\Theta(t) \end{aligned} \tag{5.2b}$$

where $N(\Theta, \dot{\Theta})$ is given by

$$N(\Theta, \dot{\Theta}) = \begin{bmatrix} -C_\theta \dot{\theta} \dot{\psi} \\ -S_\phi \dot{\phi} \dot{\theta} + C_\phi \dot{\phi} \dot{\psi} - S_\phi S_\theta \dot{\theta} \dot{\psi} \\ -C_\phi \dot{\phi} \dot{\theta} - S_\phi C_\theta \dot{\phi} \dot{\psi} - C_\phi S_\theta \end{bmatrix}$$

and T_{prop} is the resultant torques due to the gyroscopic effects given as

$$T_{prop} = \sum_{i=1}^{4} \Omega \times J_r [0, 0, (-1)^{i+1} \omega_i]^T \tag{5.3}$$

where J_r is the moment of inertia of each rotor and $\omega_i, i = 1, 2, 3, 4$ is the rotary speed of each motor.

The matrices $\Psi(\Theta)$ and $\Phi(\Theta, \dot{\Theta})$ are defined as

$$\begin{aligned} \Psi(\Theta) &= (IM(\Theta))^{-1} \\ \Phi(\Theta, \dot{\Theta}) &= -(IM(\Theta))^{-1} [IN(\Theta, \dot{\Theta}) - \Omega \times I\Omega - T_g] \end{aligned}$$

where $I = diag(I_x, I_y, I_z)$ is the inertia matrix of the quadrotor; $G = [0, 0, -g]^T m/s^2$ is the gravitational force acting along the z-axis of the inertial frame; m denotes the mass of the quadrotor. The terms $d_p = [d_x \;\; d_y \;\; d_z]^T$ and $d_\Theta = [d_\phi \;\; d_\theta \;\; d_\psi]^T$ represent the corresponding aerodynamical disturbances along with model smooth and bounded external disturbances. $S_{(\cdot)}$ and $C_{(\cdot)}$ denote the abbreviations of $\sin(\cdot)$ and $\cos(\cdot)$ functions, respectively. Each motor of quadrotor produces thrust and drag that are assumed to be proportional to the square of the motor speed. Hence, the force generated by the ith motor can be derived as by $f_i = b\omega_i^2 (i = 1, 2, 3, 4)$ where b is motor

lift coefficient. F_{prop} and T_{prop} are: the three-dimensional translational force vector and the three-dimensional reaction moment vector exerted by the propellers, respectively, as given by

$$F_{prop} = \begin{bmatrix} 0 \\ 0 \\ T \end{bmatrix} \quad T_{prop} = \begin{bmatrix} h(f_4 - f_2) \\ h(f_3 - f_1) \\ c\sum_{i=1}^{4}(-1)^i f_i \end{bmatrix}$$

where $T = \sum_{i=1}^{4} f_i$ is the total thrust, h is distance from the center of mass to the rotor, and c is he drag factor coefficient. It is easy to verify that equations (5.2a)-(5.2b) can actually be written as

$$\begin{aligned}
\ddot{\phi} &= r_1\dot{\theta}\dot{\psi} - r_2\dot{\theta}\omega + q_1 U_2 + d_\phi \\
\ddot{\theta} &= r_3\dot{\phi}\dot{\psi} + r_4\dot{\phi}\omega + q_2 U_3 + d_\theta \\
\ddot{\psi} &= r_5\dot{\theta}\dot{\phi} + q_3 U_4 + d_\psi \\
\ddot{x} &= (C_\phi S_\theta C_\psi + S_\phi S_\psi)\frac{1}{m}U_1 + d_x \\
\ddot{y} &= (C_\phi S_\theta S_\psi - S_\phi C_\psi)\frac{1}{m}U_1 + d_y \\
\ddot{z} &= -g + (C_\phi C_\theta)\frac{1}{m}U_1 + d_z
\end{aligned} \tag{5.4}$$

where $[U_1, U_2, U_3, U_4]^T = [T, T_{prop}]^T$ is the input vector.

$$\begin{aligned}
r_1 = \frac{I_y - I_z}{I_x}, r_2 = -\frac{J_r}{I_x}, r_3 = \frac{I_z - I_x}{I_y}, r_4 = \frac{J_r}{I_y}, \\
r_5 = \frac{I_x - I_y}{I_z}, q_1 = \frac{h}{I_x}, q_2 = \frac{h}{I_y}, q_3 = \frac{1}{I_z}
\end{aligned}$$

are inertia related constants and $\omega = \omega_4 + \omega_3 - \omega_2 - \omega_1$.

The state vector X can thus be defined as

$$X = [p \;\; \dot{p} \;\; \Theta \;\; \dot{\Theta}]^T \in \mathbb{R}^{12}$$

For transparency of further derivations, it is finally convenient to re-write equations (5.2a)-(5.2b) (or equivalently those in (5.4)) in the following block compact form

$$\ddot{p} = G + U_p + d_p \tag{5.5}$$

$$\ddot{\Theta} = \Phi(\Theta, \dot{\Theta}) + U_\Theta + d_\Theta \tag{5.6}$$

with

$$U_p := \frac{1}{m} R(\Theta) U_1 e_z; \tag{5.7}$$

$$U_\Theta := \Psi(\Theta)[U_2 \;\; U_3 \;\; U_4]^T \tag{5.8}$$

5.4 Observer-based tracking for the quadrotor

Tracking control objective for the quadrotor

The objective is to design and analyse the performance of a closed loop observer-based control structure that enables asymptotic tracking of the position of the center of mass and the yaw angle of the quadrotor: (p, ψ) to prescribed reference trajectories $p_r(t), \psi_r(t); t \geq 0$. The designed controllers are required to be robust with respect to the unknown force and torque disturbances d_p, d_Θ, hence necessitating the use of a disturbance observer. For the purpose of control design the dynamic model (5.4) of the quadrotor is viewed as a system composed of two subsystems, the position subsystem (5.7) and the rotational subsystem (5.8). It is seen that the attitude subsystem is decoupled from the position subsystem and that it is fully input-output acuated, with the output defined as the attitude vector Θ. Also, its disturbances d_Θ are matched to the three components of the propeller torque vector. By contrast, the position subsystem is underactuated as its only control variable is the thrust force which can be used to attenuate the disturbance component d_z while leaving the disturbances d_x,d_y unmatched by the thrust control.

5.5 Disturbance observer designs

Three different observers will be proposed and tested in closed loop tracking control structure.

5.5.1 A kernel disturbance observer (KDO)

The KDO estimates the aerodynamic disturbances by first estimating the states of the quadcopter. The state estimation employs a moving (observation) window that forwards in time as new measured system output data becomes available. The measured output is assumed to consist of: full, but possibly noisy, translational position vector $[x, y, z]$, and full angular position vector $[\phi, \theta, \psi]$. The complete state of the quadrotor $[x, y, z, \dot{x}, \dot{y}, \dot{z}, \phi, \theta, \psi, \dot{\phi}, \dot{\theta}, \dot{\psi}]$ and the accelerations $[\ddot{x}, \ddot{y}, \ddot{z}, \ddot{\phi}, \ddot{\theta}, \ddot{\psi}]$ are then estimated by the KDO over any current observation window. The development of the observer is summarized here in the particular context of the quadrotor system.

To obtain the full estimate of the state, velocity, and acceleration, at a time instant t, the KDO observer processes output data over a finite observation window preceding t. The actual estimate is calculated as "a state" of a *surrogate linear (LTI) model* that best fits the measured data over the observation window. The process of such "fitting" involves estimating the parameters of the locally defined LTI system that resembles a modified kernel-based moving-horizon version of the minimum energy filter which was first briefly introduced in (Ravichandran, 2018) with reference to a multivariable nonlinear second order system with an *unknown model*. The estimation properties of the latter observer were shown to compare favourably with a kernel adaptation of the Bayesian dynamic regression of (Särkkä, 2013).

The idea behind the kernel observer presented here is the following. First, each component of the six-dimensional position and orientation vector $[x, y, z, \phi, \theta, \psi]$, is *locally* viewed as an output $y(t), t \in [t_k, t_{k+1}]$ of a fourth order LTI system with characteristic equation of the form

$$\begin{aligned} y^{(n)}(t) + a_{n-1}y^{(n-1)}(t) + a_2 y^{(2)}(t) + a_1 y^{(1)}(t) \\ + a_0 y(t) = 0 \end{aligned} \tag{5.9}$$

The output y is assumed to be measured over the observation window $[t_k, t_{k+1}]$ and is therefore, generally, a noisy signal. The LTI model (5.9) is considered viable as it can be viewed as a natural generalization of a truncated Taylor series expansion of a function y; (a truncated expansion involving n first terms of the Taylor series would obviously satisfy the equation $y^{(n)}(t) = 0$). A yet more accurate LTI surrogate model could involve interactions between position variables, but proved unnecessary for the purpose considered. The order of the surrogate model was chosen to be $n = 4$ to permit good estimation of higher order derivatives of the quadrotor position and orientation vectors such as accelerations and jerks as the last can be used to improve motion prediction accuracy.

Fitting of the model (5.9) to any position or orientation component such as e.g. $x(t)$ over an observation window $[t_k, t_{k+1}]$ requires estimation of the parameter values $w_k := [a_0, a_1, a_2, \cdots, a_{n-1}]_k$ which is best achieved when (5.9) is represented as an integral equation because integral representations do not involve initial conditions for the system, and exact knowledge of such initial conditions cannot be assumed as the outputs are measured with noise. The procedure so described resembles the action of a skilled draftsman who fits a french curve to a cloud of data points. The kernel expressions for the integral representation of (5.9) are obtained using the theorems cited from (Ghoshal *et al.*, 2019) for the general case of an LTI system of order n.

Theorem 5.1. *Let* $[a,b]$ *be any interval on* $\mathbb{R}$. *There exists a kernel function* K_y, *defined on* $[a,b]\times[a,b]$, *such that the differential system* (5.9) *has an equivalent integral representation for* $t \in [a,b]$

$$y(t) = \int_a^b K_y(t,\tau)y(\tau)\, d\tau \tag{5.10}$$

Additionally, the kernel K_y *is a linear function of the system parameters* $a_0, \cdots, a_{n-1}$ *and is continuously differentiable* $n-1$ *times. The first* $n-1$ *derivatives of the output y,* $y^{(i)}$ *for* $i = 1, \cdots, n-1$ *, can be calculated recursively from y, as follows:*

$$y^{(i)}(t) = \sum_{m=0}^{i-1} f_y^{i,m}(t)y^{(m)}(t) + \int_a^b K_y^i(t,\tau)y(\tau)\, d\tau \tag{5.11}$$

where $f_y^i; i = 0, \cdots, n-2$, are rational functions on $[a,b]$ and the kernels K_y^i are obtained by direct differentiation of K_y with respect to t.

Since the kernel K_y is linear in the system parameters, the integral representation (5.10) can be written as

$$y(t) - g_n(t,y) = \sum_{i=0}^{n-1} a_i g_i(t,y) \tag{5.12}$$

$$g_i(t,y) := \int_a^b K_{y,i}(t,\tau) y(\tau) d\tau \;\; i = 0, \ldots, n \tag{5.13}$$

for some "component kernels" $K_{y,i}$ of K_y. Taking $a := t_k$, $b := t_{k+1}$ let $s^k := \{t_1^k, \cdots, t_N^k\} \subset (t_k, t_{k+1}]$, be a given discrete set of distinct time instants. The n copies of equation (5.12) for all members of s^k can then be stacked in the form of a matrix equation, where the index k indicates the dependence on the estimation window $[t_k, t_{k+1}]$

$$\begin{aligned}
&Q_k(y) = P_k(y)\bar{a}\;; \;\; y : [t_k, t_{k+1}] \to \mathbb{R} \\
&Q_k(y) \stackrel{def}{=} \begin{bmatrix} q(t_1^k) \\ \vdots \\ q(t_N^k) \end{bmatrix} \;\; ; \quad \bar{a} \stackrel{def}{=} \begin{bmatrix} a_0 \\ \vdots \\ a_{n-1} \end{bmatrix} \;\; ; \\
&P_k(y) \stackrel{def}{=} \begin{bmatrix} p_1(t_1^k) \cdots p_n(t_1^k) \\ \ddots \\ p_1(t_N^k) \cdots p_n(t_N^k) \end{bmatrix}
\end{aligned} \tag{5.14}$$

$$\begin{aligned}
&q(t_i^k) := y(t_i^k) - g_n(t_i^k, y);\; i = 1, \cdots, N \\
&p_j(t_i^k) := g_j(t_i^k, y);\; j = 1, \cdots, n
\end{aligned} \tag{5.15}$$

Identification and state estimation for system (5.9) of order $n = 4$, in observation window k, requires substituting: $\bar{a} := w_k$, $y(t) = y_M(t); t \in [t_k, t_{k+1}]$ in the estimation equation (5.14), where y_M denotes the measured system output (any component of the position or orientation vector of the quadrotor). Under practical identifiability condition ; see (Ghoshal & Michalska, 2019),

the knots s^k are assumed to be such that *rank* $P_k(y_M) = n$ which yields an estimate $\hat{w}_k := P_k(y_M)^\dagger Q_k(y_M)$, *in window* k, where the pseudo-inverse $P_k^\dagger$ is the left inverse of $P_k(y_m)$. The corresponding estimates $y_E, y_E^{(i)}, i = 1,2,3$, of the output and its derivatives in (5.9) over the window k, are then be calculated from the equations of Theorem 5.1; specifically

$$y_E(t) = \int_a^b K_y(t,\tau) y_M(\tau)\, d\tau\, d\tau \tag{5.16}$$

$$y_E^{(i)}(t) = \sum_{m=0}^{i-1} f_y^{i,m}(t) y_E^{(m)}(t) + \int_a^b K_y^i(t,\tau) y_M(\tau)\, d\tau \tag{5.17}$$

for $i = 1,2,3$, where all the functions and kernels depend on the value of the estimated parameters $\hat{w}_k$.

It should be noted that the procedure for estimation of a system output and its time derivatives as outlined above has important advantages:

(i) it is non-asymptotic in that it yields the estimates in finite time ;

(ii) any information about the initial conditions of the system is redundant;

(iii) no assumptions other than differentiability is needed about the estimated signals (the fitted surrogate model can be unstable);

(iv) the KDO has natural noise rejection properties as secured by the presence of the integral kernel K_y which acts as a low pass filter during the estimation process;

(v) in the absence of noise the estimation error can be made as small as desired by adjusting the order of the surrogate LTI model and the size of the observation window.

The full derivation of the development of the Double-Sided Kernel for a 4th Order LTI System can be found in (Ravichandran, 2018).

Once the position, velocity, and acceleration vectors of the quadrotor are estimated as:

$$[\hat{x}, \hat{y}, \hat{z}, \hat{\phi}, \hat{\theta}, \hat{\psi}];$$

$$[\hat{\dot{x}}, \hat{\dot{y}}, \hat{\dot{z}}, \hat{\dot{\phi}}, \hat{\dot{\theta}}, \hat{\dot{\psi}}];$$

$$[\hat{\ddot{x}}, \hat{\ddot{y}}, \hat{\ddot{z}}, \hat{\ddot{\phi}}, \hat{\ddot{\theta}}, \hat{\ddot{\psi}}];$$

over any given observation window k, the estimates of the unknown disturbances are obtained directly from the dynamical equations of the quadrotor (eq. 5.4).

$$\begin{aligned}
\hat{d}_\phi &= \hat{\ddot{\phi}} - (r_1\hat{\dot{\theta}}\hat{\dot{\psi}} - r_2\hat{\dot{\theta}}w + q_1U_2)\\
\hat{d}_\theta &= \hat{\ddot{\theta}} - (r_3\hat{\dot{\phi}}\hat{\dot{\psi}} + r_4\hat{\dot{\phi}}w + q_2U_3)\\
\hat{d}_\psi &= \hat{\ddot{\psi}} - (r_5\hat{\dot{\theta}}\hat{\dot{\phi}} + q_3U_4)\\
\hat{d}_x &= \hat{\ddot{x}} - \Big((C_{\hat{\phi}}S_{\hat{\theta}}C_{\hat{\psi}} + S_{\hat{\phi}}S_{\hat{\psi}})\frac{1}{m}U_1\Big)\\
\hat{d}_y &= \hat{\ddot{y}} - \Big((C_{\hat{\phi}}S_{\hat{\theta}}S_{\hat{\psi}} - S_{\hat{\phi}}C_{\hat{\psi}})\frac{1}{m}U_1\Big)\\
\hat{d}_z &= \hat{\ddot{z}} - \Big(-g + (C_{\hat{\phi}}C_{\hat{\theta}})\frac{1}{m}U_1\Big)
\end{aligned} \tag{5.18}$$

because the control inputs U_1, U_2, U_3 are known functions of time as produced by the designed controllers.

5.5.2 A nonlinear disturbance observer (NDO)

The NDO employed here has been previously described and analyzed in (Fethalla *et al.*, 2018). It has a similar form for each of the two sub-systems of the quadrotor (position and orientation):

$$\begin{aligned}
\dot{z}_p &= -L_pz_p - L_p[L_p\dot{p} + G + \frac{1}{m}U_p]\\
\hat{d}_p &= z_p + L_p\dot{p}
\end{aligned} \tag{5.19a}$$

$$\begin{aligned}
\dot{z}_\Theta &= -L_\Theta z_\Theta - L_\Theta[L_\Theta\dot{\Theta} + \Phi(\Theta,\dot{\Theta}) - U_\Theta]\\
\hat{d}_\Theta &= z_\Theta + L_\Theta\dot{\Theta}
\end{aligned} \tag{5.19b}$$

where $U_p = R(\Theta)e_3U_1$, $U_\Theta = \Psi(\Theta)[U_2\ \ U_3\ \ U_4]^T$, and $\widehat{d_j}$ $(j = p, \Theta)$ is the estimated disturbance. z_j is the state vector variable of the observer, and $L_j = l_jI_{3\times3}, l_j > 0,\ j = p, \Theta$, are the observer gain matrices to be tuned.

The full stability analysis of NDO was provided in our previous work (Fethalla *et al.*, 2018).

5.5.3 A super-twisting sliding mode observer (STO)

The super-twisting sliding mode observer employed here for estimation of the bounded disturbances d_j in subsystems (5.5) and (5.6) is cited below following its exposition in (Levant, 1998). To deliver the estimates of the system state vector $[\hat{p}, \hat{\dot{p}}, \hat{\Theta}, \hat{\dot{\Theta}}]$ the super-twisting sliding mode observer assumes the following structure :

$$\hat{\ddot{p}} = G + U_p + v_p \tag{5.20}$$

$$\hat{\ddot{\Theta}} = \Phi(\hat{\Theta}, \hat{\dot{\Theta}}) + U_\Theta + v_\Theta \tag{5.21}$$

where $\hat{\ddot{p}}$, and $\hat{\ddot{\Theta}}$ are the estimates of $\ddot{p}$ and $\ddot{\Theta}$, respectively, and the vectors v_p and v_Θ represent the observer injection terms as given below. The observer error dynamics defined by:

$$\dot{e}_p = \ddot{p} - \hat{\ddot{p}} \;\; ; \;\; \dot{e}_\Theta = \ddot{\Theta} - \hat{\ddot{\Theta}} \tag{5.22}$$

can be stabilized by second order sliding mode differentiators; see (Levant, 1998) , by employing the following injection terms in (5.20):

$$\begin{aligned} v_p &= -\lambda_p |e_p|^{1/2} \text{sign}(e_p) + u_p \\ \dot{u}_p &= -\alpha_p \text{sign}(e_p) \end{aligned} \tag{5.23a}$$

$$\begin{aligned} v_\Theta &= -\lambda_\Theta |e_\Theta|^{1/2} \text{sign}(e_\Theta) + u_\Theta \\ \dot{u}_\Theta &= -\alpha_\Theta \text{sign}(e_\Theta) \end{aligned} \tag{5.23b}$$

where $\text{sign}(e_p)$ and $\text{sign}(e_\Theta)$ are vector signum functions in which the signum function is applied to all components of error vectors e_p and e_Θ.

As is shown in (Levant, 1998), the estimation errors e_p and e_Θ converge to zero in finite time provided that the gain constants λ_p, α_p, λ_Θ, and α_Θ, are chosen to be sufficiently large.

Comparing (5.20) with the sub-system equations (5.5) - (5.6),

$$[\hat{p}, \hat{\dot{p}}, \hat{\ddot{p}}] \rightarrow [p, \dot{p}, \ddot{p}]$$
$$[\hat{\Theta}, \hat{\dot{\Theta}}, \hat{\ddot{\Theta}}] \rightarrow [\Theta, \dot{\Theta}, \ddot{\Theta}]$$
$$\text{implying} \quad [e_p, \dot{e}_p] \rightarrow [0,0]; \quad [e_\Theta, \dot{e}_\Theta] \rightarrow [0,0]$$

in finite time since the control inputs U_p, U_Θ are known exactly. The disturbance estimates are hence delivered immediately as: $\hat{d}_p = v_p$, and $\hat{d}_\Theta = v_\Theta$.

5.6 Tracking control designs for the quadrotor

The uncertain second order systems considered here are assumed to take the form of a vector double integrator

$$\begin{bmatrix} \dot{x}_1 \\ \dot{x}_2 \end{bmatrix} = \begin{bmatrix} 0 & I \\ 0 & 0 \end{bmatrix} \begin{bmatrix} x_1 \\ x_2 \end{bmatrix} + \begin{bmatrix} 0 \\ U \end{bmatrix} + \begin{bmatrix} 0 \\ \hat{d} \end{bmatrix} + \begin{bmatrix} 0 \\ e_d \end{bmatrix} \tag{5.24}$$

$$y = x_1 \tag{5.25}$$

with, generally, n-dimensional control, disturbance, state and output vectors, i.e. $U, \hat{d}, e_d, y, x_i \in \mathbb{R}^n \; ; i = 1,2$. It is seen that the above system is fully actuated as an input-output mapping: $U \mapsto y$, and that all disturbances are matched to the controls U.

Assumption 5.1.

- *The disturbance $\hat{d}$ is considered known while the disturbance e_d is an unknown function of time, which is, however, assumed bounded by a known constant D, i.e.,*

$$\|e_d(t)\| \leq D \;\; \textit{for all} \;\; t \in [0, \infty) \tag{5.26}$$

- *The reference trajectory to be tracked, denoted by:* $x_{1r}(t); t \geq 0,\ x_{1r}(t) \in \mathbb{R}^n$*, is required to be a twice continuously differentiable vector function of time.*
- *The full system state* $[x_1(t), x_2(t)]; t \geq 0$*, is accessible for feedback control and the control* U *is unconstrained.*

Lemma 5.1. *For all vectors* $x, y \in \mathbb{R}^n$

$$|x^T y| \leq \frac{1}{2}||x||^2 + \frac{1}{2}||y||^2 \tag{5.27}$$

Proof. It suffices to prove the inequality for the case when $x^T y > 0$. The result follows immediately by rearranging the quadratic inequality

$$0 \leq (x-y)^T (x-y) = x^T x - 2x^T y + y^T y \tag{5.28}$$

Proposition 5.1. *(Smooth high gain tracking control)*
Consider a system in vector form (5.24) *under Assumption 5.1.*

Part A (Unknown disturbances are absent i.e. $e_d \equiv 0$ *)*
Assuming that the disturbance vector $\hat{d}$ *is known, the unknown disturbances are absent,* $e_d \equiv 0$*, and the control vector* U *is unconstrained, the closed loop system* (5.24) *with the control law employing any strictly positive gain matrices* $K_1, K_2 \in \mathbb{R}^{n \times n}$*,* $K_1 > 0.5I$*,* $K_2 > 0.5I$*,*

$$\begin{aligned} U^H(x_1, x_2, x_{1r}, \hat{d}) &:= (K_2 + K_1)(\dot{x}_{1r} - x_2) \\ &+ K_2 K_1 (x_{1r} - x_1) + \ddot{x}_{1r} - \hat{d} \end{aligned} \tag{5.29}$$

achieves asymptotic tracking of any prescribed vector reference trajectory $x_{1r}(t), t \geq 0$*, in that*

$$||x_1 - x_{1r}|| \to 0 \ \text{ and } \ ||\dot{x}_1 - \dot{x}_{1r}|| \to 0 \quad \text{as } t \to \infty \tag{5.30}$$

Part B (Unknown disturbances are present)
Assuming that the disturbance vector $\hat{d}$ is known, the unknown disturbances are bounded by (5.26)*, and the control vector U is unconstrained, then for any constant $\epsilon > 0$ there exist control gains $K_1, K_2 \in \mathbb{R}^{n\times n}$ such that the tracking error for system* (5.24) *in closed loop with the control law* (5.29) *is asymptotically bounded as follows*

$$\|x_1(t) - x_{1r}(t)\|^2 + \|x_2(t) - \dot{x}_{1r}(t)\|^2 \leq \epsilon \tag{5.31}$$

for all $t \geq T^*$, for a sufficiently large time $T^* > 0$.

Proof. (*Part A) Define two new vector variables as functions of the state vectors x_1, x_2 and the vector reference trajectory x_{1r} with time derivative $\dot{x}_{1r}$:*

$$e_1 := x_{1r} - x_1 \tag{5.32}$$

$$e_2 := \dot{x}_{1r} - x_2 + K_1 e_1 = \dot{x}_{1r} - \dot{x}_1 + K_1 e_1 \tag{5.33}$$

$$= \dot{x}_{1r} - x_2 + K_1(x_{1r} - x_1) \tag{5.34}$$

for any given strictly positive definite matrix $K_1 > 0$. The following implications then clearly hold as $t \to \infty$:

$$\{e_1 \to 0\} \implies \{x_1 \to x_{1r}\} \tag{5.35}$$

$$\{e_2 \to 0\} \implies \{\dot{x}_1 \to \dot{x}_{1r}\} \tag{5.36}$$

as is required. To construct a control that results in the above, consider the Lyapunov function

$$V_e := \frac{1}{2}[e_1^T e_1 + e_2^T e_2] \tag{5.37}$$

Definitions (5.32) - (5.33) *combined with the system equations* (5.24) *imply the following expressions for the derivatives*

$$\dot{e}_1 = \dot{x}_{1r} - \dot{x}_1 = -K_1 e_1 + e_2 \tag{5.38}$$

$$= -K_1 e_1 + (\dot{x}_{1r} - x_2 + K_1 e_1) = \dot{x}_{1r} - x_2$$

$$\dot{e}_2 = \ddot{x}_{1r} - \dot{x}_2 + K_1 \dot{e}_1$$

$$= \ddot{x}_{1r} + K_1 \dot{e}_1 - U - \hat{d} \tag{5.39}$$

Hence, using (5.38) - (5.39)*, gives*

$$\dot{V}_e = e_1^T \dot{e}_1 + e_2^T \dot{e}_2$$

$$= -e_1^T K_1 e_1 + e_1^T e_2 + e_2^T (\ddot{x}_{1r} + K_1 \dot{e}_1 - U - \hat{d}) \tag{5.40}$$

Let the control U solve

$$-K_2 e_2 = +\ddot{x}_{1r} + K_1 \dot{e}_1 - U - \hat{d} \tag{5.41}$$

By virtue of (5.32) - (5.34)*, and* (5.38) - (5.39)*, the solution is*

$$U^H := K_2 e_2 + K_1 \dot{e}_1 + \ddot{x}_{1r} - \hat{d}$$

$$= K_2[(\dot{x}_{1r} - x_2) + K_1(x_{1r} - x_1)] + K_1[\dot{x}_{1r} - x_2]$$

$$+ \ddot{x}_{1r} - \hat{d} \tag{5.42}$$

$$= (K_2 + K_1)(\dot{x}_{1r} - x_2) + K_2 K_1 (x_{1r} - x_1)$$

$$+ \ddot{x}_{1r} - \hat{d} \tag{5.43}$$

From Lemma 5.1

$$e_1^T e_2 \leq \frac{1}{2}\|e_1\|^2 + \frac{1}{2}\|e_2\|^2 \tag{5.44}$$

Using this fact in (5.40) *with control* U^H *yields*

$$\begin{aligned}\dot{V}_e &= -e_1^T K_1 e_1 + e_1^T e_2 - e_2^T K_2 e_2 \\ &\leq -e_1^T (K_1 - 0.5I) e_1 - e_2^T (K_2 - 0.5I) e_2 < 0 \quad \textit{for } t \geq 0 \end{aligned} \tag{5.45}$$

provided that $K_1, K_2 > 0.5I$. *Inequality* (5.45) *then proves* (5.35) - (5.36) *and thus* (5.30) *with the tracking control as in* (5.29).

Proof. (*Part B) If the unknown disturbance is nonzero then equation* (5.39) *becomes*

$$\begin{aligned}\dot{e}_2 &= \ddot{x}_{1r} + K_1 \dot{e}_1 - \dot{x}_2 \\ &= \ddot{x}_{1r} + K_1 \dot{e}_1 - U - \hat{d} - e_d \end{aligned} \tag{5.46}$$

With the control law still satisfying (5.41)*, the inequality* (5.40) *involves an additional term*

$$\begin{aligned}\dot{V}_e &= -e_1^T K_1 e_1 + e_1^T e_2 + e_2^T (\ddot{x}_{1r} + K_1 \dot{e}_1 - U - \hat{d} - e_d) \\ &\leq -e_1^T (K_1 - 0.5I) e_1 - e_2^T (K_2 - 0.5I) e_2 - e_2^T e_d \end{aligned} \tag{5.47}$$

By Lemma 5.1

$$-e_2^T e_d \leq \frac{1}{2}\|e_2\|^2 + \frac{1}{2}\|e_d\|^2 \tag{5.48}$$

Letting $K_i, i = 1,2$ *satisfy* $K_i - 0.5I \geq k_i I_{n\times n}$*, for some constants* $k_1 > 0, k_2 > 0.5$*, inequality* (5.47) *combines with* (5.48) *and the bound* (5.26) *to yield*

$$\begin{aligned}\dot{V}_e &\leq -k_1 e_1^T e_1 - (k_2 - \frac{1}{2}) e_2^T e_2 + \frac{D^2}{2} \\ &\leq -\alpha V_e + \frac{D^2}{2} \end{aligned} \tag{5.49}$$

for $\alpha := 2\ min\{k_1, k_2 - 0.5\}$. *Invoking Proposition 5.1 proves* (5.31).

Proposition 5.2. *(First order sliding mode tracking control)*
Consider a system in vector form (5.24) *under Assumption 5.1. Let the tracking error variables be defined as in Proposition 5.1, i.e.*

$$e_1 := x_{1r} - x_1 \tag{5.50}$$

$$\begin{aligned} e_2 &:= \dot{x}_{1r} + K_1 e_1 - x_2 \\ &= \dot{x}_{1r} - \dot{x}_1 + K_1(x_{1r} - x_1) \end{aligned} \tag{5.51}$$

for some positive definite matrix $K_1 > 0$. *For simplicity of analysis it will be assumed that the tunable controller gains* K_1, K_2 *in the control law proposed below will take, or else be majorized by, the respective simple forms:* $K_1 := k_1 I_{n\times n}$, $K_2 := k_2 I_{n\times n}$ *for some constants* $k_1 > 0.5$, $k_2 > 0$ *to be selected in specific applications. Defining a sliding surface as*

$$S(x_1, x_2) := e_2 = 0 \tag{5.52}$$

the tracking control (5.29) *of Proposition 2 is augmented by a sliding mode control term as follows:*

$$\begin{aligned} U^S(x_1, x_2, x_{1r}, \hat{d}) &:= (K_2 + K_1)(\dot{x}_{1r} - x_2) \\ &+ K_2 K_1 (x_{1r} - x_1) + \ddot{x}_{1r} - \hat{d} \\ &+ A\ sign[(\dot{x}_{1r} - x_2) + K_1(x_{1r} - x_1)] \end{aligned} \tag{5.53}$$

where $A := diag\{a_1, a_2, \cdots, a_n\}$, $a_i > D, i = 1, \cdots, n$, *and for any vector* $v \in \mathbb{R}^n$, *the term* $A\ sign(v)$ *represents a column vector whose components are:* $a_i sign(v_i), i = 1, \cdots, n$.

Under these assumptions, for any initial conditions $[x_1(0), x_2(0)]$ of the system at $t = 0$, the trajectories of the closed loop system using the control law U^S reach the sliding surface $e_2 = 0$

in finite time t^* bounded by

$$t^* \leq 2 \max_i \left\{ \frac{|e_{2i}(0)|}{(a_i - D)} \right\} \tag{5.54}$$

In the absence of unknown disturbances the closed loop system trajectories remain on the sliding surface $e_2 \equiv 0$ for all times $t \geq t^*$. The system trajectories converge asymptotically to the desired reference trajectory, i.e. as $t \to \infty$:

$$\{e_1 \to 0\} \implies \{x_1 \to x_{1r}\} \tag{5.55}$$

$$\{e_2 \to 0\} \implies \{\dot{x}_1 \to \dot{x}_{1r}\} \tag{5.56}$$

The equivalent control in sliding mode is derived from the equality $\dot{S} = 0$ (with the disturbance $e_d = 0$ set to zero) thus

$$\begin{aligned} U^S_{eq} &= \ddot{x}_{1r} + K_1 \dot{e}_1 - \hat{d} \\ &= \ddot{x}_{1r} + K_1[\dot{x}_{1r}(t) - x_2(t)] - \hat{d} \end{aligned} \tag{5.57}$$

The system dynamics in sliding regime is

$$\begin{aligned} &\frac{d}{dt} x_1(t) = \dot{x}_{1r}(t) - K_1[x_1(t) - x_{1r}(t)]; \\ &\text{i..e.} \quad \frac{d}{dt} e_1(t) = -K_1 e_1(t); \quad t \geq t^* \end{aligned} \tag{5.58}$$

Proof. Employing the same definitions for the variables e_1 and e_2 as in (5.32) - (5.33), and the same Lyapunov function as that in (5.37), its derivative is

$$\dot{V}_e = e_1^T \dot{e}_1 + e_2^T \dot{e}_2 \tag{5.59}$$

$$= -e_1^T K_1 e_1 + e_1^T e_2 \tag{5.60}$$

$$+ e_2^T (\ddot{x}_{1r} + K_1 \dot{e}_1 - U^S - \hat{d} - e_d)$$

$$\text{with} \quad \dot{e}_2 = \ddot{x}_{1r} + K_1 \dot{e}_1 - U^S - \hat{d} - e_d \tag{5.61}$$

Let U^S satisfy

$$-A\ \text{sign}(e_2) - K_2 e_2 = \ddot{x}_{1r} + K_1 \dot{e}_1 - U^S - \hat{d} \tag{5.62}$$

It follows that

$$\begin{aligned} U^S &:= K_2 e_2 + A\ \text{sign}(e_2) + K_1 \dot{e}_1 + \ddot{x}_{1r} - \hat{d} \\ &= K_2[(\dot{x}_{1r} - x_2) + K_1(x_{1r} - x_1)] + K_1(\dot{x}_{1r} - x_2) \\ &\quad + \ddot{x}_{1r} - \hat{d} + A\ \text{sign}(e_2) \qquad (5.63) \\ &= (K_2 + K_1)(\dot{x}_{1r} - x_2) + K_2 K_1 (x_{1r} - x_1) \\ &\quad + \ddot{x}_{1r} - \hat{d} \\ &\quad + A\ \text{sign}[(\dot{x}_{1r} - x_2) + K_1(x_{1r} - x_1)] \qquad (5.64) \end{aligned}$$

which confirms (5.53). After substituting U^S into (5.61)

$$\dot{e}_2 = -K_2 e_2 - A\ \text{sign}(e_2) - e_d \tag{5.65}$$

With $e_{2i}, e_{di}; i = 1, \cdots, n$, denoting the entries of the vectors e_2 and e_d, respectively, (5.65) rewrites component wise as

$$\dot{e}_{2i} = -k_2 e_{2i} - a_i\ \text{sign}(e_{2i}) - e_{di};\ \ i = 1, \cdots n \tag{5.66}$$

Multiplying by e_{2i} gives

$$\begin{aligned} e_{2i}\dot{e}_{2i} = \frac{1}{2}\frac{d}{dt}e_{2i}^2 &= -k_2 e_{2i}^2 - a_i|e_{2i}| - e_{2i}e_{di}; \\ &\leq -k_2 e_{2i}^2 - (a_i - D)|e_{2i}| \qquad (5.67) \\ &\leq -(a_i - D)|e_{2i}| \ \ i = 1, \cdots n \qquad (5.68) \end{aligned}$$

because $k_2 > 0$ and

$$-e_{2i}e_{di} \leq |e_{2i}e_{di}| \leq D|e_{2i}| \tag{5.69}$$

$$\text{with } |e_{di}| \leq \|e_d\| \leq D \quad \text{for all } \; i = 1, \cdots, n. \tag{5.70}$$

From Lemma 5.1

$$e_1^T e_2 \leq \frac{1}{2}\|e_1\|^2 + \frac{1}{2}\|e_2\|^2 \tag{5.71}$$

so, using (5.67) in (5.60), yields

$$\begin{aligned} \dot{V}_e &= -k_1 e_1^T e_1 + e_1^T e_2 + e_2^T \dot{e}_2 \\ &\leq -(k_1 - 0.5)e_1^T e_1 - (k_2 - 0.5)e_2^T e_2 \qquad (5.72) \\ &\quad -(a_i - D)|e_{2i}| < 0 \;\; t \geq 0 \qquad (5.73) \end{aligned}$$

provided that $a_i > D$ for all $i = 1, \cdots, n$ and $k_1 > 0.5$, $k_2 > 0.5$.

Without loss of generality, assume that $e_{2i}(0) > 0$; then (5.67) implies

$$\begin{aligned} 2e_{2i}\frac{d}{dt}e_{2i} &\leq -(a_i - D)e_{2i} \\ \text{i.e. ,} \quad \frac{d}{dt}e_{2i} &\leq -\frac{1}{2}(a_i - D) \end{aligned} \tag{5.74}$$

Integrating the above on the interval $[0, t_i^*]$ where t_i^* is the finite reaching time for component e_{2i} renders the bound

$$\begin{aligned} e_{2i}(t_i^*) - e_{2i}(0) &\leq -\frac{1}{2}(a_i - D)(t_i^* - 0) \\ \implies t_i^* &\leq 2\frac{e_{2i}(0)}{(a_i - D)} \end{aligned} \tag{5.75}$$

as $e_{2i}(t_i^*) = 0$. Generalizing to the case of $e_{2i}(0) < 0$ and taking a maximum over i yields the total bound (5.54).

Inequality (5.72) then immediately implies the validity of (5.55) - (5.56). The dynamics in the sliding mode (5.58) is obtained by setting $e_2 = 0$ in (5.51) and the equivalent control (5.57) is calculated by assuming that $\dot{e}_2 = 0$ and $e_d = 0$ in (5.61).

The position subsystem (5.5) is clearly not in the form of (5.24). Specifically, this is because the components of the control vector $U \in \mathbb{R}^3$ of (5.24), now considered as a member of $\mathbb{R}^3$, are explicitly assumed to be functionally independent and unconstrained. By contrast, if the position subsystem (5.5) were to match the form and assumptions of (5.24), then it would have to hold that

$$U(t) = \frac{1}{m} R(\Theta(t)) T(t) e_z \quad \text{for all } t \geq 0 \tag{5.76}$$

for any desired value of the control vector $U(t)$ and any value of the attitude state vector $\Theta(t)$ of the evolving attitude subsystem. As the value of $T(t)$ is a scalar, this is impossible as the control vector $U(t)$ is clearly aligned with the vector $R(\Theta(t))e_z$ for all times t. Implied is also the fact that in the position subsystem the disturbances are not matched with the control (the disturbances cannot be cancelled instantaneously by the choice of the thrust force alone).
To find a way in which to resolve these difficulties, hypothesize that the control constraint in the position subsystem can somehow be relaxed by way of substituting it with

$$U(t) = \frac{1}{m} R(\Theta_r(t)) T(t) e_z \quad \text{for all } t \geq 0 \tag{5.77}$$

where $\Theta_r(t) := (\psi_r(t), \theta_r(t), \phi_r(t))$, with the yaw angle trajectory imposed as a reference $\psi_r(t)$ and the trajectories $\theta_r(t), \phi_r(t)$ to be chosen freely together with the value of the thrust force $T(t)$ to match any desired value of the right hand side control vector $U(t)$. Then, the position control law of Proposition 2 could be applied to steer the position system as required. By making the

following variable substitutions in the generic second order tracking system (5.24) with $n = 3$:

$$\begin{aligned} &x_1 := p;\ x_2 := \dot{p};\ x_{1r} := p_r; \\ &\hat{d} := \hat{d}_p + G;\ U^H := U_p \end{aligned} \tag{5.78}$$

the control law for tracking a given spatial reference position p_r would be given by

$$\begin{aligned} U_p := &(K_{1p} + K_{2p})(\dot{p}_r - \dot{p}) + K_{2p}K_{1p}(p_r - p) \\ &+ \ddot{p}_r - \hat{d}_p - G \end{aligned} \tag{5.79}$$

where it is assumed that the actual position and velocity vectors p and $\dot{p}$ would be available for on-line measurement. The control law U_p of (5.79) will henceforward be referred to as the "desired" position control because it would have to be "reconciled" with the U of (5.77) as, generally, $\Theta(t) \neq \Theta_r(t)$.

On the other hand, the attitude subsystem is fully actuated. As will become clear, the precision, robustness, and speed of the tracking attitude control will prove primordial towards achieving the overall tracking goal of combined position and yaw angle of the rotorcraft. Sliding mode control is hence better suited to attain tracking of the attitude. To this end the disturbance vector d_Θ is considered estimated and the following variable substitutions are made in (5.24) with $n = 3$:

$$\begin{aligned} &x_1 := \Theta;\ x_2 := \dot{\Theta};\ x_{1r} := \Theta_r; \\ &\hat{d} := \hat{d}_\Theta + \Phi(\Theta, \dot{\Theta});\ U^S := U_\Theta \end{aligned} \tag{5.80}$$

To deliver the sliding mode tracking law for the entire Θ_r with suitably chosen gain matrices A, $K_3 > 0.5I, K_4 > 0.5I$ as in Proposition 5.2.

$$
\begin{aligned}
U_\Theta := (K_{1\Theta} + K_{2\Theta})(\dot{\Theta}_r - \dot{\Theta}) + K_{2\Theta}K_{1\Theta}(\Theta_r - \Theta) \\
+ \ddot{\Theta}_r - \hat{d}_\Theta - \Phi(\Theta, \dot{\Theta}) \\
+ A_\Theta \ \text{sign}[(\dot{\Theta}_r - \dot{\Theta}) + K_{1\Theta}(\Theta_r - \Theta)]
\end{aligned} \tag{5.81}
$$

It is again assumed that the angular position and velocity vectors Θ and $\dot{\Theta}$ are available for on-line measurement.

The above control laws are abstract in the sense that they cannot be applied directly to achieve the tracking goal as stated in section 5.4, if only for the reason that the "decoupling" virtual attitude needed in (5.77) is yet undefined. However, the idea is now clear as the number of the system variables to be tracked (x_r, y_r, z_r, ψ_r) matches the number of "free" control variables (U_1, U_2, U_3, U_4) so, indirectly, the tracking problem is fully actuated. The "virtual reference trajectories" $\theta_t(t), \phi_r(t); t \geq 0$, for the "free" attitude angles θ and ϕ can be imposed as to emulate independence of the three "desired" position control components (U_{xd}, U_{yd}, U_{zd}) of U_p in (5.79). Exact tracking of full attitude in $\mathbb{R}^3$ is feasible because the components of the attitude control $U_\Theta = [U_2, U_3, U_4]$ are unconstrained and matched to the unknown disturbances thus permitting simultaneous tracking of all the three attitude reference trajectories $(\psi_r, \theta_r, \phi_r)$.
To generate the aforementioned reference trajectories θ_r and ϕ_r, it is first convenient to re-state the explicit parametrization of the desired control $U_p = (U_{xd}, U_{yd}, U_{zd})$ as given by (5.79) :

$$U_{xd} = (C_{\phi_r} S_{\theta_r} C_{\psi_r} + S_{\phi_r} S_{\psi_r}) \frac{U_{1d}}{m} \tag{5.82}$$

$$U_{yd} = (C_{\phi_r} S_{\theta_r} S_{\psi_r} - S_{\phi_r} C_{\psi_r}) \frac{U_{1d}}{m} \tag{5.83}$$

$$U_{zd} = (C_{\phi_r} C_{\theta_r}) \frac{U_{1d}}{m} \tag{5.84}$$

where, at this point, U_{1d} has the interpretation of a desired thrust force to be applied to the system. Multiplying (5.82) and (5.83) by C_{ψ_r} and S_{ψ_r}, respectively, and adding the result side by side yields

$$C_{\psi_r} U_{xd} + S_{\psi_r} U_{yd} = (C_{\phi_r} S_{\theta_r}) \frac{U_{1d}}{m} = \tan(\theta_r) U_{zd} \tag{5.85}$$

Similarly, multiplying (5.82) and (5.83) by S_{ψ_r} and $-C_{\psi_r}$, respectively, and adding the result side by side yields

$$S_{\psi_r}U_{xd} - C_{\psi_r}U_{yd} = S_{\phi_r}\frac{U_{1d}}{m} = \tan(\phi_r)\frac{U_{zd}}{C_\theta} \tag{5.86}$$

Hence, it follows that, given any desired values of U_{xd}, U_{yd} and $U_{zd} \neq 0$, that satisfy (5.79), and any reference value of the yaw angle ψ_r, one can impose corresponding "desired values" of the roll and pitch angles :

$$\theta_r = \arctan\frac{(C_{\psi_r}U_{xd} + S_{\psi_r}U_{yd})}{U_{zd}} \tag{5.87}$$

$$\phi_r = \arctan\frac{C_{\theta_r}(S_{\psi_r}U_{xd} - C_{\psi_r}U_{yd})}{U_{zd}} \tag{5.88}$$

so that any desired (U_{xd}, U_{yd}, U_{zd}) controls are replaced, albeit indirectly, by the "virtual controls" $(\theta_r, \phi_r, U_{1d})$.

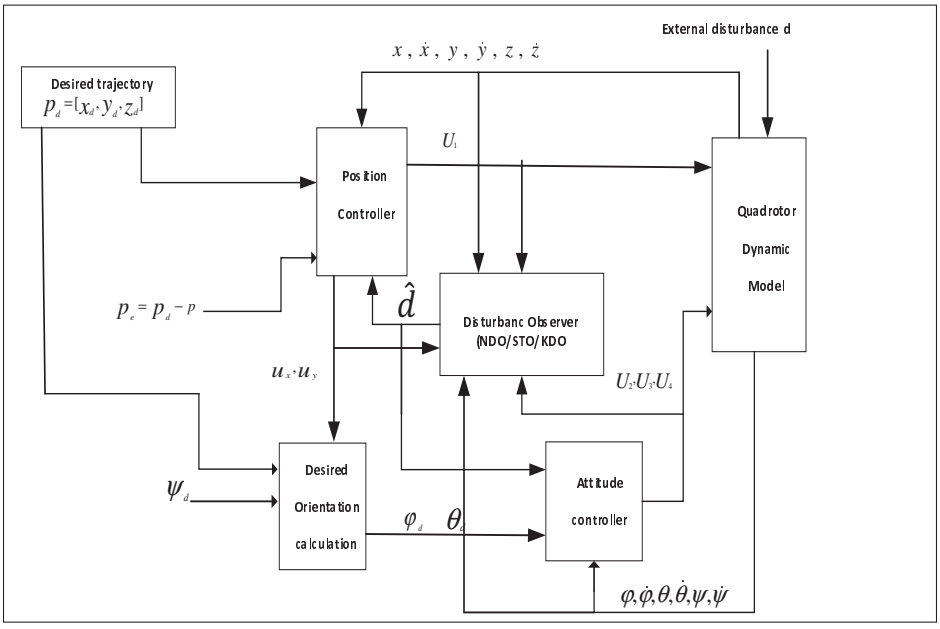

Figure 5.2 Block diagram of the controller and observer

The position and attitude control systems are coupled in such a way as to permit the desired attitude angles ϕ_r and θ_r and to be tracked by the attitude controller (see Fig. 5.2) implicitly using the position control law (5.79).

5.7 Observer-based tracking control analysis

If the unknown disturbances d_p and d_Θ are estimated by their respective observers KDO, NDO, or STO, the position and attitude closed loop subsystems with all their inaccuracies can be written as

$$\ddot{p} = G + U_p^A + \hat{d}_p + e_{d_p} + (U_p - U_p^A) \tag{5.89}$$

$$\ddot{\Theta} = \Phi(\Theta, \dot{\Theta}) + U_\Theta + \hat{d}_\Theta + e_{d_\Theta} \tag{5.90}$$

with the control laws U_p^A and U_Θ employing the estimates $\hat{d}_p$ and $\hat{d}_\Theta$. U_p^A is then given by; see (5.4):

$$U_p^A(t) = \frac{1}{m} R(\Theta(t)) T^A(t) e_z \tag{5.91}$$

where the thrust force function is calculated as

$$U_{1d}(t) := T^A(t) = m \frac{U_{zd}(t)}{C_{\phi_r(t)} C_{\theta_r(t)}} > 0 \tag{5.92}$$

as in (5.91), (5.81), with the total unknown disturbances in the position and atttude subsystems defined as

$$e_p := e_{d_p} + (U_p - U_p^A) \tag{5.93}$$

$$e_\Theta := e_{d_\Theta} \tag{5.94}$$

For simplicity of the convergence analysis and without much loss of generality it will henceforth be assumed that all the controller gains are diagonal as given by:

$$K_{ip} := k_{ip} I_{3\times 3};\ K_{i\Theta} := k_{i\Theta} I_{3\times 3};\ \ i = 1,2$$
$$A_\Theta := \text{diag}\{a_1, a_2, a_3\} \tag{5.95}$$

for some positive constants $k_{ip}, k_{i\Theta}, a_k;\ i = 1,2, k = 1,2,3$.

Therefore, the tracking control for the quadrotor is implementable only when the computed, desired altitude control component U_{zd} of U_p is strictly positive for all times.

Definition 5.1. *(Tracking control feasibility) The tracking control is feasible if the initial conditions of the system, the reference trajectories to be tracked $p_r(t), \psi_r(t); t \geq 0$, the ensemble of system disturbances, and the position controller gains $k_{ip}, i = 1,2$, are such that the computed altitude control component, and consequently the control thrust force satisfy*

$$U_{zd}(t) > 0,\ T^A(t) > 0;\quad \textit{for all } t \geq 0 \tag{5.96}$$

A brief discussion of sufficient conditions for the tracking control feasibility is in place. Since the position controller gains are assumed diagonal the instantaneously desired altitude control component of U_p is computed as

$$\begin{aligned} U_{zd} &= (k_{1p} + k_{2p}) e_{2p}(3) + (1 + k_{1p}^2) e_{1p}(3) + \ddot{z}_r \\ &\quad - \hat{d}_z + g \\ e_{1p}(3) &= z_r - z;\ \ e_{2p}(3) = \dot{z}_r - \dot{z} + k_{1p}(z_r - z) \end{aligned} \tag{5.97}$$

where $e_{ip}(3), i = 1,2$, denote the altitude i.e. z-components of the respective tracking errors. It is clear that a sufficient condition for U_{zd} to be positive is that the gravity term g dominates the sum of all other terms in (5.97) at all times. Such condition is clearly too conservative as some of the terms in (5.97) can be positive during tracking and especially during sustained ascent when $e_{1p}(3) > 0, \dot{e}_{1p}(3) > 0$ and $\ddot{z}_r > 0$. The same terms are, however, equally likely to be negative during descent and then the dominance of g might require reduction of the controller gains to preserve positivity of the thrust force during flight. In the case when the vertical

disturbance d_z is estimated without any error (i.e. when $e_{d_p}(3) \equiv 0$) the vertical component of the tracking error eventually converges to zero, so

$$U_{zd} \to \ddot{z}_r - \hat{d}_z + g \quad \text{as } t \to \infty \tag{5.98}$$

If, additionally, the reference accelerations in altitude are asymptotically zero, the necessary condition for tracking control feasibility is the dominance of the vertical disturbance acceleration by the gravitational one.

$$g > |\hat{d}_z(t)| \quad \text{for all } t \geq 0 \tag{5.99}$$

Clearly, this condition is generally not sufficient for control feasibility.

Remark 5.1. *In conclusion, feasibility of the tracking control hinges entirely on the altitude control of the quadrotor. The vertical disturbance force must not exceed the gravitational force for the tracking control to be feasible which is obvious from a practical point of view. Control feasibility is more likely to be lost during descent thus the sign of the calculated desired vertical component of the position control U_{zd} can be monitored and corrected by decreasing the controller gains adaptively during descent, if necessary.*

It is now straightforward to characterize the stability of the overall closed loop tracking control system.

Theorem 5.2. *The quadrotor system in closed loop with the control laws of the form* (5.79) *and* (5.81)*, when coupled with any of the nonlinear estimators (KDO, NDO, or STO) of the unknown disturbances d_p and d_Θ, achieves the tracking goal as specified below.*

With the assumption that the tracking control problem is feasible as defined in Definition 1, with disturbances limited as in (5.99) *, let $p_r(t) \in \mathbb{R}^3$, $\psi_r(t) \in \mathbb{R}$, $t \geq 0$, be the twice continuously differentiable position and yaw angle reference trajectories to be tracked asymptotically. Given an admissible tolerance $\epsilon_{tol} > 0$ for the total asymptotic tracking error in the position*

and yaw angle (p,ψ)*, there exist position controller gains* K_{1p}, K_{2p}*, attitude controller gains* $K_{1\Theta}, K_{2\Theta}, A_\Theta$*, and a time* $T^* > 0$ *such that*

$$\|p(t) - p_r(t)\|^2 + |\psi(t)) - \psi_r(t)|^2 \leq \epsilon_{tol} \ \ for\ t \geq T^* \tag{5.100}$$

Proof. Since the disturbance observers do not depend directly on the action of the tracking controllers, let $T_E^* > 0$ be a time such that both disturbance observer estimation errors satisfy

$$\max\{\|e_{d_p}(t)\|^2, \|e_{d_\Theta}(t)\|^2\} \leq 0.25\epsilon_{tol};\ \ t \geq T_E^* \tag{5.101}$$

By construction of the virtual attitude trajectory $\Theta_r(t); t \geq 0$, if the tracking control problem is feasible then θ_r, ϕ_r are analytic functions of their arguments, and since the reference trajectory ψ_r is twice differentiable, the following bound holds for the difference between the desired and applied position controls

$$\begin{aligned} &|U_p^A(t) - U_p(t)| \\ &\leq U_{zd}\|R(\Theta(t))e_z\| \left| \frac{1}{C_{\phi_r(t)}C_{\theta_r(t)}} - \frac{1}{C_{\phi(t)}C_{\theta(t)}} \right| \end{aligned} \tag{5.102}$$

for all $t \geq 0$. By continuity of trajectory $\Theta(t); t \geq 0$, there exists a constant $\delta_\Theta > 0$ such that

$$\begin{aligned} &|U_p^A(t) - U_p(t)| < \sqrt{0.25\epsilon_{tol}} \ \ \text{for all } t \text{ such that} \\ &\|\Theta(t) - \Theta_r(t)\| < \delta_\Theta \end{aligned} \tag{5.103}$$

where, without the loss of generality it can be assumed that $\delta_\Theta < \sqrt{0.5\epsilon_{tol}}$.

As already pointed out, convergence in the attitude tracking is completely independent of the performance of the position tracking control as the attitude subsystem is decoupled from the position subsystem and hence can be controlled independently. Given any attitude reference trajectory Θ_r the sliding mode attitude controller (5.81) in closed loop of the attitude subsystem dynamics can be tuned to deliver asymptotic tracking, in spite of its unknown disturbances e_Θ

as in (5.94)

$$\|\Theta(t) - \Theta_r(t)\| \to 0 \text{ as } t \to \infty \tag{5.104}$$

with any desired convergence rate provided the choice of controller gains $K_{1\Theta}, K_{2\theta}$ and A_Θ are unrestricted to permit full compensation of unknown disturbances. Then let $T^*_\Theta > 0$ be such that

$$\|\Theta(t) - \Theta_r(t)\|^2 \leq \delta_\Theta \leq 0.5\epsilon_{tol} \quad \text{for all } t \geq T^*_\Theta \tag{5.105}$$

It then follows from (5.101) - (5.102) that the total unknown uncertainties (5.93) to be compensated for in the position subsystem are bounded by

$$\|e_p\|^2 \leq \|e_{d_p}\|^2 + |U^A_p(t) - U_p(t)|^2 \leq 0.5\epsilon_{tol}$$
$$\text{for all } t \geq \max\{T^*_E, T^*_\Theta\} \tag{5.106}$$

By virtue of Proposition 2 there exist controller gains K_{1p}, K_{2p} and a time $T^*_p > 0$ such that

$$\|p(t) - p_r(t)\| \leq 0.5\epsilon_{tol} \quad \text{for all } t \geq T^*_p \tag{5.107}$$

in spite of the total unknown disturbances e_p as in (5.93). The inequality (5.100) then holds for

$$T^* := \max\{T_E, T^*_\Theta; T^*_p\} \tag{5.108}$$

This completes the convergence analysis of the observer-based tracking control for the quadrotor.

5.8 Results and discussion

In order to verify the effectiveness of the proposed methods, the physical parameters for the quadrotor UAV are summarized as: h= 0.225 m, $J_R = 3.357 \times 10^{-5}$ Kg m^2, g= $9.81 m/s^2$, I_{xx} =0,0126 $kg.m^2$, I_{yy} =0,0125 $kg.m^2$, and I_{zz} =0,0235 $kg.m^2$. Furthermore, the yaw angle reference trajectory was set at $x_{5r} = 0$ rad over the entire simulation horizon. The quadrotor was required to follow the desired trajectory defined as

For ($t < 10$):

$$x_d = 6x10^{-3}t^2 - 4x10^{-4}t^3$$
$$y_d = 6x10^{-3}t^2 - 4x10^{-4}t^3 \quad \text{for} \quad t < 10$$
$$z_d = 6x10^{-3}t^2 - 4x10^{-4}t^3$$

For ($10 < t \leq 20$):

$$x_d = 0.2$$
$$y_d = 0.2$$
$$z_d = 0.2$$

For ($20 < t \leq 30$)

$$x_d = 3 \times 10^{-3}(t-20)^2 - 2 \times 10^{-4}(t-20)^3$$
$$y_d = 0.2$$
$$z_d = 0.2$$

For ($30 < t \leq 40$):

$$x_d = 0.3$$
$$y_d = 3 \times 10^{-3}(t-30)^2 - 2 \times 10^{-4}(t-30)^3$$
$$z_d = 0.2$$

For $(40 < t \leq 50)$:

$$x_d = 0.3$$
$$y_d = 0.3$$
$$z_d = 0.2$$

For $(50 < t \leq 60)$:

$$x_d = -3 \times 10^{-3}(t-50)^2 + 2 \times 10^{-4}(t-50)^3$$
$$y_d = -3 \times 10^{-3}(t-50)^2 + 2 \times 10^{-4}(t-50)^3$$
$$z_d = 0.2$$

For $(t > 60)$:

$$x_d = 0.2$$
$$y_d = 0.2$$
$$z_d = 0.2$$

The position and attitude controller gains are 3×3 matrices:

$$K_{1p} = \text{diag}[k_{1x}, k_{1y}, k_{1z}],$$
$$K_{2p} = \text{diag}[k_{2x}, k_{2y}, k_{2z}],$$
$$K_{1\Theta} = \text{diag}[k_{1\phi}, k_{1\theta}, k_{1\psi}],$$
$$K_{2\Theta} = \text{diag}[k_{2\phi}, k_{2\theta}, k_{2\psi}],$$
$$A = \text{diag}[A_\phi, A_\theta, A_\psi]$$

5.8.1 Simulation Results

To exhaustively compare the performance of the KDO, NDO, and STO observers, the simulated system was subjected to four different disturbances. The disturbances were considered to be

possible models of a “combination of wind gust and aerodynamics forces". To compare the effectiveness of the observers in rapidly varying windy environments, the disturbance models proposed are chaotic in nature. For comparison of the sole convergence rates of NDO and STO, disturbances which are constant and linear with respect to time were considered. Among the chaotic models of disturbances, the results of one of these models with worst performance are considered only. The KDO has not been included in the convergence rate comparison as it is an “instantaneous” disturbance observer (with the estimation time dictated by the size of the observation window which, in the case of continuous system output measurements, can be chosen arbitrarily.

5.8.2 Disturbance model: Chaotic 1

This section presents simulation results pertaining to disturbances labelled “Chaotic 1” which are of the form,

$$d_i = ka_i(t)sin(\omega t - \phi_i) \tag{5.109}$$

where a_i for $i = 1,...,6$ are trajectories of two independent Lorenz chaotic systems, (i) first system idexed a_i for $i = 1,2,3$ and the (ii) second system indexed $i = 4,5,6$. The evolution of the Lorenz system in this case is described by :

$$\dot{a}_1(t) = 0.15(\sigma(a_2(t) - a_1(t))) \tag{5.110a}$$

$$\dot{a}_2(t) = 0.15(\rho a_1(t) - a_1(t)a_3(t) - a_2(t)) \tag{5.110b}$$

$$\dot{a}_3(t) = 0.15(a_1(t)a_2(t) - \beta a_3(t)) \tag{5.110c}$$

with constants $\sigma = 10$, $\rho = 28$, $\beta = {}^{8}/_{3}$, $k = 0.0.1$, $\omega = 0.5$ and initial conditions for a_i for $i = 1,...,6$ are given by the vector $a(0) = [-6,-5,22,-10,-12,24]$. The phase shifts values are assumed to be $\phi = [25,45,65,10,30,50]$. This results in aperiodic and chaotic system disturbances, as seen in Figures 5.3 and 5.4.

For this set of chaotic disturbances the maximum estimation errors associated with the time convergence using the three observers are summarized in the Table 5.1. The convergence time

is the time taken by NDO and STO to have an estimation error within the range ±0.1 when the observers are initialized at the same point in the observer space (all components of the observer initial state selected to be equal to 0.45).

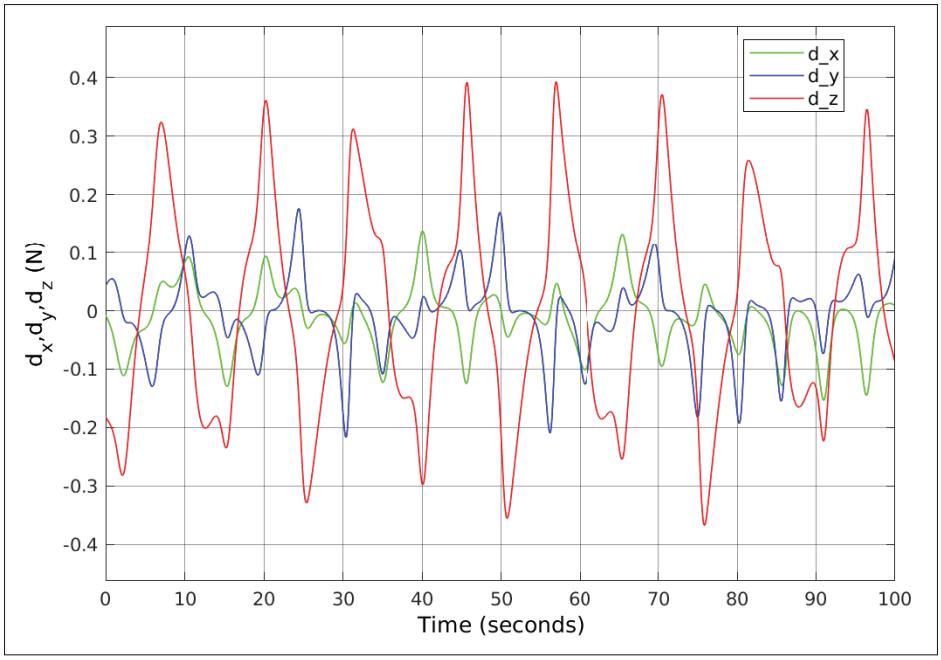

Figure 5.3 Disturbances in position subsystem; Chaotic 1

Table 5.1 Performance comparison of KDO, NDO, STO for disturbance: Chaotic 1

	NDO		STO		KDO	
	time (s)	max error (m)	time (s)	max error (m)	time (s)	max error (m)
d_z	7.266	0.112	1.721	0.096	0	$8.906 * 10^{-5}$
d_x	8.201	0.147	1.659	0.090	0	$1.487 * 10^{-4}$
d_y	4.306	0.361	3.611	0.141	0	$2.401 * 10^{-4}$
d_ϕ	34.08	0.110	1.902	0.041	0	$9.453 * 10^{-5}$
d_θ	24.52	0.183	0.650	0.089	0	$2.073 * 10^{-4}$
d_ψ	20.47	0.260	0.951	0.091	0	$1.955 * 10^{-4}$

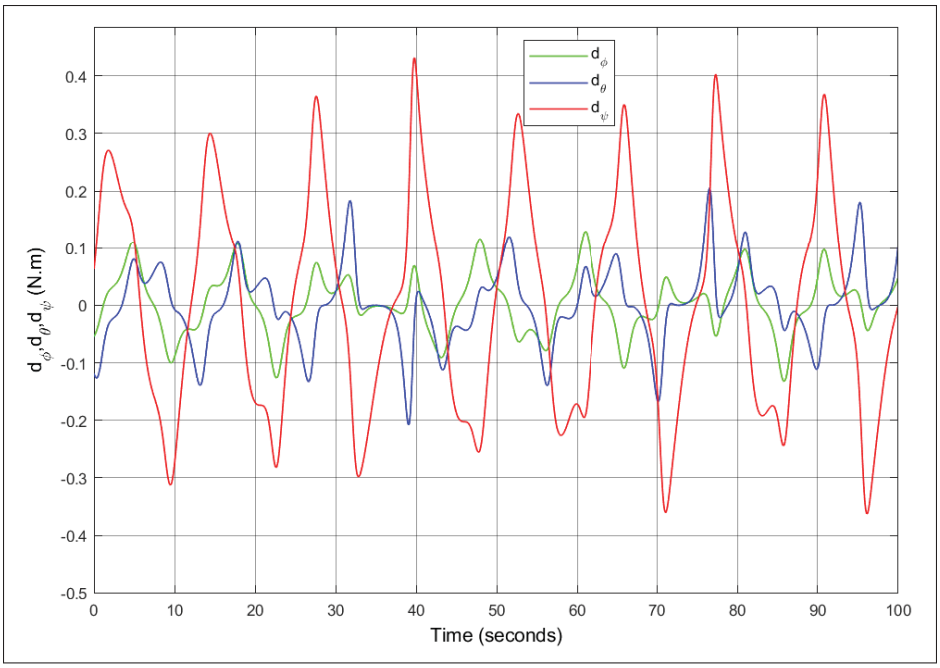

Figure 5.4 Disturbances in attitude subsystem: Chaotic 1

Using Table 5.1, the disturbance estimation with maximum estimation error (one of the worst cases) for each observer is presented in Fig. 5.5 - Fig. 5.7

From Table 5.1 and Table 5.2, it can be observed that among the two chaotic disturbances, the attitude and position tracking performance under chaotic model 1 disturbance is the worse in this case. Therefore, we chose the Chaotic 1 disturbance model to compare the three observers. The tracking results of the three observers under the effect of Chaotic 1 disturbance model are presented in Fig. 5.8- Fig. 5.25

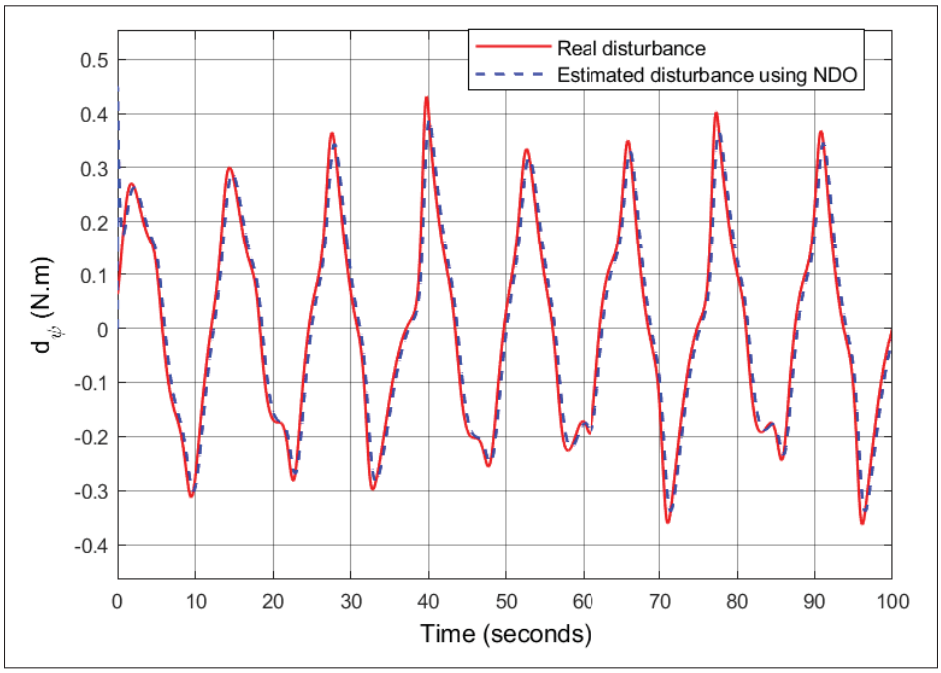

Figure 5.5 Disturbance estimation of yaw angle using NDO; Chaotic 1

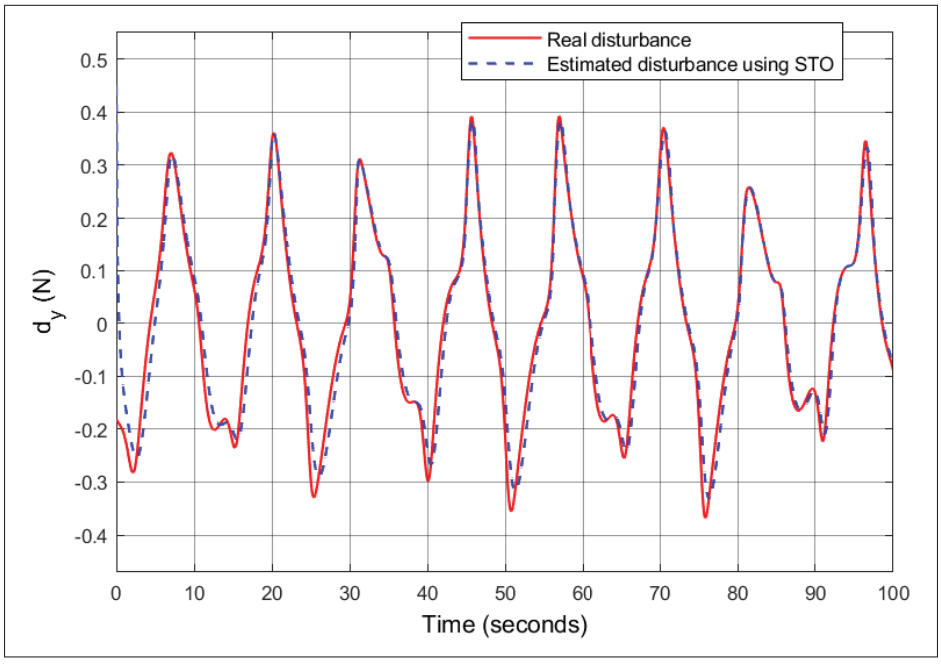

Figure 5.6 Disturbance estimation of *y* position using STO; Chaotic 1

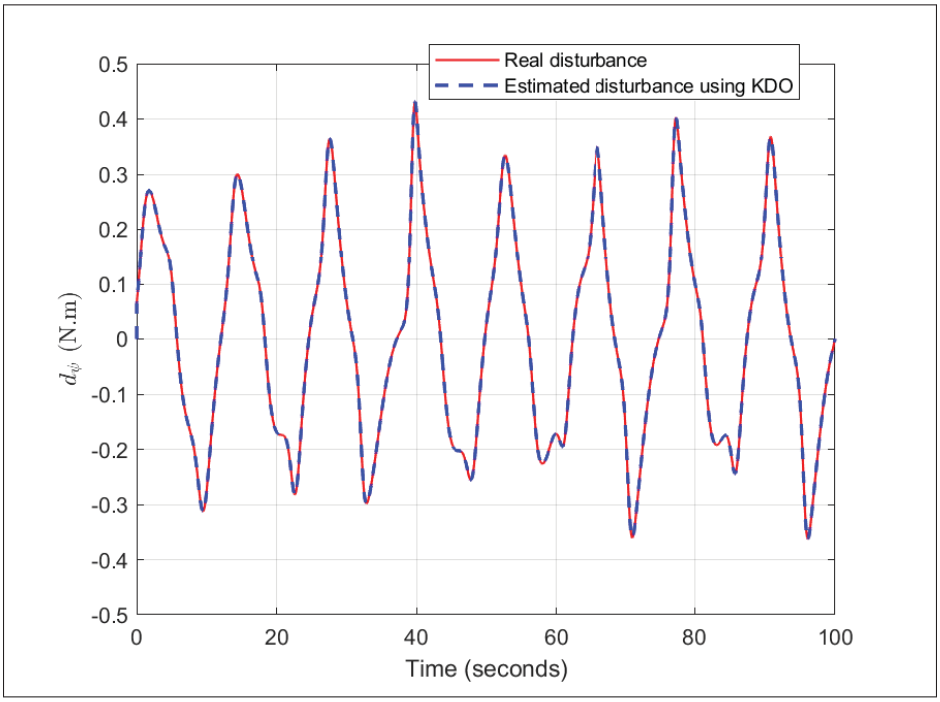

Figure 5.7 Disturbance estimation of yaw angle using KDO; Chaotic 1

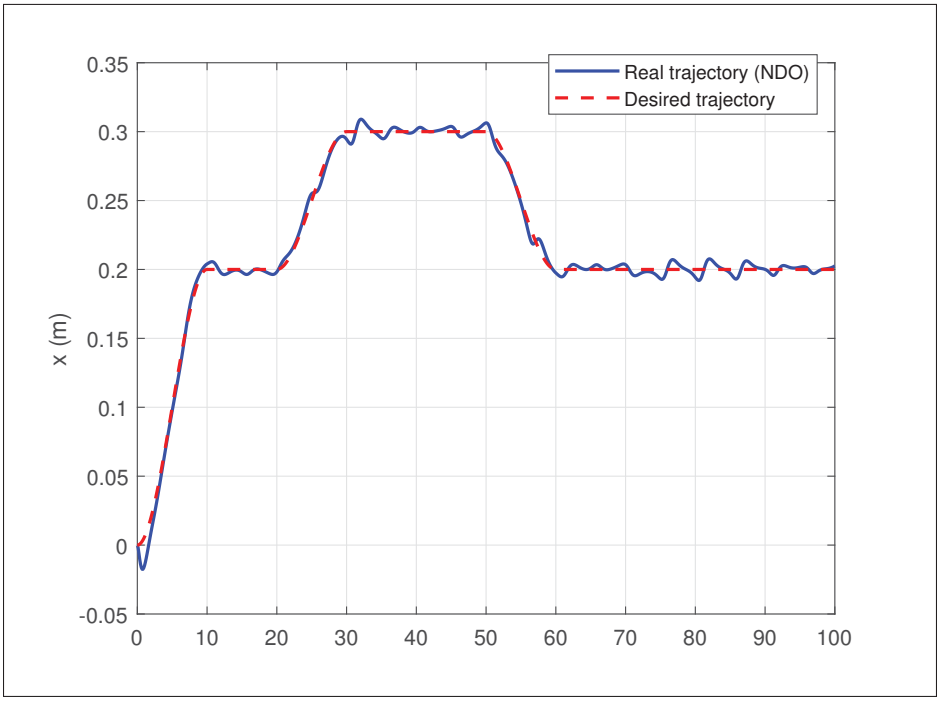

Figure 5.8 Tracking of x coordinate using NDO

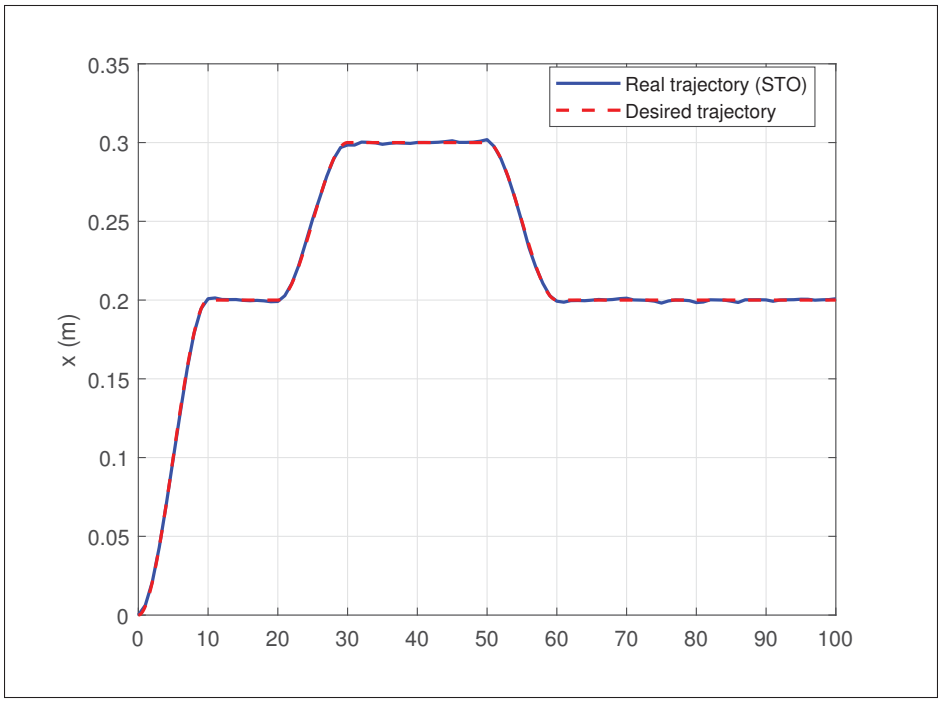

Figure 5.9 Tracking of x coordinate using STO

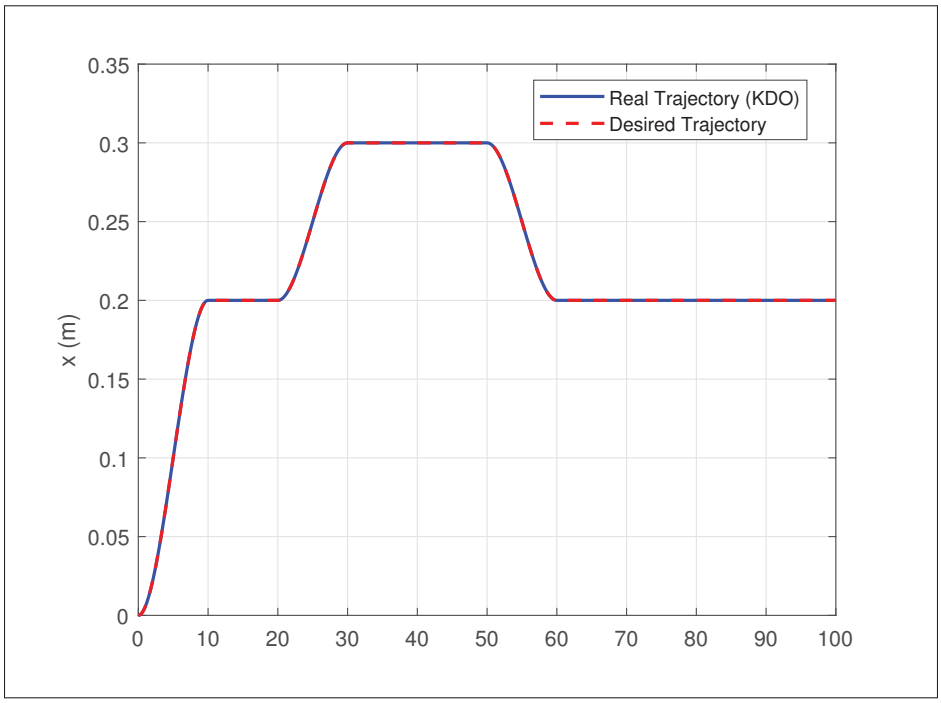

Figure 5.10 Tracking of x coordinate using KDO

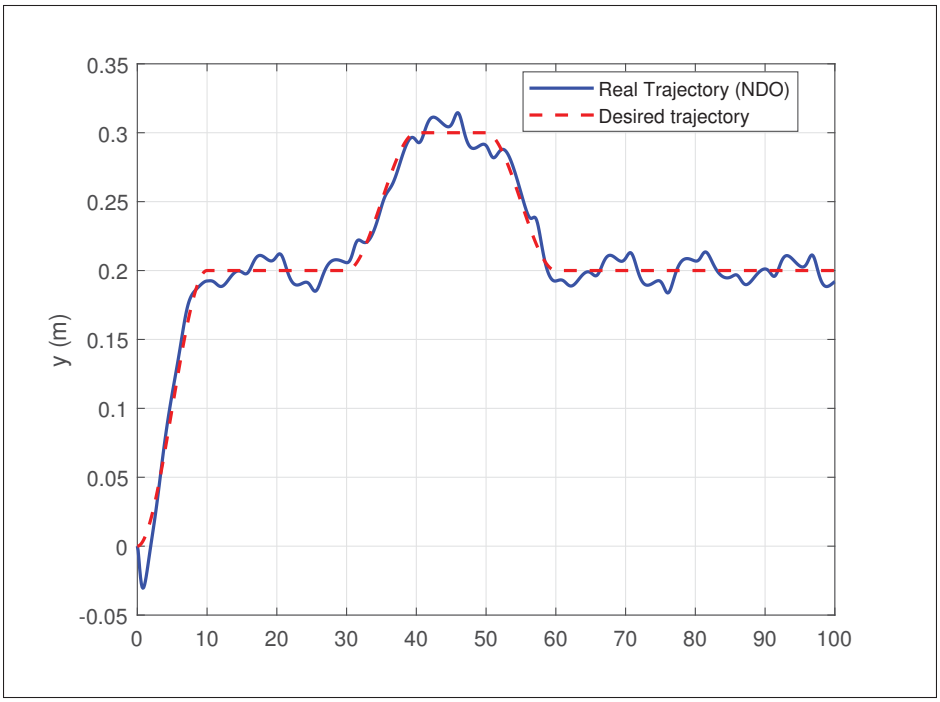

Figure 5.11 Tracking of y coordinate using NDO

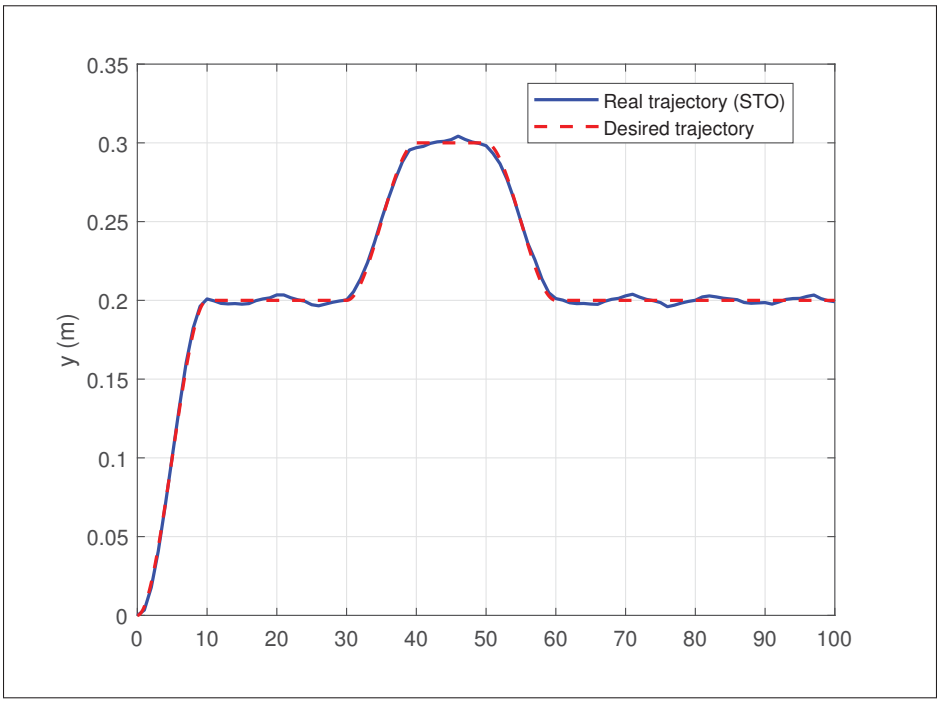

Figure 5.12 Tracking of y coordinate using STO

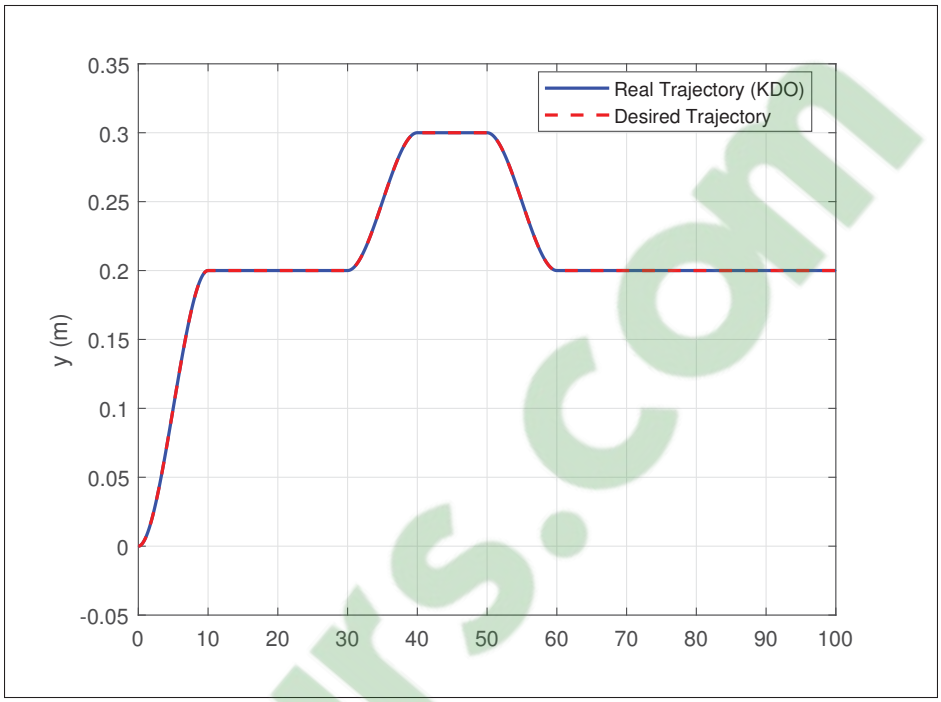

Figure 5.13 Tracking of y coordinate using KDO

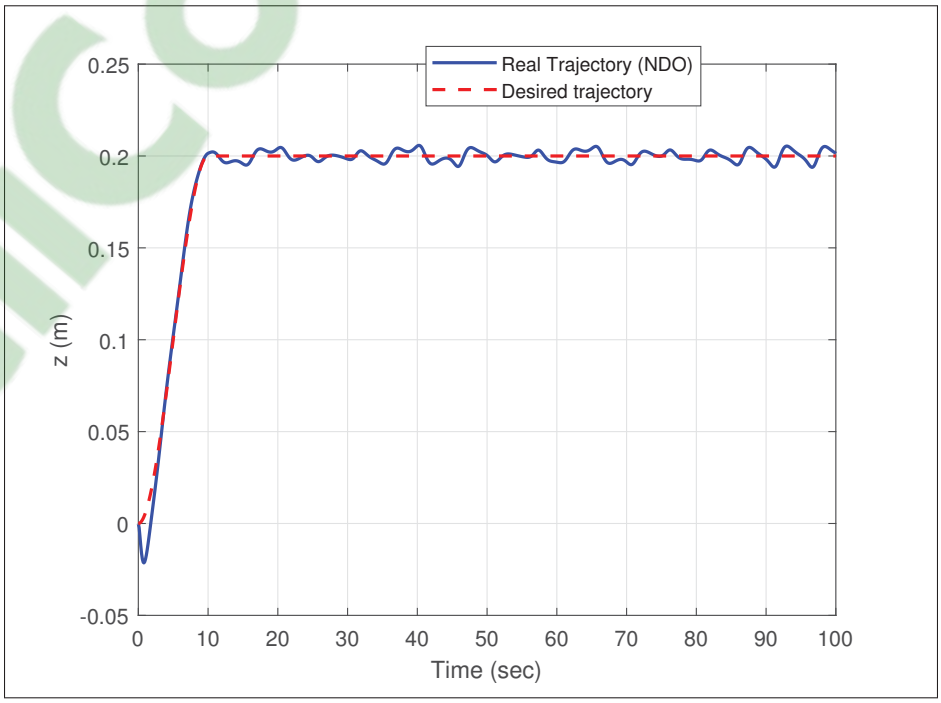

Figure 5.14 Tracking of z coordinate using NDO

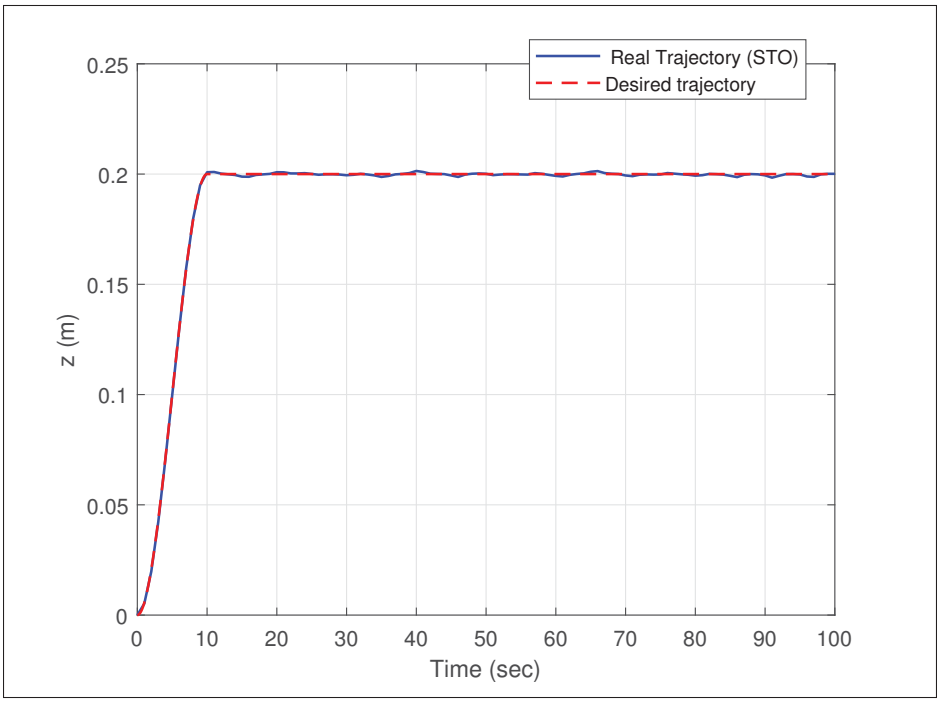

Figure 5.15 Tracking of z coordinate using STO

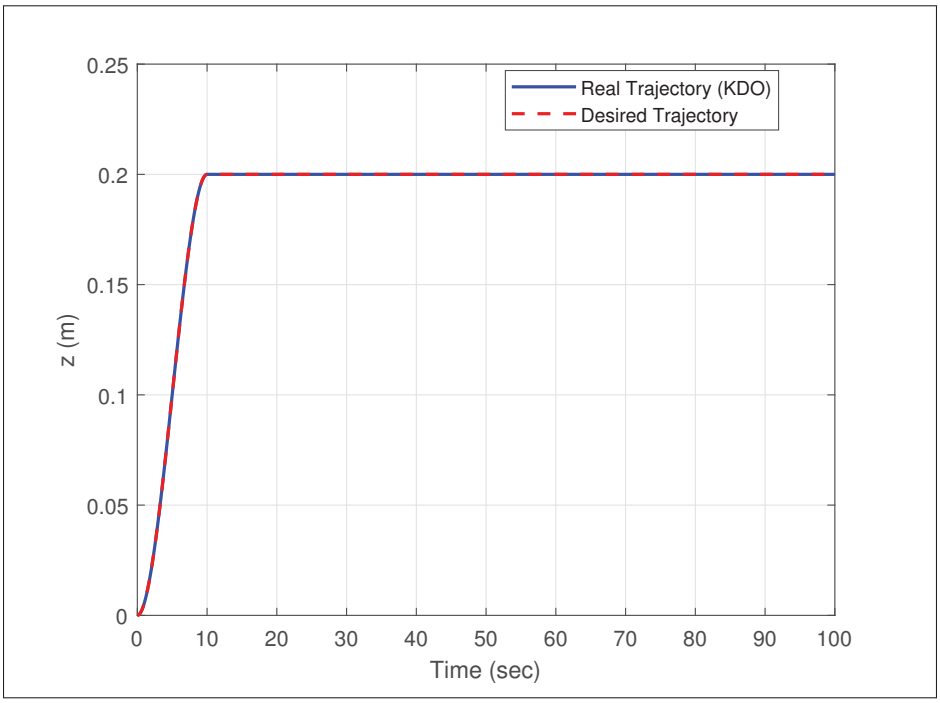

Figure 5.16 Tracking of z coordinate using KDO

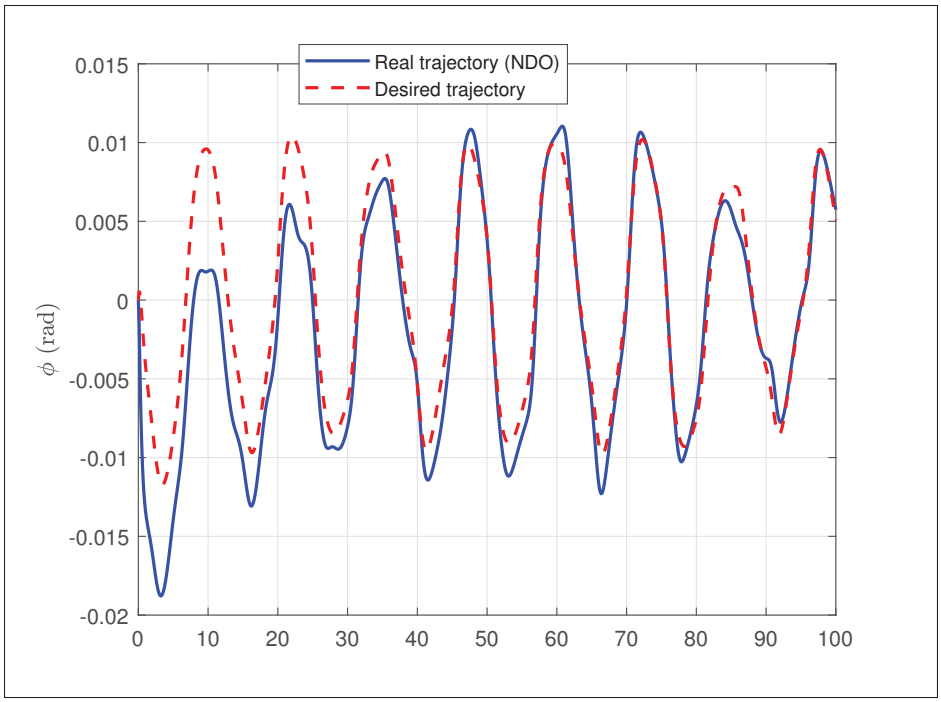

Figure 5.17 Tracking of roll angle using NDO

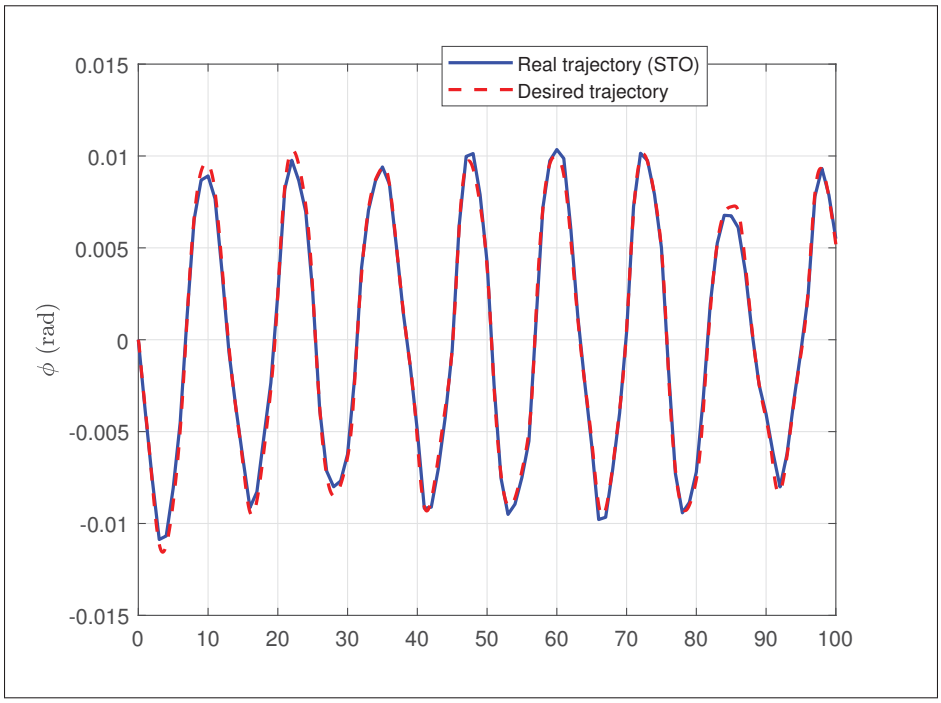

Figure 5.18 Tracking of roll angle using STO

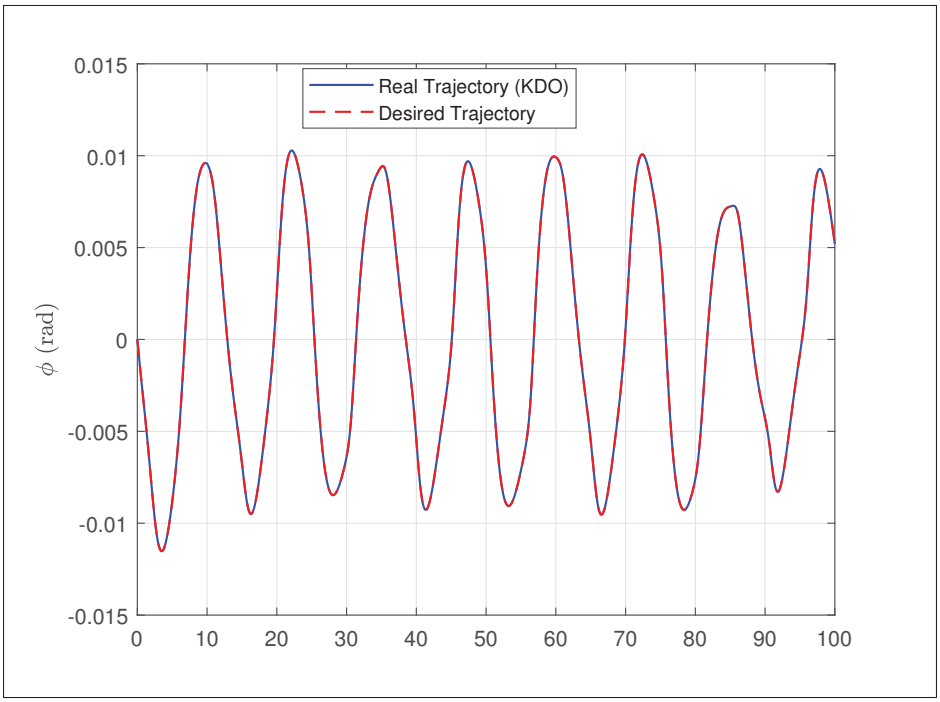

Figure 5.19 Tracking of roll angle using KDO

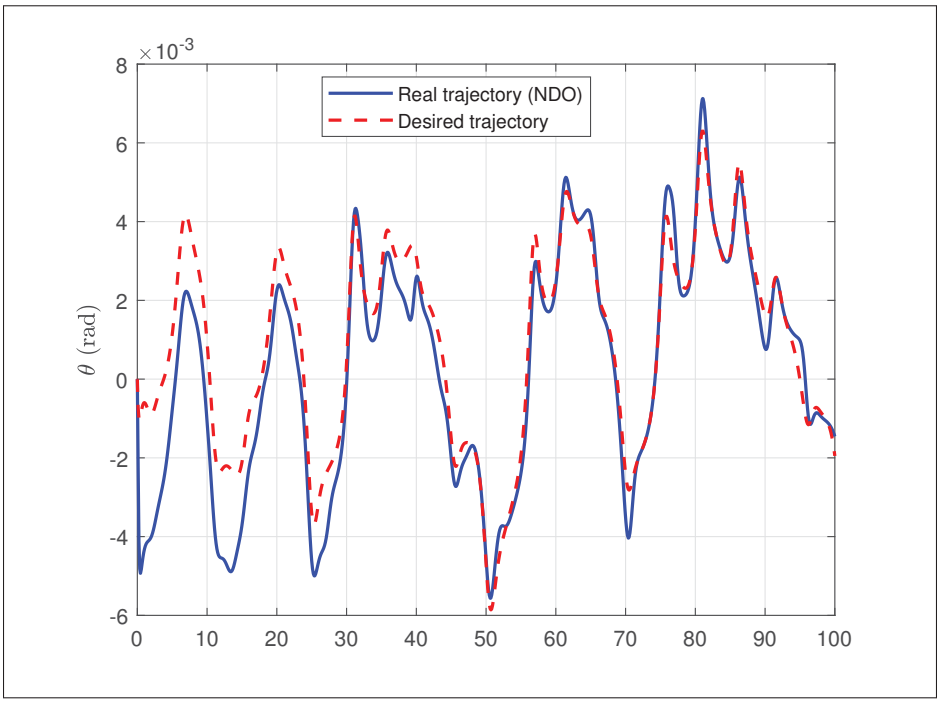

Figure 5.20 Tracking of pitch angle using NDO

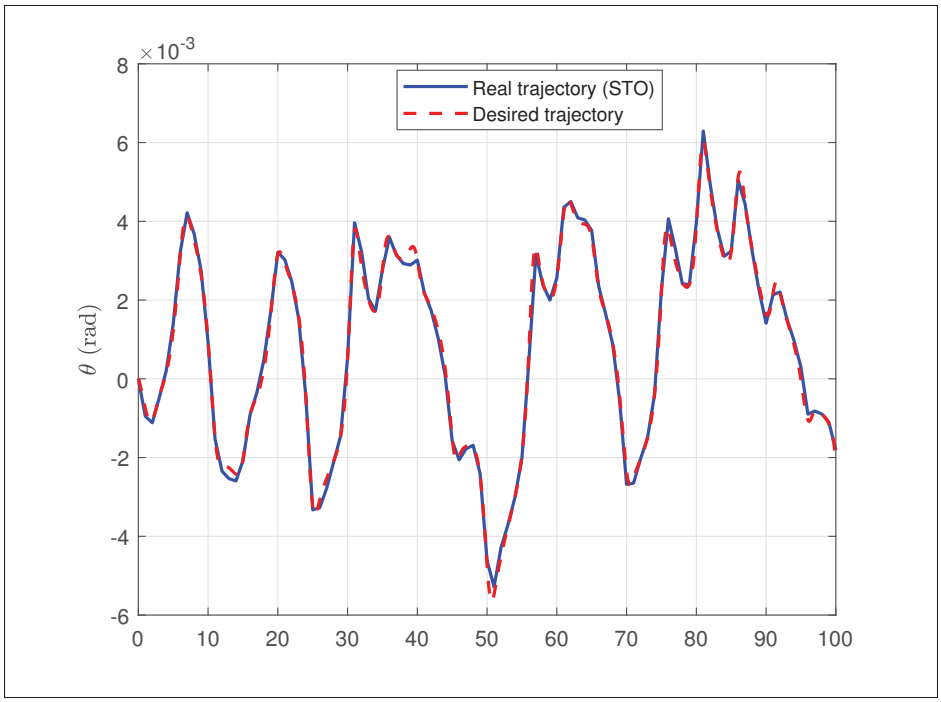

Figure 5.21 Tracking of pitch angle using STO

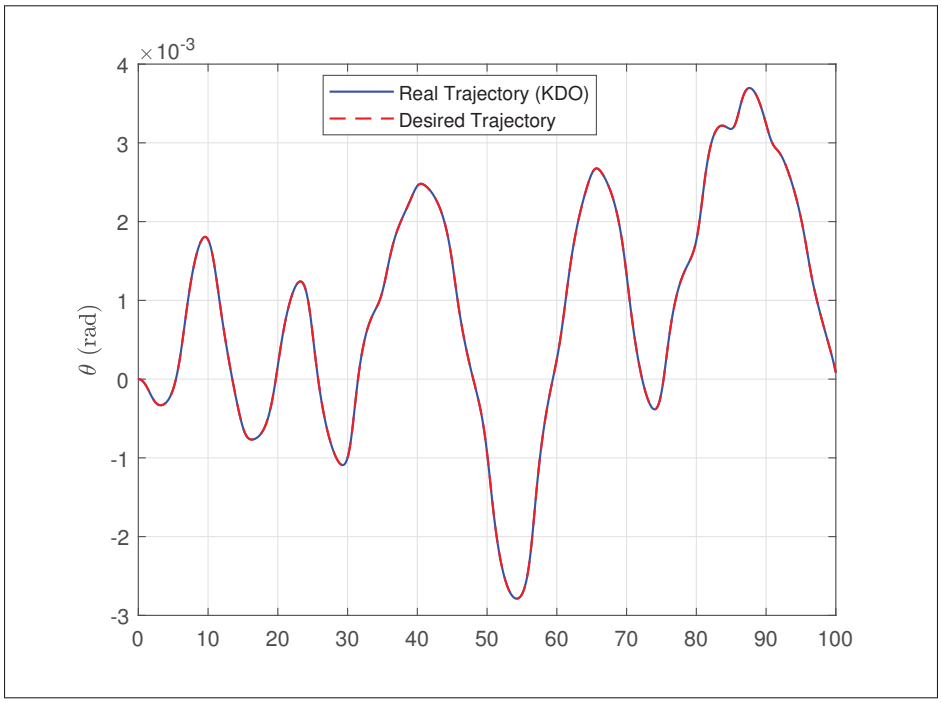

Figure 5.22 Tracking of pitch angle using KDO

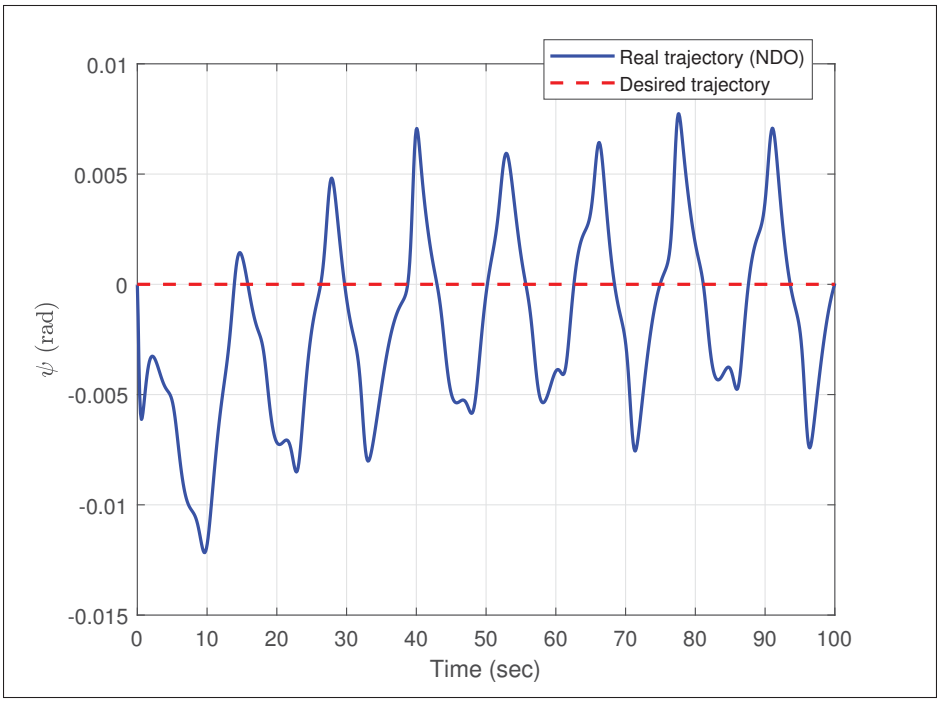

Figure 5.23 Tracking of yaw angle using NDO

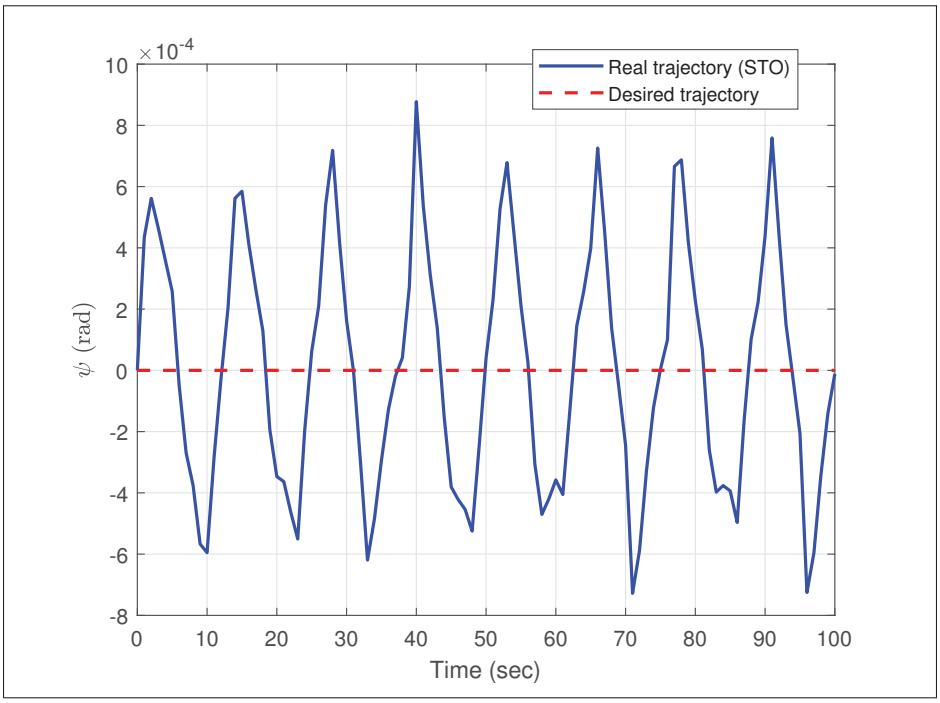

Figure 5.24 Tracking of yaw angle using STO

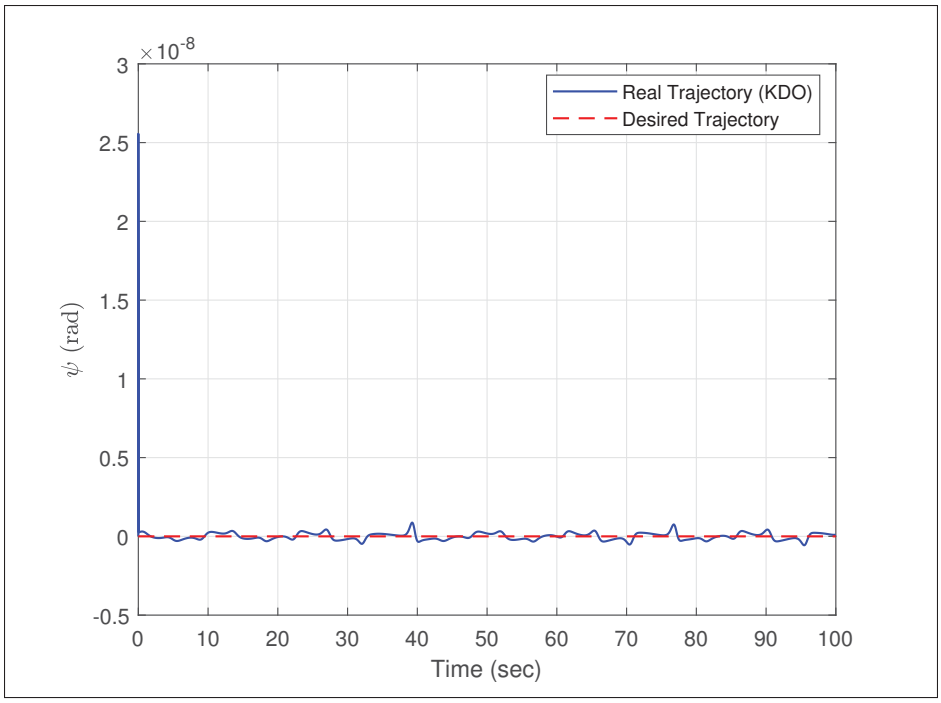

Figure 5.25 Tracking of yaw angle using KDO

5.8.3 Disturbance model: Chaotic 2

The disturbances are again of the form,

$$d_i = ka_i(t)sin(\omega t - \phi_i) \tag{5.111}$$

where the a_i for $i = 1,...,6$, are trajectories of two independent Lorenz chaotic systems a_i for $i = 1,2,3$ and the second system for $i = 4,5,6$. The Lorenz system in this case is :

$$a_1'(t) = 0.15(\sigma(a_2 - a_1)) \tag{5.112a}$$

$$a_2'(t) = 0.15(\rho a_1 - a_1 a_3 - a_2) \tag{5.112b}$$

$$a_3'(t) = 0.15(a_1 a_2 - \beta a_3) \tag{5.112c}$$

where the constants $\sigma = 10$, $\rho = 28$, $\beta = {}^{8}/_{3}$, $k = 0.0.1$, $\omega = 0.5$ with initial values of a_i for $i = 1,...,6$ are given by the vector $[-6,-5,22,-10,-12,24]$, the phase shift values, ϕ_i for $i =$

1,...,6 is given by the vector, [25,45,65,10,30,50]. This results in the applied disturbances to be non-periodic and chaotic, as seen in Figures 5.26 and 5.27.

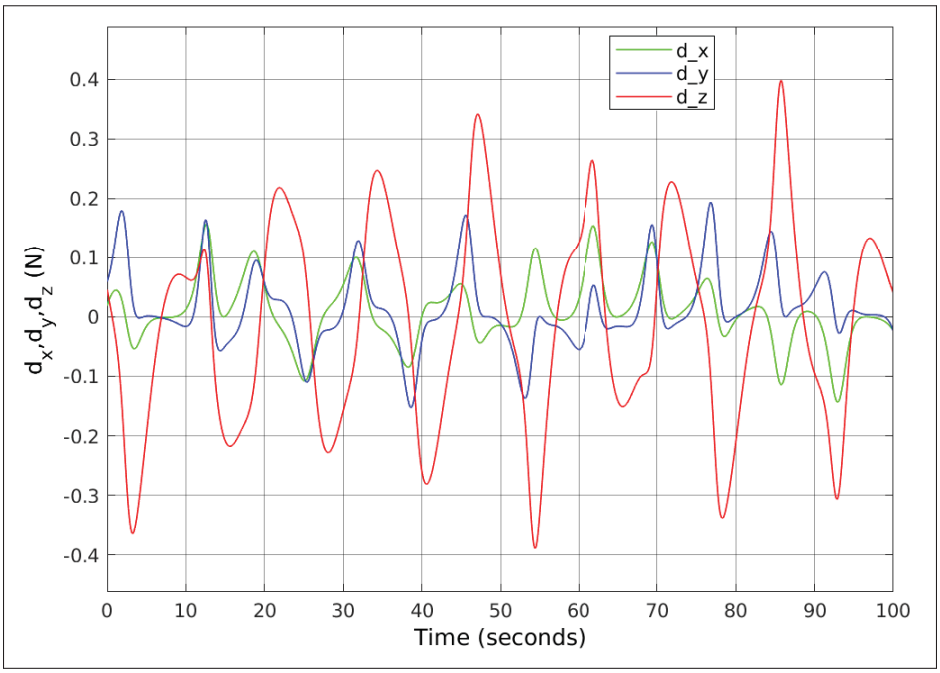

Figure 5.26 Chaotic Disturbances 2 in Position Subsystem

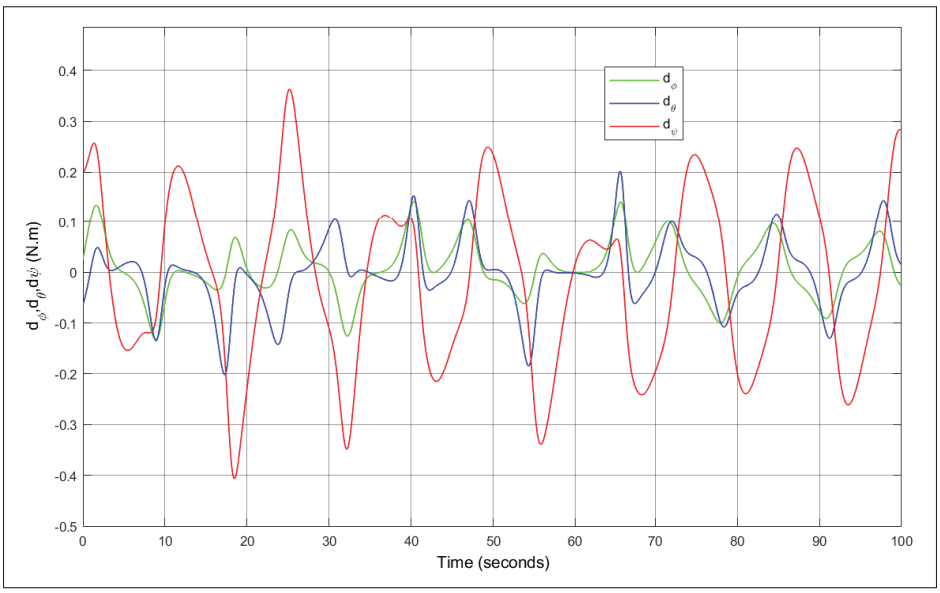

Figure 5.27 Chaotic Disturbances 2 in Attitude Subsystem

For this set of chaotic disturbances the maximum estimation errors associated with the time convergence using the three observers are summarized in the Table 5.2. The convergence time is the time taken by NDO and STO to have an estimation error within the range ±0.1 when the observers are initialized with the initial observer state of 0.45.

Using Table 5.2, the disturbance estimation with maximum estimation error (one of the worst cases) for each observer is presented in Fig. 5.28 - Fig. 5.30

Table 5.2 Performance comparison of KDO, NDO, STO for disturbance: Chaotic System 2

	NDO		STO		KDO	
	time (s)	max error (m)	time (s)	max error (m)	time (s)	max error (m)
d_z	6.03	0.136	3.075	0.551	0	$1.422 * 10^{-4}$
d_x	6.55	0.180	3.642	0.116	0	$3.446 * 10^{-4}$
d_y	3.12	0.388	2.289	0.136	0	$4.137 * 10^{-4}$
d_ϕ	26.58	0.155	1.204	0.025	0	$1.034 * 10^{-4}$
d_θ	15.82	0.194	1.328	0.072	0	$3.575 * 10^{-4}$
d_ψ	12.34	0.396	2.157	0.086	0	$4.893 * 10^{-4}$

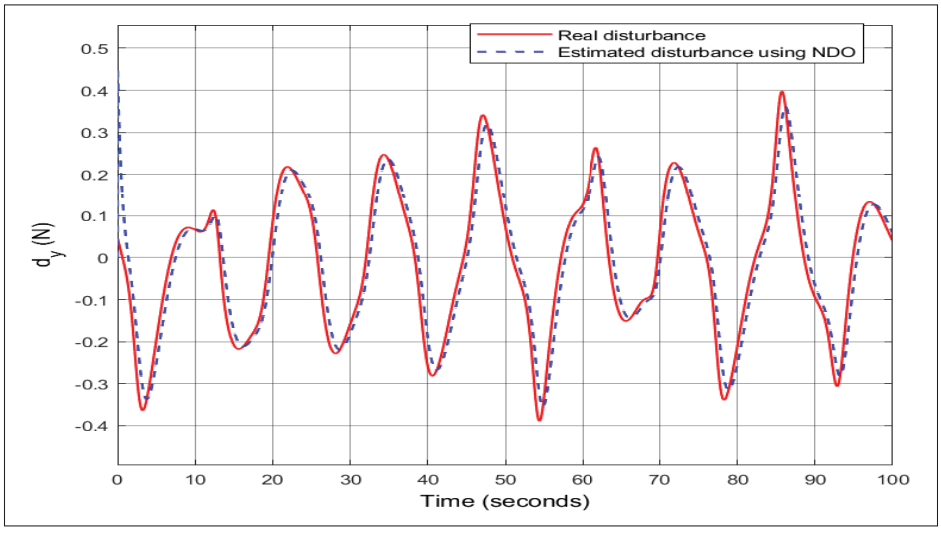

Figure 5.28 Chaotic Disturbances estimation of y component using NDO

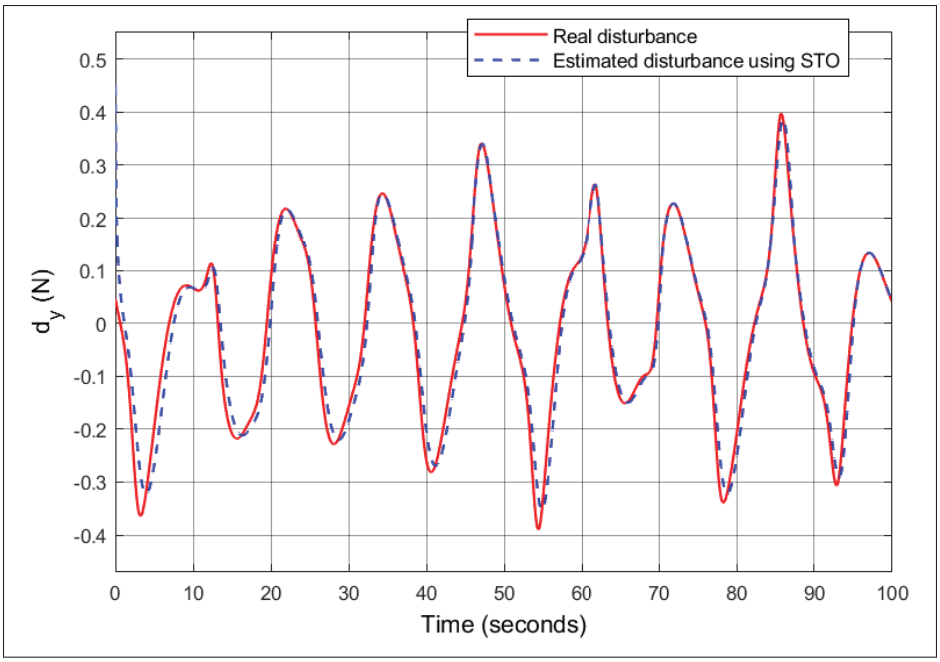

Figure 5.29 Chaotic Disturbances estimation of *y* component using STO

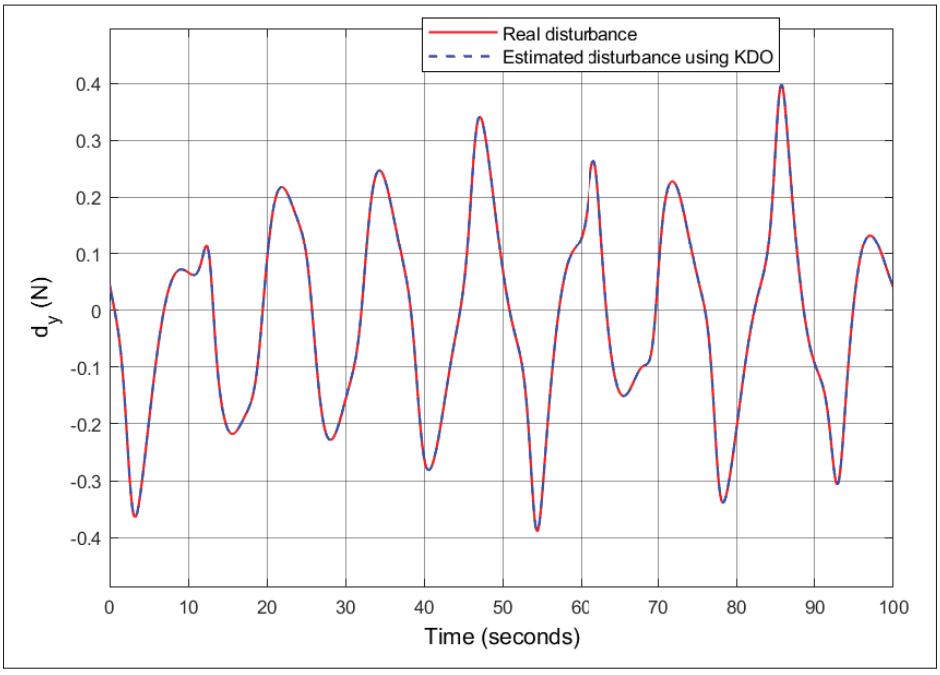

Figure 5.30 Chaotic Disturbances estimation of *y* component using KDO

5.8.4 Disturbance model: Linear

The same quadrotor system was also simulated with disturbances that increased or decreased with time. The disturbances were of the form,

$$d_i = k_i.t \tag{5.113}$$

where $i = x, y, z, \phi, \theta, \psi$ and the vector $k = [1, -3, 2, 1.5, 2.5, -2.5] * 10^{-3}$. For the set of linear disturbances, the estimation results are summarized in Table 5.3. The convergence time is the time taken by NDO and STO to have an estimation error within the range ±0.1 when the observers are initialized with the initial observer state of 0.45 for each component.

Table 5.3 Performance comparison of KDO, NDO, STO for disturbance:Linear disturbances

	NDO		STO		KDO	
	time (s)	max error (m)	time (s)	max error (m)	time (s)	max error (m)
d_z	22.757	0.005	3.549	0.0005	0	$1.002 * 10^{-6}$
d_x	20.254	0.015	5.204	0.0013	0	$3.142 * 10^{-6}$
d_y	19.584	0.001	3.420	0.0002	0	$2.435 * 10^{-6}$
d_ϕ	55.234	0.019	2.845	0.0006	0	$1.534 * 10^{-6}$
d_θ	46.565	0.045	2.594	0.0006	0	$2.532 * 10^{-6}$
d_ψ	41.543	0.052	2.487	0.0005	0	$2.504 * 10^{-6}$

5.8.5 Disturbance model: Constant

Similar to the case of applying linear disturbances, linear disturbances were applied to the same quadrotor system where the disturbances remained constant with time. The disturbances were of the form,

$$d_i = c_i \tag{5.114}$$

where $i = x, y, z, \phi, \theta, \psi$ and the vector $c_i = [0.1, 0.3, -0.2, -0.05, -0.25, 0.15]$. For the set of constant disturbances the estimation results are summarized in Table 5.4. The convergence

time is the time taken by NDO and STO to have an estimation error within the range ±0.1 when the observers are initialized with the initial observer state of 0.45 for each component.

Table 5.4 Performance comparison of KDO, NDO, STO for disturbance:Constant disturbances

	NDO		STO		KDO	
	time (s)	max error (m)	time (s)	max error (m)	time (s)	max error (m)
d_z	10.354	0.359	3.259	0.359	0	$3.553 * 10^{-7}$
d_x	10.353	0.153	2.663	0.148	0	$1.735 * 10^{-7}$
d_y	15.945	0.642	5.293	0.669	0	$2.460 * 10^{-7}$
d_ϕ	25.394	0.549	3.499	0.530	0	$4.163 ‘ * 10^{-7}$
d_θ	26.903	0.749	5.995	0.719	0	$9.702 * 10^{-7}$
d_ψ	24.959	0.392	1.639	0.344	0	$2.345 * 10^{-7}$

5.9 Conclusion

In this paper, three disturbance estimation techniques are presented; nonlinear disturbance observer, super-twisting sliding mode observer, and kernel disturbance observer in a comparable manner. A regular sliding mode control and backstepping control have engaged with all observers for the quadrotor system. The comparison is made in the presence of external disturbances and aerodynamic effects considering the behavior of states and convergence rate. The kernel disturbance observer performs better than super-twisting sliding mode observer which, in turn, performs better than the nonlinear disturbance observer under the applied external disturbances. Kernel disturbance observer does not need initial conditions and hence the results are independent of initial conditions. NDO and STO show longer convergence times in linear and constant disturbances but have a lower margin of error when compared to the chaotic disturbances; while the KDO performs better in the linear and constant disturbances on all parameters of comparison. Further, the kernel disturbance observer is a deadbeat observer by design, hence the term, "convergence time" for the observer is redundant. Meanwhile, the super-twisting sliding mode observer shows similar results to a variety of initial controller gains. This could be the main drawback in real-time flight. KDO is the most computationally

expensive observer as each iteration requires computation of kernels and the integrals. In addition, kernel disturbance observer and super-twisting sliding mode observer show a flexible environment for the initialization of the controller gains. On the other hand, nonlinear disturbance observer needs an adjusted controller gains for initialization and does not allow arbitrary gains. This leads to the fact that practical super-twisting sliding mode observer capability in the presence of bounded external disturbances result in finite time convergence as compared to NDO where the convergence is asymptotic, which is appropriate in the disturbed environment. This endeavor of exploring super-twisting sliding mode observers will be a good starting point to compare them with other observers of its kind (differential observer). Due to the computational complexity of the KDO, the observer would need to be modified for its practical implementation as future work.

CONCLUSION AND RECOMMENDATIONS

This thesis work was focused on developing a consistent control technique for a quadrotor UAV executing a tracking task in coordination. Different nonlinear controllers combined with observers were simulated and experimentally applied to a quadrotor UAV. To achieve all of the objectives of this thesis, as a first step, an experimental platform was developed and mounted in the laboratory of GREPCI-ETS to implement and validate the different designed control laws. In the second step, several observers for robust tracking control were applied, ensuring that the desired trajectory can be tracked under parameter uncertainties and external disturbances. The overall quadrotor system was divided into subsystems. The main results of this project can be summarized as follows:

- A robust control based on the observer-based approach was modified and applied to an interconnected quadrotor system; this approach was initially developed for quadrotor with different controllers. In this work, this technique was combined with different nonlinear approaches such as the backstepping technique and sliding mode control method. All these proposed control schemes ensure a good tracking of the desired trajectory under unknown external disturbances applied to the quadrotor UAV. These unknown disturbances were firstly estimated by using an observer-based approach. The overall stability of the entire system was proved based on the stability of each subsystem and the appropriate choice of the Lyapunov candidate function.
- A comparison between nonlinear control approaches based on the backstepping and sliding mode techniques combined with different observers simulated numerically and implemented experimentally on the experimental platform developed in the laboratory, as explained above. Signum function was replaced by a continuous function to reduce or limit the chattering phenomenon of sliding mode technique. The proposed control law ensures that the position and attitude errors converge to zero asymptotically. Likewise, the stability of the quadrotor system was proved by using the Lyapunov technique.

Consequently, we can conclude that the developed control strategies guarantee a good desired tracking, compensate and suppress the parametric uncertainties and external disturbances applied to the dynamic system.

Some limitations and problems can be highlighted in this thesis. First, the localization system has to be enhanced to handle more accuracy than the Kinect such as Opti-track or Vicon systems. Second, all of the developed control schemes suppose that the environment is known and do not consider the presence of any obstacle. As the next step for improved achievements, the use of a more accurate localization system is a promising objective. Furthermore, as a recommendation for future work, we will consider a more complex and unknown environment with static and dynamic obstacles. In this case, an algorithm of obstacle avoidance should be combined with the proposed controller to give the quadrotor more robustness. By considering these environments, the developed controllers will not be applied only in the laboratory but can also be implemented on real tasks such as transportation.

APPENDIX I

HARDWARE SET-UP

1. Implementation

The designed controllers are implemented on S500 platform. This section explains the ways to implement and communicate with this quadrotor platform. Several equipments are necessary for the proper functioning of experimentation. A control unit is needed to send and receive information to the quadrotor. A computer with the Ubuntu 14.04 operating system and an Intel Xeon E3-1200 v3 processor is used. This computer retrieved information from the Kinect to run the designed algorithm. Then, the received position is filtered to retrieve velocity using a Kalman filter. The desired trajectory will also be generated by the computer. Eventually, all required information (the current position, current and desired angles) are sent to the quadrotor.

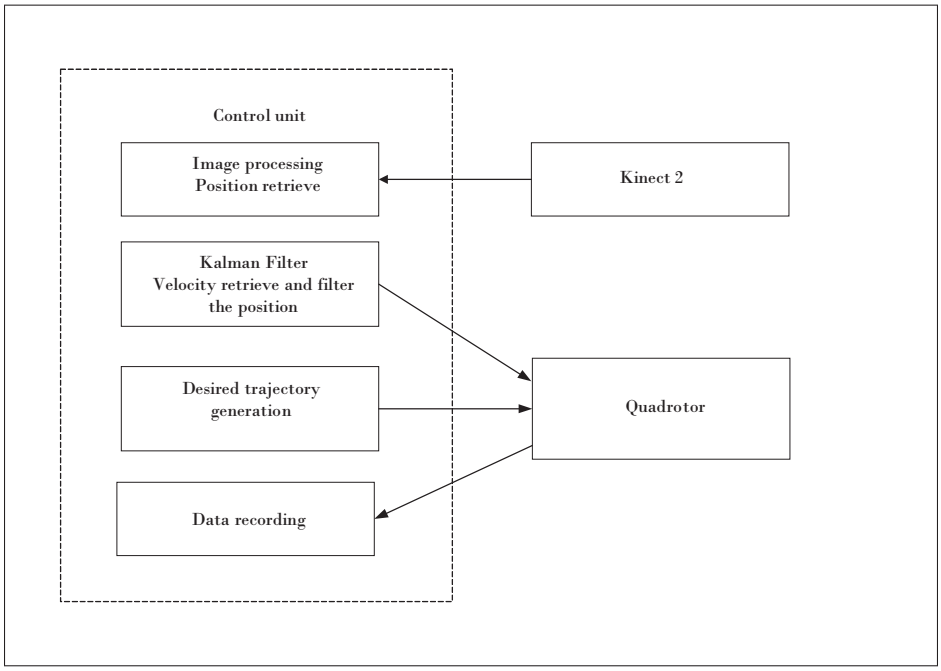

Figure-A I-1 Communication of all peripherals

It can be seen from Figure A I-1 that communication between different devices is crucial to implement the designed controller. Communication protocols are not necessarily common. Knowledge of these protocols is required to get the whole system working properly. Several tasks must be managed simultaneously and must be optimized in order to receive or send information quickly. ROS is one of the platforms that can be used externally to manage low-level devices.

1.1 Robot Operating System (ROS)

The ROS platform can handle communications between different devices at a low level. ROS is, therefore, the intermediary between the communication protocol of a device and the receiving and transmitting a message. The user must only know how to handle ROS without knowing any information on how to build the protocol and on addressing. The ROS platform is based on a server (which can be network or local) ROS (called roscore) where all messages based on the ROS protocol are received. These messages can be modified (we say that we publish information to a message) or received (we say we subscribe to a message) by any device connected to the ROS server. The procedure to establish the point between the communication protocol and ROS is called a frame Figure A I-2. The package is given most often by the developer of the device in question. We can, however, create our own package for any little device that we know the structure of the communication protocol.

The ROS compatible programming languages are Python, C ++ and Lisp. ROS contains a library to send any structure of a message (messages for positions, trajectories, Cartesian landmarks, image reading, reading of inertial centers ...). Hence, no need to know the structure of the low-level ROS protocol. Several packages have been used for the implementation of the controller:

- The Iai Kinect 2 package makes it possible to link the communication protocol of the Kinect 2 and ROS (see $https://github.com/code-iai/iai_kinect2$). It will then be possible to recover the images coming from the infra-red sensors and from the camera. We will also recover the intrinsic parameters of the camera;

- The Mavros package (available on http://wiki.ros.org/mavros) makes the relationship between the PX4 communication protocol called Mavlink (documentation is available at http://qgroundcontrol.org/mavlink/start) and ROS; We will create a package to run the designed algorithm and create ROS messages containing the position, the velocity and the desired trajectory. The designed controllers will be implemented on the Pixhawk microcontroller.

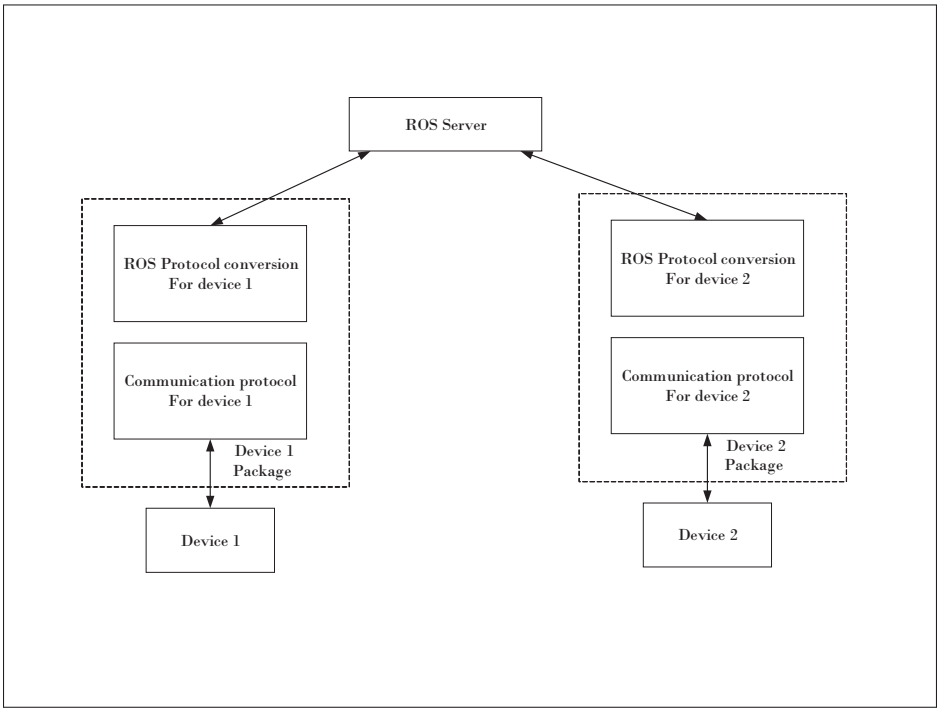

Figure-A I-2 Basic operation of ROS

1.2 Controller Implementation on the S500 quadrotor

The S500 drone has been equipped with a Pixhawk and an embedded computer (Odroid XU4) to validate the designed controller experimentally. A WI-FI router has been used to communicate with the drone from a control base. The drone uses a communication protocol called Mavlink. The use of ROS will make the link between this protocol and the control unit. Mavlink is a protocol used by a variety of firmwares. It offers a protocol structure to control

different types of quadrotor. Many quadrotors in the industry use this protocol. This also allows different firmware using Mavlink to be compatible with most ground stations. A Mavlink package can range from 8 to 263 bytes. We can send a data of 256 bytes maximum. Table A I-1 shows the structure of a Mavlink protocol package.

Table-A I-1 Structure of the Mavlink frame.

Byte Number	Name
0	Beginning of the frame
1	Size of the data
2	Frame sequence number
3	the receiving system ID
4	Component ID
5	Message ID
6 to (n+6)	Data
(n+7) to (n+8)	Control bytes

A documentation (Mavlink, 2015) provides a list of the different MAVLINK messages available. We will use for our case the messages described in Table A I-2.

Table-A I-2 Used Mavlink Messages.

Message	Description
ESTIMATION OF VISION POSITION	Send the current position
ESTIMATION OF VISION VELOCITY	Send the velocity
SET LOCAL POSITION TARGET NED	Sending the desired position, velocity and acceleration
ATTITUDE	Retrieves the current angles

ROS has been used to establish the bridge between Mavlink and the drone. The Pixhawk does not have a WI-FI antenna. We will use the Odroid XU4 embedded computer on the quadrotor to establish communication between the drone and the control base. We will communicate with the Odroid using ROS where the server will be on a network Figure A I-3.

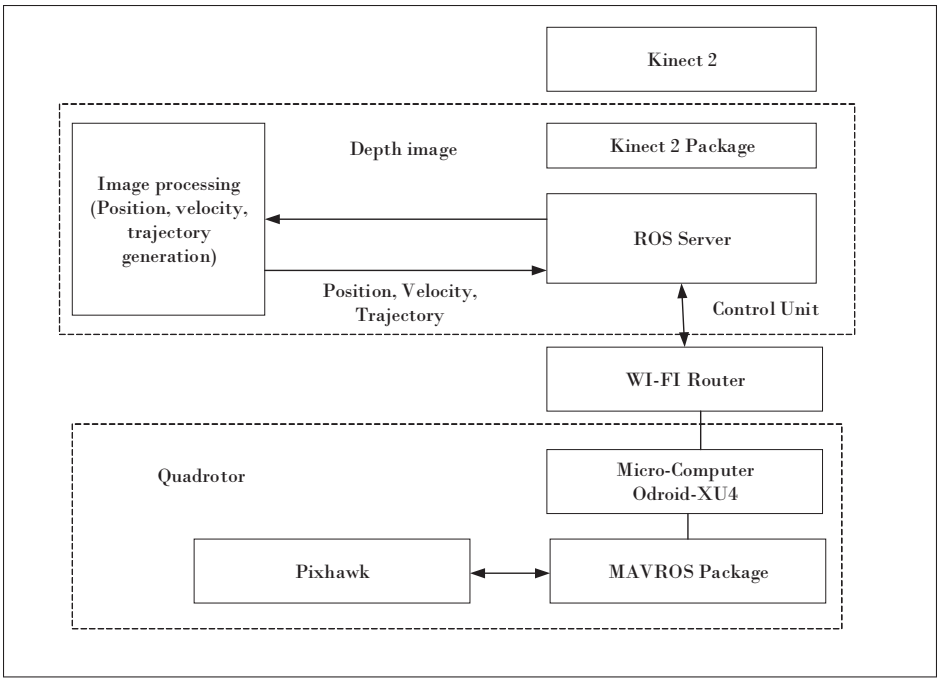

Figure-A I-3 Communication between the control unit and the S500 quadrotor

BIBLIOGRAPHY

Abdolhosseini, M., Zhang, Y. M. & Rabbath, C. A. (2013). An Efficient Model Predictive Control Scheme for an Unmanned Quadrotor Helicopter. *Journal of Intelligent & Robotic Systems*, 70(1), 27–38. doi: 10.1007/s10846-012-9724-3.

Adegas, F. D. & Stoustrup, J. Linear matrix inequalities for analysis and control of linear vector second-order systems. *International Journal of Robust and Nonlinear Control*, 25(16), 2939-2964. doi: 10.1002/rnc.3242.

Aguiar, A. P. & Hespanha, J. P. (2007). Trajectory-Tracking and Path-Following of Underactuated Autonomous Vehicles With Parametric Modeling Uncertainty. *IEEE Transactions on Automatic Control*, 52(8), 1362-1379. doi: 10.1109/TAC.2007.902731.

Alexis, K., Nikolakopoulos, G. & Tzes, A. (2010, June). Constrained optimal attitude control of a quadrotor helicopter subject to wind-gusts: Experimental studies. *Proceedings of the 2010 American Control Conference*, pp. 4451-4455. doi: 10.1109/ACC.2010.5531005.

Alexis, K., Papachristos, C., Nikolakopoulos, G. & Tzes, A. (2011, June). Model predictive quadrotor indoor position control. *2011 19th Mediterranean Conference on Control Automation (MED)*, pp. 1247-1252. doi: 10.1109/MED.2011.5983144.

Alexis, K., Nikolakopoulos, G. & Tzes, A. (2012a). Model predictive quadrotor control: attitude, altitude and position experimental studies. *IET Control Theory Applications*, 6(12), 1812-1827. doi: 10.1049/iet-cta.2011.0348.

Alexis, K., Nikolakopoulos, G. & Tzes, A. (2012b). Model predictive quadrotor control: attitude, altitude and position experimental studies. *IET Control Theory Applications*, 6(12), 1812-1827. doi: 10.1049/iet-cta.2011.0348.

Alexis, K., Papachristos, C., Siegwart, R. & Tzes, A. (2016). Robust Model Predictive Flight Control of Unmanned Rotorcrafts. *Journal of Intelligent & Robotic Systems*, 81(3), 443–469. doi: 10.1007/s10846-015-0238-7.

Amazon. (2015, March, 5). Amazon Primeair. (n.d.)[format]. Consulted at http://www.amazon.com/b?node=8037720011.

Arellano-Muro, C. A., Luque-Vega, L. F., Castillo-Toledo, B. & Loukianov, A. G. (2013, Sep.). Backstepping control with sliding mode estimation for a hexacopter. *2013 10th International Conference on Electrical Engineering, Computing Science and Automatic Control (CCE)*, pp. 31-36. doi: 10.1109/ICEEE.2013.6676026.

Benallegue, A., Mokhtari, A. & Fridman, L. (2008). High-order sliding-mode observer for a quadrotor UAV. *International Journal of Robust and Nonlinear Control*, 18(45), 427-440. doi: 10.1002/rnc.1225.

Berbra, C., Lesecq, S. & Martinez, J. J. (2008, June). A multi-observer switching strategy for fault-tolerant control of a quadrotor helicopter. *2008 16th Mediterranean Conference on Control and Automation*, pp. 1094-1099. doi: 10.1109/MED.2008.4602064.

Besnard, L., Shtessel, Y. B. & Landrum, B. (2007, July). Control of a Quadrotor Vehicle Using Sliding Mode Disturbance Observer. *2007 American Control Conference*, pp. 5230-5235. doi: 10.1109/ACC.2007.4282421.

Besnard, L., Shtessel, Y. B. & Landrum, B. (2012). Quadrotor vehicle control via sliding mode controller driven by sliding mode disturbance observer. *Journal of the Franklin Institute*, 349(2), 658 - 684. doi: https://doi.org/10.1016/j.jfranklin.2011.06.031. Advances in Guidance and Control of Aerospace Vehicles using Sliding Mode Control and Observation Techniques.

Bouabdallah, S. & Siegwart, R. (2005, April). Backstepping and Sliding-mode Techniques Applied to an Indoor Micro Quadrotor. *Proceedings of the 2005 IEEE International Conference on Robotics and Automation*, pp. 2247-2252. doi: 10.1109/ROBOT.2005.1570447.

Bouabdallah, S. & Siegwart, R. (2007, Oct). Full control of a quadrotor. *2007 IEEE/RSJ International Conference on Intelligent Robots and Systems*, pp. 153-158. doi: 10.1109/IROS.2007.4399042.

Bouabdallah, S., Murrieri, P. & Siegwart, R. (2004a, April). Design and control of an indoor micro quadrotor. *IEEE International Conference on Robotics and Automation, 2004. Proceedings. ICRA '04. 2004*, 5, 4393-4398 Vol.5. doi: 10.1109/ROBOT.2004.1302409.

Bouabdallah, S., Noth, A. & Siegwart, R. (2004b, Sep.). PID vs LQ control techniques applied to an indoor micro quadrotor. *2004 IEEE/RSJ International Conference on Intelligent Robots and Systems (IROS) (IEEE Cat. No.04CH37566)*, 3, 2451-2456 vol.3. doi: 10.1109/IROS.2004.1389776.

Bouabdallah, S. (2007). Design and control of quadrotors with application to autonomous flying. 155. doi: 10.5075/epfl-thesis-3727.

Bouadi, H., Bouchoucha, M. & Tadjine, M. (2007). Sliding Mode Control based on Backstepping Approach for an UAV Type-Quadrotor.

Bouadi, H., Aoudjif, A. & Guenifi, M. (2015, May). Adaptive flight control for quadrotor UAV in the presence of external disturbances. *2015 6th International Conference on Modeling, Simulation, and Applied Optimization (ICMSAO)*, pp. 1-6. doi: 10.1109/ICMSAO.2015.7152250.

Bouffard, P., Aswani, A. & Tomlin, C. (2012, May). Learning-based model predictive control on a quadrotor: Onboard implementation and experimental results. *2012 IEEE International Conference on Robotics and Automation*, pp. 279-284. doi: 10.1109/ICRA.2012.6225035.

Cao, N. & Lynch, A. F. (2016). Inner–Outer Loop Control for Quadrotor UAVs With Input and State Constraints. *IEEE Transactions on Control Systems Technology*, 24(5), 1797-1804. doi: 10.1109/TCST.2015.2505642.

Chen, W.-H., Ballance, D. J., Gawthrop, P. J. & O'Reilly, J. (2000). A nonlinear disturbance observer for robotic manipulators. *IEEE Transactions on Industrial Electronics*, 47(4), 932-938. doi: 10.1109/41.857974.

Cheng, Y., Jiang, L., Li, T. & Guo, L. (2018, June). Robust tracking control for a quadrotor UAV via DOBC approach. *2018 Chinese Control And Decision Conference (CCDC)*, pp. 559-563. doi: 10.1109/CCDC.2018.8407194.

Choi, Y. & Ahn, H. (2015). Nonlinear Control of Quadrotor for Point Tracking: Actual Implementation and Experimental Tests. *IEEE/ASME Transactions on Mechatronics*, 20(3), 1179-1192. doi: 10.1109/TMECH.2014.2329945.

Dai, S., Lee, T. & Bernstein, D. S. (2014, Dec). Adaptive control of a quadrotor UAV transporting a cable-suspended load with unknown mass. *53rd IEEE Conference on Decision and Control*, pp. 6149-6154. doi: 10.1109/CDC.2014.7040352.

Das, A., Lewis, F. & Subbarao, K. (2009). Backstepping Approach for Controlling a Quadrotor Using Lagrange Form Dynamics. *Journal of Intelligent and Robotic Systems*, 56(1), 127–151. doi: 10.1007/s10846-009-9331-0.

Davila, J., Fridman, L. & Levant, A. (2005). Second-order sliding-mode observer for mechanical systems. *IEEE Transactions on Automatic Control*, 50(11), 1785-1789. doi: 10.1109/TAC.2005.858636.

Derafa, L., Benallegue, A. & Fridman, L. (2012). Super twisting control algorithm for the attitude tracking of a four rotors UAV. *Journal of the Franklin Institute*, 349(2), 685 - 699. doi: https://doi.org/10.1016/j.jfranklin.2011.10.011. Advances in Guidance and Control of Aerospace Vehicles using Sliding Mode Control and Observation Techniques.

Deters, R., Ananda, G. & Selig, M. (2014, 1). Reynolds number effects on the performance of small-scale propellers. *32nd AIAA Applied Aerodynamics Conference*.

Dirac, P. (1953). The lorentz transformation and absolute time. *Physica*, 19(1-–12), 888–896. doi: 10.1016/S0031-8914(53)80099-6.

Drakunov, S. & Utkin, V. (1995, Dec). Sliding mode observers. Tutorial. *Proceedings of 1995 34th IEEE Conference on Decision and Control*, 4, 3376-3378 vol.4. doi: 10.1109/CDC.1995.479009.

Dydek, Z. T., Annaswamy, A. M. & Lavretsky, E. (2013). Adaptive Control of Quadrotor UAVs: A Design Trade Study With Flight Evaluations. *IEEE Transactions on Control Systems Technology*, 21(4), 1400-1406. doi: 10.1109/TCST.2012.2200104.

Edwards, C. & Spurgeon, S. K. (1994). On the development of discontinuous observers. *International Journal of Control*, 59(5), 1211-1229. doi: 10.1080/00207179408923128.

Edwards, C., Spurgeon, S. K. & Tan, C. P. (2002). On the Development and Application of Sliding Mode Observers. In Yu, X. & Xu, J.-X. (Eds.), *Variable Structure Systems: Towards the 21st Century* (pp. 253–282). Berlin, Heidelberg: Springer Berlin Heidelberg. doi: 10.1007/3-540-45666-X_11.

Erginer, B. & Altug, E. (2007, June). Modeling and PD Control of a Quadrotor VTOL Vehicle. *2007 IEEE Intelligent Vehicles Symposium*, pp. 894-899. doi: 10.1109/IVS.2007.4290230.

Farrell, J. A., Polycarpou, M., Sharma, M. & Dong, W. (2009). Command Filtered Backstepping. *IEEE Transactions on Automatic Control*, 54(6), 1391-1395. doi: 10.1109/TAC.2009.2015562.

Fethalla, N., Saad, M., Michalska, H. & Ghommam, J. (2017a, July). Robust tracking control for a quadrotor UAV. *2017 25th Mediterranean Conference on Control and Automation (MED)*, pp. 1269-1274. doi: 10.1109/MED.2017.7984292.

Fethalla, N., Saad, M., Michalska, H. & Ghommam, J. (2017b, April). Robust observer-based backstepping controller for a quadrotor UAV. *2017 IEEE 30th Canadian Conference on Electrical and Computer Engineering (CCECE)*, pp. 1-4. doi: 10.1109/CCECE.2017.7946754.

Fethalla, N., Saad, M., Michalska, H. & Ghommam, J. (2018). Robust Observer-Based Dynamic Sliding Mode Controller for a Quadrotor UAV. *IEEE Access*, 6, 45846-45859. doi: 10.1109/ACCESS.2018.2866208.

Feynman, R. & Vernon Jr., F. (1963). The theory of a general quantum system interacting with a linear dissipative system. *Annals of Physics*, 24, 118–173. doi: 10.1016/0003-4916(63)90068-X.

Ghoshal, D. P. & Michalska, H. (2019). Finite-interval kernel-based identification and state estimation for LTI systems with noisy output data. *American Control Conference (submitted)*.

Ghoshal, D. P., Gopalakrishnan, K. & Michalska, H. (2017). Using invariance to extract signal from noise. *American Control Conference*.

Ghoshal, D. P., Sinha, S. & Michalska, H. (2019). Algebraic Nonlinear Identification and Output Tracking Control of Synchronous Generator using Differential Flatness. *American Control Conference*.

Ginoya, D., Shendge, P. D. & Phadke, S. B. (2014). Sliding Mode Control for Mismatched Uncertain Systems Using an Extended Disturbance Observer. *IEEE Transactions on Industrial Electronics*, 61(4), 1983-1992. doi: 10.1109/TIE.2013.2271597.

Gonzalez-Hernandez, I., Palacios, F. M., Cruz, S. S., Quesada, E. S. E. & Leal, R. L. (2017). Real-time altitude control for a quadrotor helicopter using a super-twisting controller based on high-order sliding mode observer. *International Journal of Advanced Robotic Systems*, 14(1), 1729881416687113. doi: 10.1177/1729881416687113.

Guo, Y., Zhang, R. & Li, H. (2016, July). Robust trajectory control for quadrotors with disturbance observer. *2016 35th Chinese Control Conference (CCC)*, pp. 10788-10794. doi: 10.1109/ChiCC.2016.7555067.

Henrion, D., Henrion, D., Šebek, M. & Kučera, V. (2003). Robust Pole Placement for Second-Order Systems: An LMI Approach. *IFAC Proceedings Volumes*, 36(11), 419 - 424. doi: https://doi.org/10.1016/S1474-6670(17)35700-2. 4th IFAC Symposium on Robust Control Design 2003, Milan, Italy, 25-27 June 2003.

Herissé, B., Hamel, T., Mahony, R. & Russotto, F. (2012). Landing a VTOL Unmanned Aerial Vehicle on a Moving Platform Using Optical Flow. *IEEE Transactions on Robotics*, 28(1), 77-89. doi: 10.1109/TRO.2011.2163435.

Hoffmann, G. M., Huang, H., Waslander, S. L. & Tomlin, C. J. (2007a). Quadrotor Helicopter Flight Dynamics and Control : Theory and Experiment.

Hoffmann, G. M., Huang, H., Waslander, S. L. & Tomlin, C. J. (2007b). Quadrotor Helicopter Flight Dynamics and Control : Theory and Experiment .

Iskandarani, M., Givigi, S. N., Rabbath, C. A. & Beaulieu, A. (2013, June). Linear Model Predictive Control for the encirclement of a target using a quadrotor aircraft. *21st Mediterranean Conference on Control and Automation*, pp. 1550-1556. doi: 10.1109/MED.2013.6608928.

Jia, Y.-B. (2013a). Quaternions and Rotations.

Jia, Y.-B. (2013b). Quaternions and Rotations.

Khoshelham, K. & Elberink, S. O. (2012). Accuracy and Resolution of Kinect Depth Data for Indoor Mapping Applications. *Sensors*, 12(2), 1437–1454. doi: 10.3390/s120201437.

Kim, T. S., Stol, K. & Kecman, V. (2007). Control of 3 DOF Quadrotor Model. *Robot Motion and Control 2007*, pp. 29–38.

Lee, D., Kim, H. J. & Sastry, S. (2009). Feedback Linearization vs . Adaptive Sliding Mode Control for a Quadrotor Helicopter.

Levant, A. (1998). Robust exact differentiation via sliding mode technique**This paper was recommended for publication in final form by Associate Editor Hassan Khalil under the direction of Editor Tamer Basar. *Automatica*, 34(3), 379 - 384. doi: https://doi.org/10.1016/S0005-1098(97)00209-4.

Levant, A. (2003). Higher-order sliding modes, differentiation and output-feedback control. *International Journal of Control*, 76(9-10), 924-941. doi: 10.1080/0020717031000099029.

L.Meier. (2015). Software choice for Pixhawk hardware, PX4 autopilot. (n.d.)[format]. Consulted at https://pixhawk.org.

Luque-Vega, L., Castillo-Toledo, B. & Loukianov, A. G. (2012). Robust block second order sliding mode control for a quadrotor. *Journal of the Franklin Institute*, 349(2), 719 - 739. doi: https://doi.org/10.1016/j.jfranklin.2011.10.017. Advances in Guidance and Control of Aerospace Vehicles using Sliding Mode Control and Observation Techniques.

Madani, T. & Benallegue, A. (2006, Oct). Backstepping Control for a Quadrotor Helicopter. *2006 IEEE/RSJ International Conference on Intelligent Robots and Systems*, pp. 3255-3260. doi: 10.1109/IROS.2006.282433.

Madani, T. & Benallegue, A. (2007, Oct). Backstepping control with exact 2-sliding mode estimation for a quadrotor unmanned aerial vehicle. *2007 IEEE/RSJ International Conference on Intelligent Robots and Systems*, pp. 141-146. doi: 10.1109/IROS.2007.4399009.

Mahony, R., Kumar, V. & Corke, P. (2012). Multirotor Aerial Vehicles: Modeling, Estimation, and Control of Quadrotor. *IEEE Robotics Automation Magazine*, 19(3), 20-32. doi: 10.1109/MRA.2012.2206474.

Mavlink. (2015, October, 2). MAVLINK Common Message Set [Format]. Consulted at https://mavlink.io/en/messages/common.html.

McCabe, B. Y., Hamledari, H., Shahi, A., Zangeneh, P. & Azar, E. R. (2017). Roles, Benefits, and Challenges of Using UAVs for Indoor Smart Construction Applications. In *Computing in Civil Engineering 2017*. doi: 10.1061/9780784480830.043.

Meier, L., Honegger, D. & Pollefeys, M. (2015, May). PX4: A node-based multithreaded open source robotics framework for deeply embedded platforms. *2015 IEEE International Conference on Robotics and Automation (ICRA)*, pp. 6235-6240.

Michael, N., Mellinger, D., Lindsey, Q. & Kumar, V. (2010). The GRASP Multiple Micro-UAV Testbed. *IEEE Robotics Automation Magazine*, 17(3), 56-65.

Mistler, V., Benallegue, A. & M'Sirdi, N. K. (2001, Sep.). Exact linearization and noninteracting control of a 4 rotors helicopter via dynamic feedback. *Proceedings 10th IEEE International Workshop on Robot and Human Interactive Communication. ROMAN 2001 (Cat. No.01TH8591)*, pp. 586-593. doi: 10.1109/ROMAN.2001.981968.

Mokhtari, A., M'Sirdi, N. K., Meghriche, K. & Belaidi, A. (2006). Feedback linearization and linear observer for a quadrotor unmanned aerial vehicle. *Advanced Robotics*, 20(1), 71-91. doi: 10.1163/156855306775275495.

Moreno, J. A. & Osorio, M. (2008, Dec). A Lyapunov approach to second-order sliding mode controllers and observers. *2008 47th IEEE Conference on Decision and Control*, pp. 2856-2861. doi: 10.1109/CDC.2008.4739356.

Mu, B., Pei, Y. & Shi, Y. (2017, May). Integral sliding mode control for a quadrotor in the presence of model uncertainties and external disturbances. *2017 American Control Conference (ACC)*, pp. 5818-5823.

Nägeli, T., Alonso-Mora, J., Domahidi, A., Rus, D. & Hilliges, O. (2017). Real-Time Motion Planning for Aerial Videography With Dynamic Obstacle Avoidance and Viewpoint Optimization. *IEEE Robotics and Automation Letters*, 2(3), 1696-1703.

Obaid, M. A. M., Husain, A. R. & Al-Kubati, A. A. M. (2016). Robust Backstepping Tracking Control of Mobile Robot Based on Nonlinear Disturbance Observer. *International Journal of Electrical and Computer Engineering*, 6(2), 901.

O'Toole, M. D., Bouazza-Marouf, K. & Kerr, D. (2010a). Chatter Suppression in Sliding Mode Control: Strategies and Tuning Methods. *ROMANSY 18 Robot Design, Dynamics and Control*, pp. 109–116.

O'Toole, M. D., Bouazza-Marouf, K. & Kerr, D. (2010b). Chatter Suppression in Sliding Mode Control: Strategies and Tuning Methods. *ROMANSY 18 Robot Design, Dynamics and Control*, pp. 109–116.

Piersol, A. & Paez, T. (2009). *Harris' Shock and Vibration Handbook*. McGraw-Hill Education. Consulted at https://books.google.ca/books?id=6JzJmT6zSPcC.

Polyakov, A. & Poznyak, A. (2011). Invariant ellipsoid method for minimization of unmatched disturbances effects in sliding mode control. *Automatica*, 47(7), 1450 - 1454. doi: https://doi.org/10.1016/j.automatica.2011.02.013.

Pulver, A., Wei, R. & Mann, N. C. (2016). Locating AED Enabled Medical Drones to Enhance Cardiac Arrest Response Times. 20, 1-12.

Raffo, G. V., Ortega, M. G. & Rubio, F. R. Robust Nonlinear Control for Path Tracking of a Quad-Rotor Helicopter. *Asian Journal of Control*, 17(1), 142-156. doi: 10.1002/asjc.823.

Raffo, G. V., Ortega, M. G. & Rubio, F. R. (2010). An integral predictive/nonlinear H control structure for a quadrotor helicopter. *Automatica*, 46(1), 29 - 39. doi: https://doi.org/10.1016/j.automatica.2009.10.018.

Ramirez-Rodriguez, H., Parra-Vega, V., Sanchez-Orta, A. & Garcia-Salazar, O. (2014). Robust Backstepping Control Based on Integral Sliding Modes for Tracking of Quadrotors. *Journal of Intelligent & Robotic Systems*, 73(1), 51–66. doi: 10.1007/s10846-013-9909-4.

Rashad, R., Aboudonia, A. & El-Badawy, A. (2016). A novel disturbance observer-based backstepping controller with command filtered compensation for a MIMO system. *Journal of the Franklin Institute*, 353(16), 4039 - 4061. doi: https://doi.org/10.1016/j.jfranklin.2016.07.017.

Ravichandran, P. (2018). *Dynamic regression in tracking of chaotic system trajectories*. (Master's thesis, McGill University, Montreal, Canada.).

Rinaldi, F., Gargioli, A. & Quagliotti, F. (2014). PID and LQ Regulation of a Multirotor Attitude: Mathematical Modelling, Simulations and Experimental Results. *Journal of Intelligent & Robotic Systems*, 73(1), 33–50. doi: 10.1007/s10846-013-9911-x.

Robotics, T. (2018). RCbenchmark [Format]. Consulted at https://www.rcbenchmark.com/pages/series-1580-thrust-stand-dynamometer.

Runcharoon, K. & Srichatrapimuk, V. (2013, May). Sliding Mode Control of quadrotor. *2013 The International Conference on Technological Advances in Electrical, Electronics and Computer Engineering (TAEECE)*, pp. 552-557. doi: 10.1109/TAEECE.2013.6557334.

Sanca, A. S., Alsina, P. J. & Cerqueira, J. J. F. (2014, Oct). Stability Analysis of a Multirotor UAV with Robust Backstepping Controller. *2014 Joint Conference on Robotics: SBR-LARS Robotics Symposium and Robocontrol*, pp. 241-246. doi: 10.1109/SBR.LARS.Robocontrol.2014.24.

Särkkä, S. (2013). *Bayesian filtering and smoothing*. Cambridge University Press.

Shao, X., Liu, J. & Wang, H. (2018). Robust back-stepping output feedback trajectory tracking for quadrotors via extended state observer and sigmoid tracking differentiator. *Mechanical Systems and Signal Processing*, 104, 631 - 647. doi: https://doi.org/10.1016/j.ymssp.2017.11.034.

Sharifi, F., Mirzaei, M., Gordon, B. W. & Zhang, Y. (2010, Oct). Fault tolerant control of a quadrotor UAV using sliding mode control. *2010 Conference on Control and Fault-Tolerant Systems (SysTol)*, pp. 239-244. doi: 10.1109/SYSTOL.2010.5675979.

Shtessel, Y., Edwards, C., Fridman, L. & Levant, A. (2015). Sliding Mode Control and Observation.

Silva, J. M. A.-D., Edwards, C. & Spurgeon, S. K. (2009). Sliding-Mode Output-Feedback Control Based on LMIs for Plants With Mismatched Uncertainties. *IEEE Transactions on Industrial Electronics*, 56(9), 3675-3683. doi: 10.1109/TIE.2009.2024094.

Sinha, S. *Simultaneous Identification and Tracking of a Synchronous Generator*. (Master's thesis, McGill University, Canada.).

Ton, C. T. & MacKunis, W. (2012, Dec). Robust attitude tracking control of a quadrotor helicopter in the presence of uncertainty. *2012 IEEE 51st IEEE Conference on Decision and Control (CDC)*, pp. 937-942. doi: 10.1109/CDC.2012.6426266.

Wadoo, S. A. (2013). Sliding Mode Control of Crowd Dynamics. *IEEE Transactions on Control Systems Technology*, 21(3), 1008-1015. doi: 10.1109/TCST.2012.2196700.

Wang, J., He, S. & Lin, D. (2016). Robust backstepping control for a class of nonlinear systems using generalized disturbance observer. *International Journal of Control, Automation and Systems*, 14(6), 1475–1483. doi: 10.1007/s12555-014-0401-0.

Wang, Y., Zhao, D., Li, Y. & Ding, S. X. (2017). Unbiased Minimum Variance Fault and State Estimation for Linear Discrete Time-Varying Two-Dimensional Systems. *IEEE Transactions on Automatic Control*, 62(10), 5463-5469. doi: 10.1109/TAC.2017.2697210.

Xiong, J.-J. & Zheng, E.-H. (2014). Position and attitude tracking control for a quadrotor UAV. *ISA Transactions*, 53(3), 725 - 731. doi: https://doi.org/10.1016/j.isatra.2014.01.004.

Xu, B., Shi, Z. & Yang, C. (2015). Composite fuzzy control of a class of uncertain nonlinear systems with disturbance observer. *Nonlinear Dynamics*, 80(1), 341–351. doi: 10.1007/s11071-014-1872-5.

Yang, J., Li, S. & Yu, X. (2013). Sliding-Mode Control for Systems With Mismatched Uncertainties via a Disturbance Observer. *IEEE Transactions on Industrial Electronics*, 60(1), 160-169. doi: 10.1109/TIE.2012.2183841.

Yang, J., Li, S. & Chen, W.-H. (2012). Nonlinear disturbance observer-based control for multi-input multi-output nonlinear systems subject to mismatching condition. *International Journal of Control*, 85(8), 1071-1082. doi: 10.1080/00207179.2012.675520.

Younes, Y. A., Drak, A., Noura, H., Rabhi, A. & Hajjaji, A. E. (2014, May). Model-free control of a quadrotor vehicle. *2014 International Conference on Unmanned Aircraft Systems (ICUAS)*, pp. 1126-1131. doi: 10.1109/ICUAS.2014.6842366.

Yu, X. & Kaynak, O. (2009). Sliding-Mode Control With Soft Computing: A Survey. *IEEE Transactions on Industrial Electronics*, 56(9), 3275-3285. doi: 10.1109/TIE.2009.2027531.

Zhao, B., Xian, B., Zhang, Y. & Zhang, X. (2015). Nonlinear robust sliding mode control of a quadrotor unmanned aerial vehicle based on immersion and invariance method. *International Journal of Robust and Nonlinear Control*, 25(18), 3714-3731. doi: 10.1002/rnc.3290.

Zheng, E.-H., Xiong, J.-J. & Luo, J.-L. (2014). Second order sliding mode control for a quadrotor UAV. *ISA Transactions*, 53(4), 1350 - 1356. doi: https://doi.org/10.1016/j.isatra.2014.03.010. Disturbance Estimation and Mitigation.